THE UNIVERSITY *of* EDINBURGH

This thesis has been submitted in fulfilment of the requirements for a postgraduate degree (e. g. PhD, MPhil, DClinPsychol) at the University of Edinburgh. Please note the following terms and conditions of use:

- This work is protected by copyright and other intellectual property rights, which are retained by the thesis author, unless otherwise stated.
- A copy can be downloaded for personal non-commercial research or study, without prior permission or charge.
- This thesis cannot be reproduced or quoted extensively from without first obtaining permission in writing from the author.
- The content must not be changed in any way or sold commercially in any format or medium without the formal permission of the author.
- When referring to this work, full bibliographic details including the author, title, awarding institution and date of the thesis must be given.

Leveraging large-scale genetic and neuroimaging data for the study of Major Depressive Disorder: towards mechanistic insights and personalised approaches

Gladi Jinyan Thng

THE UNIVERSITY *of* EDINBURGH

Doctor of Philosophy

The University of Edinburgh

2024

Abstract

Major Depressive Disorder (MDD) is a prevalent psychiatric disorder and a leading cause of global disease burden, with women being twice as likely than men to be affected by MDD in the lifetime. Complex in nature, the symptoms of MDD are wide-ranging and its aetiology is multifactorial, involving both genetic and environmental risk factors, as well as their interaction. To elucidate mechanisms underlying MDD, large-scale neuroimaging studies have contributed robust findings on regional brain morphometric alterations and provided insights into their genetic underpinnings. There are, however, two overarching issues that remain unaddressed – (1) the use network-based approaches as a better representation of how the brain is structured as a complex network in large-scale studies, and (2) the translation of population-level neuroimaging findings to the individual level, which set the foundations for this thesis.

Most MDD studies thus far have focused on individual brain regions, but the brain is inherently structured as a network with brain regions linked together by anatomical white matter tracts (i.e., a connectome). As a complex network, the brain exhibits non-trivial organisational properties, such as having a strong "rich club" core where key brain regions are strongly connected together to function as a central backbone of brain communication. MDD is thought to be associated with dysconnectivity in the brain, where network architecture, such as the rich club core, is thought to be disrupted. However, studies adopting connectomic approaches to study these questions have been few and limited by sample size, resulting in low reproducibility. Hence, this was addressed in the first study of this thesis, where I leveraged structural connectome data that were processed locally from two large adult cohorts (UK Biobank (N=5,104), Generation Scotland (N=725)) and utilised graph theory

measures to compare the structural connectomes of MDD cases and healthy controls from the global network level down to the individual connections. Here, it was found that the rich club architecture remains robust in MDD. There were, however, subtle reductions in efficiency (i.e., a measure to reflect the efficiency of information transfer between brain regions) across the brain, which added up in the order of the connectome hierarchy to effect an overall reduction in global network efficiency in MDD. As such, brain structural connectomic differences in MDD do not consist of large effects confined to one or two distinct brain regions, but rather involves subtle effects that are distributed across the whole brain.

Having established that structural connectomic differences exist in MDD, the next step was to investigate how the connectome is affected by key MDD risk factors, such as MDD polygenic risk (MDD-PRS) and early life adversity such as childhood trauma (CT). A series of analyses were conducted using connectome data from 14,881 subjects (6,812 males and 8,069 females) from the UK Biobank. As previous studies have reported sex differences in MDD-PRS and CT associations with neuroimaging variables, the analyses here were conducted separately for males and females. Specifically, network-based statistics was first used to identify regions of the connectome (hereby called subnetworks) that were associated with MDD-PRS and CT (i.e., higher MDD-PRS or CT exposure is associated with lower network connectivity in the identified subnetwork). Next, the roles of the (1) PRS-associated subnetwork as mediator in the relation between MDD-PRS and MDD, and (2) CT-associated subnetwork as mediator in the relation between CT and MDD were examined. As the impact of MDD-PRS on MDD may differ in people with different degrees of CT exposure, further analysis using a moderated mediation model was also done to test if the direct and indirect effects of MDD-PRS on MDD were further moderated by CT. The results showed that the PRS-

and CT-associated subnetworks were largely distinctive from each other within each sex, and were also specific to each sex. For the PRS-associated subnetwork, connectivity of the subnetwork was significantly lower in MDD cases than controls in females but not males. Likewise, a significant mediation effect was present in females but not males. Both direct and indirect effects in females were, however, not moderated by CT exposure. For the CT-associated subnetworks, connectivity of the subnetwork was significantly lower in MDD cases than controls in both sexes, but a significant mediation effect was only present in females. As such, the results in this chapter showed that MDD risk factors have differential associations with male and female structural connectomes, with connectome mediation effects only observed in females.

Importantly, while these population-level neuroimaging findings are useful in providing mechanistic insights, their use is limited if they cannot be translated to the individual level. In other words, as a first step towards clinical utility, can we use neuroimaging findings to assess an individual's vulnerability to MDD? Given that brain morphometric findings by large-scale studies, such as ENIGMA, are well-established and have been shown to be reproducible, they can be used as a starting reference for the development of personalised brain-based risk scores. Thus, in the third study, I utilised ENIGMA summary statistics based on the adult cohort to generate brain-based risk scores (Regional Vulnerability Index abbreviated 'RVI') for five different brain morphometric measures for each subject in an adult subsample of Generation Scotland (N=702) and tested their associations with MDD. This was done concurrently with MDD-PRS, which can be considered a personalised genetic risk score, to use it as a benchmark to evaluate the validity of the brain-based MDD-RVIs in terms of effect sizes. The additive effect of both scores were also tested to see if they could

account for more variation in disease risk when used in combination. It was observed that MDD-RVIs, namely those based on white matter microstructural measures (mean diffusivity and fractional anisotropy), had stronger associations with MDD compared to MDD-PRS. Further, both brain-based and genetic risk scores worked additively to increase variance explained in MDD. As an exploratory study to investigate the similarities of brain features of adolescent depression with adult MDD, the same analyses were repeated in a large adolescent cohort (N=2,081 to N=3,825). In adolescents, it was observed that MDD-PRS outperformed MDD-RVIs. These results re-emphasise the notion of 'dysconnection' in MDD and highlights the dynamic nature of the brain that allows it to capture signals of additional risk factors beyond genetic risk that influence disease course. With the increasing focus on connectome studies, future research can also consider extending this work to personalised connectome-based markers.

Summarising these works, these three studies helped to fill in knowledge gaps in the existing literature, specifically pertaining to the use of connectome-based approaches and the translation of findings to the individual level. The key takeaways include: (1) the rich club architecture remains stable in MDD but there are subtle but widespread differences across the connectome, (2) genetic and environmental factors can influence the risk of MDD through the connectome and sex differences in these associations are prominent, and (3) personalised brain-based markers have potential clinical utility in aiding the early diagnosis of MDD.

Lay summary

Major Depressive Disorder (MDD) is a common mood disorder that affects approximately 3.8% of the world population, with women being twice as likely than men to be affected by MDD in the lifetime. A complex combination of genetic and environmental risk factors play a role in MDD, although the exact causes and underlying mechanisms are still unclear.

As a brain-related disorder, many studies have since shown that structural differences exist in certain brain regions in individuals with MDD versus those without. However, studying each brain region in isolation may not be ideal, as the brain is a large network where brain regions are interconnected. In recent times, network approaches, such as those used to study aviation hubs and the connections between them, have been increasingly applied to study brain networks. It has been shown that there are robust architectures in the brain to support the efficient transfer of information between brain regions. For example, similar to aviation hubs that serve as a central point for most flights to pass through and are well-connected to each other, there are stronger and more connections between key brain regions to coordinate the efficient flow of information. It is thought that such connections might be disrupted in MDD, but this remains unclear, as network approaches have not been applied at a scale for studies on MDD. Large sample sizes are essential for MDD studies to ensure the robustness and replicability of findings.

As such, in the first study of this thesis, I utilised network approaches in two large population samples (sample sizes range from 725 to 5,104 subjects) to compare the brain networks of individuals with and without MDD. It was found that in individuals with MDD, connections between key brain regions (hubs) that play a central role in the network remain robust However, there exist subtle reductions in connectivity across the entire brain, which

affected the efficiency at which brain regions communicate with each other. As such, instead of large disruptions to brain connectivity at one or two distinct brain regions, there exist subtle reductions in connectivity across the whole brain in MDD cases.

Having shown that brain networks are different in individuals with and without MDD, the next step was to see if key MDD risk factors, such as genetic risk and childhood trauma, affect the integrity of connections in the brain network. As above, studies have looked at these associations with individual brain regions, but few have looked at them from a network perspective at scale. In the second study involving 8,069 female and 6,812 male subjects, the results showed that genetic risk and childhood trauma affect different parts of the brain network, and the regions affected were also specific to each sex. Lower connectivity in these regions was associated with a higher chance of developing MDD but only in females. The results in this chapter showed that MDD risk factors have differential associations with male and female brain networks.

Besides uncovering the underlying mechanisms, one of the main goals of MDD research is also to be able to assess an individual's vulnerability to MDD. This can be done by using the results from large-scale neuroimaging and genetic studies on MDD to construct brain-based and genetic risk scores for each individual, respectively. This was done in the third study for adults and adolescents separately (sample sizes range from 782 to 3,805 subjects), and both types of scores were then compared in terms of their strength of association with MDD. Brain-based risk scores generally performed better than the genetic risk score in adults, but the converse is true for adolescents. This could possibly be due to the dynamic nature of the brain that allows it to capture signals of additional risk factors (e.g., from the environment) beyond genetic risk.

Summarising these works, these three studies demonstrate that subtle but widespread alterations in the brain network due to a combination of genetic and environmental risk factors are present in MDD. Brain-based findings also have the potential to be clinically useful biomarkers to inform early diagnosis of MDD.

Declarations

I declare that this thesis was composed by myself, that the work contained herein is my own except where explicitly stated otherwise in the text, and that this work has not been submitted for any other degree or processional qualification except as specified.

Two published papers are included in Chapters 2 and 4, respectively. As the first author, I conceived the hypotheses, conducted the analyses, and wrote these manuscripts under supervision.

Thng, G., Shen, X., Stolicyn, A., Adams, M. J., Yeung, H. W., Batziou, V., … Whalley, H. C. (2024). A comprehensive hierarchical comparison of structural connectomes in Major Depressive Disorder cases v. controls in two large population samples. *Psychological Medicine*, 1–12. https://doi.org/10.1017/S0033291724000643

Thng, G., Shen, X., Stolicyn, A., Harris, M. A., Adams, M. J., Barbu, M. C., … Whalley, H. C. (2022). Comparing personalized brain-based and genetic risk scores for major depressive disorder in large population samples of adults and adolescents. *European psychiatry: the journal of the Association of European Psychiatrists, 65*(1), e44. https://doi.org/10.1192/j.eurpsy.2022.2301

Gladi Thng

May 2024

Acknowledgements

I would first like to thank my supervisors for supporting me since day one of my PhD studies. To Heather, first and foremost, a sincere thank you for giving me the opportunity to do my PhD with you. Thank you for always being so patient and supportive, and for helping me to grow as a researcher by giving me the freedom to explore while guiding me. To Liana, thank you for the constant guidance throughout the years and for always being so encouraging. You always provide insightful feedback that help to enrich my projects and help me to think deeper. To Shen, thank you for looking out for me, for being a supervisor and a friend. I am grateful for all the help and advice that you have given me both personally and professionally. I would also like to express my heartfelt thanks to my previous supervisors Ivan, Xiang Ren, and Michael for introducing me to the world of research and for believing in me, and to A*STAR for supporting me.

Thank you to the people who have helped me in one way or another during my studies – Andy, Aleks, Mark, Keith, Colin, Ian, Simon, Colin, Miruna, Hannah, Laura, and others not mentioned here. Whether is it chatting about PhD life or answering my many silly questions and giving me constructive feedback, thank you for the conversations and for being very kind in sharing your knowledge. I have learned a lot from all of you. A special shoutout to Hon Wah for always going above and beyond to help me whenever I have trouble understanding certain concepts or when I face problems in my analyses. You have been a tremendous source of help.

To my fellow Singaporeans in Edinburgh – Jiayi, TK, Joseph, Andre, and Max, thank you for the delicious homecooked meals that remind me of home, and for taking it upon yourselves to drag me out of my flat. To my outreach leader Shawn, thank you for all the

timely advice and encouraging messages. I always feel energised after speaking to you and I would not have made it this far without your guidance, thank you very much.

Last but most importantly, thank to you my family, my number one supporters who are always there for me. To Abba, you are the first one that I turn to whenever I feel happy or sad. Thank you for walking this journey alongside me, for rejoicing with me during my highs and lifting me up during my lows. Your wise words always strengthen my heart and mind, and you know the best ways to keep me in peace. I am always in awe of you. To my parents, thank you for always enthusiastically answering my weekly zoom calls and for being a great listening ear. To Mummy, thank you for the unconditional love that you have poured out on me, the past few years felt harder for you than for me. To Daddy, thank you for the random check-in messages and for always trying your best to give me advice even when you cannot find the right words to say or something like that. To Che, thank you for being the affectionate one and I always turn to you for deep or nonsensical conversations. You are my big sister and I know I can count on you whenever I need help. To Mika, thank you for willingly participating in this family's silly antics, including holding embarrassing welcome-home signages during the early morning airport pickups. To Kotaro, the baby of the family, thank you for the joy that you bring. I always smile until my cheeks hurt just by looking at you be you. My time away from home has only made me more appreciative of the time we have together as a family, I truly treasure all of you. Thank you for being happier than me during my happiest times and sadder than me during my saddest times.

Overall, this journey, with all its ups and downs and mundane moments, has been a fruitful one. I am thankful for everything that I have experienced in the past few years, and I look forward to what the future holds for me.

Table of Contents

List of Abbreviations

ABCD	Adolescent Brain and Cognitive Development study
ACC	Anterior cingulate circuit
AIC	Akaike Information Criterion
CBCL	Child Behavioural Checklist
CBGTC	Cortico-basal ganglia-thalamo-cortical
CC	Clustering coefficient
CCA	Canonical correlation analysis
CIDI	Composite International Diagnostic Interview
CT	Childhood trauma
CTnet	CT-associated subnetwork
CTQ	Childhood Trauma Questionnaire
DLPFC	Dorsolateral prefrontal cortex
DTI	Diffusion tensor imaging
ENIGMA	Enhancing Neuroimaging Genetics through Meta-Analysis
eQTL	Expression quantitative trait loci
FA	Fractional anisotropy
FDR	False discovery rate
FWE	Family-wise error rate
GCC	Global clustering coefficient
GEFF	Global efficiency
GS	Generation Scotland

GWAS	Genome-wide association study
MD	Mean diffusivity
MDD	Major Depressive Disorder
MRI	Magnetic resonance imaging
NBS	Network-based Statistic
NEFF	Nodal efficiency
PRS	Polygenic risk score
PRSnet	PRS-associated subnetwork
pT	p-value threshold
QIDS	Quick Inventory of Depressive Symptomatology
ROI	Region-of-Interest
RVI	Regional Vulnerability Index
RVI-CorSA	RVI for cortical surface area
RVI-CorTH	RVI for cortical thickness
RVI-FA	RVI for fractional anisotropy
RVI-MD	RVI for mean diffusivity
RVI-Multi	RVI for multimodal measures
RVI-Sub	RVI for subcortical volume
SC-FC	Structural connectivity-functional connectivity
SCID	Structured Clinical Interview for DSM disorders
UKB	UK Biobank
VLPFC	Ventrolateral prefrontal cortex

List of Figures

List of Tables

Chapter 1: Introduction

1.1 Depression

Depression, characterised as having a persistently low mood or loss of pleasure, is a common but serious mental health disorder. In the 2019 Global Burden of Disease study, it was reported that approximately 280 million people in the world suffer from depressive disorders, affecting people of all ages, ethnicities, and sex (GBD 2019 Diseases and Injuries Collaborators, 2020). Despite increasing research efforts to understand and treat depression, the prevalence of depression has been rising steadily over the years, from 3.69% of the world population in 2015 to 3.8% in 2019 (Institute of Health Metrics and Evaluation, 2024).

1.1.1 Definition of Major Depressive Disorder (MDD)

MDD is a type of depression, and it is defined clinically in Diagnostic and Statistical Manual of Mental Disorders-V (DSM-V; American Psychiatric Association, 2013) as having at least five out of nine symptoms persisting daily for the most parts of the day, for at least two weeks in a row (Table 1.1). These symptoms must include either depressed mood or anhedonia, must result in significant impairment in functioning, and must not be attributed to other medical conditions.

Table 1.1. DSM-V diagnostic criteria for MDD (American Psychiatric Association, 2013)

	Symptoms
1	Depressed mood most of the day, nearly every day, as indicated by either subjective report (e.g., feels sad, empty, hopeless) or observation made by others (e.g., appears tearful).
2	Markedly diminished interest or pleasure in all, or almost all, activities most of the day, nearly every day (as indicated by either subjective account or observation)
3	Significant weight loss when not dieting or weight gain (e.g., a change of more than 5%

	of body weight in a month) or decrease or increase in appetite nearly every day.
4	Insomnia or hypersomnia nearly every day
5	Psychomotor agitation or retardation nearly every day (observable by others, not merely subjective feelings of restlessness or being slowed down)
6	Fatigue or loss of energy nearly every day
7	Feelings of worthlessness or excessive or inappropriate guilt (which may be delusional) nearly every day (not merely self-reproach or guilt about being sick)
8	Diminished ability to think or concentrate, or indecisiveness, nearly every day (either by subjective account or as observed by others)
9	Recurrent thoughts of death (not just fear of dying), recurrent suicidal ideation without a specific plan, or a suicide attempt or a specific plan for committing suicide

The heterogeneity of MDD is clearly reflected in the DSM-V diagnostic system, whereby the symptoms are not pathognomonic of MDD (i.e., not diagnostically specific to MDD as they overlap with other disorders), and a diagnosis is made using a polythetic approach. This means that there can be as many as 227 unique combinations of symptoms that fulfil the diagnostic criteria, and up to 945 combinations if considering variations within each symptom (e.g., for sleep, appetite, and psychomotor changes) (Zimmerman et al., 2015; Fried & Nesse, 2015). In other words, individuals can be commonly diagnosed as having MDD but have symptom profiles that are drastically different from each other. This high symptomatic heterogeneity is one of the reasons why MDD remains hard to understand and hence, highly prevalent.

1.1.2 Impact of MDD

The one-year prevalence of MDD is approximately 6%, and it has been estimated that one in five people will experience at least one episode of MDD at some point in their lives (Kessler & Bromet, 2013; Bromet et al., 2011). There is also a gender gap, with women being twice as likely than men to be affected by MDD in the lifetime, especially during adolescence (Salk et al., 2017; Kuehner, 2017). While the onset of MDD can occur at any age, a recent meta-

analysis of 192 studies (N=708,561) reported that the peak age for the first diagnosis of MDD is 19.5 years old, and as early as 15 years old for first symptoms of MDD (Solmi et al., 2022). The increased vulnerability to MDD in adolescents are likely to be due to a combination of biological and psychosocial changes that they undergo during puberty (Thapar et al., 2012). The early onset of MDD also likely means an increase in the number of years lived with disability, as the chance of MDD recurrence is high. Studies have shown that individuals with a history of MDD, both adults and youths, typically have five to nine separate depressive episodes in their lifetime, with an inter-episode interval of three to five years (Burcusa & Iacono, 2007; Hardeveld et al., 2010; Kovacs et al., 2016). With MDD being a chronic recurring illness, the burden associated with MDD is high and persists throughout the lifetime. Of note, due to several barriers to treatment, including the individual's inadequate mental health literacy on recognising symptoms and pathway to care, self- and societal-imposed stigma, and obstacles within the healthcare system (Waumans et al., 2022), it is likely that a substantial proportion of MDD goes undetected and undocumented. These published statistics may not fully reflect the actual prevalence of the illness and hence, the extent of the negative consequences that it brings.

As evident by the DSM-V symptoms listed above, MDD does not just affect one's mood, but it impairs overall functioning. In 2019, depressive disorders accounted for the largest proportion of mental disorder disability-adjusted life years (i.e., the sum of the number of years lost due to premature mortality and the number of years of healthy life lost due to disability) and were consistently ranked as one of the overall leading causes of global disease burden for both sexes across the lifespan, especially between ages 10 and 49 (GBD 2019 Diseases and Injuries Collaborators, 2020). Besides having a disabling effect on day-to-day activities, such as affecting one's capacity for self-care and managing social relationships

(Fried & Nesse, 2014), MDD is also associated with increased risk for all aspects of suicidality, including suicide ideation, plan, attempt, and completion (Cai et al., 2021; Dong et al., 2019). This is worrying, especially for younger individuals, as suicide was the fourth leading cause of death among 15- to 29-year-olds in 2019 (World Health Organisation, 2021). The considerable morbidity and mortality attributed to MDD are not only restricted to the individual, but they also have a significant impact on family and friends, as well as on the economy. It is estimated that approximately 12 billion productive work days costing nearly US$ 1 trillion are lost annually due to depression and anxiety alone (The Lancet Global Health, 2020). For every dollar spent on MDD direct costs (e.g., treatment), the additional indirect and comorbidity costs (e.g., suicide-related, workplace) amounted to be 6.6 times higher (Greenberg et al., 2015). Hence, with the above evidence, MDD is a disorder that has detrimental effects and warrants greater attention. To this end, many treatment options for MDD have since been explored to mitigate its effects, and in the hope of curing it.

Current treatment options for MDD include pharmacotherapy (e.g., antidepressants), psychotherapy, (e.g., cognitive behavioural therapy) and somatic treatments (e.g., deep brain stimulation, electroconvulsive therapy), which can be used independently or in combination with one another (Karrouri et al., 2021). Among them, antidepressants, such as serotonin reuptake inhibitors, have been the mainstay of MDD treatment, as they have been shown to be effective at least for short-term acute depression (Robberegt et al., 2023; Sim et al., 2015). A recent meta-analysis on the efficacy of 21 antidepressants showed that all antidepressants were more efficacious than placebos, although it should be noted that the certainty of evidence mostly ranged from moderate to very low (Cipriani et al., 2018). While antidepressant treatments and psychotherapy are effective for some people, there is still a great room for improvement for MDD treatments (Cuijpers et al., 2020). The lack of robust

treatment options, along with barriers to treatment mentioned above, collectively result in low treatment rates (34.8% globally) and even in those who seek treatment, only a minority received adequate treatment (Moitra et al., 2022; Mekonen et al., 2021). The lack of robust treatment methods likely stems from a fundamental lack of understanding of the biological basis of MDD, in part due to its highly heterogenous nature and multifactorial background.

MDD cannot be solely attributed to a single biological cause (Cui et al., 2024), but it is influenced by a host of external factors as well. Every individual has a unique pattern of symptoms that resulted from the combination of many different factors (e.g., genetic and environmental risk factors) across time. The trajectory of MDD is not linear, as evident by the high rate of recurrence, but it can fluctuate depending on certain triggers (e.g., a stressful or traumatic life event) that an individual may face at any point in life. As such, it is necessary to understand the risk factors associated with MDD and their underlying mechanisms in order to establish robust and biologically informed treatment approaches.

1.1.3 Risk factors for MDD

There is a broad range of risk factors that contribute to MDD, as detailed in the review by Remes et al (2021). Here, I focus on those that are relevant to this thesis, including genetic risk factors and childhood trauma, of which the latter is one of the most important environmental risk factors for MDD.

Genetic factors

Early evidence of MDD having a genetic component came from twin and family studies, which showed that twin-based heritability for MDD is 37% and lifetime prevalence of MDD is significantly higher in biological relatives of individuals with MDD (Sullivan et al., 2000). There

was then a shift in focus to candidate gene studies, which sought to identify specific polymorphisms in genes that were hypothesised to underlie MDD susceptibility. Prominent examples include the repeat polymorphic region in the serotonin transporter gene (5-HTTLPR) and the Val66Met polymorphism in the brain-derived neurotrophic factor (BDNF) gene. However, no significant associations between candidate genes and MDD have been reported, even in meta-analytic studies to account for the possible lack of power in the individual studies (Lohoff, 2010). The lack of significant findings was further emphasised in a recent study by Border et al (2019), where they did not find any evidence of association with MDD for the 18 most commonly studied candidate gene polymorphisms, despite using large well-powered samples with sample sizes ranging from 62,138 to 443,264 subjects. While results from these early studies may have been disappointing, they provided an important insight that MDD is not simply caused by large effects in a few genetic variants. Rather, it involves multiple variants with small effects, thus ushering in the current era of genome-wide association studies (GWAS).

In contrast to candidate gene studies, GWAS adopt a hypothesis-free approach to simultaneously test millions of genetic variants across the whole genome to identify variants that are associated with MDD. MDD GWAS, however, comes with its own set of challenges due to the unique characteristics of MDD. For example, despite having sample sizes (N~9000) that are comparable to successful GWAS for other disorders (e.g., schizophrenia), no significant genetic variants were detected in early MDD GWASs (Levinson et al., 2014). This was likely due to the high lifetime prevalence (~15%) and modest heritability of MDD, where a successful MDD GWAS would require a sample size that is four to five times larger than that required for schizophrenia which affects about 1% of the population (Wray et al., 2012; Mullins & Lewis, 2017). The increase in collaborative efforts in recent years has allowed for a

massive increase in sample size and hence, the identification of many more genetic variants associated with MDD. The number of identified variants has increased from 44 (N=480,359, 28% cases; Wray et al., 2018) to 102 (N=807,553, 30% cases; Howard et al., 2019), and finally 697 variants in the most recent MDD GWAS (N=5,050,033, 15.7% cases; Adams et al., 2024). In further downstream analyses, variants identified in the MDD GWAS by Howard et al (2019) were found to be enriched in association with synaptic structure and neurotransmission, highlighting the role of prefrontal brain regions in MDD. Of note, while GWAS has been useful in providing insights into MDD, the high polygenicity of MDD also highlights that the genetic variants, individually and collectively, still only explain a very small proportion of variance in MDD, and it is essential to take into consideration external environmental factors that may play a bigger role.

Childhood trauma

There are many environmental factors that contribute towards MDD risk (e.g., built environment, social relationships, stressful life events), as detailed in Remes et al (2021). Early life adversity is, however, of key importance as childhood is a sensitive neurodevelopmental period and negative experiences during this period can contribute towards negative mental health outcomes (Wade et al., 2022). Examples of early life adversity include exposure to violence, family economic hardship, and more importantly, child abuse and neglect (hereby referred to as childhood trauma (CT)). CT is widely studied as it is one of the strongest risk factors for MDD and other mental disorders (Teicher et al., 2022). While relatively common in the general population, CT is highly prevalent (57%) in individuals with MDD (Struck et al., 2020). There are five types of CT, including physical neglect, physical abuse, sexual abuse, emotional abuse, and emotional neglect, of which the latter two appear to be the most

important risk factors for MDD (Humphreys et al., 2020; Struck et al., 2020). In general, however, individuals who experienced multiple types of CT and at a younger age are at a greater risk for psychopathology (Medeiros et al., 2020). CT is a great cause of concern in MDD, as it is associated with an earlier onset and a more pernicious course of MDD, in terms of increased severity and chronicity, and poorer treatment outcome (Nelson et al., 2017; Wiersma et al., 2009; Nanni et al., 2012). For example, in a randomised clinical trial by Williams et al (2016) involving 1,008 adults aged 18 to 65, they found that MDD cases had four times higher rate of exposure to CT and were more likely to report more than two types of abuse as compared to healthy controls. Notably, abuse experienced between four to seven years of age was also associated with poorer response and remission rates after eight weeks of antidepressant treatment. While the exact mechanisms linking CT to MDD is not yet clear, CT has been shown to be associated with a range of alterations in brain structure, function, connectivity, and network architecture (Teicher et al., 2016; Madden et al., 2023). Some of the affected processes include reward processing, cognition, and emotion regulation, which are also commonly implicated in MDD (Yu et al., 2019). Evidently, these findings provide evidence that CT has a considerable association with MDD risk and should be taken into consideration in the study and prevention of MDD.

1.1.4 Importance of identifying biomarkers for MDD

To sum up the above, MDD is a prevalent disorder with long-term consequences that are detrimental to both the individual and the society. It remains hard to treat, mostly due to its complex, multifactorial, and heterogenous nature that preclude a robust understanding of the underlying biological mechanisms. Fundamentally, the lack of precise biological evidence not only makes it challenging to diagnose and treat MDD but may also contribute to the

stigma of MDD. Hence, the search for robust biomarkers of MDD remains important, so as to complement subjective symptom assessments with biologically informed assessments (Insel et al., 2010). The brain is a natural target for investigation of MDD, given that MDD is a brain-related disorder, and since studies on genetic and environmental risk factors have alluded to the involvement of neural mechanisms in MDD, as discussed above. This thesis therefore focuses on investigating the brain in MDD, in hope of providing more insight into the biological mechanisms underlying MDD.

1.2 Understanding the brain in MDD: neuroimaging studies

The brain made up of grey matter and white matter, with the former consisting mainly of neuronal cell bodies, dendrites, and unmyelinated axons, and the latter myelinated axons that cluster to form axonal bundles. This section talks about current evidence of alterations in grey and white matter in MDD and discusses the limitations of current work that contribute towards the motivation of this thesis.

1.2.1 Brain morphometric measures and MDD

Neuroimaging studies on grey matter typically involve studying the changes in the morphometry of specific brain regions using T1-weighted structural Magnetic Resonance Imaging (MRI). Some of the common metrics include volumetric differences of subcortical structures, and changes in the thickness and surface areas of cortical structures (Figure 1.1). Explanations on how these measures are derived can be found in Backhausen et al (2022).

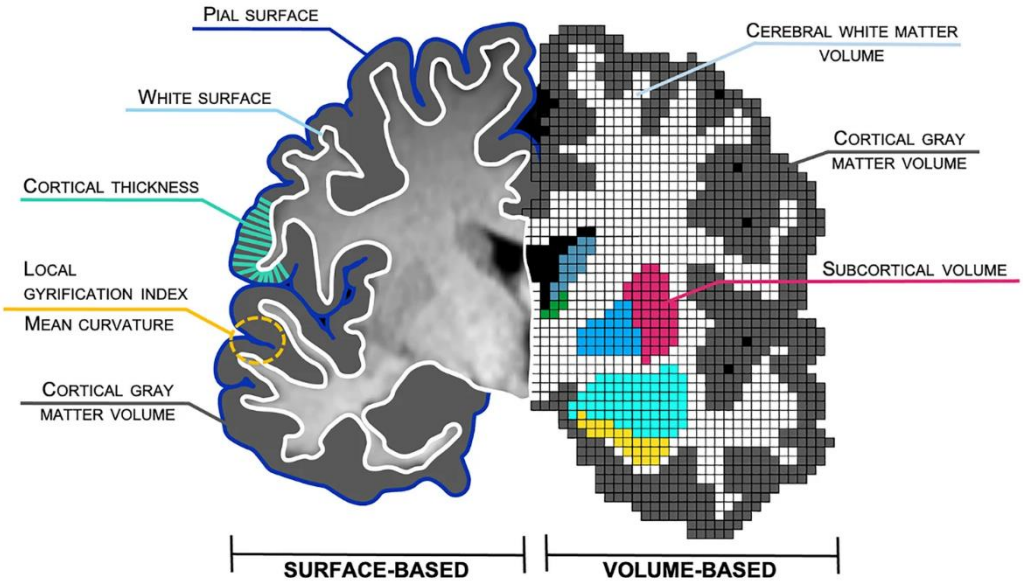

Figure 1.1. Examples of commonly used brain morphometric measures. Key measures used in this thesis include subcortical volume, cortical thickness, and cortical surface area. This figure was illustrated by Backhausen et al (2022).

In early MDD neuroimaging studies, morphometric measures of several brain regions were found to differ between MDD cases and controls, although with large variability across studies. For example, there are studies reporting increased (Papmeyer et al., 2015; Qiu et al., 2014), decreased (Järnum et al., 2011), both increased and decreased (van Eijndhoven et al., 2013), or no differences (Han et al., 2014) in cortical thickness of various brain regions in MDD cases relative to controls. A more well-known example would be the case of inconsistent reports of increase or decrease in volume of the amygdala, a region that is commonly studied due to its major role in emotion processing (Hamilton et al., 2008). A key reason for the large variability in findings is that most of these early MDD neuroimaging studies were limited by small sample sizes. For example, 60 out of 64 studies included in a meta-analysis by Koolschijn et al (2009) had less than 100 subjects. This can lead to several problems, including insufficient statistical power to detect true effects which tend to be modest, and increased chances of

reporting inflated estimates (Button et al., 2013). These lead to poor reproducibility of findings that is also in part due to inconsistencies in the scanning, processing, and analysis protocols across different study sites (Zhuo et al., 2019; Müller et al., 2017; Lorenzetti et al., 2009). Additionally, majority of the earlier neuroimaging studies typically focused on a select few regions that were commonly reported to be involved in MDD (e.g., amygdala, hippocampus). Given that MDD is a heterogenous disorder with wide-ranging symptoms, it is unlikely that only one or two distinct brain regions are involved. As such, such approaches, in contrast to data-driven approaches, may miss key associations that are unexpected and may not be able to provide a more nuanced picture of how brain structure is affected in MDD.

To address these issues, there has been an increase in the number of large population and consortia neuroimaging studies on MDD, such as those by the ENIGMA (Enhancing NeuroImaging Genetics through Meta Analysis) consortium and the UK Biobank (UKB), in the last few years (Schmaal et al., 2020). The robustness of neuroimaging findings from large-scale MDD studies was shown by Anderson et al (2020), where they were found to be consistent across three large independent datasets. These studies not only have large sample sizes, but the data were also derived using standardised protocols to avoid additional sources of heterogeneity. For subcortical volume, an ENIGMA study comprising 8,927 subjects across 15 cohorts reported significant volumetric reductions in only the hippocampus in MDD cases relative to controls (case-control Cohen's *d*: -0.14; Schmaal et al., 2016). The hippocampus is involved in processes such as learning, emotional processing, and most importantly in the holding of short-term memories and the subsequent transfer to long-term storage – deficits in these processes are commonly observed in MDD (Videbech & Ravnkilde, 2004). Likewise, a second ENIGMA study comprising 10,105 subjects across 20 cohorts found no differences in cortical surface area but reduced cortical thickness in the orbitofrontal cortex (OFC), anterior

and posterior cingulate, insula and temporal lobes in adult MDD cases (case-control Cohen's *d*: −0.10 to −0.14; Schmaal et al., 2017). Deficits in these regions are associated with symptoms that have been implicated in MDD as well as their associated risk factors (e.g., childhood trauma), including irritability/loss of social functioning due to the role of orbitofrontal cortex in modulating socially appropriate behaviour (Berlin et al., 2004), impaired motivation involving the cingulate cortex (Bonelli & Cummings, 2007), and impaired emotional processing and regulation involving the insula (Ghaziri et al., 2018). The results from these large-scale studies are useful in that they can serve as references to guide future neuroimaging studies, and the increasing availability of large-scale neuroimaging datasets is also helping to advance the field towards reproducible findings.

1.2.2 White matter microstructural measures and MDD

In contrast to grey matter studies that look at individual anatomical brain regions, white matter studies look at the myelinated axon bundles that function as tracts to connect different brain regions together. Diffusion tensor imaging (DTI) is typically used to study the architecture and integrity of the tracts, and it is based on the concept of directionality of water diffusion. Here, a brief overview of the theory (Soares et al., 2013) is given to aid understanding of subsequent measures and techniques presented in the rest of the thesis.

Unlike in the cerebrospinal fluid where water molecules are allowed to diffuse freely in all directions (i.e., isotropic), the axonal membranes and myelin sheets of axon bundles constrain the direction of diffusion in a preferred direction (i.e., anisotropic). By measuring the diffusion of water molecules and their directional preference, it is possible to deduce the local microstructure of the brain. To do so, a tensor is used to measure the distribution of water molecule diffusion along the x-, y-, and z-axes within each voxel (Figure 1.2A). The

tensor is ellipsoid in shape when diffusion is anisotropic, in which the main axis showing the direction of maximum diffusion is the principal eigenvector (Figure 1.2B). The amount of diffusion along each of the three eigenvectors is quantified as eigenvalues. Using these eigenvalues, two measures of DTI can be obtained – fractional anisotropy (FA) and mean diffusivity (MD). FA represents how strongly directional diffusion is and it ranges from 0 (complete isotropy) to 1 (complete anisotropy). Higher FA generally means increased white matter integrity (i.e., more intact myelin and greater uniformity and compactness of fibre bundles). Conversely, MD measures the magnitude of water molecule diffusion, with higher MD indicating lower structural integrity. Despite inherent limitations in FA and MD measures (e.g., the crossing of fibres in different directions can lead to low FA even if water molecules are absolutely flowing along the tracts; Jbabdi & Johansen-Berg, 2011), they are generally considered to be valid and effective measures of white matter microstructural integrity (Jones et al., 2013) and are the most commonly reported.

There are a few ways of reconstructing the white matter tracts, but I focus here on probabilistic tractography, which is generally considered a superior method and it is based on observing the probability of a given fibre moving along a specific path (Hagler et al., 2009). At this stage, the principal eigenvector of each voxel is established and serves as a fibre orientation estimate (Figures 1.2D and 1.2E). Starting from a seed region, one can trace the direction of the principal eigenvectors from voxel to voxel to form a continuous streamline until a termination criterion is reached. These streamlines represent the estimated long-range trajectories of the white matter fibres, and a large number of streamlines are typically seeded from each voxel to ensure the reproducibility and accuracy of the reconstructed fibres. Examples of termination criteria can include (1) the curvature of the streamline exceeded a particular turning angle such that the voxels are unlikely to be connected, or (2) the FA of the

voxel is too low to be meaningful (i.e., streamline likely reached the cerebrospinal fluid). Probabilistic tractography, when used with network thresholding (further discussed in section 1.3.1), is generally considered to yield valid representations of white matter tracts (Sotiropoulos & Zalesky, 2019).

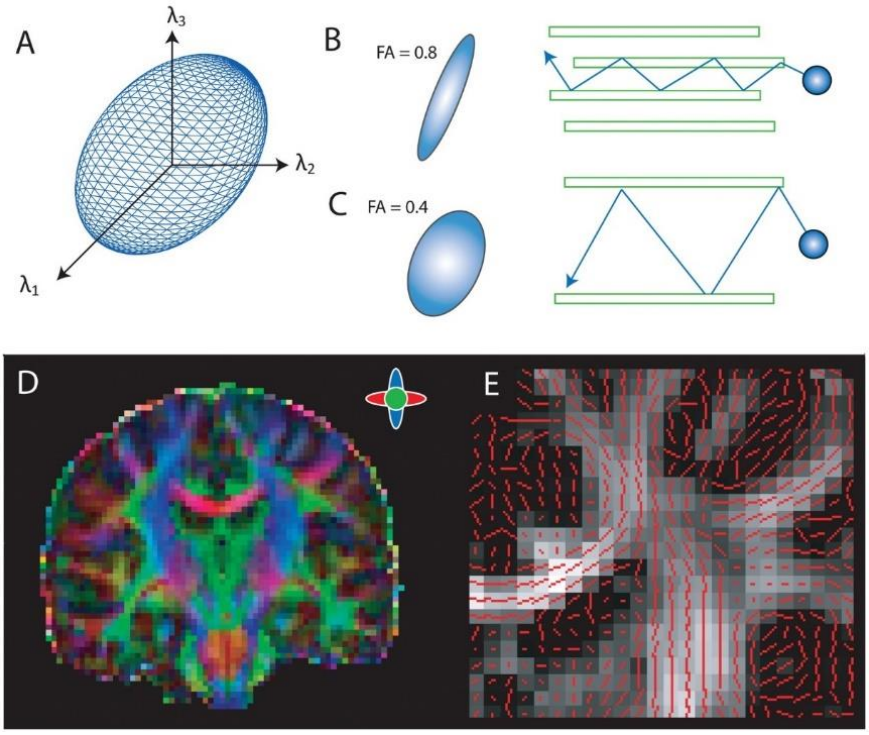

Figure 1.2. A brief overview of the theory behind diffusion tensor imaging. (A, B, C) The concept of tensors and fractional isotropy. (D and E) Examples of how white matter tracts are reconstructed from tensors. This figure was obtained from Roberts et al (2013).

Similar to brain morphometric measures described above, results from early MDD case-control studies on differences in white matter microstructural measures were highly variable, as most were underpowered and had methodological differences. For example, studies have found reduced white matter integrity (reduced FA or increased MD) in several white matter tracts like the corpus callosum and superior longitudinal fasciculus (Ota et al., 2014; Zou et al., 2008) in MDD cases relative to controls, but also no differences (Choi et al.,

2014; Olvet et al., 2015). To address this issue, an ENIGMA study involving 2,907 subjects across 20 cohorts was conducted using harmonised protocols (van Velzen et al., 2020). It was reported that subtle but widespread lower FA was observed in 16 out of 25 white matter tracts of interest (largest difference in the corpus callosum and corona radiata) in adult MDD cases relative to controls (Cohen's *d*: -0.12 to -0.26). The detection of a substantial number of tracts implicated in MDD, as compared to the handful for brain morphometric measures, seem to suggest that white matter may be more sensitive/vulnerable to changes in MDD. These findings were mostly consistent with those reported in other large-scale studies (N>1000) by Chen et al (2016) and Shen et al (2017), in terms of implicated regions and direction of effect. Collectively, these results seem to allude to the idea of dysconnectivity in MDD.

1.2.3 Research gaps in current neuroimaging studies on MDD

While it is undisputed that the use of large cohorts have allowed for significant progress to be made in identifying robust brain structural alterations associated with MDD, there still exist research gaps, which can be summarised into two main points.

Firstly, the studies discussed thus far studied each brain region or white matter tract in isolation but that is not representative of how the brain works. The brain is inherently organised as a large network (otherwise known as a connectome, with brain regions as nodes and the connections between them as edges), and the complex interactions between brain regions are thought to provide the physiological basis for the execution of coordinated high-level mental processes (Sporns et al., 2005). As discussed by Fornito et al (2015), while the interconnectedness of the connectome means that information can flow from one region to another, it also means that dysfunctions can spread easily from one region to another. This

network-based framework is supported by recent findings in studies looking at neurological and psychiatric disorders, including MDD (Cash et al., 2023; Padmanabhan et al., 2019; Chopra et al., 2023; Boes et al., 2015). The benefits of adopting a connectomics approach versus the conventional univariate approach was demonstrated in two complementary studies of functional MRI by Müller et al (2017) and Cash et al (2023). In Müller et al (2017), the authors utilised a conventional meta-analytic approach to look at neuroimaging experiments on cognitive/emotional processing in MDD. Despite a decent sample size of 1,058 patients across 57 studies, there was no significant convergence in results, suggesting that there was no convergent set of anatomical regions implicated in MDD. However, using the same data but with a connectomics approach, Cash et al (2023) showed that although the regions appeared inconsistent, they all localised to highly robust distributed brain networks of emotion and cognitive processing that are consistent with previous network models of depression. These findings clearly support the notion that MDD is associated with disruptions in functionally connected circuits and not individual regions, and can be extended to structural architecture. Hence, a connectomics approach can likewise be used for structural brain measures to identify aberrant circuits in MDD. Mathematical concepts, such as graph theory and other network approaches, can be applied to aid understanding of the brain network architecture (Sporns, 2018; Bullmore & Sporns, 2009). This is further addressed in sections 1.3 and 1.4.

Secondly, while current neuroimaging findings are informative of the underlying neurobiology in MDD, they are limited from a clinical perspective. This is because the findings were derived at the group level and hence, may not be effective in assessing an individual's vulnerability to MDD, considering that MDD is highly heterogenous. In the genetics field, progress has been made with regards to generating personalised genetic risk scores, also known as polygenic risk scores (PRS), based on effect sizes derived from large-scale GWAS

(Choi et al., 2020). Although not used in the clinic at the moment, the predictive value of MDD-PRS is constantly improving along with the size of MDD GWAS, and it is considered the best to use to validate newer personalised measures in terms of effect size. The combination of MDD-PRS with other measures, such as neuroimaging, has the potential to predict MDD and help with decision making in the clinical setting (Murray et al., 2021). However, little progress has been made in translating large-scale neuroimaging findings to the individual level, even though there is robust evidence that structural alterations are present in MDD. This search for objective brain-based markers is important in order to lessen the heavy reliance on subjective symptom report for diagnosis, and also because genetic risk score alone cannot explain a sufficient proportion of variance in MDD. With robust findings established by large MDD cohort studies discussed earlier, and with the increasing focus on normative brain modelling to map changes in brain structures both in health and in psychiatric disorders (Bethlehem et al., 2022; Marquand et al., 2019), it is a good opportunity to look into personalised brain-based markers for MDD. This is further discussed in section 1.5.

1.3 Taking a brain network approach in MDD

This section introduces the concept of the structural connectome and gives a brief overview of methods that can be used to study the connectome. The findings and limitations of existing connectome-based MDD studies are also discussed.

1.3.1 Constructing the structural connectome

To construct the structural connectome, the output from probabilistic tractography is used to identify connections between n grey matter region-of-interests (ROIs) to form a $n \times n$ connectivity matrix (Figure 1.3). ROIs are termed as nodes, and the connections between each

pair of ROIs as edges. Brain networks are usually undirected (as it is hard to determine the direction of connections) and weighted, meaning that each edge carries a value that represents the strength of the connection. Edge weight can be defined in several ways. While counting the number of streamlines that connect a pair of ROIs may seem like a feasible way of quantifying connectivity, that is generally not recommended as the density of streamlines is not consistent with underlying fibre density due to sources of error in the tracking process (Jones et al., 2013; Calamante, 2019). An alternative method would be to weight the edges using FA (i.e., a measure of fibre integrity) instead. Each streamline is weighted by the average FA of all the voxels it passes through, and the edge is calculated as the mean FA value for all reconstructed streamlines that connect each pair ROIs. This is based on the idea that changes in fibre integrity will affect the functional capacity of the edges.

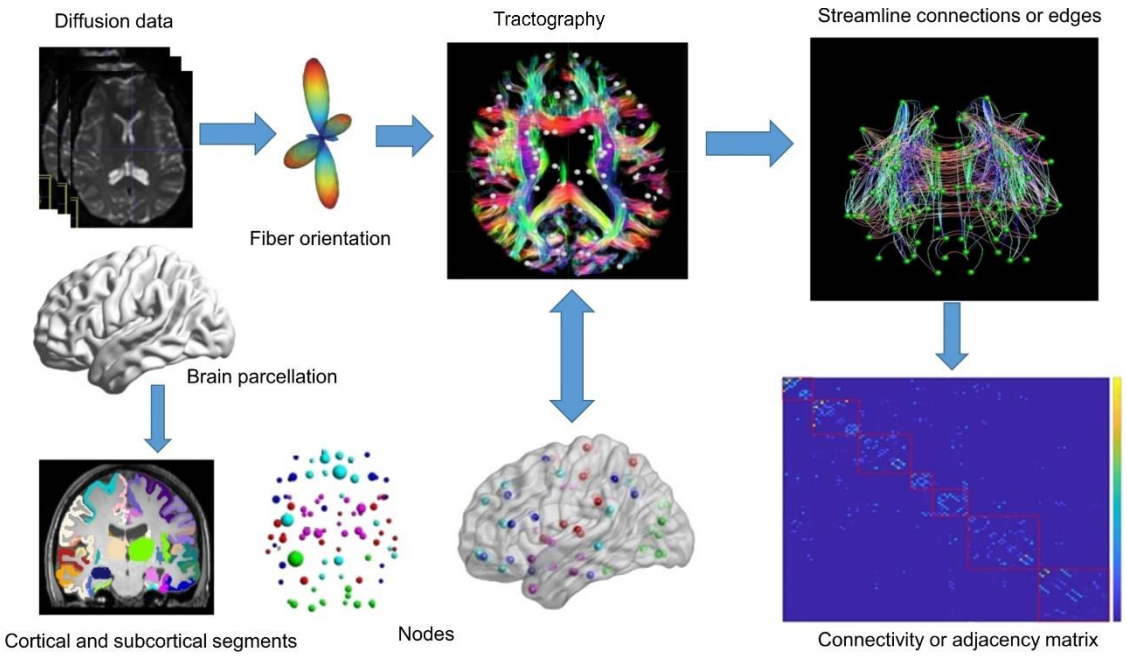

Figure 1.3. An overview of the steps taken to construct the structural connectome. This figure was adapted from Alizadeh et al (2021).

A fundamental limitation of probabilistic tractography is that it tends to generate spurious edges, causing the constructed network to be fully connected although that is not true for brain networks (Sarwar et al., 2019). This can be dealt with using thresholding, where only edges that fulfil a certain criterion are retained. There are many thresholding methods, each with their own pros and cons, and there is no current consensus on the best method to use. The studies in this thesis used density-level thresholding, which is based on the concept that each individual has a unique connectome and only retains the top *x*% of the strongest/most robust connections (Rubinov & Sporns, 2010). Of note, while thresholding is helpful, it is possible that potentially valuable or real connections may also be removed. This indicates the importance of testing a range of thresholds to avoid an arbitrary threshold, as demonstrated in Chapter 2. With the connectome defined, properties of the connectome and its associations with other variables can then be studied using various approaches, including univariate, multivariate and network-based approaches.

1.3.2 Univariate and multivariate approaches

The univariate approach to studying the connectome involves repeating the same analysis (e.g., regression) on each individual edge. However, there can be significant challenges involved, especially if a large $n \times n$ connectivity matrix is defined for each subject. For example, a network with 400 nodes defined using the ROI-by-ROI approach will have 79,600 unique edges, and this means that 79,600 statistical tests will have to be conducted. Such mass univariate testing not only requires a large amount of computational resources, but also incur a large multiple testing problem. This decreases the chances of detecting a significant effect, especially since it is known that most brain-based effects are modest. Furthermore, the

reporting and interpretation of results using this approach can also pose a significant challenge.

Aside from the univariate approach, there are multivariate approaches that can be used to study connectomic relationships. An example would be canonical correlation analysis (CCA), which has been gaining traction recently. CCA is an unsupervised technique that seeks to determine the relationship between two sets of variables measured on the same individuals, especially with multiple intercorrelated variables in each set. Many studies have since utilised this method to study connectome associations with non-neuroimaging measures and reported high canonical correlations (e.g., r=0.87 with N=461 in Smith et al (2015) and r=0.68 to 0.71 with N=663 in Xia et al (2018)). While these results may be promising, a recent paper by Helmer et al (2024) showed that the use of CCA to study brain-behaviour associations require very large sample sizes to ensure the stability of findings and to avoid inflation of canonical correlations. In comparing sample sizes of N≈1000 and N=20,000, they found that only the latter had sufficient observations for stable mappings between imaging and behavioural features. For a canonical correlation of r=0.3, approximately 50 samples per feature was recommended in order to obtain stable findings. This may be a significant challenge, especially if studying connectomic relationships with genetic factors, as the effects are even smaller and may require an even larger sample size.

As such, while the univariate and multivariate approaches described above are possible approaches that can be taken to study the association between the connectome and other variables, they are limited mainly in terms of (1) requirement for very large sample sizes and (2) usefulness and interpretability of findings. This thesis thus focuses on the use of approaches that are designed specifically for the study of networks (i.e., graph theory and network-based statistics), which may help to address some of these limitations.

1.3.3 Network approaches: network-based statistics

Efforts have been made to develop more feasible network approaches to help overcome the multiple testing problem in doing mass univariate testing. An example would be network-based statistics (NBS) by Zalesky et al (2010), which was used extensively in this thesis (Chapters 2 and 3). NBS is fundamentally based on the idea that regions of the connectome associated with the variable of interest are likely to be confined together in an interconnected subnetwork, rather than being dispersed individually throughout the connectome. By identifying subnetworks, significant statistical power can be gained as correction for multiple comparisons can be done at the level of subnetworks, in contrast to the mass univariate approach where correction has to be done considering every individual edge. The steps taken in NBS are summarised in Figure 1.4. Firstly, linear regression is done at every edge to test their individual associations with the explanatory variable. An *a priori* component-forming threshold (based on the t-statistic value from the linear regression model) is then applied to remove edges that fall below the threshold. Among those that are retained, edges that are interconnected are considered to be a component (or subnetwork), and the size of this subnetwork (i.e., the number of edges) is recorded. To evaluate the significance of the subnetwork, permutation testing is done by shuffling group membership *n* times and then repeating the above steps to obtain a null distribution of maximal subnetwork sizes. The p-value is then defined as the proportion of permutations for which the largest subnetwork was of the same size or greater as the original subnetwork (FWE-corrected for comparison of multiple subnetworks). One limitation of NBS is that the component-forming threshold is decided based on experimentation, but the choice of threshold only affects the sensitivity of the method (i.e., more stringent threshold will lead to lesser edges selected). In general, NBS

serves as a complementary method to mass univariate testing, and it has since been extensively used by multiple studies to study the connectome in both health and disease (Korgaokar et al., 2014, 2023; Baker et al., 2015; Aruldass et al., 2021).

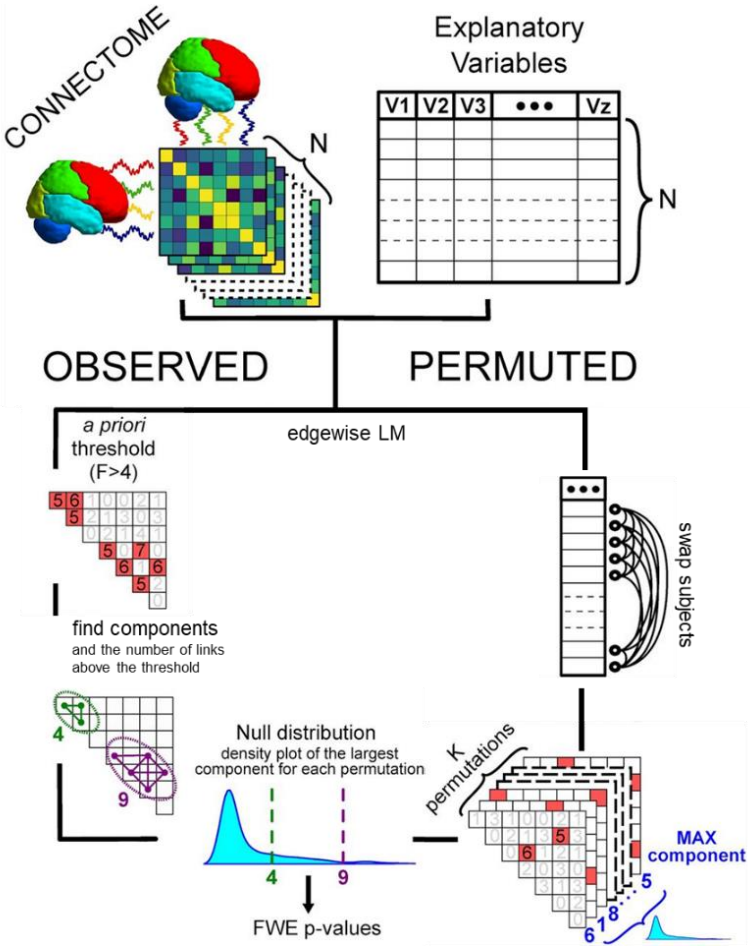

Figure 1.4. An overview of the steps involved in a NBS analysis. This figure was adapted from Gracia-Tabuenca & Alcauter (2020).

1.3.4 Network approaches: graph theory

Graph theory refers to the use of mathematical frameworks and algorithms to analyse and summarise pairwise relationships between network elements. While graph theory is not a new method and has been extensively applied in many areas of study (e.g., social and aviation networks), the use of this method to study properties of brain networks have only gained

traction in recent times. These measures are useful as they help to aggregate differences that are potentially diffusely distributed across an otherwise highly complex system that would be difficult to individually pinpoint. They can be derived at different levels of scale – global measures describe the architecture of the whole network, while nodal measures describe topological features of a single node. There are many graph theory measures as detailed in Rubinov and Sporns (2010). Here, I give a brief overview of the key measures and those that are relevant to this thesis.

The brain is a complex network and exhibits non-trivial organisational properties, which are properties that do not occur in random networks (Bullmore & Sporns, 2009). Some of these properties include the presence of a small-world topology and the presence of hubs (i.e., a subset of nodes that have a high number of connections). A small-world network is characterised as having a short path length and a high clustering coefficient. Path length refers to the number of steps required by one node to reach another node – a shorter path length represents a more efficient transfer of information. A popular graph theory measure called efficiency, is therefore defined as the inverse of path length (Figure 1.5A). Clustering coefficient, on the hand, refers to the extent of connections between a node's neighbours (Figure 1.5B). The higher the clustering coefficient, the more efficient information transfer is within that neighbourhood. As such, the small-world theory posits that nodes are highly connected together through a small number of steps to ensure a high rate of information transfer to support complex brain functions at a low energy cost. Hubs, with their high number of connections, supports this by helping to ensure that overall path lengths across the network are short, thus maximising efficiency (Figure 1.5C). An example of a hub would be the thalamus, which plays an important role as a relay centre between the frontal cortex and basal ganglia (Kumar et al., 2022). Regarding hubs, there is an interesting concept called

the “rich club organisation”, which hypothesises that hubs in the human brain network have a higher number of connections between themselves, and these connections are also stronger as compared to those of an average node (van den Heuvel et al., 2012; Figure 1.5C). The rich-club is thought to be important, as it serves as a central backbone of the brain network to coordinate and process the inflow and outflow of large amounts of information (van den Heuvel & Sporns, 2013). Collectively, both small-world and rich-club topologies reinforce the idea that the human brain is structured to maximize the efficiency of information transfer and to minimize connection cost. As both topologies have been shown to be already present during the early developmental years (Fan et al., 2011; Blesa et al., 2021), it is thus of wide interest to see if these fundamentally important measures are affected in diseases, such as MDD.

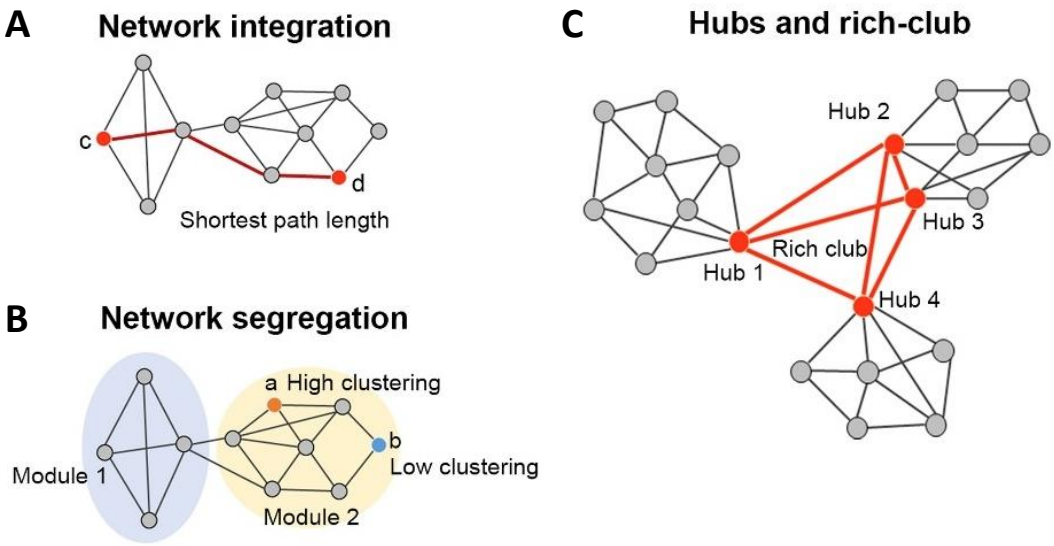

Figure 1.5. Examples of commonly used graph metrics, including (A) shortest path length (efficiency is the defined as the inverse), (B) clustering coefficient, and (C) rich club organisation. This figure was adapted from Zhao et al (2019).

1.3.5 Current connectomic studies on MDD using network approaches

Numerous studies have since utilised graph metrics and NBS to examine MDD case-control differences in brain network architecture across different scales – at the global (network-wide), nodal (individual nodes), and connection (individual edges) levels (reviews by Gong & He (2015), Yun & Kim (2021) and Chen et al (2021)). Across studies, there is a general consensus on abnormal connectivity of the structural connectome in MDD, but the results remain mixed in terms of regions implicated and the direction of effect. Globally, MDD case-control differences in graph metrics were generally not found (Sacchet et al., 2015; Korgaonkar et al., 2014; Xu et al., 2021), although some studies reported increased (Long et al., 2015) or decreased (Wang et al., 2020) efficiency in MDD cases. Node-wise, Qin et al (2014) found reduced efficiency in the superior and middle frontal gyrus, middle temporal gyrus and angular gyrus, and differences in the clustering coefficients of frontal regions, insula, and hippocampus in MDD cases. On the other hand, some studies found no differences in any nodal measures (Korgaonkar et al., 2014; Zheng et al., 2019). At the connection level using NBS, Korgaonkar et al (2014) found reduced connectivity in two subnetworks implicating the default mode networks and frontal-subcortical regions in MDD cases, while Long et al (2015) found increased connectivity in two subnetworks involving namely the orbitofrontal and subcortical regions in MDD cases. To demonstrate the inconsistency in findings, a meta-analysis by Xu et al (2021) comprising 952 patients and 1447 controls across nine studies found no significant differences for any graph metrics at both global and nodal levels. This could be due to methodological differences (e.g., different parcellation schemes, thresholding methods and node definition) and sample heterogeneity (e.g., different MDD subtypes including late-onset, treatment-resistant, treatment-naïve, remitted geriatric depression), making it highly challenging to reconcile findings. The majority of these studies also had small

sample sizes, as seen in the meta-analysis by Xu et al (2021) where seven out of the nine studies had less than 100 subjects in total. Besides the increased chances of reporting false-positives and inflated effect sizes, results from small studies may also not be generalisable to the wider population, in the context of a highly prevalent and heterogenous disorder like MDD (Fried & Nesse, 2015). As such, unlike the study of univariate brain measures in MDD, the study of structural connectomes in MDD remains largely hindered by the lack of large-scale data and the lack of standardisation of protocols.

Fortunately, recent advances have been made in the connectome field. DTI data are now available in large cohort studies, such as the UKB and Generation Scotland (GS), and the advancement of technology has made it more feasible to process large datasets that are computationally demanding. For example, Mansour et al (2023) recently made available processed structural and functional connectome data for 40,000 subjects in UKB. As with studies that have contributed robust and reproducible findings on univariate brain structural differences associated with MDD (van Velzen et al., 2020; Anderson et al., 2020), leveraging these large cohorts for connectomic studies on MDD would greatly help to advance the field.

1.4 The relationship between MDD genetic risk and the brain

Besides identifying brain differences between MDD cases and controls, it is also important to understand the origins of these differences Given the evidence for the enrichment of brain expressed genes in the MDD GWAS (Howard et al., 2019), it suggests that certain brain regions and MDD may have shared genetic architecture. This section introduces the concept of polygenic risk score (PRS), a common measure of one's genetic risk, and discusses the findings from existing studies looking at the association between MDD-PRS and the brain.

1.4.1 MDD polygenic risk score

As discussed earlier in section 1.1.3, genetic risk for MDD is contributed by multiple genetic variants each with a small effect and these effects are additive. As such, MDD-PRS, a composite score representing the additive effect of these genetic variants, is the preferred method for quantifying an individual's genetic predisposition to MDD (Choi et al., 2020). This measure is preferred, as it explains a larger proportion of variance in disease risk and hence, allows for the easier detection of any significant effect with an associated trait of interest, in contrast to studying individual genetic loci. MDD-PRS can be derived from summary statistics of a MDD GWAS that was conducted on an independent dataset. The effect sizes for each genetic variant are treated as weights and MDD-PRS is defined the sum of individual weights of each variant, with higher scores representing increased risk. Conventionally, using the clumping and thresholding method as in this thesis, MDD-PRS can be calculated at any p-value threshold (i.e., only genetic variants that pass a specified significance threshold in the MDD GWAS are included in the calculation). There is, however, no consensus on the best threshold to use, and the main threshold is typically chosen depending on the strength of association with the trait of interest, such as in Shen et al (2020). MDD-PRS has since been validated in many studies, with MDD cases having higher MDD-PRS relative to controls (Howard et al., 2020; Wray et al., 2018).

There are some limitations associated with the use of MDD-PRS (Fullerton & Nurnberger, 2019). MDD-PRS is typically derived using MDD GWAS that only consist of individuals of European ancestry, due to the lack of availability of data from other populations. As disease-associated allele frequencies can be very different between populations, the application of MDD-PRS derived from European populations to non-European populations may result in inaccurate estimations of disease risk (Lewis & Vassos, 2020). Besides that,

MDD-PRS only takes into consideration the additive effect of multiple common genetic variants of small effect and does not yet consider rare variants or more complex genetic relationships (e.g., epistasis) that can possibly account for a larger proportion of variance (Fullerton & Nurnberger, 2019). To this end, there are increasing efforts to look beyond the conventional PRS to broaden the genetic insights of MDD (Cheng et al., 2022). Despite these limitations, MDD-PRS is still generally considered as a valid measure of an individual's genetic risk for MDD, and it is widely used in this thesis (Chapters 3 and 4).

1.4.2 Current studies on MDD genetic risk and univariate brain measures

Recently published articles by Marek et al (2020) and Tervo-Clemmens et al (2023) reported that brain-wide associations studies would require more than a thousand individuals, in order to prevent inflated test statistics and to ensure reproducibility and generalisability to the wider population. Large cohorts that contain genetic and neuroimaging data are therefore useful resources that allow researchers to conduct reliable studies on brain and MDD-PRS associations. In addition, due to MDD-PRS being limited by the power of the MDD GWAS that it was derived from (Mitchell et al., 2021), the initial MDD GWAS also needs to have a large sample size. As early MDD GWASs were mostly underpowered and did not identify any variants significantly associated with MDD (Levinson et al., 2014), it may be why brain and MDD-PRS studies are few relative to other major psychiatric disorders (Cattarinussi et al., 2022) and mostly yielded no significant findings despite having large sample sizes. For example, Reus et al (2017) reported no significant associations between MDD-PRS (derived from a MDD GWAS with N=18,759) and subcortical volume and white matter microstructure in adults in UKB (N range: 816 to 978). In young adults, however, MDD-PRS was found to have

a significant impact on cortical thickness in the middle prefrontal cortex (N=432; Holmes et al., 2012), though this has not been replicated yet.

Now, with the recent increase in sample size of MDD GWASs as discussed in section 1.1.3, some progress has been made in studying brain and MDD-PRS associations (Kämpe et al., 2023; Shen et al., 2020). For example, using a large discovery (N=10,674) and replication (N=11,214) sample from UKB, Shen et al (2020) conducted a phenome-wide association study involving 209 behavioural measures and 343 neuroimaging measures with MDD-PRS (derived from a MDD GWAS with N=807,553). Among the structural neuroimaging traits, only white matter microstructural measures were significantly associated with MDD-PRS. Specifically, MDD-PRS was associated with reduced white matter integrity (lower FA and higher MD) at the global level, regional level (in association fibres and thalamic radiations), and in some individual tracts (e.g., superior longitudinal fasciculus, forceps major). Through the use of Mendelian Randomisation analysis, the authors also reported a causal effect from MDD to four of these significant measures. On the other hand, Kämpe et al (2023) found that MDD-PRS (derived from a MDD GWAS with N=470,572) was generally associated with reduced grey matter volume in the cerebellum, and also in the prefrontal, temporal and insular regions for those with current depression. Interestingly, these observations were only significant in women but not men. Collectively, these results show that MDD-PRS has a negative impact on brain structure.

1.4.3 Current studies on MDD genetic risk and the structural connectome

There are very few studies that looked at the relationship between MDD genetic risk and the structural connectome, considering that the connectomic field is still in the early stages and advances in MDD GWAS studies have only been made in recent years. In a review by Gong

and He (2015) on depression and connectomics, earlier studies only looked at structural connectivity in terms of covariance between grey matter and utilised the candidate gene approach (e.g., brain-derived neurotrophic factor, 5-HT polymorphism of the serotonin transporter), which is now known to be not ideal due to the small amount of variance explained. Since then, some progress has since been made given the increase in availability of connectome data and network-based approaches. Wainberg et al (2024) recently conducted a GWAS of 206 structural connectivity measures in a cohort comprising 26,333 subjects from UKB and looked at the genetic correlation between the structural connectivity measures and brain-related traits. However, no significant genetic correlations were found between MDD and any of the measures. Using the familial risk approach, the study by Kelsall et al (2023) involving 96 subjects found that individuals at high family risk for MDD had lower global clustering coefficient, which was also associated with current clinical symptoms. Using NBS, the authors also identified a hypoconnected subnetwork involving regions in the frontal cortex and basal ganglia in individuals with high family risk and of suicidality. Likewise, in a sample of 1,512 subjects, Hahn et al (2023) found that network controllability (i.e., a graph metric that quantifies the influence of one brain region on the dynamic transition between brain states) is related to familial risk for MDD, as well as MDD-PRS. Unlike other psychiatric disorders like schizophrenia (Cao et al., 2022; Alloza et al., 2018), Hahn et al (2023) is the only MDD connectomic study thus far that adopted a polygenic approach. Collectively, these studies seem to suggest that properties of the structural connectome is influenced by genetic risk for MDD. Further investigation will be beneficial, as the identification of disrupted circuits will provide more insight into the possible functional changes associated with MDD, as compared to studying each brain region in silos.

1.4.4 Contributions from environmental factors

As a complex multifactorial disorder, predisposition and/or the manifestation of MDD is determined by the coordinated action of many genes, their interaction with each other and also with diverse environmental factors. Studies have shown that genetic variants confer an increased risk for MDD when exposed to external stressors (Uher et al., 2008). For example, a study by Wang et al (2023) involving 41,810 subjects found that stress-related exposures, such as reduced social support, higher exposure to long-term difficulties, childhood trauma, stressful life events, and loneliness, increased the effects of MDD polygenic risk on MDD. While this PRS × environment approach has been applied to study MDD risk, few have looked at the effects of PRS × environment on the brain in the context of MDD, especially in terms of connectomic measures. This is despite the fact that environment risk factors play significant role in disease risk, and also have an impact on brain structure (Caspi & Moffitt, 2006). If the brain is deemed to be a mechanism through which gene and environment operate to effect MDD, then this should be studied in tandem. An example would be a recent study by Zhang et al (2021), which found that increased polygenic risk for MDD in the group of individuals with urban childhood (typically characterised by more stressful social environments) was associated with lower medial prefrontal cortex activation during stress, a region that plays a role in social cognition and affect regulation. This effect was, however, not observed in the group of individuals with rural childhood. Hence, although current progress is encouraging, the effects of MDD genetic risk on the brain should be studied while considering potential environmental effects. The availability of large datasets with genetic, environment, neuroimaging data presents a good opportunity to conduct such studies.

1.5 Taking a personalised approach in MDD

Personalised approaches refers to the use of individual-specific information to guide the diagnosis, prevention, and treatment of disease. It is an increasingly popular approach that has made substantial strides in certain fields, such as rare diseases and cancer (Hoeben et al., 2021). For example, personalised medicine can be used for the early identification of individuals genetically predisposed to cancer, diagnose specific cancer subtypes and tailor treatment options accordingly to obtain the best outcome The field of psychiatry is, however, lagging behind and still relies heavily on subjective retrospective diagnostic assessments because of the lack of objective and reliable biomarkers. Personalised approaches are especially important for psychiatric disorders, given the wide heterogeneity of symptoms present between individuals and possibly even within individuals for different episodes of MDD. For the field to advance, it is important to be able to objectively identify individuals at risk of or with MDD, which will in turn lead to the discovery and implementation of more effective treatment options.

For most psychiatric disorders including MDD, genetic studies have made the most progress in terms of personalised approaches, as genes are unique to each individual and causality can be easily established. As described in an earlier section, MDD-PRS is a well-established measure of an individual's genetic predisposition to MDD and it is widely used in research settings (Howard et al., 2020; Wray et al., 2018). Clinically, MDD-PRS contains useful information that can possibly help with clinical assessment. As discussed in Murray et al (2021), this can be likened to the use of family history information to assess a patient's potential trajectory especially during the earlier stages of disease and hence, help with the assignment of clinical stage to determine if treatment is required and at what level. Information on high or low PRS can be used in tandem to help to reinforce such decisions, or

possibly substitute family history in instances where the latter is not available. Unfortunately, the use of MDD-PRS is currently limited to that, as it is still unable to aid with clinical diagnosis due to several reasons. Firstly, besides having a large phenotypic overlap in terms of symptom presentation, psychiatric disorders also have a large genetic overlap (Bulik-Sullivan et al., 2015), which makes it hard to differentiate and determine the accuracy of diagnosis. Secondly, despite being a composite score, MDD-PRS ultimately accounts for a very small percentage of variance explained in MDD (5% at present). It is estimated that even with increasing sample size, the maximum variance explained in MDD is only 12% due to its high prevalence, in contrast to 25% for schizophrenia which has a lower prevalence (Murray et al., 2021). This leads to the third reason, which is that MDD-PRS is a static metric and does not capture changes in trajectories that are unique to each individual's circumstances, including those that might contribute to MDD. In other words, MDD-PRS on its own is insufficient to definitely predict a diagnosis of MDD as it only captures part of the risk. These limitations call for the need to find additional personalised markers of MDD to complement MDD-PRS.

To this end, personalised brain-based markers may come in useful. This is because structural alterations in the brain are related to the underlying mechanisms of MDD, and it is not a static metric as the dynamic nature of the brain means that it can capture the effects of various risk exposures over time. Some brain-based markers based on morphometric measures and functional connectivity have since been developed to measure individual risk and/or inter-individual variation in MDD and other psychiatric disorders as well (Doucet et al., 2020; Antoniades et al., 2021). For example, the Person-Based Similarity Index (PBSI) quantifies the variability in brain morphology of an individual to others in the same diagnostic group, which could in turn assist in quantifying the degree of brain structural heterogeneity in clinical relative to healthy control samples (Antoniades et al., 2021). With the increasing

availability of large population datasets covering individuals across all ages (e.g., UKB, Adolescent Brain and Cognitive Development study), these brain-based markers can be derived and validated using these datasets to ensure robustness, such as in Yan et al (2023) and Xie et al (2023). There may also be instances where research groups may be interested in applying these risk scores that were validated in large samples on their own study sample. This is along the same line as using summary statistics from large GWAS to derive polygenic risk scores. In this case, it will be beneficial to have a method that is based on the findings from large studies, especially since significant progress has already been made in the field in terms of establishing robust neuroimaging findings (Schmaal et al., 2016, 2017). One such method is the Regional Vulnerability Index (RVI), which utilises summary statistics by the large-scale multi-site ENIGMA studies as a reference and assesses an individual's brain pattern to see how similar it is to the disease pattern via a simple correlational approach (Kochunov et al., 2022b). As a proof of method, RVI has been tested in both large and small local samples for schizophrenia, MDD and other neurological conditions and have been shown to be useful (Kochunov et al., 2019, 2021). RVI was used in Chapter 4 and discussed in depth there.

1.6 Summary and aims of thesis

MDD is a highly prevalent and serious psychiatric disorder, but there remains a fundamental lack of understanding of the underlying biological mechanisms. This stems from the large heterogeneity of the disorder, which makes diagnosis and treatment highly challenging. Advances in the neuroimaging field through collaborative efforts and the use of large population cohorts have allowed for significant progress to be made, where differences in brain morphometric features and structural connectivity have been identified in MDD cases. Studies have also suggested that certain brain regions and white matter tracts are associated

with genetic and environmental risk factors, of which further investigation can provide insights into the mechanisms underlying MDD. However, there remains two main research gaps which form the basis of this thesis. The overall aim of this thesis is two-fold – (1) to utilise network approaches to investigate structural connectomic differences and their role in MDD, and (2) to translate the group-level brain-based findings to the individual level. With the increasing availability of large data sets, these questions can now be reliably tested, thus providing further insights to complement what is already known.

For this thesis, data from three large population cohorts, including the UKB, Generation Scotland (GS), and the Adolescent Brain and Cognitive Development (ABCD) study, were used. A brief overview of the cohorts are given here but the specifics of each sample used are detailed in the specific chapters.

(1) UKB is a large adult population-based cohort with approximately 500,000 subjects, aged 40 to 69, recruited at baseline (2006–2010) across four study locations (https://www.ukbiobank.ac.uk/; Sudlow et al., 2015). A subsample also underwent full body MRI assessments, including neuroimaging, with repeat scans already conducted and in plans (Miller et al., 2016). Brain scans for 10,000 subjects were made available in the first imaging release (diffusion data to derive structural connectomes locally were used in Chapter 2), followed by scans for 40,000 subjects at present (diffusion data to derive structural connectomes locally were used in Chapter 3). This is postulated to reach 100,000 subjects in the future.

(2) GS is also a large adult population sample based in Scotland, with approximately 24,000 subjects, aged 18 to 98, recruited at baseline (2006–2011) across two study locations (https://www.ed.ac.uk/generation-scotland; Smith et al., 2013). Like UKB, a subsample underwent neuroimaging assessments to specifically study the neuroimaging

mechanisms underlying psychiatric disorders, especially depression (Habota et al., 2021). Neuroimaging data for approximately 1,000 subjects is available – diffusion and structural data were used in Chapters 2 and 4, respectively, with the data processed locally.

(3) ABCD is the largest study of brain development and child health based in the United States, with approximately 11,000 subjects, aged 9 to 10, recruited at baseline (2017–2018) across 21 study locations (https://abcdstudy.org/; Casey et al., 2018). As a long-term study, the subjects are followed for 10 years, with annual non-imaging assessments and biannual imaging assessments conducted. The longitudinal measures of brain structure and function are the key focus of the ABCD study. Structural and diffusion neuroimaging data from the baseline and two-year follow-up timepoints were used in Chapter 4.

This thesis is structured as follows. Chapter 2 aimed to characterise structural connectomic differences between MDD cases and control using network approaches at all levels of the connectome hierarchy (global to connection level). Having established that connectomic differences exist, Chapter 3 tested the association between the structural connectome and key MDD risk factors, such as MDD-PRS and CT, to identify PRS- and CT-associated subnetworks. The role of these subnetworks in MDD was also studied using mediation and moderated mediation models. Finally, to assess the translational potential of group-level neuroimaging findings, Chapter 4 tested the utility of a recently introduced brain-based risk score called the Regional Vulnerability Index (RVI). The focus was to compare MDD-RVIs and MDD-PRS in terms of their strength of association with MDD, and the analysis was extended to ABCD as an exploratory analysis into adolescent MDD. Chapter 5 takes all the findings together and goes into an in-depth discussion of the overall takeaways from this thesis.

Chapter 2: A comprehensive hierarchical comparison of structural connectomes in Major Depressive Disorder cases versus controls in two large population samples

2.1 Chapter introduction

MDD is a brain-related disorder and studies leveraging large cohort neuroimaging datasets have shown that differences in univariate structural brain measures exist between MDD cases and controls. However, studying each brain region in isolation is not representative of how the brain functions as a network. As a complex network, the brain exhibits non-trivial organisational properties, such as having a strong rich club core where key brain regions are strongly connected together to function as the central backbone of brain communication. MDD is thought to be associated with dysconnectivity in the brain, where network architecture, such as the rich club core, is thought to be disrupted. However, studies adopting connectomic approaches to study these questions have been few and limited by sample size, resulting in low reproducibility in findings. The availability of large connectomic datasets not only presented a good opportunity to investigate MDD case-control differences using network-based approaches, but also to look into reproducibility by testing the consistency of findings in another large replication sample. This chapter presents a study of group differences between MDD cases and controls in brain network architecture, using data that were processed locally from two large adult cohorts (UKB: 5,104 subjects, GS: 725 subjects). Network-based approaches, as introduced in Chapter 1, were used to compare the structural connectomes of MDD cases and healthy controls at all levels of the connectome hierarchy, from the global network level to the individual connections.

2.2 Manuscript

This study has been published *Psychological Medicine*, titled "A comprehensive hierarchical comparison of structural connectomes in Major Depressive Disorder cases *v.* controls in two large population samples" (Thng et al. 2024). As the first author, I conceived the hypotheses, conducted the analyses, and wrote the manuscript under supervision.

2.2.1 Abstract

The brain can be represented as a network, with nodes as brain regions and edges as region-to-region connections. Nodes with the most connections (hubs) are central to efficient brain function. Current findings on structural differences in Major Depressive Disorder (MDD) identified using network approaches remain inconsistent, potentially due to small sample sizes. It is still uncertain at what level of the connectome hierarchy differences may exist, and whether they are concentrated in hubs, disrupting fundamental brain connectivity.

We utilised two large cohorts, UK Biobank (UKB, N=5,104) and Generation Scotland (GS, N=725), to investigate MDD case-control differences in brain network properties. Network analysis was done across four hierarchical levels: (1) global, (2) tier (nodes grouped into four tiers based on degree) and rich club (between-hub connections), (3) nodal, and (4) connection.

In UKB, reductions in network efficiency were observed in MDD cases globally (*d*=-0.076, pFDR=0.033), across all tiers (*d*=-0.069 to -0.079, pFDR=0.020), and in hubs (*d*=-0.080 to -0.113, pFDR=0.013 to 0.035). No differences in rich club organisation and region-to-region connections were identified. The effect sizes and direction for these associations were generally consistent in GS, albeit not significant in our lower-N replication sample.

Our results suggest that the brain's fundamental rich club structure is similar in MDD cases and controls, but subtle topological differences exist across the brain. Consistent with recent large-scale neuroimaging findings, our findings offer a connectomic perspective on a similar scale and support the idea that minimal differences exist between MDD cases and controls.

2.2.2 Introduction

Brain regions are linked together by white matter tracts formed from bundles of axonal fibres that facilitate information transfer from one region to another (Sporns, 2011). As brain function is constrained to a certain extent by anatomical connections (Suárez et al., 2020), variations in these pathways may contribute to changes in brain function. Studies have reported subtle reductions in the fractional anisotropy (FA; a measure of the coherence of axonal fibres) of multiple individual white matter tracts in Major Depressive Disorder (MDD; Chen et al., 2016; van Velzen et al., 2020), thus hinting at reduced structural connectivity. However, since the brain is organised as a network (regions as nodes, connections as edges), the use of network approaches, such as graph theory (Sporns, 2018) and network-based statistics (Zalesky et al., 2010), are better suited to study structural differences present in MDD as they can provide information on topological organisation in addition to connectivity strength. This will add to the insights that can be gained by studying individual regions in isolation.

Multiple studies have since examined MDD case-control differences in brain network architecture across different scales, at the global (network-wide), nodal (individual nodes), and connection (individual edges) levels (Gong & He, 2015; Yun & Kim, 2021). Differences were generally not found at the global level but at the nodal and connection levels (Sacchet

et al., 2015; Xu et al., 2021). For example, MDD cases had lower clustering coefficient (i.e., the extent to which nodes are clustered together) for regions involved in the cognitive-emotion circuitry (Qin et al., 2011) and reduced connectivity in subnetworks involving regions in the default mode network (Korgaonkar et al., 2014). While there is a consensus that connectomic differences do exist in MDD, there is currently no unanimity regarding specific differences due to lack of replication. Large sample sizes are needed to ensure the accurate estimation of effect sizes (Poldrack et al., 2017; Grady et al., 2021; Marek et al., 2022; Button et al., 2013) but previous studies were limited by small sample sizes (mostly N<100; Xu et al., 2021). In the context of a highly prevalent and heterogenous disorder like MDD (Fried & Nesse, 2015), results from small-scale studies may not be generalisable to the wider population too. As with large neuroimaging studies (e.g., UK Biobank) that have contributed robust findings on brain structural differences associated with MDD (van Velzen et al., 2020; Anderson et al., 2020), it is of interest to leverage these large cohorts for connectomic studies as well.

One of the features that differentiates brain networks from random networks is the presence of hubs (regions with high degree of connectivity). The concept of rich club organisation suggests that hubs are densely interconnected with one another to form a rich core that functions as the central backbone of brain communication (van den Heuvel et al., 2012; van den Heuvel & Sporns, 2013; van den Heuvel & Sporns, 2011). It has been proposed that aberrant functioning of the network, as seen in neurological and psychiatric disorders (Warren et al., 2014; Crossley et al., 2014), are due to disruptions in the connectivity of hubs. For instance, computationally simulated attacks on rich club connections were shown to impair global network efficiency (i.e., efficiency of information exchange) to a greater extent as compared to random attacks on non-rich club connections (van den Heuvel & Sporns, 2011). Given the global impact that the disruption of the rich club core has, it is possible that the rich

club core may be affected in MDD, which is characterized by a wide range of cognitive, affective, and somatic symptoms. At the same time, the importance of non-hubs was highlighted in a study investigating the complexity of connectivity patterns of nodes (i.e., how similar were the connections established by nodes of the same degree, in terms of the degrees of nodes they were connected to; Smith et al., 2019). Nodes were divided into node tiers based on node degrees, with the first tier comprising nodes in the top 25% of degrees, and so on. It was reported that the most complex nodes were found in the lower tiers, while nodes in the highest tier (hubs) were the least complex. The wide variability in connectivity patterns of non-hubs play an important role in bridging nodes across different tiers, which is needed to support the diverse functional roles of the brain. As such, disruptions at non-hubs may affect cross-tier connectivity and play a significant role in disease aetiology, possibly even more so than disruption of hubs. This, however, requires further testing. Given the above, it is of benefit to investigate the differences in the connectivity of hubs alongside non-hubs to determine key associations with MDD.

In summary, MDD is a complex disorder that is associated with structural differences in the brain network. To date, attempts to understand these associations from a connectomic perspective have been limited by small sample sizes and consequent low statistical power. Due to the lack of consensus on the regions implicated in MDD, specifically the involvement of hubs and non-hubs, the neurobiological associations of MDD remains uncertain. Thus, the goal of this study is to utilize two large adult population samples to investigate MDD case-control differences in the structural connectome using network-based methods. To this end, we adopted a comprehensive approach of making comparisons at the global, tier, nodal and connection level to tease out MDD-associated differences at each hierarchical level of the connectome (Figure 2.1).

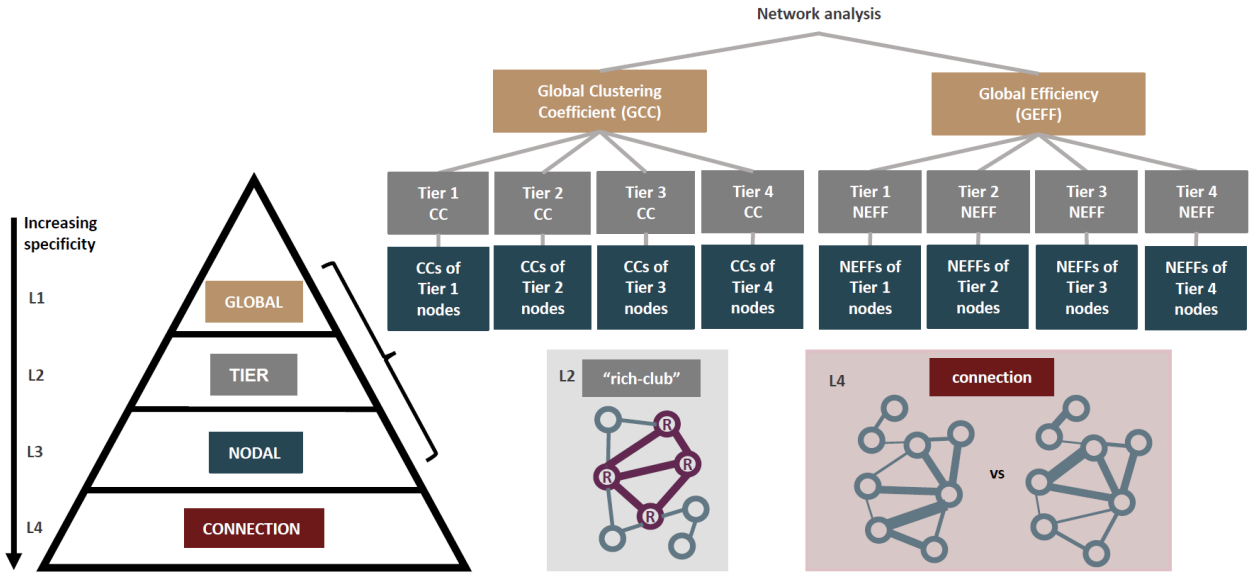

Figure 2.1. An overview of how the hierarchical order was established. We compared the structural connectomes of MDD cases and healthy controls in a hierarchical manner from Levels 1 to 4 (L1-L4), in the order of increasing specificity. At the global network-wide level at L1, network measures including global clustering coefficient (GCC) and global efficiency (GEFF) were derived. At L2, the nodes were then grouped into four tiers based on their node degrees and tier-level network measures were compared. The presence of rich club organisation looking at hub-to-hub connections was also separately studied at L2. At L3, network measures including clustering coefficient (CC) and nodal efficiency (NEFF) for each individual node were derived. At L4, Network-Based Statistics (NBS) was used to identify case-control group differences at the level of individual region-to-region connections.

2.2.3 Methods

Participants

The discovery sample consisted of participants that were part of the first 10,000 brain imaging datasets from the UK Biobank (UKB) study (Sudlow et al., 2015). The study was approved by the National Health Service Research Ethics Service (No. 11/NW/0382) and the UK Biobank Access Committee (Project No. 4844 and 10279). All participants provided informed consent. Participants were excluded if they had (1) neurological conditions including multiple sclerosis and Parkinson's disease, (2) other mental health conditions including bipolar disorder and post-traumatic stress disorder, and (3) failed neuroimaging quality control as detailed in an earlier publication (Buchanan et al., 2020). The final sample comprised N=5,104 subjects with both MDD and imaging data (Table 2.1). The replication sample consisted of participants from the imaging subsample of the Generation Scotland: the Scottish Family Health Study (GS; Habota et al., 2021). GS received ethical approval from the NHS Tayside research ethics committee. All participants provided informed consent (reference 14/SS/0039). The same exclusion criteria as UKB were applied, and the final sample comprised N=725 subjects with both MDD and imaging data (Table 2.1). Details on recruitment and assessments for both samples have been provided elsewhere (Miller et al., 2016; Alfaro-Almagro et al., 2018).

Table 2.1. Demographic information of participants from UKB and GS.

	UKB			GS		
	Cases	**Controls**	**p-value**	**Cases**	**Controls**	**p-value**
Sample size (% of cohort)	1,505 (29%)	3,599 (71%)	-	132 (18%)	593 (82%)	-
Age	60 ± 7	63 ± 7	<0.0001	57 ± 10	60 ± 10	0.004
Sex (% female)	67.1	47.3	<0.0001	80.3	56.3	<0.0001
Education (% of group)			0.651			0.844
College or University	78 (6%)	197 (6%)				
A-levels or AS levels or equivalent	74 (5%)	195 (6%)				
O-levels or GCSEs or equivalent	82 (6%)	125 (4%)				
CSEs or equivalent	294 (21%)	691 (21%)				
NVQ or HND or HNC or equivalent	216 (15%)	487 (15%)				
Other professional qualifications (e.g., nursing, teaching)	660 (47%)	1605 (48%)				
Compulsory				24 (18%)	138 (23%)	
More than compulsory				57 (43%)	204 (35%)	
Post secondary				51 (39%)	251 (42%)	
Household Income (% of group)			<0.001			0.003
Greater than £100,000	211 (15%)	348 (11%)				
£52,000 to £100,000	326 (24%)	752 (23%)				
£31,000 to £51,999	422 (31%)	992 (31%)				
£18,000 to £30,999	342 (25%)	893 (28%)				
Less than £18,000	69 (5%)	228 (7%)				
More than £70,000				11 (10%)	92 (18%)	
Between £50,000 and £70,000				7 (6%)	99 (19%)	
Between £30,000 and £50,000				36 (33%)	154 (30%)	
Between £10,000 and £30,000				48 (44%)	161 (31%)	
Less than £10,000				8 (7%)	15 (2%)	

Note: p-values represent differences between cases and controls; Abbreviations: GCSE – General Certificate of Secondary Education; CSE – Certificate of Secondary Education; NVQ – National Vocational Qualification; HND – Higher National Diploma; HNC – Higher National Certificate

Derivation of structural connectomes

Structural connectome processing was done locally and harmonized across UKB and GS using the same procedure published previously (Buchanan et al., 2020). Each T1-weighted image was parcellated into 85 neuroanatomical regions-of-interest (ROI). Eight subcortical structures per hemisphere (accumbens area, amygdala, caudate nucleus, hippocampus, pallidum, putamen, thalamus, and ventral diencephalon), and the brainstem were extracted with FreeSurfer v5.3.0, and 34 cortical structures per hemisphere were identified using the Desikan-Killany atlas (Desikan et al., 2006). Probabilistic tractography (BEDPOSTX/ProbtrackX; Behrens et al., 2007; Behrens et al., 2003) was performed and streamlines were seeded from all white matter voxels. Networks were constructed by identifying pairwise connections between the 85 ROIs and represented in the form of 85×85 matrices. FA-weighted matrices were derived by recording the mean FA along interconnecting streamlines between each pair of nodes. Given that raw networks contain many false-positive connections (Thomas et al., 2014), density-based thresholding was used to retain the top x% of strongest edges for each subject's connectome (Rubinov & Sporns, 2010), on the assumption that connections with the lowest weights are spurious and differ according to individuals. Seven thresholds ranging from 10% to 40% were applied. To select the main threshold, we took the case-control Cohen's d for all global, tier and nodal network measures, and calculated the correlation between those derived in UKB and those derived in GS. A higher correlation coefficient implies that the results between both cohorts are more agreeable, vice versa. The threshold of 35% with the strongest correlation (r_s=0.37, p=7.1×10^{-7}) was selected to be reported here. Of note, the correlation coefficient at other thresholds were also similar (Figure S1), suggesting that the replication results were consistent and there is no bias in the selection of the main

threshold. This is in line with previous studies which considered similar thresholds (Buchanan et al., 2020).

MDD status

Lifetime MDD status in UKB and GS was determined using online questionnaires based on the Composite International Diagnostic Interview Short Form (CIDI; Kessler et al., 1998). To fulfil criteria for MDD, cases were defined as ever having at least one core symptom of depression (prolonged sadness, loss of interest) for the majority or all days over a two-week period, and at least four non-core depressive symptoms (tiredness, weight change, sleep change, concentration difficulty, feeling worthless, thoughts of death) during the same period. Controls were subjects who did not endorse depression and did not screen positive for CIDI. Further details on how the case-control status was defined can be found here (Davis et al., 2020).

Network measures (L1: global; L3: nodal)

Four edge-weighted measures (two global, two nodal) focusing on clustering and efficiency were derived for each subject. The clustering coefficient (CC) measures the fraction of neighbours of the node that are also connected with each other. The weighted CC is the geometric average of the weights of the links forming all closed triplets centred on the node (Onnela et al., 2005). The global clustering coefficient (GCC) gives an overall indication of the clustering in the network and is defined as the average of all CCs. The nodal efficiency (NEFF) measures how well a node is integrated within the network via its shortest paths. It is the sum of the reciprocals of the shortest path lengths from the node to all other nodes of the network (Latora & Marchiori, 2001). The global efficiency (GEFF) measures the efficiency of

information exchange in which nodes concurrently exchange information via their shortest paths. It is defined as the average of all NEFFs.

The focus on CC and efficiency measures is because the human brain is postulated to be a 'small-world' network characterised by high CC and short path lengths. In other words, nodes are highly connected together through a small number of steps to ensure a high rate of information transfer to support complex brain functions at a low energy cost. Given that the small-network topology is already evident during the early developmental years (Fan et al., 2011), it is thus of interest to see if these fundamentally important network measures are affected in MDD.

Tier-based network measures (L2)

For each individual network, four node tiers were defined based on node degrees, using the method by Smith et al (2019). Tier 1 (T1) comprised nodes in the top 25% according to their degrees (i.e., hubs), Tier 2 (T2) comprised nodes in the next 25%, and so on for Tier 3 (T3) and Tier 4 (T4). The tiers were defined separately for each subject, as nodes may have different degrees and belong to different tiers in different subjects. For each subject and each nodal measure, measures for each tier (e.g., T1_CC, T1_NEFF) were derived by averaging the measure values of all nodes in the respective tiers.

This tier-based analysis is particularly interesting given that earlier studies showed that both neonatal and adult structural connectomes are composed of distinct hierarchical tiers, with different tiers comprising different categories of functional processing (Blesa et al., 2021). By dividing nodes into tiers, we are able to assess if there are any tiers that are particularly affected in MDD (e.g., hubs in T1 vs non-hubs in other tiers) and are possibly driving the effects observed at the global level.

Rich club organisation (L2)

A rich club organisation is present when high degree nodes are more likely to be interconnected and have stronger connection among themselves than would occur by chance (Opsahl et al., 2008). Group-averaged networks were used to calculate the weighted rich club coefficient, Φ(*k*). All non-zero connections were first ranked according to their weight (W^{rank}). For each degree *k*, a sub-graph comprising nodes with a degree larger than *k* was selected. The number of connections ($E_{>k}$) present between nodes in the sub-graph and the sum of their weights ($W_{>k}$) were determined. Φ(*k*) was then defined as the ratio between $W_{>k}$ and the sum of the top $E_{>k}$ links in the entire network (Equation 1).

$$\Phi(\mathrm{k}) = \frac{W_{>k}}{\sum_{l=1}^{E_{>k}} w_l^{rank}} \quad (1)$$

To ensure that these high degree nodes are not interconnected due to chance, 1000 random networks (with weights randomly reassigned while preserving the binary topology) were generated for each k and a corresponding $\Phi_{rand}(k)$ was calculated by averaging all 1000 random networks. A normalized rich club coefficient $\Phi_{norm}(k)$, was derived as the ratio of Φ(*k*) over $\Phi_{rand}(k)$. A $\Phi_{norm}(k)$ of greater than 1 over a continuous range of *k* would suggest the existence of rich club organisation.

Network-based statistics (NBS; L4)

NBS (v1.2; Zalesky et al, 2010) was used to test for differences in strength of each region-to-region connection. It evaluates the null hypothesis at the level of subnetworks instead of

individual connections, with the assumption that connections associated with the effect of interest are likely to be connected. A two-sample t-test was first performed to test for reduced connectivity in MDD cases at every connection, controlling for age and sex (and site for GS). A component-forming threshold of $p<0.05$ was used to select a set of suprathreshold edges, and all connected subnetworks at this level were identified. To evaluate the significance of the subnetwork, permutation testing was done by shuffling group membership (5,000 permutations) to obtain a null distribution of maximal subnetwork sizes. The p-value was defined as the proportion of permutations for which the largest subnetwork was of the same size or greater ($p<0.05$, FWE-corrected for comparison of multiple subnetworks).

Statistical analysis

The significance of (1) rich club curves for MDD cases and controls, and (2) case-control differences in rich club organisation were tested using permutation testing. (1) For each degree *k*, the 1,000 generated random networks produced a null distribution of rich club coefficients. Using this distribution, a p-value was assigned to the $\Phi_{norm}(k)$ as the proportion of $\Phi_{rand}(k)$ that exceeded $\Phi_{norm}(k)$. (2) For each degree *k*, the differences in $\Phi_{rand}(k)$ between cases and controls produced a null distribution of 1,000 differences. Using this distribution, a p-value was assigned to each case-control difference in $\Phi_{norm}(k)$ as the proportion of random differences that exceeded the observed difference. FDR correction was applied, and significance was determined at $pFDR<0.05$.

Linear regression was used to assess case-control differences in network measures, controlling for age, sex, and site (for GS only which had two sites; UKB had one site). The t-values for the group factor were used to compute Cohen's d effect sizes (Nakagawa & Cuthill, 2007). Permutation testing used to assess significance was done by shuffling group

membership to obtain a null distribution of t-values for the group factor (1,000 permutations). The p-value was defined as the proportion of permutations for which the unsigned t-value was greater than the original unsigned t-value. Given the hierarchical structure of the data (Figure 2.1), hierarchical FDR correction (Yekutieli, 2008) was performed. FDR correction was first applied across all global measures. For measures that remained significant, FDR correction was then applied across all measures at next level belonging to the same family (e.g., if GEFF remains significant, FDR correction will then be applied across all tier-based NEFFs). This process was repeated for the last level (nodal). Significance was determined at pFDR<0.05.

As sensitivity analysis, we controlled for additional covariates, including education level, household income and body mass index. To ensure that the effects were not driven by antidepressant exposure, we also tested for differences between (1) MDD cases with and without antidepressant use, and (2) MDD cases without antidepressant use and controls. The list of antidepressants is listed in Table S2.

2.2.4 Results

Global level

GEFF (*d*=-0.076, pFDR=0.033) was significantly lower in MDD cases in UKB (Figure 2.2A, Table S3). The effect size was similar in GS and in the same direction, however differences did not reach significance after FDR correction potentially due to reduced power on basis of smaller sample size (*d*=-0.108, p=0.246, pFDR=0.737; Figure 2.2A, Table S4). GCC in UKB was non-significant after FDR correction (*d*=-0.058, pFDR=0.051) and the effect size was not replicated in GS (*d*=-0.007, p=0.937, pFDR=0.937). As post-hoc analysis, we looked at case-control

differences in (1) mean FA which represents the mean weight used to construct the weighted network measures, and (2) GEFF after controlling for mean FA. No significant differences in mean FA were observed (UKB: *d*=-0.012, p=0.704; GS: *d*=-0.033, p=0.734), and GEFF remained significant with similar effect sizes after controlling for mean FA (UKB: *d*=-0.076, p=0.014; GS: *d*=-0.104, p=0.283).

Tier level

Tier membership of nodes was highly consistent between cases and controls within each cohort (UKB: r_s=0.991; GS: r_s=0.740) and were similar between cohorts (Cases: r_s=0.842; Controls: r_s=0.842) (Figure 2.2B). T1 corresponds to the rich club, and it consists of regions involved in higher-order brain functions such as the thalamus, putamen, precuneus, superior frontal gyrus and superior parietal cortex (based on results in UKB). NEFF of all tiers were significantly lower in MDD cases (T1: *d*=-0.076, pFDR=0.020; T2: *d*=-0.069, pFDR=0.020; T3: *d*=-0.075, pFDR=0.020; T4: *d*=-0.079, pFDR=0.020; Figure 2.2C) and the above effect sizes were well-replicated in GS, albeit non-FDR-significant (T1: *d*=-0.108, p=0.312, pFDR=0.416; T2: *d*=-0.097, p=0.306, pFDR=0.416; T3: *d*=-0.075, p=0.429, pFDR=0.429; T4: *d*=-0.123, p=0.205, pFDR=0.416; Figure 2.2C). Effect sizes for CC tier-based measures were less consistent between cohorts. Given the hierarchical structure of the data, significance of CC tier-based measures after multiple correction was not tested due to GCC not reaching significance.

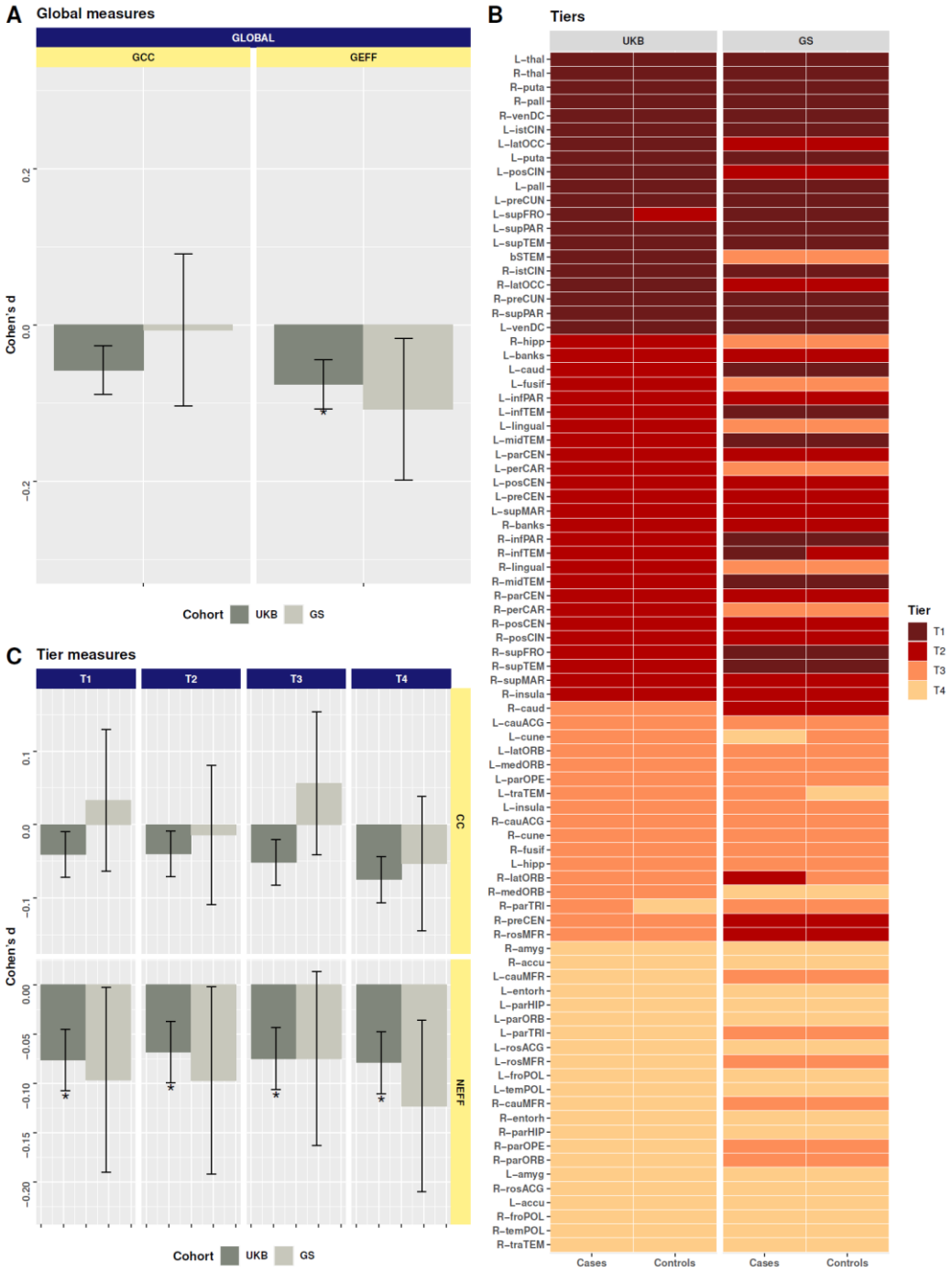

Figure 2.2. (A) Effect sizes for MDD case-control differences for the global network measures (GCC: global clustering coefficient; GEFF: global efficiency) for UKB and GS. The error bars represent the standard error of the estimate derived from the regression analysis. (B) All 85 nodes were ranked according to their node degree and sorted into four node tiers. T1 consist of nodes that are in the top 25% according to their degrees, and so on. To assess tier membership of nodes within each cohort, each node is assigned to the node tier that is the most dominant across all subjects in the subject group (cases or controls). (C) Effect sizes for MDD case-control differences for the tier-level network measures (tier-based CC; tier-based NEFF) for UKB and GS. The error bars represent the standard error of the estimate derived from the regression analysis. Note: the list of nodes along with their abbreviations can be found in Table S1.

Rich club organisation

Both cases and controls in UKB exhibited rich club organisation, as $\Phi_{norm}(k)$ were greater than one over a range of degree *k* (*k*=13 to *k*=63, pFDR<0.005) (Figure 2.3A and 2.3B). Similar results were observed in GS (Figure S2). In UKB, significant case-control differences were observed at *k*=16, *k*=23 and *k*=24 (pFDR=0.017 to 0.027; Figure 2.3C). However, these degree thresholds do not implicate the rich club and the absence of significant findings at the highest degrees suggest that there are no case-control differences in rich club organisation. Likewise, no significant case-control differences were found in GS at all values of degree *k* (pFDR<0.05, Figure S2).

Nodal level

The effect sizes for CC and NEFF of all nodes were generally consistent across cohorts (r_s =0.30), with cases consistently having lower values than controls (Figure 2.4A and 2.4B). In UKB, the NEFF of nodes belonging predominantly to T1 were significantly lower in cases. These include the right thalamus (*d*=-0.085, pFDR=0.035), right and left putamen (right: *d*=-0.094, pFDR=0.013; left: *d*=-0.099, pFDR=0.013), right and left pallidum (right: *d*=-0.113, pFDR=0.013; left: *d*=-0.079, pFDR=0.035), left precuneus (*d*=-0.080, pFDR=0.035), left ventral diencephalon (*d*=-0.080, pFDR=0.033), and the left insula (*d*=-0.099, pFDR=0.016) belonging to T3 (Figure 2.4C). No CC measures were significantly different in both cohorts.

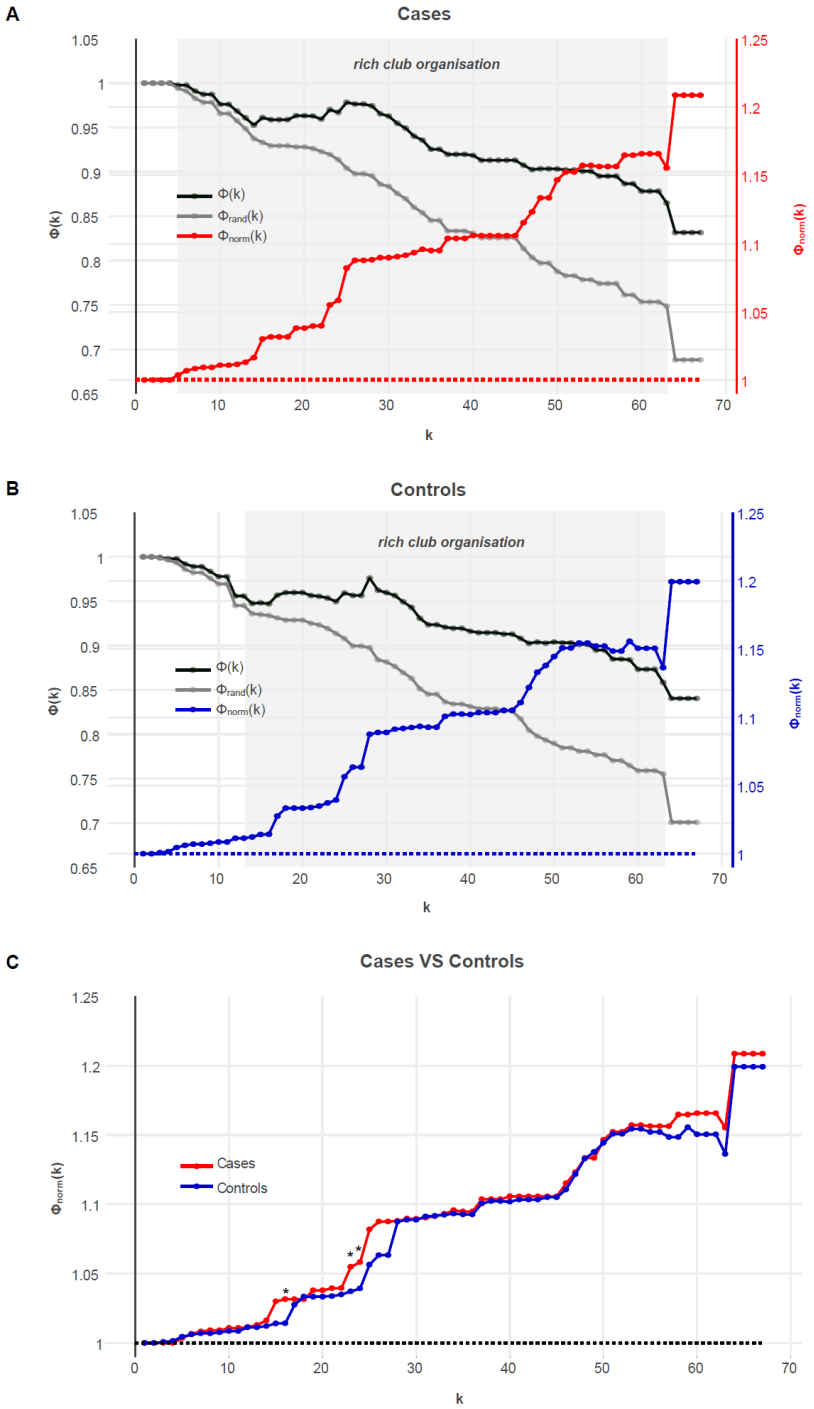

Figure 2.3. We tested for the presence of rich club organisation (i.e., whether hubs are more likely to be interconnected and have stronger connection among themselves than would occur by chance) in (A) cases and (B) controls in UKB. For (A) and (B), the x-axis represents the range of degree (k) tested, the primary y-axis represents the rich club coefficients derived from the original network ($\Phi(k)$; black line) and the randomly generated networks ($\Phi_{rand}(k)$; grey line), and the secondary y-axis represents the normalized rich-club coefficients ($\Phi_{norm}(k)$; red line in (A), blue line in (B)). The shaded area represents the range of degree that showed significant rich club organisation, which is indicated by a $\Phi_{norm}(k)$ of greater than 1 over a continuous range of *k*. A comparison of $\Phi_{norm}(k)$ for cases and controls is shown in (C).

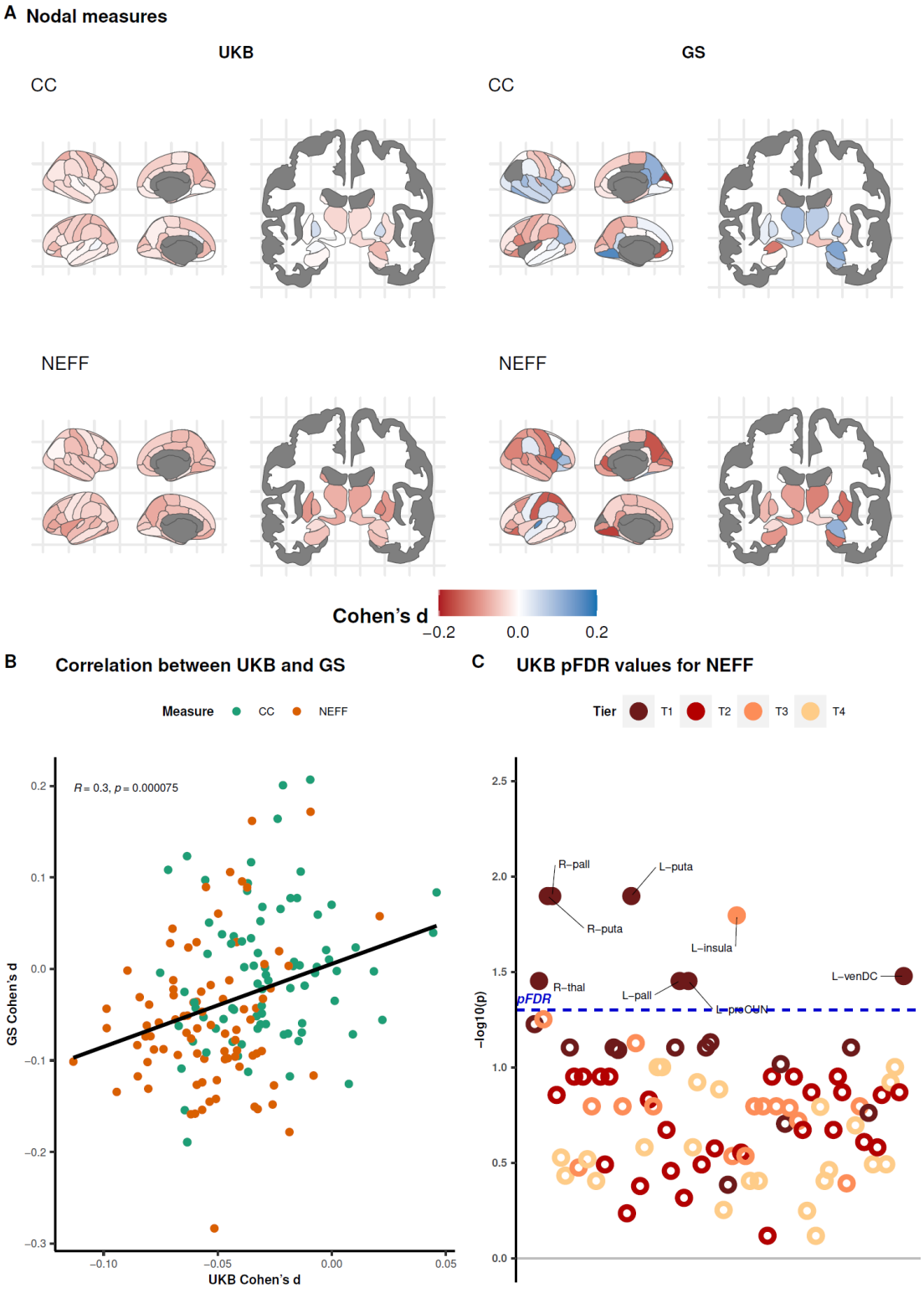

Figure 2.4. (A) Effect sizes for MDD case-control differences in nodal network measures (CC: clustering coefficient; NEFF: nodal efficiency) in UKB and GS. For each network measure, segmentation maps representing cortical (left) and subcortical (right) regions are shown. (B) Correlation of the effect sizes for CC and NEFF of all regions in UKB and GS. (C) FDR-corrected p-values for the NEFF of all nodes in UKB, grouped according to their tier membership. The blue dashed line represents the significance threshold at pFDR<0.05. Filled and labelled circles represent regions that survived FDR correction.

Connection level

No significant subnetworks were identified at the component-forming threshold of $p<0.05$ in either UKB or GS. As recommended by the authors of NBS, the analysis was repeated at other component-forming thresholds ($p<0.005$, $p<0.01$, $p<0.1$) but still no significant subnetworks were identified. As supplementary analysis, mass univariate testing for case-control differences at every connection was performed with permutation testing (50,000 times) and FDR correction applied across all tests. Again, no significant differences were found ($pFDR>0.05$).

Sensitivity analysis

Results at the global, tier and nodal levels remained largely unchanged after additionally controlling for education level, household income and body mass index (Tables S5-S6). Additionally, there were no significant differences between MDD cases with and without antidepressant use, suggesting that the effects of antidepressants on network measures are minimal in this sample (Table S7). There were no significant differences between MDD cases without antidepressant use and controls (Table S8), but the correlation of the effect sizes obtained here with those obtained in the main analysis was high ($r_s=0.934$, $p<0.001$). Given that more severe cases are likely to take medication and our samples were community-based, it is possible that the removal of cases with antidepressant use may have simultaneously removed the more severe MDD cases, thus eliminating the significance of effects Collectively, these results show that our main findings are related to the features of MDD and not driven by antidepressant exposure.

Null results

For null findings in the main analysis and sensitivity analysis, we additionally conducted Bayes factor (BF) analysis to better understand the strength of these findings (Keysers et al., 2020). Further information and discussion of the results derived from the BF analysis can be found in the Supplementary Materials (Tables S9 and S10).

2.2.5 Discussion

This study examined the connectomic differences between MDD cases and controls in a hierarchical manner. In the discovery sample, reduction in network efficiency in MDD cases were observed globally, across all tiers, and mainly in hubs locally. No case-control differences were observed for rich club organisation and at the connection level. The effect sizes were generally consistent, albeit not significant, in the smaller replication sample, which we also statistically tested in a meta-analysis (Figure S3).

The reduction of global network efficiency in MDD cases suggests that there is an overall reduction in the capacity of the network to communicate between regions. Efficiency measures are based on shortest path lengths, and the brain is optimized towards a low average shortest path length to ensure efficient communication (Kaiser et al., 2007). As edge-weighted network measures were used, differences in efficiency could be attributed to differences in weights or topology. Given the absence of case-control differences in mean FA and the significant reduction in global efficiency in MDD even after controlling for mean FA, the differences in network efficiency may possibly be due to topological differences. The differences are, however, likely to be subtle and dispersed across the network, given that no connected subnetworks were found to be significantly different between groups at the connection level. Likewise, the inability to detect significantly different connections at the

current statistical power using mass univariate testing also hints at the subtlety of effects. Nevertheless, these results are still insightful as they seem to suggest that the brain is configured slightly differently in MDD and point to the importance of studying network organisation alongside connectivity strength. These topological differences can be diathetic, a sequelae, or a form of adaptation to MDD, all of which are interesting possibilities that warrant further investigation.

Interestingly, the overall reduction in network efficiency is unlikely to be associated with hub-hub connections, as indicated by the absence of significant case-control differences in rich club organisation. This could be because the rich club plays a crucial role in integrating information from numerous functionally specialized regions across the brain (van den Heuvel & Sporns, 2011; Kaiser et al., 2007), and contribute towards providing a foundational basis for the development and functional specialisation of lower tier regions (Blesa et al., 2021). It is arguably evolutionarily adaptive to prioritize maintaining a stable and robust core to make it resilient to changes that could critically compromise functioning. While biologically costly to maintain the rich core, the high biological cost is offset by the functional benefits it confers for neural communication (Bullmore & Sporns, 2012; Collin et al., 2014). The manifestation of the effects of MDD in a subtle yet cumulative manner, unlike radiologically defined abnormalities that are immediately damaging, also lends support to the assertion that the rich core remains intact in MDD.

Hubs, however, may remain a key area of focus in MDD research, given that significant reductions in efficiency at the nodal level were mostly observed in T1 nodes. As rich connections between hubs have been shown above to be resilient to MDD-related changes, the differences seen in T1 may be driven by differences in feeder connections (hub to non-hub connections) instead. Hubs of interest include the thalamus, putamen, pallidum,

precuneus and ventral diencephalon, deficits in which have been shown to be implicated in MDD (Kim et al., 2019; Lu et al., 2016; Li et al., 2018; Zhang et al., 2022; Lebedeva et al., 2017). Of note, these regions are mostly involved in reward processing and emotion regulation. The pallidum, putamen and thalamus are part of the cortico-basal ganglia loop, which plays a central role in developing goal-directed behaviours (Haber, 2016). Specifically, the putamen is part of the striatum (the main input structure of the basal ganglia) and receives input from various cortical structures including the anterior cingulate cortex and prefrontal cortex which comprise regions associated with reward and motivation. The pallidum, especially the ventral pallidum, is also key player in emotion processing, where it receives input from the limbic areas via the ventral striatum. Both putamen and pallidum project to the thalamus, which functions as a core information relay station from basal ganglia to the cerebral cortex and also contribute towards higher order functions (Kumar et al., 2022). Disruptions to this corticostriatal circuitry have been implicated in neuropsychiatric disorders including MDD (Gunaydin & Kreitzer, 2016). The precuneus and ventral diencephalon are also involved in related processes, with the former playing a central role in the default mode network (DMN) responsible for internally orientated cognition (e.g., rumination) and the latter containing the hypothalamus which is a key region for stress response (Zhou et al., 2020). Thus, the implication of multiple regions involved in reward/emotion regulation processes suggests that differences in this circuitry may be more important in MDD (Park et al., 2019; Ng et al., 2019).

While our results point to the importance of hubs, they also suggest that hubs are not solely involved in the reduction of overall network efficiency in MDD. Reduction in tier-level efficiency was observed across all four hierarchical tiers, indicating that MDD-associated brain differences are pervasive, involving both hubs and non-hubs. Since the four tiers cover a

broad set of categories of functional processing (Smith et al., 2019; Blesa et al., 2021), the widespread somatic, affective, and cognitive dysfunctions often observed in MDD may possibly be associated with changes in information flow in multiple regions belonging to different tiers. Interestingly, although MDD cases had lower efficiency at T2 to T4, there was an absence of significant findings at the nodal level for these tiers unlike for T1. This suggests that differences at these lower tiers may be a result of the accumulation of subtle reductions in the nodal efficiency of multiple nodes that were too small/insignificant to be detected individually at the nodal level. An exception would be the insula, which despite being a T3 node, also showed significant reduction in nodal efficiency. This could be due to its close proximity and connections with the abovementioned T1 nodes like the thalamus and putamen, likely necessary to support its diverse functions (including affective processes; Ghaziri et al., 2018), thus rendering its paths more susceptible to changes associated with MDD. In the same light, the significant reduction in efficiency of T1 nodes, as discussed above, is likely not attributable to large differences in only a few connections, but a result of the accumulation of subtle differences in the large number of connections surrounding it. In other words, the ability to identify significant findings in T1 nodes may be by virtue of the fact that these nodes have the highest number of connections and hence, the accumulation of more subtle differences around them.

Taking all these together, our results suggest that there are subtle, widespread, and possibly topology-related differences in the structural connectomes of MDD cases. The differences potentially build up in the order of hierarchy to effect changes that are detectable at the higher network organisation levels (global, tier and nodes in the top tier). The reasonable consistency of effect sizes in both samples suggests that the findings are likely true, although this can be determined definitively in the future using larger samples with

preferably more than a thousand subjects for reliable results (Marek et al., 2022). While the small effect sizes may seem trivial, they are actually in line with recent meta-analytic and large consortia studies that found very small differences (<2% variance explained) in MDD across all neuroimaging modalities (Feng et al., 2022; Winter et al., 2022). Our study conducted at a similar scale thus offers a connectomic perspective and provides further evidence for the notion that very subtle and potentially diffusely distributed brain-related differences exist in MDD.

While not the first to examine network measures in MDD, this study is one of the largest, well-powered and most comprehensive hierarchical connectomic explorations of MDD to date. The use of two large samples is a strength, in that the results are generally replicable and can serve as a reliable reference for future studies. Limitations should, however, be considered. Firstly, it is known that network metrics can vary depending on various factors, such as the atlas used, thresholding method and tractography parameters, which still lack consensus in the scientific community (Adamovich et al., 2022; Wei et al., 2017). Our results may thus not hold if different approaches were taken. Secondly, our results may not be directly applicable to the more severe MDD cases, as GS and UKB are community-based cohorts consisting mainly of relatively healthy individuals. Our results, however, have the benefit of better generalisability to the community and likely cover abnormalities common across different severities/subtypes, thus providing a starting point for future in-depth analyses. We considered it essential to maximise sample size by minimising exclusions to ensure sufficient power needed to detect small effects present in MDD.

Conclusion

This study presents a comprehensive approach to the hierarchical comparison of the structural connectomes of MDD cases relative to controls in two large population cohorts. The key takeaways include: (1) there is an overall reduction in network efficiency in MDD, (2) the rich club core remains robust in MDD, and (3) the connectomic differences in MDD are subtle but widespread involving both hubs and non-hubs. This work can be extended in future studies by integrating functional connectivity data (e.g., the coupling between structural and functional connectivity) to gain further insights into the basis and consequences of reduced network efficiency in MDD.

2.3 Chapter conclusion

Using two large discovery and replication structural connectome datasets, the findings from this chapter showed that subtle but widespread differences outside the rich club core exist between MDD cases and healthy controls, resulting in an overall reduction in network efficiency in MDD cases. The results here provided the impetus to look into the origins of connectomic differences in the next chapter, specifically to investigate structural connectomic associations with key MDD risk factors.

Chapter 3: A sex-stratified analysis on structural connectomic associations with childhood trauma and polygenic risk score for Major Depressive Disorder in the UK Biobank

3.1 Chapter introduction

MDD polygenic risk (MDD-PRS) and childhood trauma (CT) are key risk factors for MDD, and previous neuroimaging studies have reported significant associations between both MDD-PRS and CT with reduced white matter integrity (Shen et al., 2020; He et al., 2023). These associations are, however, understudied from a connectome perspective (Gong & He, 2015), and especially in large samples needed for the reliable assessment of brain-wide associations (Marek et al., 2022). Beyond the identification of regions of the structural connectome (hereby referred to as subnetworks) associated with each MDD risk factor, it was also of interest to understand the role of the subnetworks in the pathogenesis of MDD, in that whether MDD-PRS and CT operate through the respective subnetworks to increase MDD risk. The study of mediation effects was further extended by using a moderated mediation model to take into consideration that MDD is a multifactorial disorder and there can be possible interactions between genetic and environmental factors. Collectively, these analyses help to provide more insight into how MDD-PRS, CT, the structural connectome, and MDD are related to one another. For this study, the full sample consisted of 14,881 subjects from the UKB, with 8,069 females and 6,812 males. Due to reports of sex differences in MDD-PRS and CT associations with neuroimaging variables in earlier studies (Kämpe et al., 2023; Gui et al., 2022; Tozzi et al., 2020), the analyses described above were conducted separately for males and females.

3.2 Manuscript

This study has been written up as a manuscript titled “A sex-stratified analysis on structural connectomic associations with childhood trauma and polygenic risk for Major Depressive Disorder in the UK Biobank”. As the first author, I conceived the hypotheses, conducted the analyses, and wrote the manuscript under supervision.

3.2.1 Abstract

Major Depressive Disorder (MDD) is more prevalent in females, and it is a multifactorial disorder associated with brain structural dysconnectivity. This study sought to understand the relationship between the structural connectome and key MDD risk factors, including MDD polygenic risk (PRS) and childhood trauma (CT).

The sample consisted of 14,881 subjects (6,812 males, 8,069 females) from the UK Biobank. In males and females separately, we (1) looked at the association between the connectome and MDD-PRS/CT to identify PRS- and CT-associated subnetworks (i.e., higher MDD-PRS/CT is associated with lower connectivity in the identified subnetwork), (2) examined the role of the respective subnetworks as a mediator between MDD-PRS/CT and MDD, and (3) tested if the direct and indirect effects by the PRS-associated subnetworks were moderated by CT.

The PRS- and CT-associated subnetworks were distinct and were also unique to each sex. For the PRS-associated subnetworks, network connectivity was lower in MDD cases than controls in females (d=-0.101, p<0.001) but not males (d=-0.006, p=0.834). A significant mediation effect was present in females (ab=0.007, 95% CI [0.003, 0.012]), but both direct and indirect effects were not moderated by CT. For the CT-associated subnetworks, network connectivity was lower in MDD cases than controls in females (d=-0.103, p<0.001) and males

(*d*=-0.082, p=0.007), but a significant mediation effect was only present in females (*ab*=0.006, 95% CI [0.0007, 0.012]).

MDD risk factors have differential associations with male and female structural connectomes, with connectome mediation effects only observed in females.

3.2.2 Introduction

Major Depressive Disorder (MDD) is a prevalent psychiatric disorder, with women being twice as likely to be diagnosed with MDD in their lifetime as compared to men (Salk et al., 2017). Extensive neuroimaging research has since been done in hopes of understanding the neurobiological basis of MDD, and the rise in the number of large population studies has allowed for significant progress to be made in identifying robust brain structural alterations that are present in MDD across different neuroimaging measures (Schmaal et al., 2016; Schmaal et al., 2017; van Velzen et al., 2020; Harris et al., 2022). Large-scale brain connectome studies using network approaches, such as in Sha et al (2023), have also gained traction in recent years, given that the brain is organised as a large network and dysfunctions are unlikely to be confined to a single brain region. In relation to MDD, a recent study by our group found that global network efficiency is lower in MDD cases relative to controls, suggesting less efficient communication across the whole structural connectome (Thng et al., 2024). With the knowledge that MDD is multifactorial and is associated with alterations in the structural connectome, it then raises the question of whether genetic and environmental risk factors for MDD operate via the connectome to increase vulnerability to MDD.

The latest MDD genome-wide association study (GWAS) identified 697 associated genetic variants (Adams et al., 2024), re-emphasising that MDD is highly polygenic with many variants of small effect. Each genetic variant, however, contributes very little to disease

liability and there is limited clinical value in studying their individual associations with other phenotypes. MDD polygenic risk score (PRS) is more representative of liability to MDD (up to 5.8% in Adams et al (2024)) and can be used to identify brain regions whose genetic architecture is shared with MDD more accurately. Previous neuroimaging studies have adopted this approach in large cohort settings, such as in Shen et al (2020) and Kämpe et al (2023) who reported significant associations between higher MDD-PRS and reductions in white matter integrity and gray matter volume, respectively. This is, however, understudied from a connectome perspective (Gong & He, 2015), especially in terms of using a polygenic approach and having sample sizes that are large enough to reliably assess brain-wide associations (Marek et al., 2022). The use of a polygenic and network approach in a large cohort, would therefore better inform our understanding on how genetic risk for MDD can influence structural connectivity at a macroscale brain network level. Beyond the identification of PRS-associated subnetworks, it was also of interest to test if the subnetworks mediate the relationship between MDD-PRS and MDD. That is, if genes exert their influence on the subnetwork, which in turn effect downstream changes or symptoms seen in MDD. This will help us to understand the relevance of the subnetworks in the pathogenesis of MDD.

In terms of environmental risk factors, childhood trauma (CT) is a well-established and significant risk factor for many mental disorders including MDD (Teicher et al., 2022). MDD cases often reported higher rates of exposure to CT as compared to healthy controls (Negele et al., 2015; Humphreys et al., 2020). While the exact mechanisms linking CT to MDD is not yet clear, CT has been shown to be associated with a range of alterations in brain morphology, functional and structural connectivity, and network architecture (Teicher et al., 2014, 2016; Madden et al., 2023; Korgaonkar et al., 2023), which may be relevant to MDD (Yu et al., 2019; Tozzi et al., 2020). However, similar to studies looking at the associations between MDD-PRS

and the brain, the relationship between CT and the brain is understudied from a connectome perspective, especially for structural connectomes (Yeung et al., 2024). Thus, to complement existing findings, here we utilised large-cohort data to identify structural brain circuits associated with CT and tested the relevance of the identified subnetworks as a mediator in MDD.

Of note, while the effects of MDD-PRS and CT can be studied separately, both risk factors can also operate in tandem to bring about MDD. The interaction between MDD-PRS and CT is commonly studied for the direct effect (i.e., MDD-PRS × CT → MDD), but seldom studied for the indirect or mediated effect. One of the assumptions of the traditional mediation model is that the mediated effect can be generalised to all circumstances, although it is possible for mediated effects to operate differently in different circumstances. In other words, although genetic predisposition to MDD is determined since birth, the manifestation of MDD-PRS on MDD both directly and indirectly through the PRS-associated subnetwork can be different between individuals with and without CT. As such, we were also interested in using a moderated mediation model to study the role of the PRS-associated subnetwork as a mediator linking MDD-PRS to MDD, while allowing the effects to be contingent on different levels of CT exposure. Doing so will provide us with more insight into how genes, the connectome, CT and MDD are related to one another.

As sex differences in the manifestation of MDD is known (Salk et al., 2017), there may be potential sex differences in the mechanisms underlying MDD. Recent studies have reported sex differences in MDD-PRS and CT associations with neuroimaging variables (Kämpe et al., 2023; Gui et al., 2022; Tozzi et al., 2020). For example, in Kämpe et al (2023), MDD-PRS was found to be associated with grey matter volumetric changes in females but not males. In Tozzi et al (2020), CT severity was associated with higher cortical thickness of the

rostral anterior cingulate cortex but only in males. The analyses in this study were thus conducted separately for males and females. The use of a stratification approach is because this study has one of the largest sample sizes (N=14,881) to date for the investigation of structural connectomic associations with MDD risk factors, which allows for sufficient statistical power in each group to reliably detect any significant differences between MDD cases and controls. Additionally, stratification also allows for a more nuanced understanding of the specific connectomic associations in males and females. This is especially since the analyses involve identifying entire subnetworks from the ground up which can be highly variable between sexes, as compared to using already well-defined variables (e.g., morphometric measures). Such level of detail may be lost when combining both sexes in a single analysis to identify the subnetworks. Although stratification does not allow for the statistical testing of sex differences as with an interaction approach, the focus of this study is to better understand the specific subnetworks that are potentially involved in MDD within each sex.

In summary, MDD is a complex disorder that is associated with structural brain differences, and these differences may possibly play a mediating role between MDD risk factors and the manifestation of MDD itself. To date, attempts to understand the role of the brain as a mediator from a connectomic perspective have been few, constrained by small sample sizes and the inclusion of environmental factors as possible moderators remains largely unexplored. Thus, the goal of this study is to use a large sample from the UK Biobank to (1) look at the associations between the structural connectome and MDD-PRS/CT to identify PRS- and CT-associated subnetworks, (2) examine the role of the respective subnetworks as a mediator, and (3) test if the mediated effects by the PRS-associated subnetworks are moderated by CT, in males and females separately (Figure 3.1).

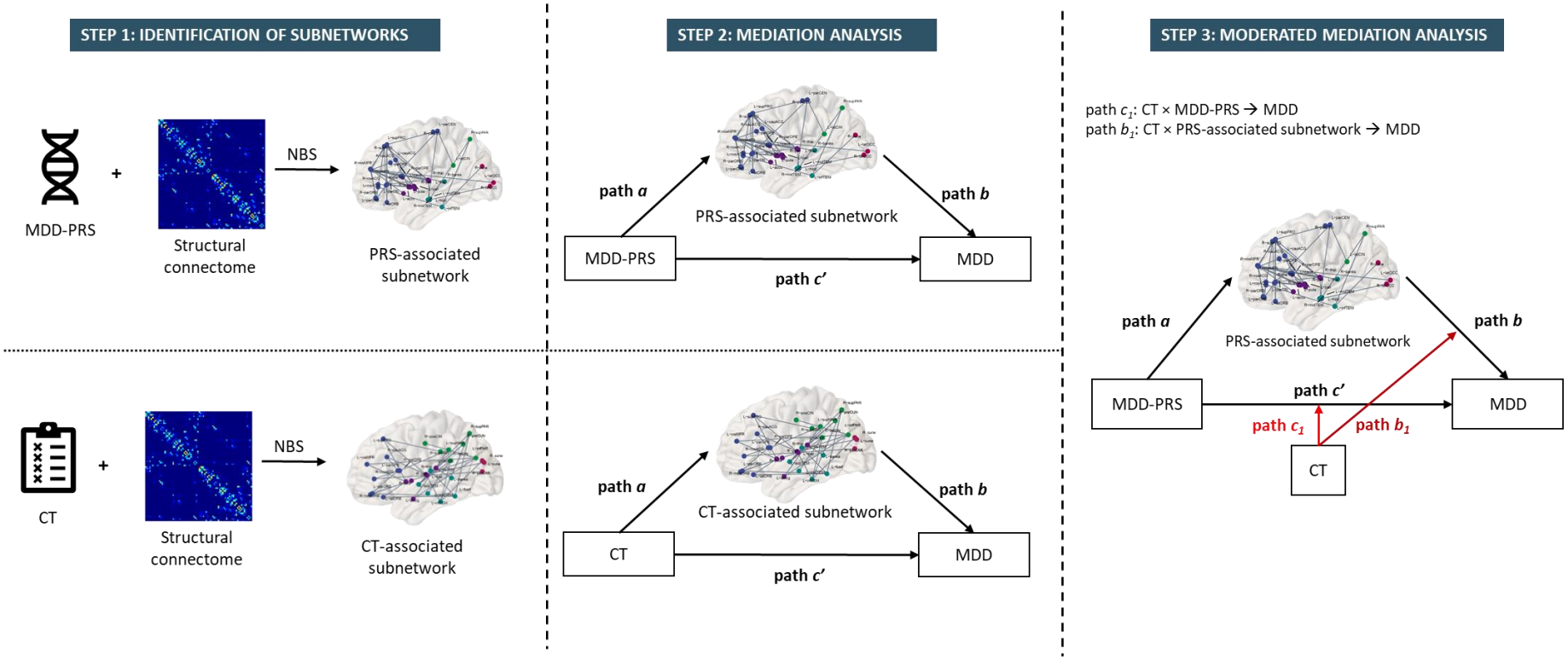

Figure 3.1. An overview of the analyses conducted in males and females separately. PRS- and CT-associated subnetworks were first identified using network-based statistics (Step 1). The role of the subnetworks as mediators were then evaluated (Step 2). A moderated mediation model was then used to test if the effect of MDD-PRS on MDD directly and indirectly through the PRS-associated subnetwork were conditional on the level of CT exposure (Step 3).

3.2.3 Methods

Participants

The sample consisted of participants from the imaging subsample of the UK Biobank (UKB) study (Sudlow et al., 2015). The study was approved by the National Health Service Research Ethics Service (No. 11/NW/0382) and the UK Biobank Access Committee (Project No. 4844 and 10279). All participants provided informed consent. Details on recruitment and assessments have been provided elsewhere (Miller et al., 2016; Alfaro-Almagro et al., 2018). The sample was restricted to unrelated and European-only subjects, due to the use of summary statistics based on European-only subjects to generate MDD-PRS. Further details on the exclusion criteria are available in the Supplementary Material. The final sample comprised N=14,881 subjects, of which N=8,049 were females and N=6,812 were males (Table 3.1).

Derivation of structural connectomes

Structural connectome processing was done locally, using methods that have been previously described (Buchanan et al., 2020; Thng et al., 2024), to derive FA-weighted connectivity matrices for 85 regions of interest. Briefly, the brain stem and eight subcortical structures per hemisphere (accumbens area, amygdala, caudate nucleus, hippocampus, pallidum, putamen, thalamus, and ventral diencephalon) were extracted with FreeSurfer v5.3.0, and 34 cortical structures per hemisphere were identified using the Desikan-Killany atlas (Desikan et al., 2006). Density-based thresholding was applied to the 85×85 connectivity matrices to retain the top *x*% of strongest edges for each subject (Rubinov & Sporns, 2010), on the assumption that connections with the lowest weights are spurious and differ according to individuals. A

threshold of 35% was applied, following an earlier publication (Thng et al., 2024) and in line with previous studies which considered similar thresholds (Buchanan et al., 2020).

Table 3.1. Demographic information

	Females (N=8,069)			Males (N=6,812)			p-value^{+}
	Cases	**Controls**	**p-value$^{\wedge}$**	**Cases**	**Controls**	**p-value$^{\wedge}$**	
Sample size (% of group)	2,865 (36%)	5,204 (64%)	-	1,339 (20%)	5,473 (80%)	-	-
Age (mean ± SD)	62 ± 7	64 ± 7	<0.001	63 ± 7	66 ± 8	<0.001	<0.001
CT score (% ≥ 7)	10.6	2.9	<0.001	8.7	1.7	<0.001	<0.001
Education (% college)	50	48.6	0.252	51.7	51.9	0.905	<0.001

Note: CT score above 7 was used as a point of comparison because CT<7 was defined as the cutoff for no CT exposure in this study. p-value$^{\wedge}$ represents MDD group difference within each sex, while p-value^{+} represent difference between sexes.

MDD status

Lifetime MDD status in UKB was determined using online questionnaires based on the Composite International Diagnostic Interview Short Form (CIDI; Kessler et al., 1998). To fulfil criteria for MDD, cases were defined as ever having at least one core symptom of depression (prolonged sadness, loss of interest) for the majority or all days over a two-week period, and at least four non-core depressive symptoms (tiredness, weight change, sleep change, concentration difficulty, feeling worthless, thoughts of death) during the same period. Controls were subjects who did not endorse depression and did not screen positive for CIDI. Further details on how the case-control status was defined can be found here (Davis et al., 2020).

Polygenic risk score (MDD-PRS)

MDD-PRS was derived using the latest MDD GWAS summary statistics from the Psychiatric Genomics Consortium MDD Working Group (Adams et al., 2024). To avoid bias, subjects included in this study were excluded in the calculation of the summary statistics. PRSice v2.1.11 (Choi & O'Reilly, 2019) was then used to calculate MDD-PRS using the clumping and thresholding method (clump-p = 1, clump-r2 = 0.25, clump-kb = 250 kb). The p-value threshold of 0.01 was used in this analysis, as previous studies have shown that this threshold had the strongest associations with neuroimaging phenotypes in UKB (Shen et al., 2020).

Childhood Trauma (CT)

The 5-item Childhood Trauma Screener (CTS; Glaesmer et al., 2013), a shortened version of the Childhood Trauma Questionnaire (CTQ; Bernstein et al., 2003), was used to rate adverse events that may have happened during childhood. This was assessed at the same time as MDD as part of the mental health questionnaire. Five aspects of childhood trauma (field: 20487 to 20491), including "felt loved", "physically abused by family", "felt hated by family member", "sexually molested", and "someone to take to doctor when needed", were evaluated using a five-point Likert scale (0=never true, 1=rarely true, 2=sometimes true, 3=often, 4=very often true). The total sum across all items was taken as the final CT score. We note that the CTS is an abbreviated measure of the original CTQ, but it is generally considered a valid screening instrument for the retrospective assessment of CT in the general population (Witt et al., 2022) and has been used in earlier studies (Orellana et al., 2024).

Network-based statistics (NBS)

NBS (version 1.2; Zalesky et al., 2010) was used to identify subnetworks associated with MDD-PRS and CT. NBS is fundamentally based on the idea that regions of the connectome associated with the variable of interest are likely to be confined together in an interconnected subnetwork, rather than being dispersed individually throughout the connectome. By identifying subnetworks, significant statistical power can be gained as correction for multiple comparisons can be done at the level of subnetworks, in contrast to the mass univariate approach where correction has to be done considering every individual edge. A linear regression model was first applied on each connection, with MDD-PRS or CT as predictor, and age, site, scanner position on the x-, y-, z- axes, first 10 genetic principal components (for MDD-PRS), genotyping array (for MDD-PRS), and the Townsend index (for CT) as covariates. A component-forming threshold of $p<0.01$ (corresponding to a t-statistic of 2.32 from the linear regression model) was applied to select a set of suprathreshold edges, and all connected subnetworks at this level were identified. To evaluate the significance of the subnetwork, permutation testing was done by shuffling group membership and repeating the above steps to obtain a null distribution of maximal network sizes (5,000 permutations). The p-value was determined as the proportion of permutations for which the largest subnetwork was of the same size or greater ($p<0.05$, FWE-corrected for comparison of multiple subnetworks).

Network properties

Beyond just identifying the subnetworks, we further characterised the subnetworks by looking at the extent of involvement of hubs and non-hubs in the subnetwork. This is because hubs (i.e., brain regions with the highest number of connections in the network) are important

in ensuring efficient brain communication (Crossley et al., 2014), and disruption to hub connectivity is generally considered to play a role in disease. For each subject, using the method by Smith et al (2019), nodes (i.e., brain regions) were ranked according to their degree (i.e., the number of connections each node has), and those in the top 25% of degrees were selected as hubs. In addition, the type of edges or connections in the subnetwork were also identified. They include rich, feeder, and local connections, which refer to connections that are between hubs, hubs and non-hubs, and non-hubs and non-hubs, respectively.

Mediation

A single summary measure for the connectivity of the PRS- and CT-associated subnetworks was each derived by taking the average weight of all edges in the subnetwork (hereby called PRSnet or CTnet). Using the PROCESS macro in R (Hayes, 2013), mediation analysis (PROCESS model #4) was conducted to determine if the respective subnetworks (mediator *M*) mediated relationship between MDD-PRS or CT (predictor *X*) and MDD (outcome *Y*). The indirect effect was defined as the product of *a* and *b* (i.e., *ab*; Figure 3.1*)*, which represent the regression coefficient of (1) *X* on *M*, and (2) *X* on *Y* controlling for *M*, respectively. Covariates included age, site, array (for MDD-PRS), the first ten genetic principal components (for MDD-PRS), and the Townsend index (for CT). Significance of the indirect effect was determined by deriving a 95% bootstrapped confidence interval (10,000 times). For both mediation and moderated mediation analyses, the measures were standardised to account for the difference in scale before running the models.

Moderated mediation

Moderated mediation was then done to test if the direct effect of MDD-PRS on MDD and indirect effect via PRSnet differed at different levels of CT. Specifically, we used PROCESS model #15 (Figure 3.1) to test if CT (moderator *W*) moderated the paths between (1) MDD-PRS and MDD, and (2) PRSnet and MDD. For levels of CT, we used four levels corresponding to CT scores of 0, 7, 10 and 14 (out of 20) to represent no, low, moderate, and high CT exposure, corresponding to the equivalent cutoffs for the CTQ (MacDonald et al., 2016). The indirect effect is defined as the function $ab+ab_1W$ (Figure 3.1), and evidence of moderation of the indirect effect can be determined by assessing if the weight of the moderator in the function (i.e., ab_1) is different from zero (Hayes, 2013). ab_1 quantifies the change in the indirect effect of MDD-PRS on MDD through PRSnet as CT changes by one unit. If ab_1 is not equal to zero, the indirect effect depends on the moderator and hence, mediation is moderated. Significance of ab_1, otherwise known as the index of moderated mediation, was determined by deriving a 95% bootstrapped confidence interval (5,000 times).

Sensitivity analyses

Given the higher percentage of females in these analyses, to ensure that the results were not driven by this difference, a sensitivity analysis was conducted on N=6,812 females randomly selected to match the number of males and the previous analyses were repeated. For completeness, we also tested if CT moderated the path between MDD-PRS and PRSnet (path a). A significant interaction would mean that the effect of MDD-PRS on PRSnet will differ according to different levels of CT.

3.2.4 Results

Features of the PRS-associated subnetwork

For females, higher MDD-PRS was significantly associated (p=0.008) with lower connectivity for all connections in a subnetwork involving 55 nodes and 71 edges (Figure 3.2A; Table S2). These nodes were primarily in the frontal and subcortical regions, with majority of the connections being frontal-subcortical (15 edges) and frontal-frontal (12 edges). For frontal regions, the rostral middle frontal gyrus, superior frontal gyrus, and regions on the inferior frontal gyrus (e.g., pars triangularis, pars orbitalis, pars opercularis), were the dominant nodes. For subcortical regions, regions part of the basal ganglia including the thalamus, putamen, and pallidum, were the dominant nodes. Hubs included regions such as the basal ganglia, precuneus, superior parietal, superior frontal and superior temporal gyrus, lateral occipital gyrus, ventral diencephalon, and isthmus of cingulate gyrus. A number of rich connections between the basal ganglia, superior frontal cortex and parietal regions were involved in the subnetwork, but majority were feeder and local connections.

For males, higher MDD-PRS was significantly associated (p=0.043) with lower connectivity for all connections in a subnetwork involving 45 nodes and 50 edges (Figure 3.2B; Table S3). These nodes were primarily in the frontal and parietal regions, with majority of the connections being frontal-parietal (13 edges) and frontal-frontal (12 edges). For the frontal-parietal connections, some of the key nodes included the superior and middle frontal gyrus, supramarginal gyrus, postcentral gyrus and precuneus. For frontal regions, the superior frontal gyrus, regions on the inferior frontal gyrus (e.g., pars triangularis, pars orbitalis), and the anterior cingulate gyrus were the dominant nodes. Hubs remained mostly consistent with

those identified in females, and most of the connections in the subnetwork were feeder and local connections, with only one rich connection observed.

In comparing MDD case-control difference in network connectivity for each sex, PRSnet (the average edge weight of the PRS-associated subnetwork) was significantly lower in MDD cases relative to controls in females (d=-0.101, p<0.001) but not in males (d=-0.006, p=0.834).

Features of CT-associated subnetworks

For females, higher CT score was significantly associated (p=0.007) lower connectivity for all edges in a subnetwork involving 58 nodes and 77 edges (Figure 3.3A; Table S4). These nodes were primarily in the frontal and subcortical regions, with majority of the connections being frontal-subcortical (17 edges) and subcortical-temporal (10 edges). For the frontal-subcortical connections, regions similar to the PRS-associated subnetwork were implicated, along with the orbitofrontal regions. For the subcortical-temporal connections, the main nodes included the basal ganglia and the superior, inferior, and middle temporal regions. Similar to the PRS-associated subnetwork, a number of rich connections between the basal ganglia, frontal, parietal and temporal regions were involved in the subnetwork, but majority of the connections were feeder and local connections.

For males, higher CT score was significantly associated (p=0.046) lower connectivity for all edges in a subnetwork involving 33 nodes and 39 edges (Figure 3.3A; Table S5). Unlike females, the nodes/connections were more diffused and evenly spread over parietal (e.g., inferior parietal gyrus, precuneus), subcortical (e.g., basal ganglia), occipital (e.g., lateral occipital), and temporal (e.g., inferior, transverse temporal, parahippocampal) regions. A number of rich connections mainly between the parietal, basal ganglia and occipital regions

were involved in the subnetwork, but majority of the connections were again feeder and local connections.

In comparing MDD case-control difference in network connectivity for each sex, CTnet (the average edge weight of the CT-associated subnetwork) was significantly lower in MDD cases relative to controls in both females (*d*=-0.103, p<0.001) and males (*d*=-0.082, p=0.007).

Similarity of subnetworks within and between sexes

The Jaccard Index (JI) can be used to quantify the degree of the similarity of the subnetworks. It ranges from 0 (no similarity) to 1 (perfectly similar), and it is measured as the ratio of the number of observations in both sets and the number of observations in either set. Within each sex, there were minimal overlaps in the connections of the PRS- and CT-associated subnetworks (Females JI: 0.050, Males JI: 0.023; Figure 3.4A). Between sexes, there were also minimal to no overlaps in the connections of the PRS- associated subnetworks and CT-associated subnetworks (PRS JI: 0.034, CT JI: 0; Figure 3.4B). These findings show that the identified subnetworks are largely distinctive to MDD-PRS or CT and specific to each sex.

Mediation

For the PRS-associated subnetworks, there was a significant indirect effect in females (*a*=-0.088, *b*=-0.079, *c'*=0.324, *ab*=0.007, 95% CI [0.003, 0.012]; Figure 3.5A). The positive indirect effect means that higher MDD-PRS increased the risk of MDD via lower connectivity of the PRS-associated subnetwork. No significant indirect effect was observed in males (*a*=-0.076, *b*=0.021, *c'*=0.320, *ab*=-0.002, 95% CI [-0.007, 0.003]; Figure 3.5B).

For the CT-associated subnetworks, there was a significant indirect effect in females (*a*=-0.106, *b*=-0.056, *c'*=0.524, *ab*=0.006, 95% CI [0.0007, 0.012]; Figure 3.5C). The positive

indirect effect means that higher CT exposure increased the risk of MDD via lower connectivity of the CT-associated subnetwork. No significant indirect effect was observed in males (*a*=-0.114, *b*=-0.020, *c'*=0.453, *ab*=-0.002, 95% CI [-0.005, 0.010]; Figure 3.5D).

Moderated mediation

For females, there was no significant interaction between MDD-PRS and CT (c_1=-0.012, p=0.675), and between PRSnet and CT (b_1=-0.031, p=0.250; Figure 3.5E), suggesting that both direct and indirect effects of MDD-PRS on MDD did not vary across different levels of CT exposure (Figure 3.5F). The index of moderated mediation was also not significant (index=0.003, 95% CI [-0.002, 0.008]), implying that the effects of MDD-PRS and CT do not overlap and are largely independent of each other. For males, moderated mediation analysis was not done given that there was no significant mediation effect.

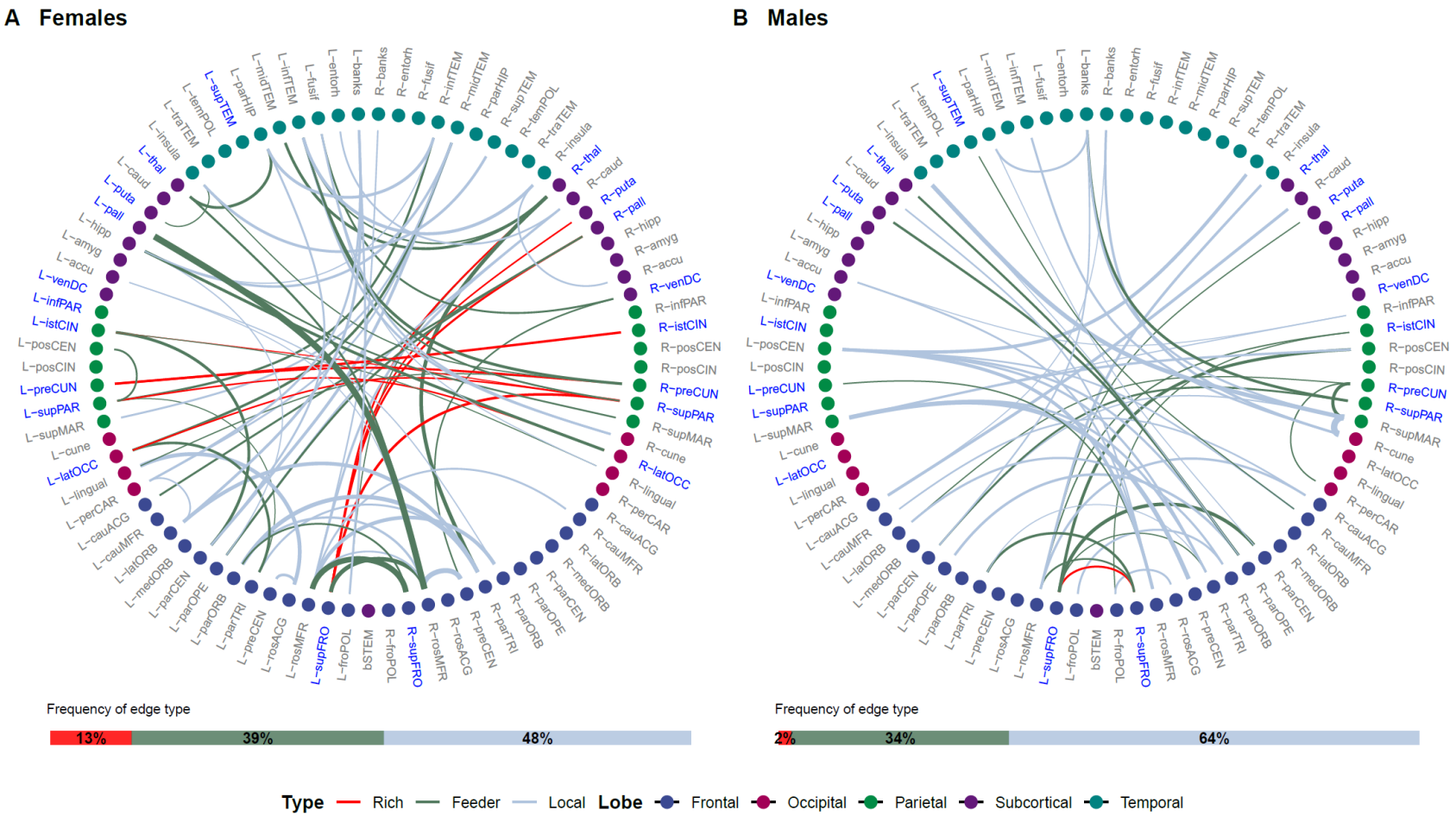

Figure 3.2. PRS-associated subnetworks for (A) females and (B) males. The colour of the nodes represent the lobe it belongs to (frontal, occipital, parietal, subcortical, and temporal) and the colour of the edges represent the type of connection (rich, feeder, or local) between a pair of nodes. The bar at the bottom of each plot represent the frequency of edge type. The edges are weighted based on the t-statistic value in the NBS analysis, with thicker edges representing a greater difference between MDD cases and controls. Hubs are highlighted in blue.

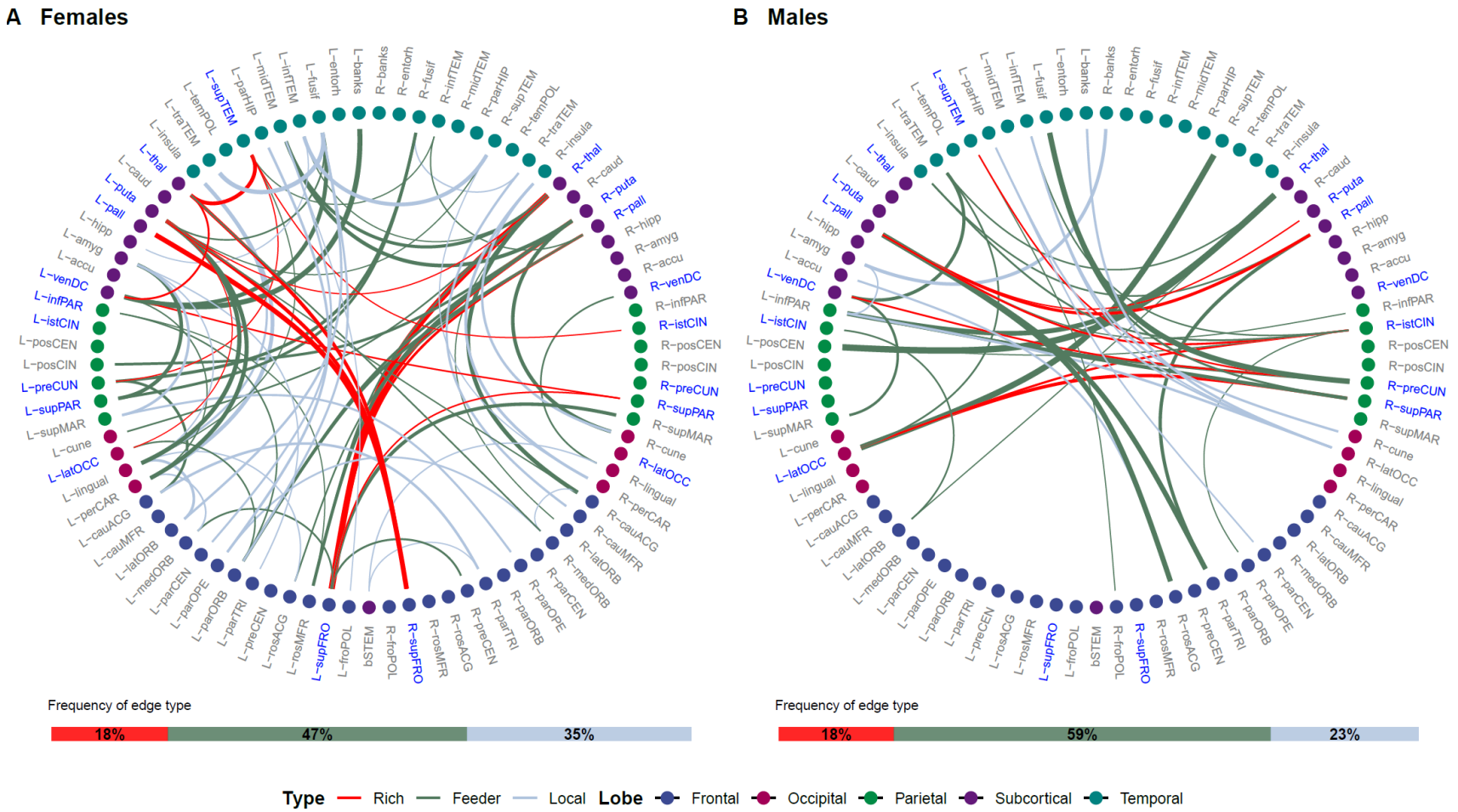

Figure 3.3. CT-associated subnetworks for (A) females and (B) males. The colour of the nodes represent the lobe it belongs to (frontal, occipital, parietal, subcortical, and temporal) and the colour of the edges represent the type of connection (rich, feeder, or local) between a pair of nodes. The bar at the bottom of each plot represent the frequency of edge type. The edges are weighted based on the t-statistic value in the NBS analysis, with thicker edges representing a greater difference between MDD cases and controls. Hubs are highlighted in blue.

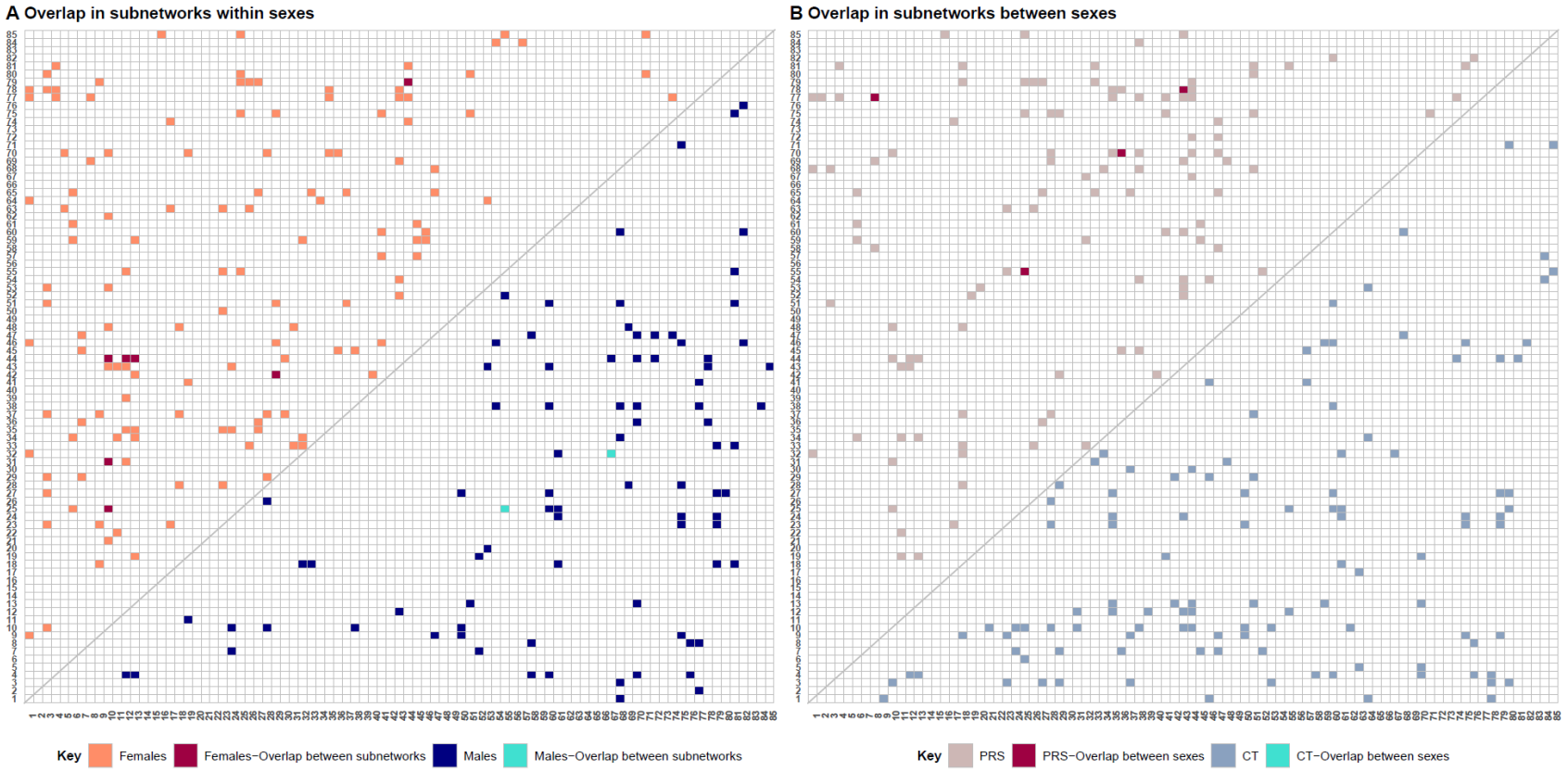

Figure 3.4. (A) Comparing the overlap between the PRS- and CT-associated subnetworks within each sex. The upper triangle represent females (F) and the lower triangle represent males (M). Regions highlighted in orange (F)/navy (M) represent all edges in both PRS- and CT-associated subnetworks, regions in red (F)/turquoise (M) represent the overlapping edges between both subnetworks. (B) Comparing the overlap between sexes for the PRS- and CT-associated subnetworks. The upper triangle represent the PRS-associated subnetworks and the lower triangle represent the CT-associated subnetworks. Regions highlighted in plum (PRS)/blue (CT) represent all edges of the subnetwork for both sexes, regions in red (PRS)/turquoise (CT) represent the overlapping edges for the subnetwork between sexes. The numbers along the axis represent the position of each node in the 85 × 85 connectivity matrix. The list of nodes and their positions is in Table S1.

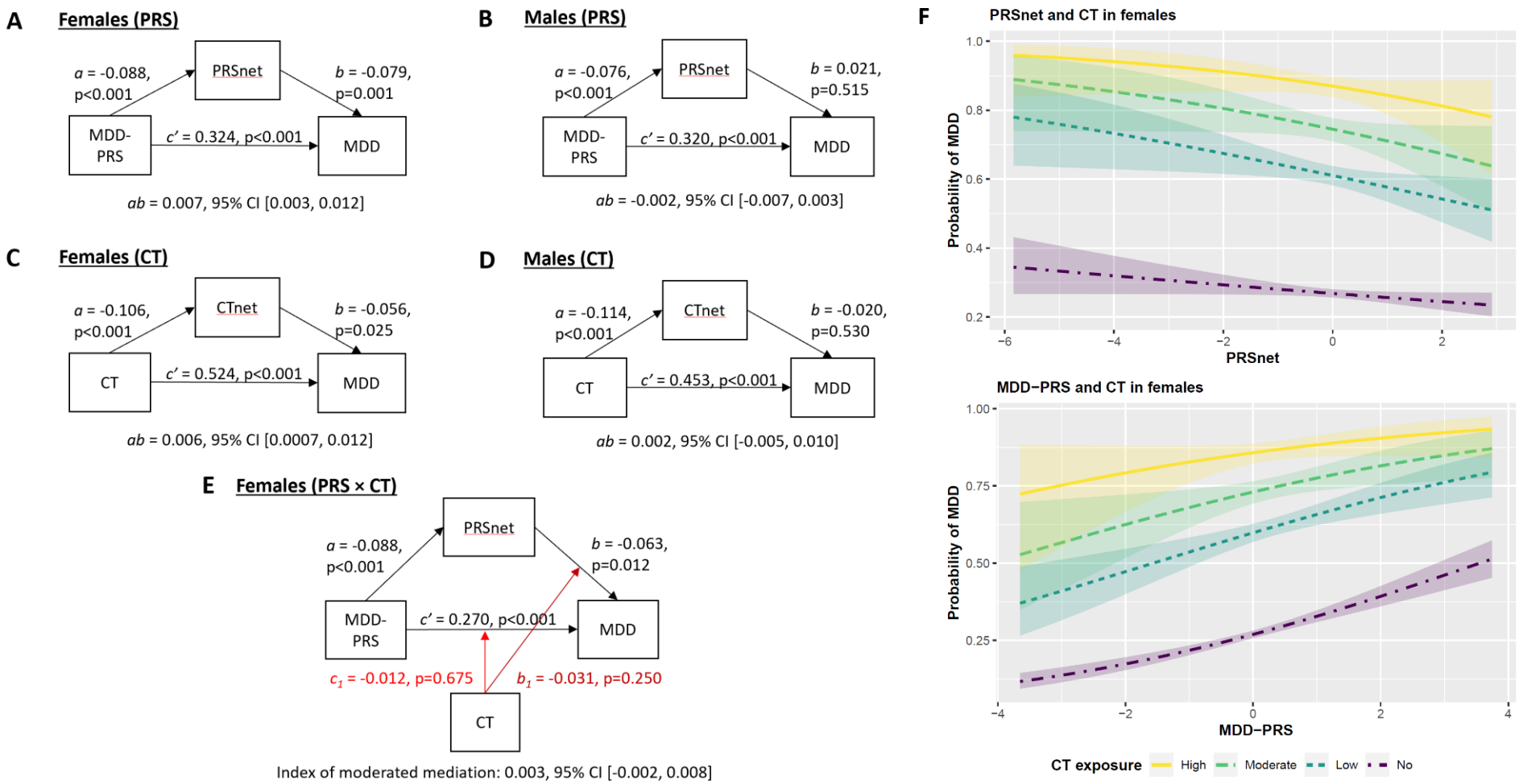

Figure 3.5. Mediation models looking at the relationship between MDD-PRS, PRSnet and MDD in (A) females and (B) males. Mediation models looking at the relationship between CT, CTnet and MDD in (C) females and (D) males. For females, (E) moderated mediation analysis was done to see if CT moderates the path between MDD-PRS and MDD (in red), and PRSnet and MDD (in dark red). (F) Interaction plot showing the interaction between CT and PRSnet (higher values of PRSnet = higher connectivity; top), and CT and MDD-PRS (bottom).

Sensitivity analyses

The results for the mediation and moderated mediation analysis for the matched female sample (N=6,812) were consistent with those in the main analysis, suggesting that the observed differences between males and females were not driven by the difference in sample sizes (Figures S1-S2; Tables S6-S7). Notably, in comparing the connections in the PRS-associated subnetwork for the matched female sample with that of the main female sample, it is useful to note that there was more consistency in terms of frequency of edge type for the feeder and local connections, as compared to the rich connections. Despite the decrease in the number of rich connections involved, the mediation effect remained significant, thus suggesting that the effects were likely to be driven by feeder and local connections instead.

Additionally, in the main female sample, CT did not significantly interact with MDD-PRS to influence the connectivity of PRSnet (β=-0.005, p=0.535), suggesting that the relationship between MDD-PRS and PRSnet is not influenced by CT.

3.2.5 Discussion

The goal of this study was to identify subnetworks associated with MDD risk factors including MDD-PRS and CT in both sexes, and to investigate their roles as mediators between MDD-PRS/CT and MDD, respectively. A key finding is that the identified subnetworks were largely distinctive to PRS or CT, and also specific to each sex. For the PRS-associated subnetwork, connectivity of the subnetwork was significantly lower in MDD cases than controls and a significant mediation effect was present (even in the sensitivity analysis) in females. The opposite findings were observed for males. For the CT-associated subnetworks, although connectivity of the subnetwork was significantly lower in MDD cases than controls in both sexes, a significant mediation effect was only present in females (even in the sensitivity analysis). For the moderated mediation analysis in females, both direct and indirect effects were, however, not moderated by CT exposure.

PRS-associated subnetworks

The prefrontal cortex (PFC), best known for its role in higher-order executive functions (e.g., decision making, working memory) (Friedman & Robbins, 2022; Yuan & Raz, 2014), was heavily involved the PRS-associated subnetworks for both sexes, thus suggesting that individuals genetically predisposed to MDD are more likely to have dysfunctions in the frontal circuits. This finding on the role of the PFC in MDD is also supported by earlier genetic (Howard et al., 2019) and neuroimaging studies (Cattarinussi et al., 2022). Specifically, there were a number of frontal-frontal connections involving the dorsolateral (DLPFC) and ventrolateral prefrontal cortex (VLPFC). Besides their roles in cognition – the DLPFC in processes such as cognitive flexibility and planning (Alvarez & Emory, 2006) and the VLPFC in response inhibition (Aron et al., 2004) – findings also suggest their involvement in emotion processing (Nejati et

al., 2022; Sturm et al., 2016). While vastly interconnected, the PFC is not exclusively responsible for executive functions, and it has extensive connections with other brain regions. In females, frontal-subcortical connections as part of the cortico-basal ganglia-thalamo-cortical loop (CBGTC; Haber, 2016) were prominent. The CBGTC loop is a system of neural circuits and those relevant to the female PRS-associated subnetwork include the DLPFC circuit and the anterior cingulate circuit (ACC), with the former implicated to a larger extent here. The DLPFC circuit mainly supports the cognitive functions described above and the ACC is mainly involved in motivated behaviour. In males, instead of frontal-basal ganglia connections, frontal-parietal connections were dominant along with frontal-frontal connections. These frontal-parietal connections likewise included regions in the DLPFC and are similarly involved in cognitive demanding tasks such as goal-directed behaviours (Marek & Dosenbach, 2018). Deficits in these regions are associated with cognitive dysfunctions (e.g., poor organisational strategies) and impaired motivation (Berlin et al., 2004; Bonelli & Cummings, 2007; Mega & Cummings, 1994). Despite the different regions implicated, both female and male PRS-associated subnetworks commonly suggest that genetic predisposition to MDD predominantly affected cognitive-related brain regions. The affected regions observed here have some overlap with previous neuroimaging studies (e.g., MDD-PRS was associated with reduced white matter integrity in thalamic radiations in Shen et al (2020)), and the associated cognitive and behavioural changes have also been observed in MDD studies (Scheurich et al., 2008; Joormann & Gotlib, 2010; Davidson et al., 2002; Zhang et al., 2018).

While there were general similarities between sexes in terms of the brain functions affected by MDD-PRS, the subnetworks between sexes were distinct. For example, it was observed here that frontal-basal ganglia regions were disproportionately affected in females for both PRS- and CT associated subnetworks, and this is in line with a recent study by Silveria

et al (2023) where they sought to identify expression quantitative trait loci (eQTLs; genetic variants that affect gene expression) among the genetic variants associated with MDD in the respective sex-specific MDD GWAS. They found that there was a highly sex-specific distribution of identified eQTLs across brain regions, with females having significantly higher eQTLs in regions including the caudate-basal ganglia and putamen-basal ganglia, as compared to males. As such, it seems that the basal ganglia regions are more susceptible to changes in females as compared to males. Sex differences remain to be further studied but these differences in the subnetwork may be possibly account for sex-specific symptoms of MDD – for example, cognition is affected in both sexes but the specific cognitive domains that are affected may differ (Mao et al., 2024).

CT-associated subnetworks

For the CT-associated subnetworks, similar observations were made in that although different regions were implicated for males and females, there was a point of convergence as the subnetworks seemed to involve more regions that are associated with sensory/social-related functions. For females, frontal-basal ganglia circuits like the DLFPC circuit and ACC circuit described above were again dominant, but with the inclusion of the orbitofrontal circuit (OFC). The OFC modulates social control/socially appropriate behaviour (Berlin et al., 2004) and plays a role in decision making for reward-related behaviours (Rolls et al., 2020). Dysfunctions in the OFC circuits are associated with irritability, loss of empathy and social functioning (Berlin et al., 2004; Stone et al., 1998; Mega & Cummings, 1994). For males, there were no dominant connections but there was generally an increase in parietal, temporal and occipital connections with each other and with the basal ganglia regions, an observation that can be seen in females as well. The processes which these regions are involved in are interlinked –

e.g., parietal regions are involved in functions such as processing of somatosensory inputs from the thalamus, the occipital regions are mainly involved in visual processing, and the temporal regions are involved in auditory processing and also in the memory system (Jawabri & Sharma, 2023). Our findings here complement previous CT neuroimaging studies that found gray matter changes in similar regions (Hanson et al., 2010), such as in a recent large-scale study by ENIGMA whereby cortical volume and surface area of temporal and parietal regions were disproportionately affected (Tozzi et al., 2020). The symptoms associated with dysfunction in these areas are symptoms observed in MDD as well (Kupferberg et al., 2016; Rolls et al., 2020).

As with the PRS-associated subnetworks, while there were general similarities between sexes in terms of the brain functions affected by CT, the distinctiveness of the subnetworks between sexes suggest that the underlying mechanisms may differ. The absence of overlap in the CT-associated subnetworks may potentially be associated with the difference in the type of abuse experienced by males and females. For example, emotional and sexual abuse are more commonly reported and have stronger associations with psychopathology in females, as with emotional and physical neglect in males (Prachason et al., 2023). However, as our study does not have sufficient information to look into CT subtypes, this remains conjectural and can be looked at in more depth in future studies.

Type of connections in the subnetworks

Notably, the type of connections involved in the subnetworks may partly explain the sex differences in the findings, specifically with regards to network connectivity differences between MDD cases and controls and the presence or absence of a significant mediation effect. In a study by Zhao et al (2021), they found that cognitive function was differentially

associated with regional structural-functional coupling (SC-FC) in males and females – poorer working memory in females was related to weaker SC-FC coupling in non-hub connections while better reasoning ability was related to stronger SC–FC coupling in rich connections. Similarly, Vandewouw et al (2023) also observed sex-specific developmental trajectories of the rich club organisation, with females engaging more distributed and less rich-club-centric networks by adolescence, as compared to males. In line with these findings, our findings here showed that there were more rich connections in the CT-associated subnetwork as compared to the PRS-associated subnetwork for males, and this coincided with the presence and absence of a significant reduction in subnetwork connectivity in MDD cases relative to controls, respectively. For females, in comparing the main and matched samples, feeder and local connections, especially for the PRS-associated subnetwork, were found to be more consistent in both samples and hence, were likely the ones driving the significant findings instead of the rich connections. As such, the type of connections affected by MDD-PRS or CT seem to be important in males and females, as structural changes in regions where SC-FC coupling is stronger will have a greater impact on function. As this study only utilised a single UKB cohort, the analyses here can be repeated in another large-scale cohort to confirm the role of the type of connections in males and females. Of note, the lack of significant mediation effect by the CT-associated subnetwork in males does not necessarily diminish its role in MDD, but it suggests that CT may operate through other biological pathways (Berens et al., 2017) to a larger extent as compared to the brain. This can be further investigated, perhaps by using a multiple mediator model.

Distinctive effects of MDD-PRS and CT on the structural connectome

Besides the differences in the PRS- and CT-associated subnetworks between sexes, it is also clear that the PRS- and CT-associated subnetwork within each sex were largely distinct from each other. As discussed earlier, MDD-PRS and CT seem to affect different domains of the structural connectome, with MDD-PRS affecting cognitive-related regions and CT affected social/sensory-related regions to a larger extent. Due to this distinctiveness, it may be why there was no significant interaction between CT and MDD-PRS and the PRS-associated subnetwork in the moderated mediation analysis for the females. The effects of both MDD risk factors likely work alongside each other to bring about the wide range of cognitive, affective, somatic issues that characterise MDD. The lack of significant interaction between MDD-PRS and CT was also previously reported in a meta-analytic study Peyrot et al (2018).

While the absence of a significant moderated mediation effect may be a true finding and was expected given the lack of overlapping regions between the PRS- and CT-associated subnetworks in this sample, there might be other factors involved, such as sample size and the type of interaction effect studied For example, multiplicative interaction (the combined effects of MDD-PRS and CT is greater than the product of their individual effects) was studied here due to the use of a binary measure of MDD, but significant findings were previously reported only for additive interaction (the combined effects of MDD-PRS and CT is greater than the sum of their individual effects), which is thought to better capture the biological mechanisms of gene × environment (Knol et al., 2007). This was demonstrated in Thorp et al (2023) and Coleman et al (2020), which had sample sizes ranging from 102,182 to 126,522 subjects. The study by Peyrot et al (2018) mentioned earlier likewise looked at additive interaction but did not observe a significant effect possibly due to the smaller sample size of N=5,765. As such, this is an area to follow-up on. The analysis can be repeated in a larger sample using a continuous outcome variable to test for additive interaction effects.

Strengths and limitations

This is one of the largest studies looking structural connectomic associations with MDD-PRS and CT in males and females separately. Limitations should, however, be considered. Firstly, results from connectomic studies are dependent on the type of processing conducted (e.g., atlas, thresholding and tractography parameters) (Adamovich et al., 2022; Wei et al., 2017). Secondly, CT in UKB was measured using the screening version of the original questionnaire, with just one question for each of the five types of childhood trauma. Due to limited information, we also did not look into CT subtypes, which may have different effects on the brain, and possibly different roles in males and females (Teicher et al., 2022; Everaerd et al., 2016). In addition, UKB is a community-based cohort with relatively healthy participants, and majority of the subjects had no or low CT. It will be beneficial to repeat the above analyses in a well-powered cohort using a more comprehensive CT variable with a good distribution of subjects with no, low, moderate, and high exposure to CT, to check that the results hold and in order to extend to different CT subtypes. Lastly, our results may not generalise to other ethnic groups as our sample was restricted to individuals of European ancestry (important for the calculation of MDD-PRS). While we acknowledge the above limitations, we believe that our results help to provide a starting point for future in-depth analyses. The large sample size also ensures enough statistical power to detect the small effects that are characteristic of brain-based differences.

Conclusion

The key takeaways of this study are that MDD-PRS and CT both affect structural connectivity but in unique regions, and there are potential sex differences in the mechanisms underlying MDD. From a clinical perspective, given that separate networks are impacted by MDD-PRS and CT, it might be that particular therapeutic approaches would work better for people who have/have not been traumatised, or who do/do not have a strong family history. This work can be extended in future studies by looking into the specific subtypes of CT and MDD, which may be differentially associated with the structural connectome, and also by extending to functional connectomes to further elucidate the structure-function relationships.

3.3 Chapter conclusion

The results in this chapter highlight the importance of considering both gene and environmental risk factors in the study of a complex and multifactorial disorder like MDD, due to their potential additive effects on the structural connectome. The results in this chapter also showed that MDD risk factors have differential associations with male and female structural connectomes, with connectome mediation effects only observed in females.

Chapter 4: Comparing personalised brain-based and genetic risk scores for Major Depressive Disorder in large population samples of adults and adolescents

4.1 Chapter introduction

The availability of large neuroimaging datasets coupled with collaborative efforts have allowed for significant progress to be made in identifying robust brain structural differences in MDD (Schmaal et al., 2016, 2017; van Velzen et al., 2020). This then calls for the translation of these population-level findings to the individual level, specifically to test if these findings can be used to assess an individual's vulnerability to MDD. Personalised approaches are especially important in the context of MDD, due to its large heterogeneity between individuals. Although MDD-PRS, a personalised genetic risk score, is rather well-established in the field, its use is limited as it only captures genetic risk, which explains a small proportion of variance in MDD. To this end, brain-based personalised scores may come in useful, as the dynamic nature of the brain is able to capture risk exposures beyond that of genetic risk. This chapter thus presents a study looking at a relative new method of constructing brain-based risk score and compared its performance with that of MDD-PRS in terms of their strength of association with MDD. GS, also called GS-Imaging in this chapter, was used as the main adult sample (N=702). Due to MDD having an early onset during adolescence, it was also of interest to investigate the similarities of brain features of adolescent depression with adult MDD, and also to test if it is possible to predict the trajectory of adolescent MDD. This was done using a large adolescent sample from the ABCD study, using data from the baseline (N=3,805) and two-year follow-up (N=2,081) timepoint.

4.2 Manuscript

This study has been published in *European Psychiatry*, titled "Comparing personalised brain-based and genetic risk scores for Major Depressive Disorder in large population samples of adults and adolescents" (Thng et al. 2022). As the first author, I conceived the hypotheses, conducted the analyses, and wrote the manuscript under supervision.

4.2.1 Abstract

Major Depressive Disorder (MDD) is a polygenic disorder associated with brain alterations but until recently, there have been no brain-based metrics to quantify individual-level variation in brain morphology. Here, we evaluated and compared the performance of a new brain-based 'Regional Vulnerability Index' (RVI) with polygenic risk scores (PRS), in the context of MDD. We assessed associations with syndromal MDD in an adult sample (N=702, age=59±10), and with subclinical depressive symptoms in a longitudinal adolescent sample (baseline N=3,825, age=10±1; two-year follow-up N=2,081, age=12±1).

MDD-RVIs quantify the correlation of the individual's corresponding brain metric with the expected pattern for MDD derived in an independent sample. Using the same methodology across samples, subject-specific MDD-PRS and six MDD-RVIs based on different brain modalities (subcortical volume, cortical thickness, cortical surface area, mean diffusivity, fractional anisotropy, and multimodal) were computed.

In adults, MDD-RVIs (based on white matter and multimodal measures) were more strongly associated with MDD (β=0.099–0.281, pFDR=0.001-0.043) than MDD-PRS (β=0.056-0.152, pFDR=0.140-0.140). In adolescents, depressive symptoms were associated with MDD-PRS at baseline and follow-up (β=0.084-0.086, $p=1.38\times10^{-4}$-4.77×10^{-4}), but not with any MDD-RVIs (β<0.05, p>0.05).

Our results potentially indicate the ability of brain-based risk scores to capture a broader range of risk exposures than genetic risk scores in adults and are also useful in helping us to understand the temporal origins of depression-related brain features. Longitudinal data, specific to the developmental period and on white matter measures, will be useful in informing risk for subsequent psychiatric illness.

4.2.2 Introduction

Major Depressive Disorder (MDD) is a serious psychiatric disorder that significantly contributes to global disease burden (GBD 2019 Diseases and Injuries Collaborators, 2020; Whiteford et al., 2013). Large-scale neuroimaging approaches, such as the Enhancing Neuro Imaging Genetics through Meta-Analysis (ENIGMA) consortium, have greatly advanced the field by contributing robust findings on brain structural abnormalities associated with MDD (Schmaal et al., 2016, 2017; van Velzen et al., 2020; Anderson et al., 2020). However, these findings have limited clinical utility as they are based on group-level inferences and cannot be generalised across individuals that can have very different MDD profiles. This reflects the need for a more personalised approach to improve understanding of the biological origins of MDD. Recently, several novel brain-based metrics have been introduced to capture individual-level variation in brain morphology (Doucet et al., 2019; Antoniades et al., 2021; Kochunov et al., 2019, 2021, 2022a, 2022b). We focus here on the Regional Vulnerability Index (RVI) (Kochunov et al., 2019, 2021, 2022a, 2022b).

RVI is a personalised score that quantifies the degree of similarity (i.e., a correlation coefficient) between an individual's brain pattern and the expected pattern of brain differences seen in a disorder, as determined by case-control effect sizes derived from large-scale meta-analyses (e.g., ENIGMA). Higher RVI indicates a stronger correlation and therefore,

a higher vulnerability to the given disorder. An example would be that RVI based on white matter microstructural measures has been shown to differentiate schizophrenia patients from controls in clinical samples (Kochunov et al., 2019, 2022a), and also MDD cases from healthy individuals in a large epidemiological sample (Kochunov et al., 2021).

In this study, we derived six MDD-RVIs using different brain modalities (subcortical volume, cortical thickness, cortical surface area, mean diffusivity, fractional anisotropy and multimodal) and examined their associations with syndromal MDD in a large adult sample. The comparison across modalities will help in identifying tissue types that are most implicated in MDD. Besides comparing MDD-RVIs, this study also evaluated the performance of MDD-RVIs relative to polygenic risk scores (PRS) for MDD. PRS is derived from the weighted sum of the number of risk alleles in an individual and has been shown to be associated with MDD across samples (Wray et al., 2018; Howard et al., 2019). We were therefore interested in using MDD-PRS as a benchmark to evaluate the validity of MDD-RVI in terms of effect sizes and sought to ascertain if both scores combined could account for more variation in disease risk than when used in isolation. Our hypothesis was that MDD-RVIs will show stronger associations with MDD than MDD-PRS, as the dynamic nature of brains structure across the lifespan may capture signals of additional risk factors beyond genetic risk that influence disease course.

Additionally, we repeated the analysis in a large adolescent sample, given that adolescence is the peak period for the onset of MDD (Giedd et al., 2008; Thapar et al., 2012; Casey et al., 2019). However, adolescent MDD is often undiagnosed as symptoms are covert (Mullen, 2018), resulting in continuity to adulthood (Carballo et al., 2011). We considered the investigation of MDD-RVI and MDD-PRS in the younger sample as exploratory, to determine the association between these personalised scores with cross-sectional and subsequent

subclinical depressive symptoms. Specifically, MDD-RVIs for adolescents will be derived using effect sizes based on the adult meta-analyses in ENIGMA, to ensure sufficient statistical power and to see if brain features of vulnerable adolescents are similar to the adult MDD brain phenotypes. If brain-psychopathology associations are beginning to be established, this would have important implications for the identification of adolescents at increased risk of MDD. A continuous measure of depressive symptoms was used for the younger sample to better accommodate diagnostic uncertainty and capture the entire spectrum of severity (Bjelland et al., 2009).

4.2.3 Methods

Participants

Adult participants were from the deeply phenotyped imaging subsample of Generation Scotland: the Scottish Family Health Study (GS-Imaging). GS-Imaging received ethical approval from the NHS Tayside research ethics committee and all participants provided informed consent (reference 14/SS/0039). Information on the recruitment, assessment and brain imaging procedures for this sample has been provided elsewhere (Habota et al., 2021). The full GS-Imaging sample included 1,188 adults recruited across two sites in Scotland. The currently analysis comprised 702 unrelated and neurologically healthy individuals of European ancestry (age: 59±10, 59% female). Further details in Table 4.1 and in the supplementary materials.

Adolescent participants were from the Adolescent Brain and Cognitive Development (ABCD) study. The baseline sample comprised 11,875 youths recruited across 21 sites in the United States. Ethical approval was obtained from a central or local institutional review board

(Auchter et al., 2018). Informed consent and assent were obtained from all parents and participants. Baseline and follow-up data from curated annual release 2.0 and 3.0, respectively, were obtained through the NDA database (https://nda.nih.gov/general-query.html?q=query=featured-datasets:Adolescent%20Brain%20Cognitive%20Development%20Study%20(ABCD); Federal-Wide Assurance: FWA00018101). The analysis sample comprised 3,825 unrelated and neurologically healthy individuals of European ancestry at baseline (age: 10±1, 47% female) and a subset of 2,081 individuals (age: 12±1, 44% female) at two-year follow-up. Further details in Table 4.1 and in the supplementary materials.

Table 4.1. Demographic information for GS-Imaging, ABCD (Baseline) and ABCD (Two-year). For the calculation of MDD-RVIs in our sample, subjects were deemed as healthy if they did not self-report any psychiatric diagnoses and were not taking antidepressants at the point of assessment.

		Unit	GS-Imaging	ABCD (Baseline)	ABCD (Two-year)
Demographics	Sample size	N	702	3,825	2,081
	Age	years ± SD	59 ± 10	10 ± 1	12 ± 1
	Sex	% Females	59	47	44
MDD-RVI	Subcortical	N (Healthy)	702 (524)	3,825 (3,218)	2,081 (1,732)
	Cortical	N (Healthy)	702 (524)	3,825 (3,218)	2,081 (1,732)
	DTI	N (Healthy)	686 (508)	3,630 (3,056)	2,032 (1,698)
MDD-PRS	MDD-PRS	N	702	3825	2081
Depressive Phenotypes	Lifetime-MDD	N (Cases/Controls)	602 (223/379)	-	-
	TotalQIDS	N	702	-	-
		Mean ± SD	4.5 ± 3.7	-	-
	CBCL-DSM Depressed	N	-	3,825	2,081
		Mean ± SD	-	1.3 ± 2.0	1.6 ± 2.3

Imaging Measures

For GS-Imaging, T1-weighted imaging and diffusion imaging data were obtained using the same protocol at either the Aberdeen study site (3T Philips Achieva TX-series MRI system Philips Healthcare, Best, Netherlands) or at the Dundee study site (Siemens 3T Prisma-FIT Siemens, Erlangen, Germany). T1 scans were processed using FreeSurfer 5.3.0 and the Desikan-Killiany atlas (Desikan et al., 2006) was used for subcortical segmentation and cortical parcellation. Fractional anisotropy (FA) and mean diffusivity (MD) for white matter tracts were derived using TBSS toolkit within FSL following the ENIGMA DTI analysis protocol (http://enigma.ini.usc.edu/protocols/dti-protocols/). The John-Hopkins University white matter atlas (Mori & van Zijl, 2007) was used to define white matter tracts. Full details on image acquisition and quality control measures are described in the supplementary materials and elsewhere (Habota et al., 2021; Stolicyn et al., 2020; Green et al., 2021).

For ABCD, minimally processed data for baseline and two-year follow-up from the ABCD repository were used. Participants were scanned at 21 sites using 3T Siemens Prisma, General Electric 750 or Phillips scanner. Data acquisition and image processing methods were harmonised between sites and scanners (Hagler et al., 2019; Casey et al., 2018). T1 scans were processed using FreeSurfer 5.3.0 and the Desikan-Killiany atlas was used for subcortical segmentation and cortical parcellation. Major white matter tracts were labelled using AtlasTrack (Hagler et al., 2009). Quality control was conducted following recommendations from the ABCD data team (Hagler et al., 2019), and full details in the supplementary materials.

Regional Vulnerability Index

MDD-related alterations in subcortical volume (Schmaal et al., 2016), cortical surface area and thickness (Schmaal et al., 2017), and tract-based MD and FA measures (van Velzen et al.,

2020) were established by ENIGMA. Case-control effect sizes from these meta-analyses (Tables S1 to S4) were used as the reference data. MDD-RVIs were computed using the RVIpkg package (version 0.2.3) in R (https://cran.r-project.org/web/packages/RVIpkg/RVIpkg.pdf) and following the procedures specified by Kochunov et al (2022b). Briefly, for each brain region used in the calculation of an MDD-RVI type, the effects of covariates were first regressed out (see supplementary materials) and the residuals were z-normalised using the mean and standard deviation of healthy individuals in the sample. Subject-specific MDD-RVI was then calculated as a single Pearson's correlation coefficient between the vector of the region-wise z-values and the corresponding regional effect sizes in the ENIGMA meta-analyses (see Figure 4.1A and the supplementary materials for details). The procedures were conducted separately for GS-Imaging and ABCD to define six MDD-RVIs for each subject: RVI-Sub for subcortical volumes, RVI-CorTH for cortical thickness, RVI-CorSA for cortical surface area, RVI-MD for mean diffusivity, RVI-FA for fractional anisotropy, and RVI-Multi, a multimodal index calculated as the average of the five RVIs (Figure 4.1B). GS-Imaging and ABCD were not part of the ENIGMA meta-analyses, thus ensuring no overlap between the discovery and testing samples.

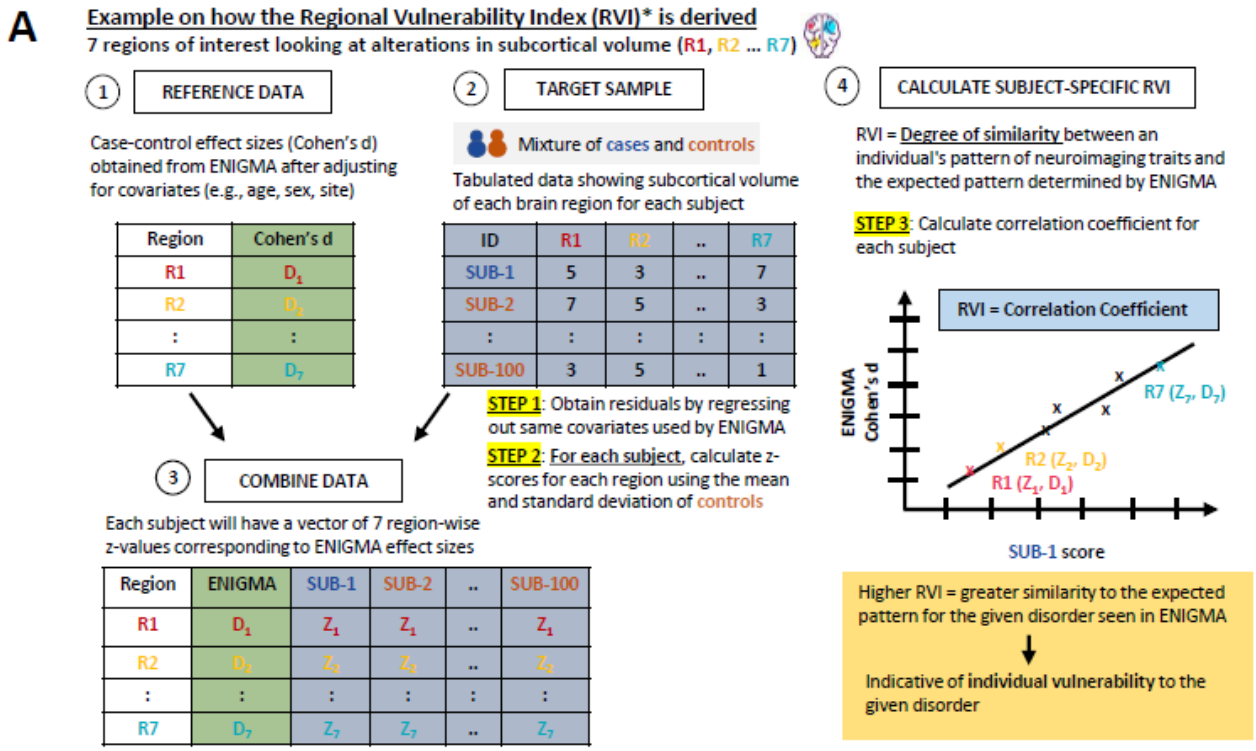

*Kochunov P, Fan F, Ryan MC, Hatch K S, Tan S, Jahanshad N, *et al*. Translating ENIGMA schizophrenia findings using the regional vulnerability index: Association with cognition, symptoms, and disease trajectory. *Hum Brain Mapp* 2020; 43: 566-575.

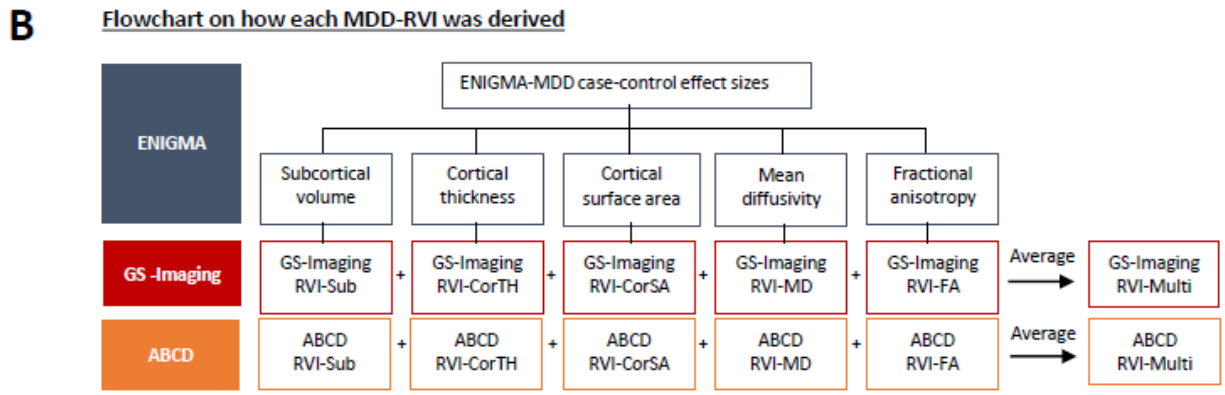

Figure 4.1. (A) A brief explanation on how MDD-RVIs for each modality is calculated, using alterations in subcortical volume as an example. The RVI method was developed by Kochunov et al (2022b). (B) The different types of MDD-RVIs that were derived for the GS-Imaging and ABCD samples, using MDD case-control effect sizes from ENIGMA meta-analyses.

Polygenic Risk Scores

For GS-Imaging, MDD-PRS was calculated for the full GS cohort, as detailed in Howard et al (2019). Briefly, standard quality control measures and imputation using the Haplotype Reference Consortium dataset (Nagy et al., 2017) were undertaken before deriving MDD-PRS using Plink v1.90b4 (Chang et al., 2015). For the current analysis, only MDD-PRS for individuals within the GS-Imaging sample were included. Six p-value thresholds (pT_0.001, pT_0.01, pT_0.05, pT_0.1, pT_0.5 and pT_1) were considered but only results for pT_0.1 are reported as the score at this threshold outperformed scores at different thresholds in this analysis in terms of effect sizes.

For ABCD, the ABCD team conducted quality control on the genotyped data following the Ricopili pipeline (Lam et al., 2020) and then imputation using mixed ancestry and Eagle v2.4 phasing on the TOPMed imputation server using the full sample. Here, we only used imputed genetics data from unrelated individuals of European ancestry. In this subsample, we did post-imputation quality control by filtering out variants with INFO<0.8 and minor allele frequency <0.005. PRSice v2.1.11 (Choi & Reilly et al., 2019) was used to calculate MDD-PRS using summary statistics by Howard et al (2019) using the clumping and thresholding method (clump-p=1, clump-r2=0.25, clump-kb=250kb). A description of the phenotypes used in the summary statistics can be found in the supplement. A linkage disequilibrium reference panel using the 1000 Genomes central European population (The 1000 Genomes Project Consortium et al., 2015) was specified. MDD-PRS were obtained across the same p-value thresholds as in GS-Imaging, and pT_0.1 was chosen for subsequent analysis.

Depressive Phenotypes

For GS-Imaging, participants rated their symptoms over the past seven days using a four-point Likert scale on the Quick Inventory of Depressive Symptomatology (QIDS; Rush et al., 1986). The total score (TotalQIDS) was used as a dimensional measure of current depressive symptoms. Categorical lifetime diagnosis of MDD (Lifetime-MDD) was determined using the Composite International Diagnostic Interview Short Form (CIDI-SF; Kessler et al., 1998) and the Structured Clinical Interview for DSM disorders (SCID; First et al., 2002). Both assessments were administered at overlapping intervals and were thus used to detect more MDD cases. Participants were defined as cases if they met the diagnostic criteria for CIDI or SCID, and controls if they did not meet the criteria for both.

For ABCD, the primary caregiver completed the Child Behavioural Checklist (CBCL; Achenbach, 2009) by rating the child's behaviour over the last six months using a three-point Likert scale (Barch et al., 2018). Only caregiver-reported scores were used, as child-reported scores were not available. Other instruments completed by both caregiver and child were considered suboptimal, as binary measures may not be as effective in accommodating diagnostic uncertainty in adolescents. The total raw scores for the CBCL DSM-oriented depressive problems subscale (CBCL-DSM-Depressed) obtained at baseline and two-year follow-up were used as dimensional measures of current depressive psychopathology.

Statistical Analysis

All statistical analyses were conducted using R (version 3.6.3). The associations between MDD-RVIs/MDD-PRS with depressive phenotypes were assessed separately in GS-Imaging and ABCD. For GS-Imaging, we used linear and logistic regression for models with TotalQIDS and Lifetime-MDD as outcomes, respectively. For ABCD, study site was modelled as a random

effect in linear mixed models to account for the nested structure of the data. In GS-Imaging, site was included as a covariate as subjects were recruited only across two sites. In all models, covariates included age, age^2, sex, site (for GS-Imaging), individual/parent education level and family income (Kochunov et al., 2022a). We additionally controlled for the top 15 genetic principal components and genotype plate number for analyses that included MDD-PRS as predictor. False discovery rate correction (FDR) was applied within each MDD-RVI type and within the selected MDD-PRS p-value threshold (pT_0.1). The change in R^2 was used to quantify the individual and combined explanatory power of MDD-RVI/MDD-PRS in terms of improvements in model fit relative to the null model (which only included covariates). The McFadden's pseudo R^2 and marginal R^2 were used for logistic and linear mixed models, respectively. Analysis using the Akaike Information Criterion (AIC) was conducted to provide further evidence for the R^2 analysis. The above analytic approach was repeated for ABCD baseline and two-year follow-up. We examined associations with CBCL-DSM-Depressed at each time point, and with the change in symptoms between assessments. For the latter, we adopted a residualised change approach (Castro-Schilo & Grimm, 2018), whereby we residualised the two-year CBCL-DSM-Depressed scores by regressing out baseline scores, sex, age difference, parent education, family income and study site. Residuals were then regressed against baseline MDD-RVIs and MDD-PRS.

4.2.4 Results

Association between MDD-RVIs and depressive phenotypes

For GS-imaging, Lifetime-MDD was strongly associated with RVI-MD (β=0.281, pFDR=0.001), RVI-FA (β=0.206, pFDR=0.043) and RVI-Multi (β=0.241, pFDR=0.021) (Figure 4.2A). Similar

results were found for TotalQIDS for RVI-FA (β=0.085, pFDR=0.043) and RVI-Multi (β=0.099, pFDR=0.021), but not RVI-MD (β=0.052, pFDR=0.169). Subcortical and cortical-based RVIs had no associations with either depressive phenotype (pFDR>0.05).

For ABCD, CBCL-DSM-Depressed score was not associated with any MDD-RVIs either at baseline or at the two-year follow-up (β<0.05, p>0.05, Figure 4.3A).

Association between MDD-PRS and depressive phenotypes

For GS-Imaging, MDD-PRS (at pT_0.1) was not associated with Lifetime-MDD (β=0.152, pFDR=0.140) and TotalQIDS (β=0.056, pFDR=0.140, Figure 4.2A). The results for other p-value thresholds of PRS are reported in Figure S3. This finding may be related to reduced power in the imaging sample as analyses using the full unrelated GS sample (N=6,946, including non-imaged participants; Howard et al., 2019) revealed strong associations between MDD-PRS and lifetime MDD at all p-value thresholds (β=0.182-0.204, $p=1.14\times10^{-7}$–1.57×10^{-6}, Figure S4A).

For ABCD: MDD-PRS was associated with CBCL-DSM-Depressed score at baseline (β=0.086, $p=4.77\times10^{-4}$) and at two-year follow-up (β=0.084, $p=1.38\times10^{-4}$, Figure 4.3A). Results for other p-value thresholds are reported in Figure S6.

Comparing associations of MDD-RVI and MDD-PRS with depressive phenotypes

For GS-Imaging, the effect sizes for the associations of RVI-MD, RVI-FA and RVI-Multi with Lifetime-MDD (β=0.206-0.281, pFDR=0.001-0.043) were higher than for MDD-PRS (at pT_0.1) (β=0.152, pFDR=0.140, Figure 4.2A). The same was observed for RVI-Multi (β=0.099, pFDR=0.021) and MDD-PRS (β=0.056, pFDR=0.140, Figure 4.2A) in their associations with TotalQIDS.

For ABCD, the effect sizes for the association between CBCL-DSM-Depressed for all RVIs ($\beta<0.05$, $p>0.05$) were consistently lower than those for MDD-PRS (at pT_0.1) at both time points ($\beta=0.084$-0.086, $p=1.38\times10^{-4}$–4.77×10^{-4}, Figure 4.3A), and for other p-value thresholds (Figure S6).

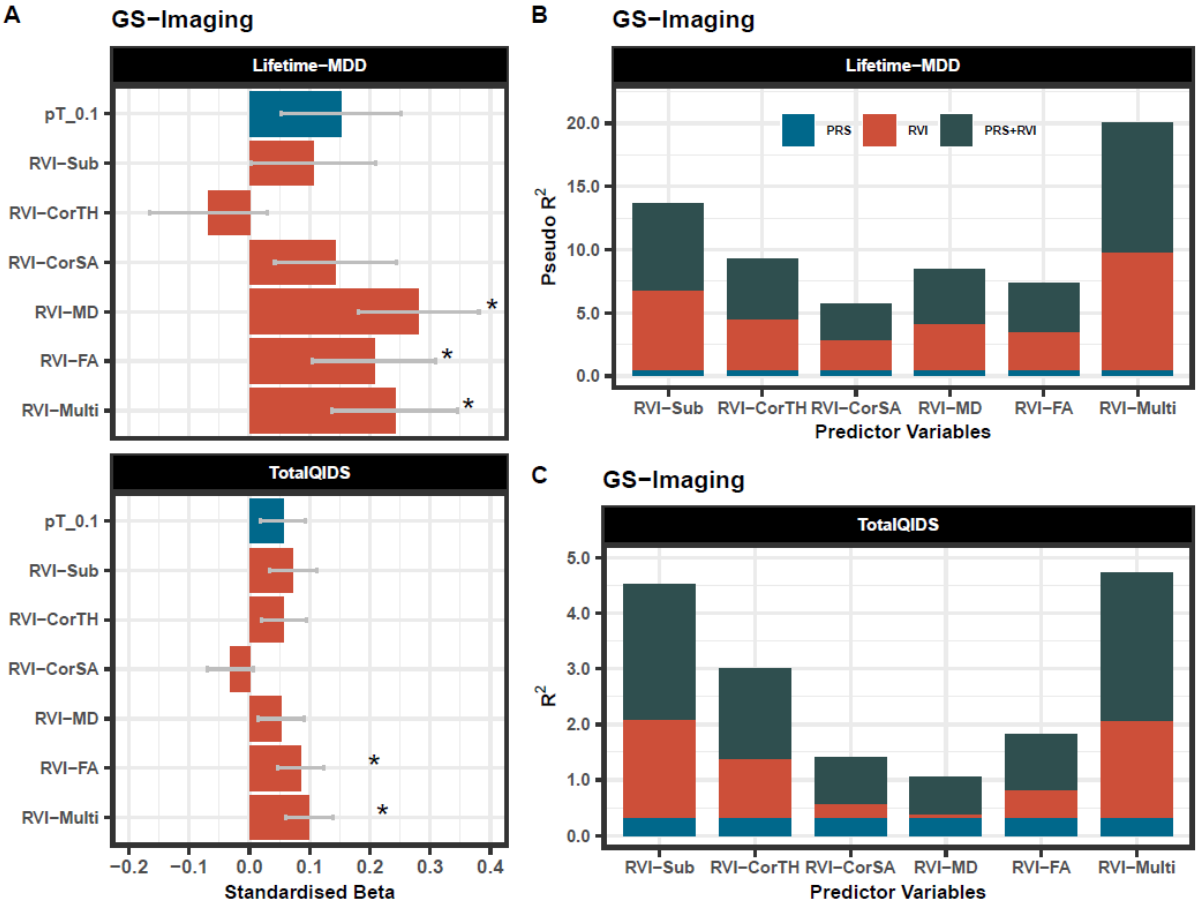

Figure 4.2. (A) Association between MDD-RVIs/MDD-PRS with Lifetime-MDD and TotalQIDS in GS-Imaging. The x-axis represents the standardised effect sizes and the y-axis represent the different MDD-RVIs and the MDD-PRS calculated at pT_0.1 threshold. (B) The change in McFadden Pseudo-R^2 (in %) contributed by each variable type (PRS, RVI or PRS + RVI) when compared to a null model (i.e., covariates only) for Lifetime-MDD. (C) The change in R^2 (in %) contributed by each variable type (PRS, RVI or PRS + RVI) when compared to a null model (i.e., covariates only) for TotalQIDS.

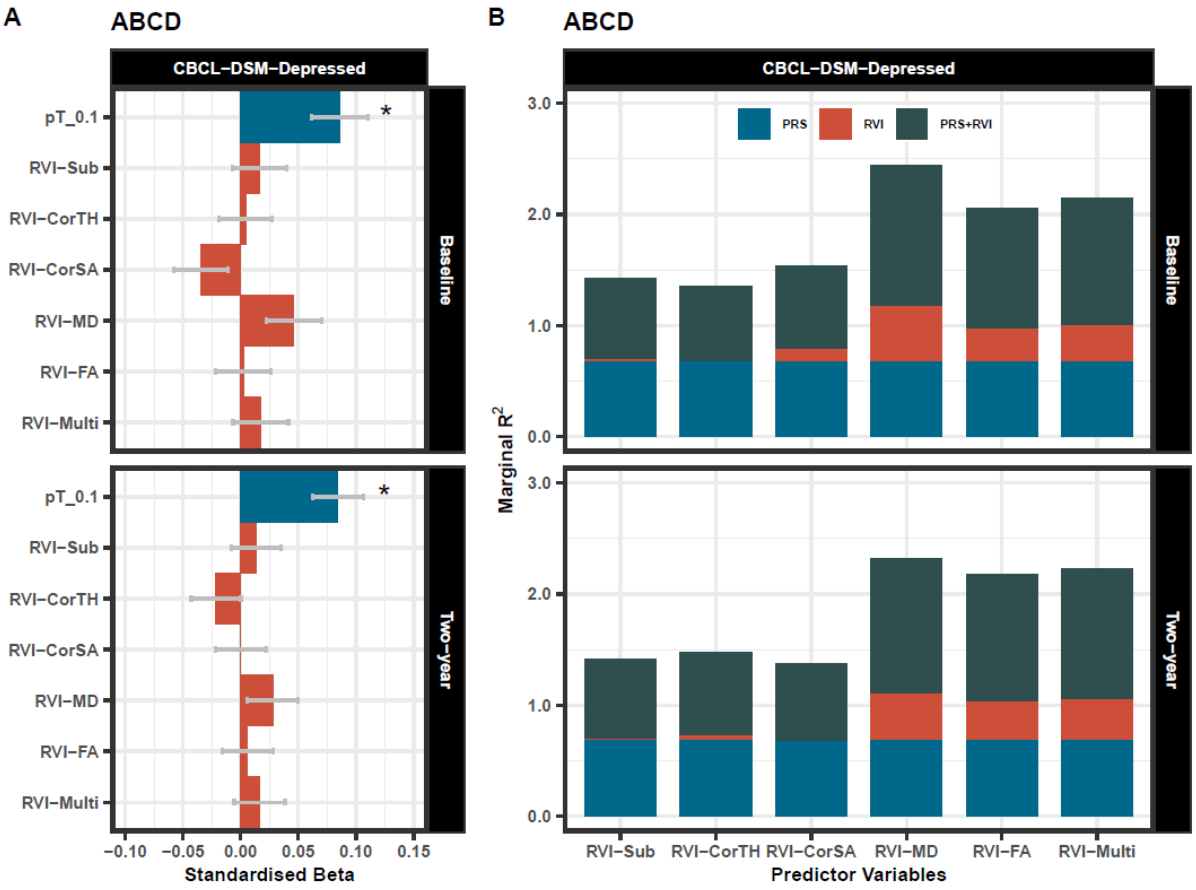

Figure 4.3. (A) Association between MDD-RVIs/MDD-PRS with CBCL-DSM-Depressed in ABCD at baseline and at two-year follow-up. The x-axis represents the standardised effect sizes and the y-axis represent the different MDD-RVIs and the MDD-PRS calculated at pT_0.1 threshold. (B) The change in marginal R^2 (in %) contributed by each variable type (PRS, RVI or PRS + RVI) when compared to a null model (i.e., covariates only) for CBCL-DSM-Depressed. The results at baseline and two-year follow-up are reported.

Comparing change in R^2 and AIC values of different model types using MDD-RVI and MDD-PRS as individual or combined predictors of depressive phenotypes

For GS-Imaging, in models with Lifetime-MDD as the outcome, each MDD-RVI individually contributed to a greater change in R^2 (Pseudo-R^2 = 2.5-9.5%) than MDD-PRS (Pseudo-R^2 = 0%), with the strongest effect from RVI-Multi (Figure 4.2B). All MDD-RVIs contributed towards an improvement in model fit individually (compare M1 and M2) and additively with MDD-PRS (compare M3, M4 and M5) given the relative decrease in AIC values upon the addition of MDD-RVIs (Table 4.2). RVI-Multi contributed towards the largest decrease in AIC value in the full model relative to the null model. A similar pattern was observed with TotalQIDS as the outcome: all MDD-RVIs contributed towards an improvement in model fit individually and in combination with MDD-PRS (Table 4.2). Likewise, RVI-Multi contributed the largest change in R^2 individually (R^2 = 1.8%, Figure 4.2C) and had the largest additive contribution with MDD-PRS (Table 4.2), compared to other MDD-RVIs and MDD-PRS. Further calculations using delta AIC can be found in Table S7.

For ABCD, for both timepoints, among the MDD-RVIs, RVI-MD, RVI-FA and RVI-Multi had the largest change in R^2 when added to the model individually (Baseline R^2 = 0.3%-0.5%, Two-year R^2 = 0.3%-0.4%, Figure 4.3B). These three MDD-RVIs also contributed towards an improvement in model fit individually (compare M1 and M2) and in combination with MDD-PRS (compare M3, M4 and M5) at both timepoints, in contrast to the other MDD-RVIs (Table 4.2). MDD-PRS, however, accounted for a greater change in R^2 than each individual MDD-RVI at baseline (MDD-PRS R^2 = 0.7%, MDD-RVIs R^2 =0%-0.5%, Figure 4.3B) and at two-year follow-up (MDD-PRS R^2 = 0.7%, MDD-RVIs R^2 = 0%-0.4%, Figure 4.3B). MDD-PRS also contributed towards an improvement in model fit individually at both time points (Table 4.2).

Table 4.2. Absolute AIC values for each model type (M1 to M5) when MDD-PRS and MDD-RVIs are used as predictors individually or in conjunction with each other. AIC is a metric used to select the most parsimonious model that best explain the variance in the dependent variable. For example, the relative increase in AIC with the addition of new variable to the model would mean that the new predictor does not help to explain additional variance in the dependent variable. For model comparison, relative lower AIC values (typically at least 2 AIC units lower) are indicative of better model fit. The results for both GS-Imaging and ABCD are reported.

GS-Imaging

		Lifetime-MDD						TotalQIDS					
Model	**Variables**	**RVI-Sub**	**RVI-CorTH**	**RVI-CorSA**	**RVI-MD**	**RVI-FA**	**RVI-Multi**	**RVI-Sub**	**RVI-CorTH**	**RVI-CorSA**	**RVI-MD**	**RVI-FA**	**RVI-Multi**
M1	Covs (for RVI)	655.568						1770.973					
M2	RVI+Covs (for RVI)	617.14	631.196	641.74	633.603	637.521	597.874	1648.444	1681.766	1733.443	1718.084	1714.972	1596.433
M3	Covs	672.293						1792.363					
M4	PRS+Covs	671.93						1792.09					
M5	PRS+RVI+Covs	633.582	647.215	659.033	649.654	652.779	613.38	1667.764	1701.706	1753.004	1737.658	1735.256	1614.54

ABCD

		CBCL-DSM-Depressed (Baseline)						CBCL-DSM-Depressed (Two-year)					
Model	**Variables**	**RVI-Sub**	**RVI-CorTH**	**RVI-CorSA**	**RVI-MD**	**RVI-FA**	**RVI-Multi**	**RVI-Sub**	**RVI-CorTH**	**RVI-CorSA**	**RVI-MD**	**RVI-FA**	**RVI-Multi**
M1	Covs (for RVI)	4970.509						5791.486					
M2	RVI+Covs (for RVI)	4972.006	4972.475	4970.297	4713.946	4717.684	4717.155	5793.091	5792.503	5793.486	5628.348	5629.907	5629.424
M3	Covs	5117.664						5808.395					
M4	PRS+Covs	5106.279						5795.573					
M5	PRS+RVI+Covs	5107.171	5108.268	5106.773	4852.654	4856.309	4855.112	5797.077	5796.307	5797.55	5630.852	5632.173	5631.698

*Covs: Covariates; “Covs (for RVI)“ models do not include the 15 genetic principal components and genotype plate number that were included in the “Covs” models

Association of MDD-RVIs and MDD-PRS with symptom change in ABCD

Mean CBCL-DSM-Depressed scores increased slightly from baseline (1.3±2.0) to two-year follow-up (1.6±2.3). No MDD-RVIs nor MDD-PRS at any p-value thresholds were associated with symptom change ($\beta<0.05$, $p>0.05$, Table S8).

4.2.5 Discussion

This study examined associations between MDD-RVIs/MDD-PRS and depressive phenotypes in adults, and further explored their utility in adolescents. White matter integrity-based MDD-RVIs (RVI-MD, RVI-FA) and RVI-Multi had the strongest associations among the MDD-RVIs in adults. These MDD-RVIs outperformed MDD-PRS in terms of effect sizes and contributed additively with MDD-PRS to model fit. This pattern did not generalise to early adolescence, where no significant associations were observed for any MDD-RVIs. MDD-PRS was however, associated with adolescent depressive symptoms cross-sectionally but not with symptom change.

Our key findings on white matter integrity-based MDD-RVIs having the strongest associations with MDD phenotypes in adults are in line with results reported by previous studies looking at other adult cohorts using standard approaches (Shen et al., 2017, 2020). This suggests that reduced white matter integrity may be an important neurobiological feature of adult MDD and provides a rationale to look into finer details of the brain's structural connectivity (e.g., connectomes) to elucidate the underlying mechanisms. Our findings also broadly replicate prior reports of RVI methods applied to UK Biobank, which reported significant associations between MDD and RVI-FA and RVI-Multi (Kochunov et al., 2021). Notably, the FA and MD measures of individual tracts (rather than as a combined risk score) had very small effect sizes and no significant associations with symptom severity scores in the

original ENIGMA meta-analysis (van Velzen et al., 2020; see Tables S5 and S6). This suggests that brain-based deviation of small effect sizes when considered collectively and across modalities can create individualised summary scores that are better measures of psychopathology than individual brain metrics in isolation.

Our results also support the role of MDD-PRS as an indicator of depressive phenotypes across the lifespan. The absence of any significant association in adults in this study is likely due to the lack of power given the relatively small sample size, and since MDD-PRS has been shown to be predictive in larger case-control studies (Wray et al., 2018; Howard et al., 2019), including here in the larger GS sample. However, we considered it necessary to restrict the sample to individuals with both imaging and genetic data to ensure a fair comparison between MDD-RVIs and MDD-PRS. Given that MDD-PRS in adults also generalise to adolescents (i.e., effect sizes for continuous depressive phenotypes were comparable in this study; Halldorsdottir et al., 2019), MDD-PRS may be useful as an early indicator of adolescent depression. The lack of association between MDD-PRS and the change in depressive symptoms in adolescents could be due to lower statistical power at the two-year follow-up, or it could suggest that the changes are minimal due to the short time interval. Future work can consider following these young individuals over a longer time period for a more robust assessment of genetic contributions to MDD risk.

In evaluating the comparative performance of MDD-RVIs and MDD-PRS in adults, RVI-MD, RVI-FA and RVI-Multi had higher associations with depressive phenotypes compared to MDD-PRS, especially for lifetime MDD. This may be because MDD-PRS and MDD-RVI operate on different timescales, with MDD-PRS being a snapshot one's genetic susceptibility that is fixed since birth and MDD-RVI capturing the cumulative effects of non-genetic factors (e.g., environmental, biological) on the brain across the lifespan. The additive contribution to model

fit by MDD-RVI and MDD-PRS, as well as the absence of a correlation between them (Figure S2), indeed suggest that they each contribute towards unique variance. As such, it could be argued that MDD-RVI may be a useful additional measure of MDD risk in adults, since non-genetic risk factors can have an important influence on MDD risk, especially with the increase in exposure with age (Vinkers et al., 2014). For example, depressed individuals who face stressful life events may have reductions in white matter integrity (Poletti et al., 2018), which may play a mediating role between the environmental exposure and clinical outcome that is not captured to the same extend by genetic risk scores (Wang et al., 2022). Given the significant role of environmental factors, future work could explore the effects of different environmental exposures on brain structural connectivity, such as through the use of methylation risk scores (Barbu et al., 2021), which can also be combined with MDD-RVI and MDD-PRS to study their additive effects on MDD risk.

Notably, MDD-RVIs were not associated with depressive symptoms in the adolescent sample and underperformed compared to the MDD-PRS. This could be due to the use of effect sizes from the adult ENIGMA meta-analyses to derive the MDD-RVIs. The effect sizes were based on cases with established MDD, and such estimates may not be directly relevant to cases with milder and less chronic depressive symptoms like in ABCD. Given that adults are likely to have more episodes and longer disease duration, the estimates may be more relevant within age group instead – e.g., GS-Imaging cases with lifetime MDD, on average, have had three episodes of depression, each lasting for approximately 20 weeks (Figure S5). In line with the above, adolescents may not yet demonstrate the same degree of detectable brain structural changes associated with depressive symptoms as adults, as psychopathology in adolescents can be transient and diagnostically uncertain (Blok et al., 2022; Calkins et al., 2017). They might also have had lesser exposure to environmental/biological stressors of

MDD, thereby cumulating lesser detrimental changes to the brain which are harder to detect. Given that adolescent brains are still undergoing significant developmental structural changes (Tamnes et al., 2017), the accuracy of the MDD-RVIs could have also been compromised due to the incorporation of variation attributed to neurodevelopment. As such, with the increase in sample sizes over the coming years, deriving adolescent MDD-RVIs using adolescent-specific effect sizes would be something important to look at in future, in order to identify brain-psychopathology associations, if any, that are unique to this age group. Nonetheless, it is interesting that adolescent RVI-MD, RVI-FA and RVI-Multi (i.e., the best performing MDD-RVIs in the adult sample) had the highest proportion of variance explained among the other MDD-RVIs, and were the only ones that contributed towards improved model fit individually and in combination with MDD-PRS. It is of interest to continue monitoring this longitudinal sample to see if the results become increasingly comparable to those seen in adults. We consider these findings critical for furthering the understanding of the role of neurodevelopment in shaping brain-psychopathology associations.

It is important to note that both MDD-RVI and MDD-PRS still only capture a small proportion of variance within the clinical phenotype and are not of clinical utility at present, either individually or in combination (Martin et al., 2019; Lewis & Vassos, 2020). Brain-based measures like MDD-RVI, however, are still potentially clinically useful, given our findings that effects of non-genetic risk factors can be captured by changes in brain structure. Its clinical potential may be enhanced in the near future, considering the steady increase in sample sizes of imaging studies (and genome wide association studies), which is indicative of a corresponding increase in power to detect more brain deviations (and genetic variants) that can hopefully contribute towards higher explained variance (Wray et al., 2013; Smith & Nichols, 2018). Though not directly clinically useful yet, observations from such brain-based

measures still inform our understanding of the biology of depression, which may aid in the development of future diagnostic biomarkers.

Strengths and Limitations

Strengths of this study include the large sample sizes, comparison of imaging and genetic predictors across different age groups and the use of longitudinal data. Our findings should however be interpreted in the context of some limitations. Both GS-Imaging and ABCD are community-based samples consisting mainly of healthy individuals. We thus may not have captured the effects of moderate to severe MDD, but our results have the benefit of higher generalisability to the community. Our results may also not generalise to other ethnic groups as our sample was restricted to individuals of European ancestry. Future work can replicate this study in multi-ethnic cohorts when discovery data and analysis tools become more widely available. Additionally, we note that multiple factors, such as variations in protocols, can influence the reproducibility of imaging findings across sites. However, it was recently noted that neuroimaging findings, especially from large-scale studies, are generally consistent (Anderson et al., 2020). For RVI specifically, it has been shown that the method was effective when applied in different cohorts (Kochunov et al., 2019, 2021, 2022a). Along with the increase in adoption of standardised protocols (e.g., the use of ENIGMA's DTI protocol in this study), there is more confidence in the replicability and applicability of results across sites (Gountouna et al., 2010; Gradin et al., 2010; Bearden & Thompson, 2017).

Conclusion

This study presents a comprehensive comparison of brain-based and genetic risk scores in terms of their association with MDD at different stages of the lifespan. MDD-RVIs, mainly

those derived from white-matter microstructural measures, had stronger associations with MDD and outperformed MDD-PRS in adults. While the contrary is true for adolescents, white matter-based MDD-RVIs, like in adults, contributed towards the highest proportion of variance explained among the MDD-RVIs. These findings are significant, as they inform our understanding of the temporal origins of depression-related brain features. They also highlight the importance of longitudinal studies for developing measures of risk for psychiatric illness, and the increasing influence of environmental exposures on brain structure and MDD risk across the lifespan.

4.3 Chapter conclusion

In this study, personalised brain-based and genetic risk scores were derived using summary statistics from large-scale group-level findings. Brain-based risk scores based on white matter microstructural measures outperformed genetic risk scores in adults, in terms of the strength of their associations with MDD. Although genetic risk scores outperformed all brain-based risk scores in adolescents, signs of adult MDD brain-like features in white matter tracts were also more detectable in adolescents. Collectively, the results in this study highlight the role of structural connectivity in MDD, the contributions of MDD genetic risk at different stages of life, and also the benefits of combining information from different risk scores to better assess MDD risk.

Chapter 5: General discussion

5.1 Chapter introduction

To recap, the main focus of the three studies can be briefly summarised as – (1) to utilise network approaches to investigate structural connectomic differences in MDD, (2) to identify structural connectomic associations with key MDD risk factors, and (3) to test the utility of personalised MDD brain-based risk score in adults and adolescents. The analyses were conducted using large population datasets and the findings collectively help to address two main research gaps in the current literature, including the lack of large-scale connectomic studies in MDD, and the translation of group-level findings to the individual level. The specifics were already discussed within each chapter. Here, I discuss the common themes and salient points from all three studies and discuss how they relate to the wider literature. This is followed by discussion on the strengths and limitations of this thesis, and possible future work that can be undertaken.

5.2 Summary of main findings

5.2.1 Evidence of structural dysconnectivity in MDD

White matter tracts are important as they form the anatomical basis for information transfer between brain regions. Perturbations to this underlying architecture can have fundamental implications on how the brain operates, and the results from all three studies in this thesis collectively provide evidence that disruption in brain structural connectivity is a feature of MDD. In Chapter 2, it was shown that there were subtle changes across the whole structural

connectome leading to an overall reduction in network efficiency in MDD cases. In Chapter 3, it was shown that key risk factors for MDD, including MDD-PRS and CT, both resulted in reduced connectivity in distinct subnetworks. In Chapter 4, brain-based risk scores based on white matter microstructural measures (FA and MD) were not only the most strongly associated with MDD in adults, but also contributed the highest proportion of variance explained in adolescents with depressive symptoms, as compared to other morphological measures. The significant role of white matter in MDD is also supported by findings in earlier UKB neuroimaging studies – significant reductions in white matter integrity but not subcortical volumes were observed in MDD cases relative to controls in a UKB neuroimaging study (Shen et al., 2017), and MDD-PRS was only found to be associated with reduced integrity in several white matter tracts among the structural neuroimaging variables in a phenome-wide association study (Shen et al., 2020). Collectively, there seem to be a consensus that structural dysconnectivity plays a key role in MDD.

The findings from Chapters 2 and 3 also demonstrate the value of studying the structural connectome using network approaches, as they added to the insights that can be gained by studying individual regions in isolation. The use of graph theory allowed the study of MDD-associated effects at each hierarchical level of the connectome and showed the build-up of effects in MDD. Likewise, specific structural circuits and their associated functions affected by MDD-PRS and CT (e.g., the disproportionate role of frontal-basal ganglia circuits in females) could be identified through the use of NBS. Recent findings, including those from large-scale studies like ENIGMA, also further highlight the value of studying the structural connectome in psychiatric disorders as it may be linked to morphological alterations. Georgiadis et al (2024) found that the structural connectome architecture shapes patterns of cortical atrophy (i.e., reduction in cortical thickness) in schizophrenia, in that cortical atrophy

were not randomly distributed but regions structurally connected to each other had similar patterns of atrophy (Georgiadis et al., 2024). Likewise, Han et al (2023) found that grey matter atrophy (i.e., reduction in volume) in MDD is constrained by the structural network architecture, and regions with stronger connections to disease epicentres (i.e., regions where disease propagates from) involving the thalamus, hippocampus, striatum and frontal regions have greater atrophy. These findings, coupled with the findings in this thesis, collectively suggest that the structural connectome may play a fundamental role in terms of propagating disease spread in grey matter regions. Additionally, the results here also tie in with existing grey matter findings in MDD. For example, ENIGMA studies reported reductions in the cortical thickness of the orbitofrontal cortex, cingulate cortex, insula and temporal lobes (Schmaal et al., 2017), and connectivity of these regions were likewise found to be affected in the PRS- and CT-associated subnetworks detailed in Chapter 3. As such, it is clear that grey and white matter effects in MDD are correlated with each other, and future studies should thus leverage the increase in large-scale connectomic datasets to conduct more in-depth and replicable studies to better understand the role of the structural connectome in MDD.

5.2.2 The involvement of both hubs and non-hubs in MDD

Hubs are considered to be key components of the brain network as they play an integral role in coordinating a large proportion of region-to-region signal traffic. In this study and consistent with the existing literature, regions identified as hubs typically include the superior frontal and superior parietal cortex, precuneus, as well as components of the basal ganglia including the thalamus and putamen (van den Heuvel & Sporns, 2011, 2013). While hubs are crucial for efficient brain communication, their high biological cost (e.g., high metabolic cost of hub activity and high wiring cost to support long-distance connections) also render them more

vulnerable to adverse circumstances such as stress (Van den Heuvel & Sporns, 2013). Hubs are therefore widely studied in neurological and psychiatric disorders (Crossley et al., 2014). In line with this, Chapter 2 showed that only hubs had significantly lower nodal efficiency in MDD cases relative to controls, and Chapter 3 showed that hubs were also extensively involved in subnetworks associated with higher MDD polygenic risk and exposure to childhood trauma. Collectively, these findings provide evidence to support the involvement of hubs in MDD.

Importantly, although non-hubs are traditionally overlooked due to the heavy emphasis on hubs, the findings in this thesis also provide evidence to support the significant involvement of non-hubs in MDD. In Chapter 2, differences in network efficiency were present across all four hierarchical tiers of the connectome, indicating that hubs and non-hubs alike were affected. In Chapter 3, although some rich connections were implicated in the PRS- and CT-associated subnetworks, majority of the connections were feeder (hub to non-hub) and local (non-hub to non-hub) connections. In line with this, recent structural connectome studies, as mentioned earlier, also found that disease epicentres in schizophrenia and MDD are not necessarily the regions with the highest level of atrophy (aka hubs), but instead are regions that are connected to hubs. (Georgiadis et al., 2024; Han et al., 2023). In addition to this, multiple epicentres, instead of the commonly hypothesised single epicentre, was found to be present in MDD (Han et al., 2023). Collectively, these findings and the findings in this thesis seem to indicate that non-hubs do play a key role in MDD, in that changes in multiple non-hub regions across the brain are likely to build up and effect changes that were more detectable in hubs due to their higher number of connections.

With regards to the involvement of the rich club in MDD, the rich club was found to be stable in MDD cases in Chapter 2, but rich connections were implicated in subnetworks associated with key MDD risk factors in Chapter 3 and connectivity of these subnetworks were

lower in MDD cases. While seemingly conflicting, there are a few considerations to be made when interpreting these findings. In Chapter 2, rich club coefficients (used to examine the presence of rich club) at each level of degree *k* was defined as the sum of weights of *x* rich connections relative to the sum of top *x* weights in the network. The stability of the rich club in MDD does not necessarily mean that there were no disruptions to the rich connections, but that even with disruptions to some rich connections, the sum of weights of all rich connections still exceeded that of average connections, such that the rich club coefficients remained similar to those observed in controls. The disruptions to the individual rich connections in MDD were thus likely to be (1) minimal: were the disruptions substantial, the NBS step in Chapter 2 would have detected subnetworks involving the rich connections but no significant findings were found, and (2) few: the number of rich connections implicated in the PRS- and CT-associated subnetworks were relatively few. As such, minimal disruption to a handful of individual rich connections may not have destabilised the rich club. It is likely that the differences in MDD were driven by feeder and local connections outside the rich club, as discussed earlier. Nevertheless, given that the analyses in Chapter 2 were conducted using the full sample and rich connections may potentially have a bigger role to play in males as discussed in Chapter 3, it may still be of benefit to repeat the analyses in Chapter 2 for males and females separately to fully understand the role of the rich club in MDD.

5.2.3 The impact of genetic and environmental risk factors for MDD on the connectome

The structural connectome is shaped over the years by genetic and environmental inputs (Feng et al., 2024), whereby disruptions to the normal developmental process, including initial formation to maturation of the connectome, may underlie brain-related disorders (Collin & Keshavan, 2018). A key finding from Chapter 3 is that MDD-PRS and CT both affect the

structural connectome and in unique ways – genetic risk affects cognitive-related regions while CT affects social/sensory-related regions to a larger extent. Abnormalities during the initial formation of the structural connectome may already be present due to MDD genetic risk, and these inherent deficits become apparent when functional systems start to appear over the course of development. For example, a large-scale (N=5,315) longitudinal study by Morales-Muñoz et al (2021) found that cognitive deficits (e.g., working memory, attentional control) assessed during childhood (as early as eight years of age) were associated with subsequent psychopathological symptoms (e.g., depression, psychosis) assessed during adolescence and young adulthood. Over time, subsequent negative experiences, especially during the sensitive neurodevelopmental period, may further affect the integrity of the structural connectome and contribute towards increased risk for MDD. While these factors may contribute towards increased risk of developing MDD through alterations in the structural connectome, it is also possible that the manifestation of MDD will in turn result in further maladaptive changes in the connectome, resulting in a continual negative cycle of events that exacerbate MDD. This complex relationship makes it challenging to infer causality between brain structure and MDD. There are studies that utilised Mendelian Randomisation (MR), which is a technique that uses genome-wide significant variants as instruments to determine the direction of causality between MDD and different phenotypes. For example, Shen et al (2020) reported a causal effect of MDD on neuroimaging phenotypes such as white matter microstructural measures. However, there is a known bias, in that there is a relative lack of genome-wide significant loci for brain measures, resulting in weaker genetic instruments for MR and hence, reduced power to detect causal effects on MDD. Furthermore, given that MDD has large genetic and phenotypic overlap with multiple psychiatric disorders (Borque et al., 2024), it is also not possible to conclude that the identified brain measures are

exclusively related to MDD. Future studies can work towards establishing causality between brain structure and MDD, which can only be determined through the use of longitudinal imaging data and studies of high-risk participants in order to identify the trajectory of brain differences before and after the onset of MDD.

Beyond studying the impact of key MDD risk factors on the structural connectome, the analyses in Chapter 3 provided further insight by looking at sex differences as well. Specifically, it was found that the subnetworks associated with MDD-PRS and CT were unique to each sex, in terms of the regions implicated and their roles as mediators in the relationship between MDD-PRS/CT and MDD. The results re-emphasised the well-established phenomenon of sex differences in MDD and highlight the importance of identifying more factors that contribute towards this disparity (e.g., sex hormones, sociocultural factors; Piccinelli & Wilkinson, 2018, Hyde et al., 2020) and understanding the underlying mechanisms. In line with this, there has been increasing efforts in recent years to look at the association between such factors and the brain in mental disorders. For example, the ENIGMA-Neuroendocrinology working group was recently launched to address knowledge gaps about how sex hormones affect the brain across the female lifespan (e.g., during prenatal, puberty, reproductive years, and menopause) and contribute towards the preponderance of mental disorders such as MDD in females (Heller et al., 2024). Likewise, the current work here can be extended to factors other than MDD-PRS and CT to study their impact on the structural connectome in males and females separately. By considering more factors, this will allow for a more complete understanding of the complex aetiology of sex disparities in MDD.

5.2.4 Utility and practicality of brain-based markers for MDD

A common theme of the results obtained in Chapters 2 to 4 is that the effect sizes for case-control differences in structural brain measures in MDD are very small, likely detectable due to the large sample sizes used in each study. While the minimal differences may possibly be due to the use of population cohorts that consist of participants that are generally healthy, similar findings were reported by Winter et al (2022) where they investigated case-control differences in a clinical population consisting of 861 MDD cases and 948 healthy controls, across all neuroimaging modalities that were measured using harmonised protocols. They found that the maximum explained variance by an individual neuroimaging measure was only 2%, and even measures with the largest differences between MDD cases and controls had a large distributional overlap of 86.6% to 94.8%. Based on these findings, it is highly likely that all the neuroimaging measures combined will still be unable to explain sufficient variance in MDD to be of diagnostic value. However, these small effects do not rule out brain-based markers as relevant tools in MDD research. Rather, they highlight certain points that should be considered moving forward, in order to maximise the value of brain-based markers.

Firstly, personalised approaches should be considered. MDD affects a wide range of brain functions that can vary drastically between individuals and even within individuals for different episodes of MDD. As such, while group-level neuroimaging findings may be useful in identifying the general mechanisms underlying MDD, the results may not appear to be as impactful in diagnosis or treatment as the findings were based on the group average. Personalised neuroimaging approaches are already increasingly applied to study psychiatric disorders (Rutherford et al., 2023; Marquand et al., 2019). As shown in Chapter 4, the regional vulnerability index derived based on white matter microstructural measures were significantly associated with both lifetime MDD and current depressive symptoms, thus

showing potential in terms of aiding MDD diagnosis. As for treatment, a recent study by Cash et al (2023) also showed that therapeutic outcome for transcranial magnetic stimulation was better using personalised functional connectivity brain maps instead of the group-averaged brain map. These results clearly demonstrate the clinical potential of personalised brain-based markers, and further research can be conducted to improve or discover more of such metrics. For example, having established the benefits of studying the structural connectome, future work can also consider looking into generating personalised connectome-based metrics in addition to existing brain metrics that are mostly based on morphological features.

Secondly, brain-based markers should be used in tandem with other measures. Even by taking individual-level approach, it is possible that brain-based markers alone are still insufficient to explain risk in MDD. This was shown in a recent study by ENIGMA on psychosis, where normative modelling of brain morphometry did not reveal any significant difference detected individuals at clinical high risk for psychosis and healthy controls (ENIGMA Clinical High Risk for Psychosis Working Group, 2024). However, even without diagnostic value, brain-based markers can still help with predictive and prognosis of MDD along with other markers, as shown in Chapter 4, where MDD-PRS along with MDD-RVI worked additively to explain a larger proportion of variance in MDD. Similar to the concept of allostatic load where many biological factors are considered to assess an individual's level of chronic stress in the body, risk assessment for MDD should also consider combining a range of factors since MDD affects multiple functions not restricted to just the brain (Kennis et al., 2020). This includes genetic factors (e.g., MDD-PRS), brain-based measures, immune factors (e.g., CRP, IL-6; Miller & Raison et al., 2016), hormonal factors (e.g., cortisol (Kennis et al., 2020)), metabolites (e.g., gut microbiota; Liu et al., 2023), lifestyle/environmental factors (e.g., measured in the form of methylation risk scores (Barbu et al., 2021)), and even data from wearables (e.g., sleep

patterns, physical activity; Abd-Alrazaq et al., 2023). The combination of these measures can provide a more accurate view of MDD, and the use of such objective measures will avoid the heavy reliance on subjective retrospective assessments of symptoms. While more work still needs to be done – more data across more settings are needed to be collected, best practices need to be established with regards to collection, measurement, and analysis, and methods need to be devised to integrate these measures (e.g., machine learning to identify patterns of association in the data) – personalised approaches are promising and should be worked towards. Hence, given that it is known that brain effects are modest, it is now insufficient to just keep increasing sample size. The larger the sample sizes, the more we are able to detect differences but the less useful they are due to the very small effect sizes. Approaches such as these typically aggregate the measures so it might be useful in contributing towards bigger effect sizes, thus making brain research more relevant (Kong et al., 2022).

Lastly, sex stratification can be considered when studying the brain in MDD. In line with the extensive literature on sex differences in MDD, such as in genetic mechanisms (Silveria et al., 2023; Labonté et al., 2017), inflammation markers (Kim et al., 2021) and brain morphology (Mou et al., 2023), the results in Chapter 3 also clearly demonstrated that there are distinct sex differences in the way the structural connectome is affected by key MDD risk factors. As such, aggregating males and females into a single sample may mask signals that are only apparent in one group, produce more noise resulting in inconsistent findings across samples, and lead to incomplete understanding of the mechanisms underlying MDD as only shared signals will be identified. With the growing sample size of neuroimaging and connectomic studies, there might be sufficient statistical power to allow for sex stratification instead of simply covarying for sex in analyses. The practice of sex stratification will not only promote reproducibility but also the deeper understanding for differential MDD

pathophysiology in males and females, thus advancing the discovery of sex-specific biomarkers for MDD. In addition to sex stratification, subtyping is also an important but it will be addressed in the next section under limitations, as it was not applied in this thesis.

5.2.5 Further methodological considerations

There are additional methodological factors that should be taken into consideration when interpreting the results in this thesis.

Firstly, the studies in this thesis mainly focused on lifetime MDD although the effects of MDD can be further categorised as being state or trait (Krohne et al., 2002). State is considered a transitory condition where current depressive symptoms are characterised by the intensity of symptoms (e.g., how does one feel at the moment), while trait refers to an individual's propensity to be depressed (e.g., how one generally feels). For lifetime MDD, an individual is classified as a case as long as an episode of MDD occurred at any point in life. The reason for analysing MDD as a single unified construct is because one of the key aims of this thesis is to maximise sample size in order to reliably identify brain-related differences that tend to be very subtle. Furthermore, there are likely to be shared characteristics between the two forms of depression. This was shown in a recent study by Dutt et al (2022), where they found that five different measures of current and lifetime MDD in UKB were moderately correlated with one another. As such, the findings here sought to identify underlying biology that is present in at least a notable proportion of MDD cases and serve to act as a reference point for future studies to zoom in onto specific subtypes. This point was emphasised in Supplementary information of Chapter 2, which showed that majority of the cases with lifetime MDD did not have current depressive symptoms, and the observed effects are likely to be a generic MDD phenomenon.

Secondly, similar to how MDD-PRS is limited by the MDD GWAS it was derived from, MDD-RVI is also limited by the ENIGMA-MDD study it was derived from. Although ENIGMA-MDD studies have contributed significantly to the neuroimaging field, they have some inherent limitations which may affect the effectiveness or validity of MDD-RVI as a potential clinical tool to assess an individual's vulnerability to MDD. For example, data collection protocols can vary widely across different ENIGMA study sites, such as the use of different scanners, scanning parameters, and even different instruments for the diagnosis of MDD that may compromise the validity of case-control status (Schmaal et al., 2020). As such, there might be potential confounds (e.g., head motion) associated with differences in scanning methodologies and other characteristics between cohorts, which must be considered and modelled. Most ENIGMA study sites also consist of fairly Eurocentric samples, which suggest that MDD-RVI may lack generalisability to other ethnicities. Efforts to improve ENIGMA protocols and/or develop alternative large-scale cohorts to base MDD-RVI on are important so as to improve the validity of MDD-RVI as a potential clinical tool.

5.3 Strengths and limitations of current work, and possible future work

This thesis has two main strengths. Firstly, the use of data from large and well-phenotyped population cohorts (UKB, GS, and ABCD) to conduct the analyses. The use of large samples ensures sufficient statistical power for the more accurate detection of small effects, which are typical of neuroimaging and genetic studies. This is especially important for structural connectomic studies, considering that current literature still mostly consist of studies that were limited by small sample sizes (N<100). The use of large connectomic samples in Chapters 2 and 3 (N range: 725 to 14,881), along with the increasing availability of bulk connectomic data processed using harmonised protocols such as in UKB (Mansour et al., 2023), will allow

for significant progress to be made in the study of connectomes in health and disease. Secondly, specifically to Chapters 2 and 4, the use of a large discovery cohort was coupled with the use of a second large replication/exploratory cohort to test if the results can be replicated and extended to a separate age group, respectively. Doing so is important, as it increases the reliability of results and also allows for the extension or generalisation of results to a wider population.

These strengths are, however, also accompanied by limitations, which should be taken into consideration when interpreting the results. Limitations specific to the studies were already discussed in their respective chapters. Here, I discuss the salient points that apply to all three studies, and these limitations can also form the basis for future work.

Firstly, the studies mainly considered lifetime MDD and did not look into different MDD subtypes, such as symptom subtypes (e.g., melancholic vs atypical), symptom severity (e.g., mild, moderate, severe), remitted or current MDD, and more. This is a limitation as it has been suggested that not only do MDD subtypes have different symptom presentation, but they can also have different associations with various biological mechanisms, including brain structure and function (Woelfer et al., 2019; Toenders et al., 2022). Stratifying the cohort into subtypes, rather than aggregating them into a single sample, will therefore provide a more accurate understanding of the specific mechanisms underlying each subtype. The adoption of a broad approach here is based on the idea that core MDD symptoms shared across cases will probably share a common neurobiological basis. Considering that large-scale connectomic studies are still relatively rare, the findings here can serve as a starting point to guide future connectomic investigations, such as adopting a bottom-up approach to study well-phenotyped severe subtypes first. In order to look into subtypes, it is, however, likely that more data must be collected from many more participants to ensure sufficient statistical

power. This is especially so if stratification into MDD subtypes is to be based on biological and/or genetic measures in addition to self-reported symptoms, which might be subjective if used alone. This will be possible, considering that the UKB aims to conduct neuroimaging assessments for 100,000 participants in total and are on track to do so.

Secondly, differences in methodology have to be considered. Unlike the significant progress that has been made in harmonising imaging and analysis protocols in the study of univariate brain measures, the connectome field is relatively nascent and there is still no scientific consensus on the best approaches to take with regards to parcellation scheme, network construction, thresholding methods, and more (Adamovich et al., 2022). Different methods have their pros and cons – for example, parcellating a connectome into many ROIs as compared to 85 ROIs in this study can allow for fine-grained resolution but at the same time, are more susceptible to noise. As such, the results and their interpretations can vary according to the approaches taken, unless protocols are harmonised. Fortunately, understanding this, Mansour et al (2023) recently made available processed structural and functional connectome data for 40,000 subjects from the UKB. The availability of this large connectome dataset processed using a single protocol serves as a useful starting point for replicable research, considering that groups can access and work on the same dataset without having to worry too much about methodological differences.

Thirdly, the results here may not be applicable to clinical samples as data from community-based cohorts, such as the UKB and GS, were used. It is known that such cohorts have a selection bias, where participants are healthier and are from less deprived areas than the general population (Fry et al., 2017). Such healthy volunteer bias compromises the generalisability of findings to more vulnerable populations who account for most of the burden of disease. Furthermore, early-life experiences, such as childhood adversity, are

significant predictors of future mental health trajectories, but these older adult cohorts can only gather participants' retrospective reports of childhood, which may be subjected to recall bias and hence, compromise the validity of findings (Brayne & Moffitt, 2022). Due to these limitations, the findings here can only provide a broad overview/common characteristic of people with depression. These limitations do not render the findings in this thesis irrelevant, but rather they provide a starting point to investigate further in smaller clinical samples. Such large studies provide the statistical power to detect small effects, which can be studied in greater detail in smaller and better phenotyped clinical samples. Likewise, the results here may not be directly applicable to other ethnicities, age groups, or under-represented populations, as they are mostly based on older adults (age 50 and above) that are of European ancestry. With the increasing availability of large-scale datasets beyond that of UKB and GS, the analyses in this thesis can be replicated using those datasets to assess the generalisability of findings. For example, the number of studies on the adolescent structural connectome in the context of MDD is currently low but connectomic data, such as from the ABCD study and the Human Connectome Project (both Developmental and Young Adult), are now widely available. The findings in this thesis can serve as a reference to compare features of adult and adolescent MDD. Additionally, the data from ABCD are also longitudinal, thus allowing for the tracking of brain changes over multiple time points. This is important, since MDD has a non-linear disease course depending on life experiences, and since the results in Chapter 4 also suggest that adult MDD-related brain changes may already be observed in adolescents.

Lastly, while not a limitation in itself, the studies in this thesis only focused on structural brain measures (morphometry and structural connectivity), which is insufficient for a holistic understanding of brain changes in MDD. MDD is associated with both structural and functional deficits (Zhuo et al., 2019), and functional properties are constrained to a certain

extent by structural properties (Suárez et al., 2020). The analyses done in this thesis can be extended to functional connectomes and the structure-function relationship can be inferred (e.g., will disruption in certain subnetworks lead to changes in certain brain functions?). In the same light, there has been a growing interest in integrating multi-omics (e.g., genomics, methylomics, transcriptomics, spatial omics) to study psychiatric disorders (Sathyanarayanan et al., 2023). Currently, the findings in this thesis gives an idea of brain regions affected in MDD but the exact molecular mechanisms are still unclear. Integrating connectomics with these multi-omics approaches, such as in Fornito et al (2019) and Hansen et al (2022), would bridge the gap between molecular function and large-scale connectome organisation, thus providing much more insight into the mechanisms underlying MDD.

5.4 General conclusions

MDD is a highly prevalent and serious psychiatric disorder. Despite years of research, the complex nature of MDD has made it challenging to elucidate its neurobiological underpinnings. However, advancements in recent years have provided new perspectives on how to better study the brain in MDD. The first being the need to study the brain as it is innately structured (i.e., a network), so as to understand the implications of structural changes at the systems level. The second being the need to integrate different disciplines (e.g., imaging genetics) to better inform understanding of MDD, instead of studying them independently of each other. The third being the increasing realisation that personalised approaches are necessary to study a heterogenous disorder like MDD. At the same time, there has been an increase in large, comprehensive, and publicly available datasets, thus allowing for more in-depth and reproducible research to be done. By leveraging these recent advancements, this thesis contributes three studies that can add to or complement what is

already known about MDD. The results here provide evidence that structural dysconnectivity is present in MDD, with effects that are subtle but widespread across the entire brain network, resulting in lower global efficiency in information transfer. Key MDD risk factors, such as MDD polygenic risk and childhood trauma, were also shown to affect structural connectivity in distinct regions, and the effects were also different between sexes. In translating group-level neuroimaging findings to the individual level, personalised brain-based risk scores based on white matter microstructural measures show potential in assessing an individual's risk for MDD but due to the small effects, they have to be integrated with other genetic or biological markers in order to provide a more accurate and holistic measure of MDD risk. Collectively, the studies in this thesis provide fresh insights into the brain in MDD and can help to guide future studies that are planning to adopt similar or more in-depth analyses to extend these results.

References

Abd-Alrazaq, A., AlSaad, R., Shuweihdi, F., Ahmed, A., Aziz, S., & Sheikh, J. (2023). Systematic review and meta-analysis of performance of wearable artificial intelligence in detecting and predicting depression. *NPJ digital medicine*, *6*(1), 84. https://doi.org/10.1038/s41746-023-00828-5

Achenbach, T. M. (2009). The Achenbach system of empirically based assessment (ASEBA): Development, findings, theory, and applications. Burlington, VT: University of Vermont Research Center for Children, Youth,& Families.

Adamovich, T., Zakharov, I., Tabueva, A., & Malykh, S. (2022). The thresholding problem and variability in the EEG graph network parameters. *Scientific Reports*, *12*(1), 18659. https://doi.org/10.1038/s41598-022-22079-2

Adams, M. J., Streit, F., Awasthi, S., Ripke, S., Lewis, C. M., Wray, N. R., … Major Depressive Disorder Working Group of the Psychiatric Genomics Consortium Genome-wide study of half a million individuals with major depression identifies 697 independent associations, infers causal neuronal subtypes and biological targets for novel pharmacotherapies. *medxriv*, https://doi.org/10.1101/2024.04.29.24306535

Alfaro-Almagro, F., Jenkinson, M., Bangerter, N. K., Andersson, J. L. R., Griffanti, L., Douaud, G., … Smith, S. M. (2018). Image processing and Quality Control for the first 10,000 brain

imaging datasets from UK Biobank. *NeuroImage, 166*, 400–424. https://doi.org/10.1016/j.neuroimage.2017.10.034

Alizadeh, M., Manmatharayan, A. R., Johnston, T., Thalheimer, S., Finley, M., Detloff, M., … Mohamed, F. B. (2021). Graph theoretical structural connectome analysis of the brain in patients with chronic spinal cord injury: preliminary investigation. *Spinal cord series and cases*, *7*(1), 60. https://doi.org/10.1038/s41394-021-00424-3

Alloza, C., Cox, S. R., Blesa Cábez, M., Redmond, P., Whalley, H. C., Ritchie, S. J., … Bastin, M. E. (2018). Polygenic risk score for schizophrenia and structural brain connectivity in older age: A longitudinal connectome and tractography study. *NeuroImage*, *183*, 884–896. https://doi.org/10.1016/j.neuroimage.2018.08.075

Alvarez, J. A., & Emory, E. (2006). Executive function and the frontal lobes: a meta-analytic review. *Neuropsychology review, 16*(1), 17–42. https://doi.org/10.1007/s11065-006-9002-x

American Psychiatric Association, DSM-5 Task Force. (2013). *Diagnostic and statistical manual of mental disorders: DSM-5™* (5th ed.). American Psychiatric Publishing, Inc..

Anderson, K. M., Collins, M. A., Kong, R., Fang, K., Li, J., He, T., … Holmes, A. J. (2020). Convergent molecular, cellular, and cortical neuroimaging signatures of major depressive disorder. *Proceedings of the National Academy of Sciences of the United States of America*, *117*(40), 25138–25149. https://doi.org/10.1073/pnas.2008004117

Antoniades, M., Haas, S. S., Modabbernia, A., Bykowsky, O., Frangou, S., Borgwardt, S., & Schmidt, A. (2021). Personalized Estimates of Brain Structural Variability in Individuals With Early Psychosis. *Schizophrenia bulletin*, *47*(4), 1029–1038. https://doi.org/10.1093/schbul/sbab005

Aron, A. R., Robbins, T. W., & Poldrack, R. A. (2004). Inhibition and the right inferior frontal cortex. *Trends in cognitive sciences, 8*(4), 170–177. https://doi.org/10.1016/j.tics.2004.02.010

Aruldass, A. R., Kitzbichler, M. G., Morgan, S. E., Lim, S., Lynall, M. E., Turner, L., … Bullmore, E. T. (2021). Dysconnectivity of a brain functional network was associated with blood inflammatory markers in depression. *Brain, behavior, and immunity, 98*, 299–309. https://doi.org/10.1016/j.bbi.2021.08.226

Auchter, A. M., Hernandez Mejia, M., Heyser, C. J., Shilling, P. D., Jernigan, T. L., Brown, S. A., … Dowling, G. J. (2018). A description of the ABCD organizational structure and communication framework. *Developmental cognitive neuroscience*, *32*, 8–15. https://doi.org/10.1016/j.dcn.2018.04.003

Backhausen, L. L., Herting, M. M., Tamnes, C. K., & Vetter, N. C. (2022). Best Practices in Structural Neuroimaging of Neurodevelopmental Disorders. *Neuropsychology review*, *32*(2), 400–418. https://doi.org/10.1007/s11065-021-09496-2

Baker, S. T., Lubman, D. I., Yücel, M., Allen, N. B., Whittle, S., Fulcher, B. D., … Fornito, A. (2015). Developmental Changes in Brain Network Hub Connectivity in Late Adolescence. *The Journal of neuroscience : the official journal of the Society for Neuroscience*, *35*(24), 9078–9087. https://doi.org/10.1523/JNEUROSCI.5043-14.2015

Barbu, M. C., Shen, X., Walker, R. M., Howard, D. M., Evans, K. L., Whalley, H. C., … McIntosh, A. M. (2021). Epigenetic prediction of major depressive disorder. *Molecular psychiatry*, *26*(9), 5112–5123. https://doi.org/10.1038/s41380-020-0808-3

Barch, D. M., Albaugh, M. D., Avenevoli, S., Chang, L., Clark, D. B., Glantz, M. D., … Sher, K. J. (2018). Demographic, physical and mental health assessments in the adolescent brain and cognitive development study: Rationale and description. *Developmental cognitive neuroscience*, *32*, 55–66. https://doi.org/10.1016/j.dcn.2017.10.010

Bearden, C. E., & Thompson, P. M. (2017). Emerging Global Initiatives in Neurogenetics: The Enhancing Neuroimaging Genetics through Meta-analysis (ENIGMA) Consortium. *Neuron*, *94*(2), 232–236. https://doi.org/10.1016/j.neuron.2017.03.033

Behrens, T. E., Berg, H. J., Jbabdi, S., Rushworth, M. F., & Woolrich, M. W. (2007). Probabilistic diffusion tractography with multiple fibre orientations: What can we gain?. *NeuroImage*, *34*(1), 144–155. https://doi.org/10.1016/j.neuroimage.2006.09.018

Behrens, T. E., Woolrich, M. W., Jenkinson, M., Johansen-Berg, H., Nunes, R. G., Clare, S., … Smith, S. M. (2003). Characterization and propagation of uncertainty in diffusion-weighted

MR imaging. *Magnetic Resonance in Medicine*, *50*(5), 1077–1088. https://doi.org/10.1002/mrm.10609

Berlin, H. A., Rolls, E. T., & Kischka, U. (2004). Impulsivity, time perception, emotion and reinforcement sensitivity in patients with orbitofrontal cortex lesions. *Brain : a journal of neurology, 127*(Pt 5), 1108–1126. https://doi.org/10.1093/brain/awh135

Bernstein, D. P., Stein, J. A., Newcomb, M. D., Walker, E., Pogge, D., Ahluvalia, T., … Zule, W. (2003). Development and validation of a brief screening version of the Childhood Trauma Questionnaire. *Child abuse & neglect, 27*(2), 169–190. https://doi.org/10.1016/s0145-2134(02)00541-0

Bethlehem, R. A. I., Seidlitz, J., White, S. R., Vogel, J. W., Anderson, K. M., Adamson, C., … Alexander-Bloch, A. F. (2022). Brain charts for the human lifespan. *Nature, 604*(7906), 525–533. https://doi.org/10.1038/s41586-022-04554-y

Bjelland, I., Lie, S. A., Dahl, A. A., Mykletun, A., Stordal, E., & Kraemer, H. C. (2009). A dimensional versus a categorical approach to diagnosis: anxiety and depression in the HUNT 2 study. *International journal of methods in psychiatric research*, *18*(2), 128–137. https://doi.org/10.1002/mpr.284

Blesa, M., Galdi, P., Cox, S. R., Sullivan, G., Stoye, D. Q., Lamb, G. J., … Boardman, J. P. (2021). Hierarchical Complexity of the Macro-Scale Neonatal Brain. *Cerebral Cortex (New York, N.Y. : 1991)*, *31*(4), 2071–2084. https://doi.org/10.1093/cercor/bhaa345

Blok, E., de Mol, C. L., van der Ende, J., Hillegers, M. H. J., Althoff, R. R., Shaw, P., & White, T. (2022). Stability and Change of Psychopathology Symptoms Throughout Childhood and Adolescence. *Child psychiatry and human development*, *53*(6), 1330–1339. https://doi.org/10.1007/s10578-021-01212-8

Boes, A. D., Prasad, S., Liu, H., Liu, Q., Pascual-Leone, A., Caviness, V. S., Jr, & Fox, M. D. (2015). Network localization of neurological symptoms from focal brain lesions. *Brain : a journal of neurology*, *138*(Pt 10), 3061–3075. https://doi.org/10.1093/brain/awv228

Bonelli, R. M., & Cummings, J. L. (2007). Frontal-subcortical circuitry and behavior. *Dialogues in clinical neuroscience, 9*(2), 141–151. https://doi.org/10.31887/DCNS.2007.9.2/rbonelli

Border, R., Johnson, E. C., Evans, L. M., Smolen, A., Berley, N., Sullivan, P. F., & Keller, M. C. (2019). No Support for Historical Candidate Gene or Candidate Gene-by-Interaction Hypotheses for Major Depression Across Multiple Large Samples. *The American journal of psychiatry*, *176*(5), 376–387. https://doi.org/10.1176/appi.ajp.2018.18070881

Bourque, V. R., Poulain, C., Proulx, C., Moreau, C. A., Joober, R., Forgeot d'Arc, B., … Jacquemont, S. (2024). Genetic and phenotypic similarity across major psychiatric disorders: a systematic review and quantitative assessment. *Translational psychiatry, 14*(1), 171. https://doi.org/10.1038/s41398-024-02866-3

Brayne, C., & Moffitt, T. E. (2022). The limitations of large-scale volunteer databases to address inequalities and global challenges in health and aging. *Nature aging, 2*(9), 775–783. https://doi.org/10.1038/s43587-022-00277-x

Bromet, E., Andrade, L. H., Hwang, I., Sampson, N. A., Alonso, J., de Girolamo, G., … Kessler, R. C. (2011). Cross-national epidemiology of DSM-IV major depressive episode. *BMC medicine*, *9*, 90. https://doi.org/10.1186/1741-7015-9-90

Buchanan, C. R., Bastin, M. E., Ritchie, S. J., Liewald, D. C., Madole, J. W., Tucker-Drob, E. M., … Cox, S. R. (2020). The effect of network thresholding and weighting on structural brain networks in the UK Biobank. *NeuroImage*, *211*, 116443. https://doi.org/10.1016/j.neuroimage.2019.116443

Bulik-Sullivan, B., Finucane, H. K., Anttila, V., Gusev, A., Day, F. R., Loh, P. R., … Neale, B. M. (2015). An atlas of genetic correlations across human diseases and traits. *Nature genetics*, *47*(11), 1236–1241. https://doi.org/10.1038/ng.3406

Bullmore, E., & Sporns, O. (2009). Complex brain networks: graph theoretical analysis of structural and functional systems. *Nature reviews. Neuroscience*, *10*(3), 186–198. https://doi.org/10.1038/nrn2575

Burcusa, S. L., & Iacono, W. G. (2007). Risk for recurrence in depression. *Clinical psychology review, 27*(8), 959–985. https://doi.org/10.1016/j.cpr.2007.02.005

Button, K. S., Ioannidis, J. P., Mokrysz, C., Nosek, B. A., Flint, J., Robinson, E. S., & Munafò, M. R. (2013). Power failure: why small sample size undermines the reliability of neuroscience. *Nature reviews. Neuroscience*, *14*(5), 365–376. https://doi.org/10.1038/nrn3475

Cai, H., Xie, X. M., Zhang, Q., Cui, X., Lin, J. X., Sim, K., … Xiang, Y. T. (2021). Prevalence of Suicidality in Major Depressive Disorder: A Systematic Review and Meta-Analysis of Comparative Studies. *Frontiers in psychiatry*, *12*, 690130. https://doi.org/10.3389/fpsyt.2021.690130

Calamante F. (2019). The Seven Deadly Sins of Measuring Brain Structural Connectivity Using Diffusion MRI Streamlines Fibre-Tracking. *Diagnostics (Basel, Switzerland)*, *9*(3), 115. https://doi.org/10.3390/diagnostics9030115

Calkins, M. E., Moore, T. M., Satterthwaite, T. D., Wolf, D. H., Turetsky, B. I., Roalf, D. R., … Gur, R. E. (2017). Persistence of psychosis spectrum symptoms in the Philadelphia Neurodevelopmental Cohort: a prospective two-year follow-up. *World psychiatry : official journal of the World Psychiatric Association (WPA)*, *16*(1), 62–76. https://doi.org/10.1002/wps.20386

Cao, H., Zhou, H., & Cannon, T. D. (2021). Functional connectome-wide associations of schizophrenia polygenic risk. *Molecular psychiatry*, *26*(6), 2553–2561. https://doi.org/10.1038/s41380-020-0699-3

Carballo, J. J., Muñoz-Lorenzo, L., Blasco-Fontecilla, H., Lopez-Castroman, J., García-Nieto, R., Dervic, K., … Baca-García, E. (2011). Continuity of depressive disorders from childhood and adolescence to adulthood: a naturalistic study in community mental health centers. *The primary care companion for CNS disorders*, *13*(5), PCC.11m01150. https://doi.org/10.4088/PCC.11m01150

Casey, B. J., Cannonier, T., Conley, M. I., Cohen, A. O., Barch, D. M., Heitzeg, M. M., … ABCD Imaging Acquisition Workgroup (2018). The Adolescent Brain Cognitive Development (ABCD) study: Imaging acquisition across 21 sites. *Developmental cognitive neuroscience*, *32*, 43–54. https://doi.org/10.1016/j.dcn.2018.03.001

Casey, B. J., Heller, A. S., Gee, D. G., & Cohen, A. O. (2019). Development of the emotional brain. *Neuroscience letters*, *693*, 29–34. https://doi.org/10.1016/j.neulet.2017.11.055

Cash, R.F.H., Müller, V.I., Fitzgerald, P.B., Eickhoff, S. B., & Zalesky, A. (2023). Altered brain activity in unipolar depression unveiled using connectomics. *Nature Mental Health* **1**, 174–185. https://doi.org/10.1038/s44220-023-00038-8

Caspi, A., & Moffitt, T. E. (2006). Gene-environment interactions in psychiatry: joining forces with neuroscience. *Nature reviews. Neuroscience*, *7*(7), 583–590. https://doi.org/10.1038/nrn1925

Castro-Schilo, L., & Grimm, K. J. (2018). Using residualized change versus difference scores for longitudinal research. *Journal of Social and Personal Relationships, 35*(1), 32-58. https://doi.org/10.1177/0265407517718387

Cattarinussi, G., Delvecchio, G., Sambataro, F., & Brambilla, P. (2022). The effect of polygenic risk scores for major depressive disorder, bipolar disorder and schizophrenia on morphological brain measures: A systematic review of the evidence. *Journal of affective disorders*, *310*, 213–222. https://doi.org/10.1016/j.jad.2022.05.007

Chang, C. C., Chow, C. C., Tellier, L. C., Vattikuti, S., Purcell, S. M., & Lee, J. J. (2015). Second-generation PLINK: rising to the challenge of larger and richer datasets. *GigaScience*, *4*, 7. https://doi.org/10.1186/s13742-015-0047-8

Chen, G., Hu, X., Li, L., Huang, X., Lui, S., Kuang, W., … Gong, Q. (2016). Disorganization of white matter architecture in major depressive disorder: a meta-analysis of diffusion tensor imaging with tract-based spatial statistics. *Scientific Reports*, *6*, 21825. https://doi.org/10.1038/srep21825

Chen, T., Chen, Z., & Gong, Q. (2021). White Matter-Based Structural Brain Network of Major Depression. *Advances in experimental medicine and biology*, *1305*, 35–55. https://doi.org/10.1007/978-981-33-6044-0_3

Cheng, S., Cheng, B., Liu, L., Yang, X., Meng, P., Yao, Y., … Zhang, F. (2022). Exome-wide screening identifies novel rare risk variants for major depression disorder. *Molecular psychiatry, 27*(7), 3069–3074. https://doi.org/10.1038/s41380-022-01536-4

Choi, K. S., Holtzheimer, P. E., Franco, A. R., Kelley, M. E., Dunlop, B. W., Hu, X. P., & Mayberg, H. S. (2014). Reconciling variable findings of white matter integrity in major depressive disorder. *Neuropsychopharmacology : official publication of the American College of Neuropsychopharmacology*, *39*(6), 1332–1339. https://doi.org/10.1038/npp.2013.345

Choi, S. W., & O'Reilly, P. F. (2019). PRSice-2: Polygenic Risk Score software for biobank-scale data. *GigaScience*, *8*(7), giz082. https://doi.org/10.1093/gigascience/giz082

Choi, S. W., Mak, T. S., & O'Reilly, P. F. (2020). Tutorial: a guide to performing polygenic risk score analyses. *Nature protocols*, *15*(9), 2759–2772. https://doi.org/10.1038/s41596-020-0353-1

Chopra, S., Segal, A., Oldham, S., Holmes, A., Sabaroedin, K., Orchard, E. R., … Fornito, A. (2023). Network-Based Spreading of Gray Matter Changes Across Different Stages of Psychosis. *JAMA psychiatry*, *80*(12), 1246–1257. https://doi.org/10.1001/jamapsychiatry.2023.3293

Cipriani, A., Furukawa, T. A., Salanti, G., Chaimani, A., Atkinson, L. Z., Ogawa, Y., … Geddes, J. R. (2018). Comparative efficacy and acceptability of 21 antidepressant drugs for the acute treatment of adults with major depressive disorder: a systematic review and network meta-

analysis. *Lancet (London, England)*, *391*(10128), 1357–1366. https://doi.org/10.1016/S0140-6736(17)32802-7

Coleman, J. R. I., Peyrot, W. J., Purves, K. L., Davis, K. A. S., Rayner, C., Choi, S. W., … Breen, G. (2020). Genome-wide gene-environment analyses of major depressive disorder and reported lifetime traumatic experiences in UK Biobank. *Molecular psychiatry, 25*(7), 1430–1446. https://doi.org/10.1038/s41380-019-0546-6

Collin, G., & Keshavan, M. S. (2018). Connectome development and a novel extension to the neurodevelopmental model of schizophrenia. *Dialogues in clinical neuroscience*, *20*(2), 101–111. https://doi.org/10.31887/DCNS.2018.20.2/gcollin

Collin, G., Sporns, O., Mandl, R. C., & van den Heuvel, M. P. (2014). Structural and functional aspects relating to cost and benefit of rich club organization in the human cerebral cortex. *Cerebral cortex (New York, N.Y. : 1991)*, *24*(9), 2258–2267. https://doi.org/10.1093/cercor/bht064

Crossley, N. A., Mechelli, A., Scott, J., Carletti, F., Fox, P. T., McGuire, P., & Bullmore, E. T. (2014). The hubs of the human connectome are generally implicated in the anatomy of brain disorders. *Brain : A Journal of Neurology*, *137*(Pt 8), 2382–2395. https://doi.org/10.1093/brain/awu132

Cui, L., Li, S., Wang, S., Wu, X., Liu, Y., Yu, W., … Li, B. (2024). Major depressive disorder: hypothesis, mechanism, prevention and treatment. *Signal transduction and targeted therapy, 9*(1), 30. https://doi.org/10.1038/s41392-024-01738-y

Cuijpers, P., Stringaris, A., & Wolpert, M. (2020). Treatment outcomes for depression: challenges and opportunities. *The lancet. Psychiatry*, *7*(11), 925–927. https://doi.org/10.1016/S2215-0366(20)30036-5

Davidson, R. J., Pizzagalli, D., Nitschke, J. B., & Putnam, K. (2002). Depression: perspectives from affective neuroscience. *Annual review of psychology, 53*, 545–574. https://doi.org/10.1146/annurev.psych.53.100901.135148

Davis, K. A. S., Coleman, J. R. I., Adams, M., Allen, N., Breen, G., Cullen, B., … Hotopf, M. (2020). Mental health in UK Biobank - development, implementation and results from an online questionnaire completed by 157 366 participants: a reanalysis. *BJPsych open, 6*(2), e18. https://doi.org/10.1192/bjo.2019.100

Desikan, R. S., Ségonne, F., Fischl, B., Quinn, B. T., Dickerson, B. C., Blacker, D., … Killiany, R. J. (2006). An automated labeling system for subdividing the human cerebral cortex on MRI scans into gyral based regions of interest. *NeuroImage, 31*(3), 968–980. https://doi.org/10.1016/j.neuroimage.2006.01.021

Dong, M., Zeng, L. N., Lu, L., Li, X. H., Ungvari, G. S., Ng, C. H., … Xiang, Y. T. (2019). Prevalence of suicide attempt in individuals with major depressive disorder: a meta-analysis

of observational surveys. *Psychological medicine*, *49*(10), 1691–1704. https://doi.org/10.1017/S0033291718002301

Doucet, G. E., Lin, D., Du, Y., Fu, Z., Glahn, D. C., Calhoun, V. D., … Frangou, S. (2020). Personalized estimates of morphometric similarity in bipolar disorder and schizophrenia. *NPJ schizophrenia*, *6*(1), 39. https://doi.org/10.1038/s41537-020-00128-x

Dutt, R. K., Hannon, K., Easley, T. O., Griffis, J. C., Zhang, W., & Bijsterbosch, J. D. (2022). Mental health in the UK Biobank: A roadmap to self-report measures and neuroimaging correlates. *Human brain mapping, 43*(2), 816–832. https://doi.org/10.1002/hbm.25690

ENIGMA Clinical High Risk for Psychosis Working Group, Haas, S. S., Ge, R., Agartz, I., Amminger, G. P., Andreassen, O. A., … Frangou, S. (2024). Normative Modeling of Brain Morphometry in Clinical High Risk for Psychosis. *JAMA psychiatry*, *81*(1), 77–88. https://doi.org/10.1001/jamapsychiatry.2023.3850

Everaerd, D., Klumpers, F., Zwiers, M., Guadalupe, T., Franke, B., van Oostrom, I., … Tendolkar, I. (2016). Childhood abuse and deprivation are associated with distinct sex-dependent differences in brain morphology. *Neuropsychopharmacology: official publication of the American College of Neuropsychopharmacology, 41*(7), 1716–1723. https://doi.org/10.1038/npp.2015.344

Fan, Y., Shi, F., Smith, J. K., Lin, W., Gilmore, J. H., & Shen, D. (2011). Brain anatomical networks in early human brain development. *NeuroImage, 54*(3), 1862–1871. https://doi.org/10.1016/j.neuroimage.2010.07.025

Feng, C., Thompson, W. K., & Paulus, M. P. (2022). Effect sizes of associations between neuroimaging measures and affective symptoms: A meta-analysis. *Depression and Anxiety*, *39*(1), 19–25. https://doi.org/10.1002/da.23215

Feng, G., Chen, R., Zhao, R., Li, Y., Ma, L., Wang, Y., … Shu, N. (2024). Author Correction: Longitudinal development of the human white matter structural connectome and its association with brain transcriptomic and cellular architecture. *Communications biology*, *7*(1), 85. https://doi.org/10.1038/s42003-024-05771-z

First, M. B., Spitzer, R. L., Gibbon, M., & Williams, J. B. W. (2002). Structured clinical interview for DSM-IV-TR axis I disorders, research version, patient edition. (SCID-I/P) New York: Biometrics Research, New York State Psychiatric Institute.

Fornito, A., Arnatkevičiūtė, A., & Fulcher, B. D. (2019). Bridging the Gap between Connectome and Transcriptome. *Trends in cognitive sciences*, *23*(1), 34–50. https://doi.org/10.1016/j.tics.2018.10.005

Fornito, A., Zalesky, A., & Breakspear, M. (2015). The connectomics of brain disorders. *Nature reviews. Neuroscience*, *16*(3), 159–172. https://doi.org/10.1038/nrn3901

Fried, E. I., & Nesse, R. M. (2014). The impact of individual depressive symptoms on impairment of psychosocial functioning. *PloS one*, *9*(2), e90311. https://doi.org/10.1371/journal.pone.0090311

Fried, E. I., & Nesse, R. M. (2015). Depression is not a consistent syndrome: An investigation of unique symptom patterns in the STAR*D study. *Journal of affective disorders*, *172*, 96–102. https://doi.org/10.1016/j.jad.2014.10.010

Friedman, N. P., & Robbins, T. W. (2022). The role of prefrontal cortex in cognitive control and executive function. *Neuropsychopharmacology : official publication of the American College of Neuropsychopharmacology, 47*(1), 72–89. https://doi.org/10.1038/s41386-021-01132-0

Fry, A., Littlejohns, T. J., Sudlow, C., Doherty, N., Adamska, L., Sprosen, T., … Allen, N. E. (2017). Comparison of Sociodemographic and Health-Related Characteristics of UK Biobank Participants With Those of the General Population. *American journal of epidemiology, 186*(9), 1026–1034. https://doi.org/10.1093/aje/kwx246

Fullerton, J. M., & Nurnberger, J. I. (2019). Polygenic risk scores in psychiatry: Will they be useful for clinicians?. *F1000Research*, *8*, F1000 Faculty Rev-1293. https://doi.org/10.12688/f1000research.18491.1

GBD 2019 Diseases and Injuries Collaborators (2020). Global burden of 369 diseases and injuries in 204 countries and territories, 1990-2019: a systematic analysis for the Global

Burden of Disease Study 2019. *Lancet (London, England)*, *396*(10258), 1204–1222. https://doi.org/10.1016/S0140-6736(20)30925-9

Georgiadis, F., Larivière, S., Glahn, D., Hong, L. E., Kochunov, P., Mowry, B., … Kirschner, M. (2024). Connectome architecture shapes large-scale cortical alterations in schizophrenia: a worldwide ENIGMA study. *Molecular psychiatry*, 10.1038/s41380-024-02442-7. Advance online publication. https://doi.org/10.1038/s41380-024-02442-7

Ghaziri, J., Tucholka, A., Girard, G., Boucher, O., Houde, J. C., Descoteaux, M., … Nguyen, D. K. (2018). Subcortical structural connectivity of insular subregions. *Scientific Reports*, *8*(1), 8596. https://doi.org/10.1038/s41598-018-26995-0

Giedd, J. N., Keshavan, M., & Paus, T. (2008). Why do many psychiatric disorders emerge during adolescence?. *Nature reviews. Neuroscience*, *9*(12), 947–957. https://doi.org/10.1038/nrn2513

Glaesmer, H., Schulz, A., Häuser, W., Freyberger, H. J., Brähler, E., & Grabe, H. J. (2013). Der Childhood Trauma Screener (CTS) - Entwicklung und Validierung von Schwellenwerten zur Klassifikation [The childhood trauma screener (CTS) - development and validation of cut-off-scores for classificatory diagnostics]. *Psychiatrische Praxis, 40*(4), 220–226. https://doi.org/10.1055/s-0033-1343116

Gong, Q., & He, Y. (2015). Depression, neuroimaging and connectomics: a selective overview. *Biological Psychiatry, 77*(3), 223–235. https://doi.org/10.1016/j.biopsych.2014.08.009

Gountouna, V. E., Job, D. E., McIntosh, A. M., Moorhead, T. W., Lymer, G. K., Whalley, H. C., … Lawrie, S. M. (2010). Functional Magnetic Resonance Imaging (fMRI) reproducibility and variance components across visits and scanning sites with a finger tapping task. *NeuroImage*, *49*(1), 552–560. https://doi.org/10.1016/j.neuroimage.2009.07.026

Gracia-Tabuenca, Z., & Alcauter, S. (2020). NBR: Network-based R-statistics for (unbalanced) longitudinal samples. *bioRxiv*. https://doi.org/10.1101/2020.11.07.373019

Gradin, V., Gountouna, V. E., Waiter, G., Ahearn, T. S., Brennan, D., Condon, B., … Steele, J. D. (2010). Between- and within-scanner variability in the CaliBrain study n-back cognitive task. *Psychiatry research*, *184*(2), 86–95. https://doi.org/10.1016/j.pscychresns.2010.08.010

Grady, C. L., Rieck, J. R., Nichol, D., Rodrigue, K. M., & Kennedy, K. M. (2021). Influence of sample size and analytic approach on stability and interpretation of brain-behavior correlations in task-related fMRI data. *Human Brain Mapping*, *42*(1), 204–219. https://doi.org/10.1002/hbm.25217

Green, C., Shen, X., Stevenson, A. J., Conole, E. L. S., Harris, M. A., Barbu, M. C., … Whalley, H. C. (2021). Structural brain correlates of serum and epigenetic markers of inflammation in major depressive disorder. *Brain, behavior, and immunity*, *92*, 39–48. https://doi.org/10.1016/j.bbi.2020.11.024

Greenberg, P. E., Fournier, A. A., Sisitsky, T., Pike, C. T., & Kessler, R. C. (2015). The economic burden of adults with major depressive disorder in the United States (2005 and 2010). *The Journal of clinical psychiatry*, *76*(2), 155–162. https://doi.org/10.4088/JCP.14m09298

Gui, Y., Zhou, X., Wang, Z., Zhang, Y., Wang, Z., Zhou, G., … Zhao, H. (2022). Sex-specific genetic association between psychiatric disorders and cognition, behavior and brain imaging in children and adults. *Translational psychiatry, 12*(1), 347. https://doi.org/10.1038/s41398-022-02041-6

Gunaydin, L. A., & Kreitzer, A. C. (2016). Cortico-Basal Ganglia Circuit Function in Psychiatric Disease. *Annual Review of Physiology*, *78*, 327–350. https://doi.org/10.1146/annurev-physiol-021115-105355

Haber S. N. (2016). Corticostriatal circuitry. *Dialogues in Clinical Neuroscience, 18*(1), 7–21. https://doi.org/10.31887/DCNS.2016.18.1/shaber

Habota, T., Sandu, A. L., Waiter, G. D., McNeil, C. J., Steele, J. D., Macfarlane, J. A., … McIntosh, A. M. (2021). Cohort profile for the STratifying Resilience and Depression Longitudinally (STRADL) study: A depression-focused investigation of Generation Scotland, using detailed clinical, cognitive, and neuroimaging assessments. *Wellcome Open Research, 4*, 185. https://doi.org/10.12688/wellcomeopenres.15538.2

Hagler, D. J., Jr, Ahmadi, M. E., Kuperman, J., Holland, D., McDonald, C. R., Halgren, E., & Dale, A. M. (2009). Automated white-matter tractography using a probabilistic diffusion

tensor atlas: Application to temporal lobe epilepsy. *Human brain mapping*, *30*(5), 1535–1547. https://doi.org/10.1002/hbm.20619

Hagler, D. J., Jr, Hatton, S., Cornejo, M. D., Makowski, C., Fair, D. A., Dick, A. S., … Dale, A. M. (2019). Image processing and analysis methods for the Adolescent Brain Cognitive Development Study. *NeuroImage*, *202*, 116091. https://doi.org/10.1016/j.neuroimage.2019.116091

Hahn, T., Winter, N. R., Ernsting, J., Gruber, M., Mauritz, M. J., Fisch, L., … Repple, J. (2023). Genetic, individual, and familial risk correlates of brain network controllability in major depressive disorder. *Molecular psychiatry*, *28*(3), 1057–1063. https://doi.org/10.1038/s41380-022-01936-6

Halldorsdottir, T., Piechaczek, C., Soares de Matos, A. P., Czamara, D., Pehl, V., Wagenbuechler, P., … Binder, E. B. (2019). Polygenic Risk: Predicting Depression Outcomes in Clinical and Epidemiological Cohorts of Youths. *The American journal of psychiatry*, *176*(8), 615–625. https://doi.org/10.1176/appi.ajp.2019.18091014

Hamilton, J. P., Siemer, M., & Gotlib, I. H. (2008). Amygdala volume in major depressive disorder: a meta-analysis of magnetic resonance imaging studies. *Molecular psychiatry*, *13*(11), 993–1000. https://doi.org/10.1038/mp.2008.57

Han, K. M., Choi, S., Jung, J., Na, K. S., Yoon, H. K., Lee, M. S., & Ham, B. J. (2014). Cortical thickness, cortical and subcortical volume, and white matter integrity in patients with their

first episode of major depression. *Journal of affective disorders*, *155*, 42–48. https://doi.org/10.1016/j.jad.2013.10.021

Han, S., Fang, K., Zheng, R., Li, S., Zhou, B., Sheng, W., … Zhang, Y. (2023). Gray matter atrophy is constrained by normal structural brain network architecture in depression. *Psychological medicine*, 1–11. Advance online publication. https://doi.org/10.1017/S0033291723003161

Hansen, J. Y., Shafiei, G., Vogel, J. W., Smart, K., Bearden, C. E., Hoogman, M … Misic, B. (2022). Local molecular and global connectomic contributions to cross-disorder cortical abnormalities. *Nature communications*, *13*(1), 4682. https://doi.org/10.1038/s41467-022-32420-y

Hanson, J. L., Chung, M. K., Avants, B. B., Shirtcliff, E. A., Gee, J. C., Davidson, R. J., & Pollak, S. D. (2010). Early stress is associated with alterations in the orbitofrontal cortex: a tensor-based morphometry investigation of brain structure and behavioral risk. *The Journal of neuroscience : the official journal of the Society for Neuroscience, 30*(22), 7466–7472. https://doi.org/10.1523/JNEUROSCI.0859-10.2010

Hardeveld, F., Spijker, J., De Graaf, R., Nolen, W. A., & Beekman, A. T. (2010). Prevalence and predictors of recurrence of major depressive disorder in the adult population. *Acta psychiatrica Scandinavica*, *122*(3), 184–191. https://doi.org/10.1111/j.1600-0447.2009.01519.x

Harris, M. A., Cox, S. R., de Nooij, L., Barbu, M. C., Adams, M. J., Shen, X., … Whalley, H. C. (2022). Correction: Structural neuroimaging measures and lifetime depression across levels of phenotyping in UK biobank. *Translational psychiatry, 12*(1), 282. https://doi.org/10.1038/s41398-022-02062-1

Hayes, A. F. (2013). Introduction to mediation, moderation, and conditional process analysis: A regression-based approach. Guilford Press.

He, J., Zhong, X., Cheng, C., Dong, D., Zhang, B., Wang, X., & Yao, S. (2023). Characteristics of white matter structural connectivity in healthy adults with childhood maltreatment. *European journal of psychotraumatology, 14*(1), 2179278. https://doi.org/10.1080/20008066.2023.2179278

Heller, C., Barth, C., Silk, T. J., Vijayakumar, N., Carmona, S., Martínez-García, M., … Petersen, N. (2024). The ENIGMA-Neuroendocrinology working group to bridge gaps in female mental health research. *Nature Mental Health, 2*, 348-350. https://doi.org/10.1038/s44220-024-00224-2

Helmer, M., Warrington, S., Mohammadi-Nejad, A. R., Ji, J. L., Howell, A., Rosand, B., … Murray, J. D. (2024). On the stability of canonical correlation analysis and partial least squares with application to brain-behavior associations. *Communications biology*, *7*(1), 217. https://doi.org/10.1038/s42003-024-05869-4

Hoeben, A., Joosten, E. A. J., & van den Beuken-van Everdingen, M. H. J. (2021). Personalized Medicine: Recent Progress in Cancer Therapy. *Cancers*, *13*(2), 242. https://doi.org/10.3390/cancers13020242

Holmes, A. J., Lee, P. H., Hollinshead, M. O., Bakst, L., Roffman, J. L., Smoller, J. W., & Buckner, R. L. (2012). Individual differences in amygdala-medial prefrontal anatomy link negative affect, impaired social functioning, and polygenic depression risk. *The Journal of neuroscience : the official journal of the Society for Neuroscience*, *32*(50), 18087–18100. https://doi.org/10.1523/JNEUROSCI.2531-12.2012

Howard, D. M., Adams, M. J., Clarke, T. K., Hafferty, J. D., Gibson, J., Shirali, M., … McIntosh, A. M. (2019). Genome-wide meta-analysis of depression identifies 102 independent variants and highlights the importance of the prefrontal brain regions. *Nature neuroscience, 22*(3), 343–352. https://doi.org/10.1038/s41593-018-0326-7

Humphreys, K. L., LeMoult, J., Wear, J. G., Piersiak, H. A., Lee, A., & Gotlib, I. H. (2020). Child maltreatment and depression: A meta-analysis of studies using the Childhood Trauma Questionnaire. *Child abuse & neglect*, *102*, 104361. https://doi.org/10.1016/j.chiabu.2020.104361

Hyde, J. S., & Mezulis, A. H. (2020). Gender Differences in Depression: Biological, Affective, Cognitive, and Sociocultural Factors. *Harvard review of psychiatry, 28*(1), 4–13. https://doi.org/10.1097/HRP.0000000000000230

Insel, T., Cuthbert, B., Garvey, M., Heinssen, R., Pine, D. S., Quinn, K., … Wang, P. (2010). Research domain criteria (RDoC): toward a new classification framework for research on mental disorders. *The American journal of psychiatry*, *167*(7), 748–751. https://doi.org/10.1176/appi.ajp.2010.09091379

Institute of Health Metrics and Evaluation. Global Health Data Exchange (GHDx). https://vizhub.healthdata.org/gbd-results/ (Accessed 4 March 2023).

Järnum, H., Eskildsen, S. F., Steffensen, E. G., Lundbye-Christensen, S., Simonsen, C. W., Thomsen, I. S., … Larsson, E. M. (2011). Longitudinal MRI study of cortical thickness, perfusion, and metabolite levels in major depressive disorder. *Acta psychiatrica Scandinavica*, *124*(6), 435–446. https://doi.org/10.1111/j.1600-0447.2011.01766.x

Jawabri, K. H., & Sharma, S. (2023). Physiology, Cerebral Cortex Functions. In StatPearls. StatPearls Publishing.

Jbabdi, S., & Johansen-Berg, H. (2011). Tractography: where do we go from here?. *Brain connectivity*, *1*(3), 169–183. https://doi.org/10.1089/brain.2011.0033

Jones, D. K., Knösche, T. R., & Turner, R. (2013). White matter integrity, fiber count, and other fallacies: the do's and don'ts of diffusion MRI. *NeuroImage*, *73*, 239–254. https://doi.org/10.1016/j.neuroimage.2012.06.081

Joormann, J., & Gotlib, I. H. (2010). Emotion regulation in depression: relation to cognitive inhibition. *Cognition & emotion, 24*(2), 281–298. https://doi.org/10.1080/02699930903407948

Kaiser, M., Martin, R., Andras, P., & Young, M. P. (2007). Simulation of robustness against lesions of cortical networks. *The European Journal of Neuroscience, 25*(10), 3185–3192. https://doi.org/10.1111/j.1460-9568.2007.05574.x

Kämpe, R., Paul, E. R., Östman, L., Heilig, M., Howard, D. M., & Hamilton, J. P. (2023). Contributions of polygenic risk and disease status to grey matter abnormalities in major depression. *Biological psychiatry. Cognitive neuroscience and neuroimaging*, S2451-9022(23)00338-5. Advance online publication. https://doi.org/10.1016/j.bpsc.2023.12.001

Karrouri, R., Hammani, Z., Benjelloun, R., & Otheman, Y. (2021). Major depressive disorder: Validated treatments and future challenges. *World journal of clinical cases*, *9*(31), 9350–9367. https://doi.org/10.12998/wjcc.v9.i31.9350

Kelsall, N. C., Wang, Y., Gameroff, M. J., Cha, J., Posner, J., Talati, A., … van Dijk, M. T. (2023). Differences in White Matter Structural Networks in Family Risk of Major Depressive Disorder and Suicidality: A Connectome Analysis. *medRxiv: the preprint server for health sciences*, 2023.09.07.23295211. https://doi.org/10.1101/2023.09.07.23295211

Kennis, M., Gerritsen, L., van Dalen, M., Williams, A., Cuijpers, P., & Bockting, C. (2020). Prospective biomarkers of major depressive disorder: a systematic review and meta-analysis. *Molecular psychiatry*, *25*(2), 321–338. https://doi.org/10.1038/s41380-019-0585-z

Kessler, R. C., & Bromet, E. J. (2013). The epidemiology of depression across cultures. *Annual review of public health*, *34*, 119–138. https://doi.org/10.1146/annurev-publhealth-031912-114409

Kessler, R.C., Andrews, G., Mroczek, D., Ustun, B., & Wittchen, H. (1998). The world health organisation composite international diagnostic interview short-form (CIDI-SF). *International Journal of Methods in Psychiatric Research, 7*(4), 171–185. https://doi.org/10.1002/mpr.47

Keysers, C., Gazzola, V., & Wagenmakers, E. J. (2020). Using Bayes factor hypothesis testing in neuroscience to establish evidence of absence. *Nature neuroscience, 23*(7), 788–799. https://doi.org/10.1038/s41593-020-0660-4

Kim, J., Kim, J. H., & Chang, K. A. (2021). Sex Difference in Peripheral Inflammatory Biomarkers in Drug-Naïve Patients with Major Depression in Young Adulthood. *Biomedicines, 9*(7), 708. https://doi.org/10.3390/biomedicines9070708

Kim, K., Shin, J. H., Myung, W., Fava, M., Mischoulon, D., Papakostas, G. I., … Jeon, H. J. (2019). Deformities of the Globus Pallidus are Associated with Severity of Suicidal Ideation and Impulsivity in Patients with Major Depressive Disorder. *Scientific Reports*, *9*(1), 7462. https://doi.org/10.1038/s41598-019-43882-4

Knol, M. J., van der Tweel, I., Grobbee, D. E., Numans, M. E., & Geerlings, M. I. (2007). Estimating interaction on an additive scale between continuous determinants in a logistic regression model. *International journal of epidemiology, 36*(5), 1111–1118. https://doi.org/10.1093/ije/dym157

Kochunov, P., Fan, F., Ryan, M. C., Hatch, K. S., Tan, S., Jahanshad, N., … Hong, L. E. (2022a). Translating ENIGMA schizophrenia findings using the regional vulnerability index: Association with cognition, symptoms, and disease trajectory. *Human brain mapping*, *43*(1), 566–575. https://doi.org/10.1002/hbm.25045

Kochunov, P., Hong, L. E., Dennis, E. L., Morey, R. A., Tate, D. F., Wilde, E. A., … Jahanshad, N. (2022b). ENIGMA-DTI: Translating reproducible white matter deficits into personalized vulnerability metrics in cross-diagnostic psychiatric research. *Human brain mapping*, *43*(1), 194–206. https://doi.org/10.1002/hbm.24998

Kochunov, P., Huang, J., Chen, S., Li, Y., Tan, S., Fan, F., … Hong, L. E. (2019). White Matter in Schizophrenia Treatment Resistance. *The American journal of psychiatry*, *176*(10), 829–838. https://doi.org/10.1176/appi.ajp.2019.18101212

Kochunov, P., Ryan, M. C., Yang, Q., Hatch, K. S., Zhu, A., Thomopoulos, S. I., … Hong, L. E. (2021). Comparison of regional brain deficit patterns in common psychiatric and neurological disorders as revealed by big data. *NeuroImage. Clinical*, *29*, 102574. https://doi.org/10.1016/j.nicl.2021.102574

Kong, X, Zhang, C., Liu, Y., & Pu, Y. (2022). Scanning reproducible brain-wide associations: sample size is all you need? *Psychoradiology, 2*(3), 67-68. https://doi.org/10.1093/psyrad/kkac010

Koolschijn, P. C., van Haren, N. E., Lensvelt-Mulders, G. J., Hulshoff Pol, H. E., & Kahn, R. S. (2009). Brain volume abnormalities in major depressive disorder: a meta-analysis of magnetic resonance imaging studies. *Human brain mapping*, *30*(11), 3719–3735. https://doi.org/10.1002/hbm.20801

Korgaonkar, M. S., Breukelaar, I. A., Felmingham, K., Williams, L. M., & Bryant, R. A. (2023). Association of Neural Connectome With Early Experiences of Abuse in Adults. *JAMA network open, 6*(1), e2253082. https://doi.org/10.1001/jamanetworkopen.2022.53082

Korgaonkar, M. S., Fornito, A., Williams, L. M., & Grieve, S. M. (2014). Abnormal structural networks characterize major depressive disorder: a connectome analysis. *Biological Psychiatry*, *76*(7), 567–574. https://doi.org/10.1016/j.biopsych.2014.02.018

Kovacs, M., Obrosky, S., & George, C. (2016). The course of major depressive disorder from childhood to young adulthood: Recovery and recurrence in a longitudinal observational study. *Journal of affective disorders*, *203*, 374–381. https://doi.org/10.1016/j.jad.2016.05.042

Krohne, H. W., Schmukle, S. C., Spaderna, H. & Spielberger, C. D. (2002). The State-Trait Depression Scales: An International Comparison. *Anxiety, Stress, & Coping, 15*(2), 105-122. https://doi.org/10.1080/10615800290028422

Kuehner C. (2017). Why is depression more common among women than among men?. *The lancet. Psychiatry*, *4*(2), 146–158. https://doi.org/10.1016/S2215-0366(16)30263-2

Kumar, V. J., Beckmann, C. F., Scheffler, K., & Grodd, W. (2022). Relay and higher-order thalamic nuclei show an intertwined functional association with cortical-networks. *Communications Biology, 5*(1), 1187. https://doi.org/10.1038/s42003-022-04126-w

Kupferberg, A., Bicks, L., & Hasler, G. (2016). Social functioning in major depressive disorder. *Neuroscience and biobehavioral reviews, 69*, 313–332. https://doi.org/10.1016/j.neubiorev.2016.07.002

Labonté, B., Engmann, O., Purushothaman, I., Menard, C., Wang, J., Tan, C., … Nestler, E. J. (2017). Sex-specific transcriptional signatures in human depression. *Nature medicine, 23*(9), 1102–1111. https://doi.org/10.1038/nm.4386

Lam, M., Awasthi, S., Watson, H. J., Goldstein, J., Panagiotaropoulou, G., Trubetskoy, V., … Ripke, S. (2020). RICOPILI: Rapid Imputation for COnsortias PIpeLIne. *Bioinformatics (Oxford, England)*, *36*(3), 930–933. https://doi.org/10.1093/bioinformatics/btz633

Latora, V., & Marchiori, M. (2001). Efficient behavior of small-world networks. *Physical Review Letters*, *87*(19), 198701. https://doi.org/10.1103/PhysRevLett.87.198701

Lebedeva, A. K., Westman, E., Borza, T., Beyer, M. K., Engedal, K., Aarsland, D., … Haberg, A. K. (2017). MRI-Based Classification Models in Prediction of Mild Cognitive Impairment and Dementia in Late-Life Depression. *Frontiers in Aging Neuroscience*, *9*, 13. https://doi.org/10.3389/fnagi.2017.00013

Levinson, D. F., Mostafavi, S., Milaneschi, Y., Rivera, M., Ripke, S., Wray, N. R., & Sullivan, P. F. (2014). Genetic studies of major depressive disorder: why are there no genome-wide association study findings and what can we do about it?. *Biological psychiatry*, *76*(7), 510–512. https://doi.org/10.1016/j.biopsych.2014.07.029

Lewis, C. M., & Vassos, E. (2020). Polygenic risk scores: from research tools to clinical instruments. *Genome medicine*, *12*(1), 44. https://doi.org/10.1186/s13073-020-00742-5

Li, G., Rossbach, K., Zhang, A., Liu, P., & Zhang, K. (2018). Resting-state functional changes in the precuneus within first-episode drug-naive patients with MDD. *Neuropsychiatric Disease and Treatment, 14*, 1991–1998. https://doi.org/10.2147/NDT.S168060

Liu, L., Wang, H., Chen, X., Zhang, Y., Zhang, H., & Xie, P. (2023). Gut microbiota and its metabolites in depression: from pathogenesis to treatment. *EBioMedicine, 90*, 104527. https://doi.org/10.1016/j.ebiom.2023.104527

Lohoff F. W. (2010). Overview of the genetics of major depressive disorder. *Current psychiatry reports*, *12*(6), 539–546. https://doi.org/10.1007/s11920-010-0150-6

Long, Z., Duan, X., Wang, Y., Liu, F., Zeng, L., Zhao, J. P., & Chen, H. (2015). Disrupted structural connectivity network in treatment-naive depression. *Progress in neuro-psychopharmacology & biological psychiatry*, *56*, 18–26. https://doi.org/10.1016/j.pnpbp.2014.07.007

Lorenzetti, V., Allen, N. B., Fornito, A., & Yücel, M. (2009). Structural brain abnormalities in major depressive disorder: a selective review of recent MRI studies. *Journal of affective disorders*, *117*(1-2), 1–17. https://doi.org/10.1016/j.jad.2008.11.021

Lu, Y., Liang, H., Han, D., Mo, Y., Li, Z., Cheng, Y., … Sun, X. (2016). The volumetric and shape changes of the putamen and thalamus in first episode, untreated major depressive disorder. *NeuroImage. Clinical*, *11*, 658–666. https://doi.org/10.1016/j.nicl.2016.04.008

MacDonald, K., Thomas, M. L., Sciolla, A. F., Schneider, B., Pappas, K., Bleijenberg, G., … Wingenfeld, K. (2016). Minimization of Childhood Maltreatment Is Common and Consequential: Results from a Large, Multinational Sample Using the Childhood Trauma Questionnaire. *PloS one, 11*(1), e0146058. https://doi.org/10.1371/journal.pone.0146058

Madden, R. A., Atkinson, K., Shen, X., Green, C., Hillary, R. F., Hawkins, E., … Whalley, H. C. (2023). Structural brain correlates of childhood trauma with replication across two large,

independent community-based samples. *European psychiatry : the journal of the Association of European Psychiatrists*, *66*(1), e19. https://doi.org/10.1192/j.eurpsy.2022.2347

Mansour L, S., Di Biase, M. A., Smith, R. E., Zalesky, A., & Seguin, C. (2023). Connectomes for 40,000 UK Biobank participants: A multi-modal, multi-scale brain network resource. *NeuroImage, 283*, 120407. https://doi.org/10.1016/j.neuroimage.2023.120407

Mao, R., Wang, C., Cui, L., Mellor, D., Wu, Z., & Fang, Y. (2024). Gender differences in prevalence and associations between cognitive symptoms and suicidal ideation in patients with recurrent major depressive disorder: findings from the Chinese NSSD study. *BMC psychiatry, 24*(1), 83. https://doi.org/10.1186/s12888-024-05557-x

Marek, S., & Dosenbach, N. U. F. (2018). The frontoparietal network: function, electrophysiology, and importance of individual precision mapping. *Dialogues in clinical neuroscience, 20*(2), 133–140. https://doi.org/10.31887/DCNS.2018.20.2/smarek

Marek, S., Tervo-Clemmens, B., Calabro, F. J., Montez, D. F., Kay, B. P., Hatoum, A. S., … Dosenbach, N. U. F. (2022). Reproducible brain-wide association studies require thousands of individuals. *Nature*, *603*(7902), 654–660. https://doi.org/10.1038/s41586-022-04492-9

Marquand, A. F., Kia, S. M., Zabihi, M., Wolfers, T., Buitelaar, J. K., & Beckmann, C. F. (2019). Conceptualizing mental disorders as deviations from normative functioning. *Molecular psychiatry*, *24*(10), 1415–1424. https://doi.org/10.1038/s41380-019-0441-1

Martin, A. R., Daly, M. J., Robinson, E. B., Hyman, S. E., & Neale, B. M. (2019). Predicting Polygenic Risk of Psychiatric Disorders. *Biological psychiatry*, *86*(2), 97–109. https://doi.org/10.1016/j.biopsych.2018.12.015

Medeiros, G. C., Prueitt, W. L., Minhajuddin, A., Patel, S. S., Czysz, A. H., Furman, J. L., Mason, B. L., Rush, A. J., Jha, M. K., & Trivedi, M. H. (2020). Childhood maltreatment and impact on clinical features of major depression in adults. *Psychiatry research, 293*, 113412. https://doi.org/10.1016/j.psychres.2020.113412

Mega, M. S., & Cummings, J. L. (1994). Frontal-subcortical circuits and neuropsychiatric disorders. *The Journal of neuropsychiatry and clinical neurosciences, 6*(4), 358–370. https://doi.org/10.1176/jnp.6.4.358

Mekonen, T., Chan, G. C. K., Connor, J. P., Hides, L., & Leung, J. (2021). Estimating the global treatment rates for depression: A systematic review and meta-analysis. *Journal of affective disorders*, *295*, 1234–1242. https://doi.org/10.1016/j.jad.2021.09.038

Miller, A. H., & Raison, C. L. (2016). The role of inflammation in depression: from evolutionary imperative to modern treatment target. *Nature reviews. Immunology*, *16*(1), 22–34. https://doi.org/10.1038/nri.2015.5

Mitchell, B. L., Thorp, J. G., Wu, Y., Campos, A. I., Nyholt, D. R., Gordon, S. D., … Byrne, E. M. (2021). Polygenic Risk Scores Derived From Varying Definitions of Depression and Risk of

Depression. *JAMA psychiatry*, *78*(10), 1152–1160. https://doi.org/10.1001/jamapsychiatry.2021.1988

Moitra, M., Santomauro, D., Collins, P. Y., Vos, T., Whiteford, H., Saxena, S., & Ferrari, A. J. (2022). The global gap in treatment coverage for major depressive disorder in 84 countries from 2000-2019: A systematic review and Bayesian meta-regression analysis. *PLoS medicine*, *19*(2), e1003901. https://doi.org/10.1371/journal.pmed.1003901

Morales-Muñoz, I., Upthegrove, R., Mallikarjun, P. K., Broome, M. R., & Marwaha, S. (2021). Longitudinal Associations Between Cognitive Deficits in Childhood and Psychopathological Symptoms in Adolescence and Young Adulthood. *JAMA network open*, *4*(4), e214724. https://doi.org/10.1001/jamanetworkopen.2021.4724

Mori, S., & van Zijl, P. (2007). Human white matter atlas. *The American journal of psychiatry*, *164*(7), 1005. https://doi.org/10.1176/ajp.2007.164.7.1005

Mou, J., Zheng, T., Long, Z., Mei, L., Wang, Y., Yuan, Y., …Qiu, L. (2023). Sex differences of brain cortical structure in major depressive disorder. *Psychoradiology, 3*, 2023, kkad014. https://doi.org/10.1093/psyrad/kkad014

Mullen S. (2018). Major depressive disorder in children and adolescents. *The mental health clinician*, *8*(6), 275–283. https://doi.org/10.9740/mhc.2018.11.275

Müller, V. I., Cieslik, E. C., Serbanescu, I., Laird, A. R., Fox, P. T., & Eickhoff, S. B. (2017). Altered Brain Activity in Unipolar Depression Revisited: Meta-analyses of Neuroimaging Studies. *JAMA psychiatry*, *74*(1), 47–55. https://doi.org/10.1001/jamapsychiatry.2016.2783

Mullins, N., & Lewis, C. M. (2017). Genetics of Depression: Progress at Last. *Current psychiatry reports*, *19*(8), 43. https://doi.org/10.1007/s11920-017-0803-9

Murray, G. K., Lin, T., Austin, J., McGrath, J. J., Hickie, I. B., & Wray, N. R. (2021). Could Polygenic Risk Scores Be Useful in Psychiatry?: A Review. *JAMA psychiatry*, *78*(2), 210–219. https://doi.org/10.1001/jamapsychiatry.2020.3042

Nagy, R., Boutin, T. S., Marten, J., Huffman, J. E., Kerr, S. M., Campbell, A., … Hayward, C. (2017). Exploration of haplotype research consortium imputation for genome-wide association studies in 20,032 Generation Scotland participants. *Genome medicine*, *9*(1), 23. https://doi.org/10.1186/s13073-017-0414-4

Nakagawa, S., & Cuthill, I. C. (2007). Effect size, confidence interval and statistical significance: a practical guide for biologists. *Biological reviews of the Cambridge Philosophical Society, 82*(4), 591–605. https://doi.org/10.1111/j.1469-185X.2007.00027.x

Nanni, V., Uher, R., & Danese, A. (2012). Childhood maltreatment predicts unfavorable course of illness and treatment outcome in depression: a meta-analysis. *The American journal of psychiatry*, *169*(2), 141–151. https://doi.org/10.1176/appi.ajp.2011.11020335

Negele, A., Kaufhold, J., Kallenbach, L., & Leuzinger-Bohleber, M. (2015). Childhood Trauma and Its Relation to Chronic Depression in Adulthood. *Depression research and treatment, 2015*, 650804. https://doi.org/10.1155/2015/650804

Nejati, V., Majidinezhad, M., & Nitsche, M. (2022). The role of the dorsolateral and ventromedial prefrontal cortex in emotion regulation in females with major depressive disorder (MDD): A tDCS study. *Journal of psychiatric research, 148*, 149–158. https://doi.org/10.1016/j.jpsychires.2022.01.030

Nelson, J., Klumparendt, A., Doebler, P., & Ehring, T. (2017). Childhood maltreatment and characteristics of adult depression: meta-analysis. *The British journal of psychiatry : the journal of mental science*, *210*(2), 96–104. https://doi.org/10.1192/bjp.bp.115.180752

Ng, T. H., Alloy, L. B., & Smith, D. V. (2019). Meta-analysis of reward processing in major depressive disorder reveals distinct abnormalities within the reward circuit. *Translational Psychiatry*, *9*(1), 293. https://doi.org/10.1038/s41398-019-0644-x

Olvet, D. M., Delaparte, L., Yeh, F. C., DeLorenzo, C., McGrath, P. J., Weissman, M. M., … Parsey, R. V. (2016). A COMPREHENSIVE EXAMINATION OF WHITE MATTER TRACTS AND CONNECTOMETRY IN MAJOR DEPRESSIVE DISORDER. *Depression and anxiety*, *33*(1), 56–65. https://doi.org/10.1002/da.22445

Onnela, J. P., Saramäki, J., Kertész, J., & Kaski, K. (2005). Intensity and coherence of motifs in weighted complex networks. *Physical review. E, Statistical, nonlinear, and soft matter physics*, *71*(6 Pt 2), 065103. https://doi.org/10.1103/PhysRevE.71.065103

Opsahl, T., Colizza, V., Panzarasa, P., & Ramasco, J. J. (2008). Prominence and control: the weighted rich-club effect. *Physical Review Letters*, *101*(16), 168702. https://doi.org/10.1103/PhysRevLett.101.168702

Orellana, S. C., Bethlehem, R. A. I., Simpson-Kent, I. L., van Harmelen, A. L., Vértes, P. E., & Bullmore, E. T. (2024). Childhood maltreatment influences adult brain structure through its effects on immune, metabolic, and psychosocial factors. *Proceedings of the National Academy of Sciences of the United States of America, 121*(16), e2304704121. https://doi.org/10.1073/pnas.2304704121

Ota, M., Noda, T., Sato, N., Hattori, K., Hori, H., Sasayama, D., … Kunugi, H. (2015). White matter abnormalities in major depressive disorder with melancholic and atypical features: A diffusion tensor imaging study. *Psychiatry and clinical neurosciences*, *69*(6), 360–368. https://doi.org/10.1111/pcn.12255

Padmanabhan, J. L., Cooke, D., Joutsa, J., Siddiqi, S. H., Ferguson, M., Darby, R. R., … Fox, M. D. (2019). A Human Depression Circuit Derived From Focal Brain Lesions. *Biological psychiatry*, *86*(10), 749–758. https://doi.org/10.1016/j.biopsych.2019.07.023

Papmeyer, M., Giles, S., Sussmann, J. E., Kielty, S., Stewart, T., Lawrie, S. M., … McIntosh, A. M. (2015). Cortical Thickness in Individuals at High Familial Risk of Mood Disorders as They Develop Major Depressive Disorder. *Biological psychiatry*, *78*(1), 58–66. https://doi.org/10.1016/j.biopsych.2014.10.018

Park, C., Rosenblat, J. D., Lee, Y., Pan, Z., Cao, B., Iacobucci, M., & McIntyre, R. S. (2019). The neural systems of emotion regulation and abnormalities in major depressive disorder. *Behavioural Brain Research, 367*, 181–188. https://doi.org/10.1016/j.bbr.2019.04.002

Peyrot, W. J., Van der Auwera, S., Milaneschi, Y., Dolan, C. V., Madden, P. A. F., Sullivan, P. F., … Penninx, B. W. J. H. (2018). Does Childhood Trauma Moderate Polygenic Risk for Depression? A Meta-analysis of 5765 Subjects From the Psychiatric Genomics Consortium. *Biological psychiatry, 84*(2), 138–147. https://doi.org/10.1016/j.biopsych.2017.09.009

Piccinelli, M., & Wilkinson, G. (2000). Gender differences in depression. Critical review. *The British journal of psychiatry : the journal of mental science, 177*, 486–492. https://doi.org/10.1192/bjp.177.6.486

Poldrack, R. A., Baker, C. I., Durnez, J., Gorgolewski, K. J., Matthews, P. M., Munafò, M. R., … Yarkoni, T. (2017). Scanning the horizon: towards transparent and reproducible neuroimaging research. *Nature Reviews. Neuroscience*, *18*(2), 115–126. https://doi.org/10.1038/nrn.2016.167

Poletti, S., Aggio, V., Brioschi, S., Bollettini, I., Falini, A., Colombo, C., & Benedetti, F. (2018). Impact of early and recent stress on white matter microstructure in major depressive disorder. *Journal of affective disorders*, *225*, 289–297. https://doi.org/10.1016/j.jad.2017.08.017

Prachason, T., Mutlu, I., Fusar-Poli, L., Menne-Lothmann, C., Decoster, J., van Winkel, R., … Guloksuz, S. (2023). Gender differences in the associations between childhood adversity and psychopathology in the general population. Social psychiatry and psychiatric epidemiology, 10.1007/s00127-023-02546-5. Advance online publication. https://doi.org/10.1007/s00127-023-02546-5

Qin, J., Wei, M., Liu, H., Yan, R., Luo, G., Yao, Z., & Lu, Q. (2014). Abnormal brain anatomical topological organization of the cognitive-emotional and the frontoparietal circuitry in major depressive disorder. *Magnetic resonance in medicine*, *72*(5), 1397–1407. https://doi.org/10.1002/mrm.25036

Qiu, L., Lui, S., Kuang, W., Huang, X., Li, J., Li, J., … Gong, Q. (2014). Regional increases of cortical thickness in untreated, first-episode major depressive disorder. *Translational psychiatry*, *4*(4), e378. https://doi.org/10.1038/tp.2014.18

Remes, O., Mendes, J. F., & Templeton, P. (2021). Biological, Psychological, and Social Determinants of Depression: A Review of Recent Literature. *Brain sciences*, *11*(12), 1633. https://doi.org/10.3390/brainsci11121633

Reus, L. M., Shen, X., Gibson, J., Wigmore, E., Ligthart, L., Adams, M. J., … McIntosh, A. M. (2017). Association of polygenic risk for major psychiatric illness with subcortical volumes and white matter integrity in UK Biobank. *Scientific reports*, *7*, 42140. https://doi.org/10.1038/srep42140

Robberegt, S. J., Brouwer, M. E., Kooiman, B. E. A. M., Stikkelbroek, Y. A. J., Nauta, M. H., & Bockting, C. L. H. (2023). Meta-Analysis: Relapse Prevention Strategies for Depression and Anxiety in Remitted Adolescents and Young Adults. *Journal of the American Academy of Child and Adolescent Psychiatry*, *62*(3), 306–317. https://doi.org/10.1016/j.jaac.2022.04.014

Roberts, R. E., Anderson, E. J., & Husain, M. (2013). White matter microstructure and cognitive function. *The Neuroscientist : a review journal bringing neurobiology, neurology and psychiatry*, *19*(1), 8–15. https://doi.org/10.1177/1073858411421218

Rolls, E. T., Cheng, W., & Feng, J. (2020). The orbitofrontal cortex: reward, emotion and depression. *Brain communications, 2*(2), fcaa196. https://doi.org/10.1093/braincomms/fcaa196

Rubinov, M., & Sporns, O. (2010). Complex network measures of brain connectivity: uses and interpretations. *NeuroImage*, *52*(3), 1059–1069. https://doi.org/10.1016/j.neuroimage.2009.10.003

Rush, A. J., Giles, D. E., Schlesser, M. A., Fulton, C. L., Weissenburger, J., & Burns, C. (1986). The Inventory for Depressive Symptomatology (IDS): preliminary findings. *Psychiatry research*, *18*(1), 65–87. https://doi.org/10.1016/0165-1781(86)90060-0

Rutherford, S., Barkema, P., Tso, I. F., Sripada, C., Beckmann, C. F., Ruhe, H. G., & Marquand, A. F. (2023). Evidence for embracing normative modeling. *eLife*, *12*, e85082. https://doi.org/10.7554/eLife.85082

Sacchet, M. D., Prasad, G., Foland-Ross, L. C., Thompson, P. M., & Gotlib, I. H. (2015). Support vector machine classification of major depressive disorder using diffusion-weighted neuroimaging and graph theory. *Frontiers in Psychiatry*, *6*, 21. https://doi.org/10.3389/fpsyt.2015.00021

Salk, R. H., Hyde, J. S., & Abramson, L. Y. (2017). Gender differences in depression in representative national samples: Meta-analyses of diagnoses and symptoms. *Psychological bulletin*, *143*(8), 783–822. https://doi.org/10.1037/bul0000102

Sarwar, T., Ramamohanarao, K., & Zalesky, A. (2019). Mapping connectomes with diffusion MRI: deterministic or probabilistic tractography?. *Magnetic resonance in medicine*, *81*(2), 1368–1384. https://doi.org/10.1002/mrm.27471

Sathyanarayanan, A., Mueller, T. T., Ali Moni, M., Schueler, K., ECNP TWG Network members, Baune, B. T., … Xicota, L. (2023). Multi-omics data integration methods and their applications in psychiatric disorders. *European neuropsychopharmacology : the journal of the European*

College of Neuropsychopharmacology, *69*, 26–46. https://doi.org/10.1016/j.euroneuro.2023.01.001

Scheurich, A., Fellgiebel, A., Schermuly, I., Bauer, S., Wölfges, R., & Müller, M. J. (2008). Experimental evidence for a motivational origin of cognitive impairment in major depression. *Psychological medicine, 38*(2), 237–246. https://doi.org/10.1017/S0033291707002206

Schmaal, L., Hibar, D. P., Sämann, P. G., Hall, G. B., Baune, B. T., Jahanshad, N., … Veltman, D. J. (2017). Cortical abnormalities in adults and adolescents with major depression based on brain scans from 20 cohorts worldwide in the ENIGMA Major Depressive Disorder Working Group. *Molecular psychiatry, 22*(6), 900–909. https://doi.org/10.1038/mp.2016.60

Schmaal, L., Pozzi, E., C Ho, T., van Velzen, L. S., Veer, I. M., Opel, N., … Veltman, D. J. (2020). ENIGMA MDD: seven years of global neuroimaging studies of major depression through worldwide data sharing. *Translational psychiatry*, *10*(1), 172. https://doi.org/10.1038/s41398-020-0842-6

Schmaal, L., Veltman, D. J., van Erp, T. G., Sämann, P. G., Frodl, T., Jahanshad, N., … Hibar, D. P. (2016). Subcortical brain alterations in major depressive disorder: findings from the ENIGMA Major Depressive Disorder working group. *Molecular psychiatry, 21*(6), 806–812. https://doi.org/10.1038/mp.2015.69

Sha, Z., Schijven, D., Fisher, S. E., & Francks, C. (2023). Genetic architecture of the white matter connectome of the human brain. *Science advances, 9*(7), eadd2870. https://doi.org/10.1126/sciadv.add2870

Shen, X., Howard, D. M., Adams, M. J., Hill, W. D., Clarke, T. K., Major Depressive Disorder Working Group of the Psychiatric Genomics Consortium, … McIntosh, A. M. (2020). A phenome-wide association and Mendelian Randomisation study of polygenic risk for depression in UK Biobank. *Nature communications, 11*(1), 2301. https://doi.org/10.1038/s41467-020-16022-0

Shen, X., Reus, L. M., Cox, S. R., Adams, M. J., Liewald, D. C., Bastin, M. E., … McIntosh, A. M. (2017). Subcortical volume and white matter integrity abnormalities in major depressive disorder: findings from UK Biobank imaging data. *Scientific reports*, *7*(1), 5547. https://doi.org/10.1038/s41598-017-05507-6

Silveira, P. P., Pokhvisneva, I., Howard, D. M., & Meaney, M. J. (2023). A sex-specific genome-wide association study of depression phenotypes in UK Biobank. *Molecular psychiatry, 28*(6), 2469–2479. https://doi.org/10.1038/s41380-023-01960-0

Sim, K., Lau, W. K., Sim, J., Sum, M. Y., & Baldessarini, R. J. (2015). Prevention of Relapse and Recurrence in Adults with Major Depressive Disorder: Systematic Review and Meta-Analyses of Controlled Trials. *The international journal of neuropsychopharmacology*, *19*(2), pyv076. https://doi.org/10.1093/ijnp/pyv076

Smith, B. H., Campbell, A., Linksted, P., Fitzpatrick, B., Jackson, C., Kerr, S. M., … Morris, A. D. (2013). Cohort Profile: Generation Scotland: Scottish Family Health Study (GS:SFHS). The study, its participants and their potential for genetic research on health and illness. *International journal of epidemiology*, *42*(3), 689–700. https://doi.org/10.1093/ije/dys084

Smith, K., Bastin, M. E., Cox, S. R., Valdés Hernández, M. C., Wiseman, S., Escudero, J., & Sudlow, C. (2019). Hierarchical complexity of the adult human structural connectome. *NeuroImage, 191*, 205–215. https://doi.org/10.1016/j.neuroimage.2019.02.028

Smith, S. M., & Nichols, T. E. (2018). Statistical Challenges in "Big Data" Human Neuroimaging. *Neuron*, *97*(2), 263–268. https://doi.org/10.1016/j.neuron.2017.12.018

Smith, S. M., Nichols, T. E., Vidaurre, D., Winkler, A. M., Behrens, T. E., Glasser, M. F., …Miller, K. L. (2015). A positive-negative mode of population covariation links brain connectivity, demographics and behavior. *Nature neuroscience*, *18*(11), 1565–1567. https://doi.org/10.1038/nn.4125

Soares, J. M., Marques, P., Alves, V., & Sousa, N. (2013). A hitchhiker's guide to diffusion tensor imaging. *Frontiers in neuroscience*, *7*, 31. https://doi.org/10.3389/fnins.2013.00031

Solmi, M., Radua, J., Olivola, M., Croce, E., Soardo, L., Salazar de Pablo, G., … Fusar-Poli, P. (2022). Age at onset of mental disorders worldwide: large-scale meta-analysis of 192

epidemiological studies. *Molecular psychiatry*, *27*(1), 281–295. https://doi.org/10.1038/s41380-021-01161-7

Sotiropoulos, S. N., & Zalesky, A. (2019). Building connectomes using diffusion MRI: why, how and but. *NMR in biomedicine*, *32*(4), e3752. https://doi.org/10.1002/nbm.3752

Sporns O. (2011). The human connectome: a complex network. *Annals of the New York Academy of Sciences, 1224*, 109–125. https://doi.org/10.1111/j.1749-6632.2010.05888.x

Sporns O. (2018). Graph theory methods: applications in brain networks. *Dialogues in clinical neuroscience*, *20*(2), 111–121. https://doi.org/10.31887/DCNS.2018.20.2/osporns

Sporns, O., Tononi, G., & Kötter, R. (2005). The human connectome: A structural description of the human brain. *PLoS computational biology*, *1*(4), e42. https://doi.org/10.1371/journal.pcbi.0010042

Stolicyn, A., Harris, M. A., Shen, X., Barbu, M. C., Adams, M. J., Hawkins, E. L., … Whalley, H. C. (2020). Automated classification of depression from structural brain measures across two independent community-based cohorts. *Human brain mapping*, *41*(14), 3922–3937. https://doi.org/10.1002/hbm.25095

Struck, N., Krug, A., Yuksel, D., Stein, F., Schmitt, S., Meller, T., … Brakemeier, E. L. (2020). Childhood maltreatment and adult mental disorders - the prevalence of different types of

maltreatment and associations with age of onset and severity of symptoms. *Psychiatry research*, *293*, 113398. https://doi.org/10.1016/j.psychres.2020.113398

Sturm, V. E., Haase, C. M., & Levenson, R. W. (2016). Emotional dysfunction in psychopathology and neuropathology: Neural and genetic pathways. In T. Lehner, B. L. Miller, & M. W. State (Eds.), Genomics, circuits, and pathways in clinical neuropsychiatry (pp. 345–364). Elsevier Academic Press. https://doi.org/10.1016/B978-0-12-800105-9.00022-6

Suárez, L. E., Markello, R. D., Betzel, R. F., & Misic, B. (2020). Linking Structure and Function in Macroscale Brain Networks. *Trends in cognitive sciences*, *24*(4), 302–315. https://doi.org/10.1016/j.tics.2020.01.008

Sudlow, C., Gallacher, J., Allen, N., Beral, V., Burton, P., Danesh, J., … Collins, R. (2015). UK biobank: an open access resource for identifying the causes of a wide range of complex diseases of middle and old age. *PLoS Medicine*, *12*(3), e1001779. https://doi.org/10.1371/journal.pmed.1001779

Sullivan, P. F., Neale, M. C., & Kendler, K. S. (2000). Genetic epidemiology of major depression: review and meta-analysis. *The American journal of psychiatry*, *157*(10), 1552–1562. https://doi.org/10.1176/appi.ajp.157.10.1552

Tamnes, C. K., Herting, M. M., Goddings, A. L., Meuwese, R., Blakemore, S. J., Dahl, R. E., … Mills, K. L. (2017). Development of the Cerebral Cortex across Adolescence: A Multisample Study of Inter-Related Longitudinal Changes in Cortical Volume, Surface Area, and

Thickness. *The Journal of neuroscience : the official journal of the Society for Neuroscience*, *37*(12), 3402–3412. https://doi.org/10.1523/JNEUROSCI.3302-16.2017

Teicher, M. H., Anderson, C. M., Ohashi, K., & Polcari, A. (2014). Childhood maltreatment: altered network centrality of cingulate, precuneus, temporal pole and insula. *Biological psychiatry, 76*(4), 297–305. https://doi.org/10.1016/j.biopsych.2013.09.016

Teicher, M. H., Gordon, J. B., & Nemeroff, C. B. (2022). Recognizing the importance of childhood maltreatment as a critical factor in psychiatric diagnoses, treatment, research, prevention, and education. *Molecular psychiatry*, *27*(3), 1331–1338. https://doi.org/10.1038/s41380-021-01367-9

Teicher, M. H., Samson, J. A., Anderson, C. M., & Ohashi, K. (2016). The effects of childhood maltreatment on brain structure, function and connectivity. *Nature reviews. Neuroscience, 17*(10), 652–666. https://doi.org/10.1038/nrn.2016.111

Tervo-Clemmens, B., Marek, S., Chauvin, R. J., Van, A. N., Kay, B. P., Laumann, T. O., … Dosenbach, N. U. F. (2023). Reply to: Multivariate BWAS can be replicable with moderate sample sizes. *Nature*, *615*(7951), E8–E12. https://doi.org/10.1038/s41586-023-05746-w

Thapar, A., Collishaw, S., Pine, D. S., & Thapar, A. K. (2012). Depression in adolescence. *Lancet (London, England)*, *379*(9820), 1056–1067. https://doi.org/10.1016/S0140-6736(11)60871-4

The 1000 Genomes Project Consortium, Auton, A., Brooks, L. D., Durbin, R. M., Garrison, E. P., Kang, H. M., … Abecasis, G. R. (2015). A global reference for human genetic variation. *Nature*, *526*(7571), 68–74. https://doi.org/10.1038/nature15393

The Lancet Global Health (2020). Mental health matters. *The Lancet. Global health*, *8*(11), e1352. https://doi.org/10.1016/S2214-109X(20)30432-0

Thng, G., Shen, X., Stolicyn, A., Adams, M. J., Yeung, H. W., Batziou, V., … Whalley, H. C. (2024). A comprehensive hierarchical comparison of structural connectomes in Major Depressive Disorder cases v. controls in two large population samples. *Psychological Medicine*, 1–12. https://doi.org/10.1017/S0033291724000643

Thng, G., Shen, X., Stolicyn, A., Harris, M. A., Adams, M. J., Barbu, M. C., … Whalley, H. C. (2022). Comparing personalized brain-based and genetic risk scores for major depressive disorder in large population samples of adults and adolescents. *European psychiatry: the journal of the Association of European Psychiatrists*, *65*(1), e44. https://doi.org/10.1192/j.eurpsy.2022.2301

Thomas, C., Ye, F. Q., Irfanoglu, M. O., Modi, P., Saleem, K. S., Leopold, D. A., & Pierpaoli, C. (2014). Anatomical accuracy of brain connections derived from diffusion MRI tractography is inherently limited. *Proceedings of the National Academy of Sciences of the United States of America*, *111*(46), 16574–16579. https://doi.org/10.1073/pnas.1405672111

Thorp, J. G., Gerring, Z. F., Colodro-Conde, L., Byrne, E. M., Medland, S. E., Middeldorp, C. M., & Derks, E. M. (2023). The association between trauma exposure, polygenic risk and individual depression symptoms. *Psychiatry research, 321*, 115101. https://doi.org/10.1016/j.psychres.2023.115101

Toenders, Y. J., Schmaal, L., Nawijn, L., Han, L. K. M., Binnewies, J., van der Wee, N. J. A., … Penninx, B. W. J. H. (2022). The association between clinical and biological characteristics of depression and structural brain alterations. *Journal of affective disorders*, *312*, 268–274. https://doi.org/10.1016/j.jad.2022.06.056

Tozzi, L., Garczarek, L., Janowitz, D., Stein, D. J., Wittfeld, K., Dobrowolny, H., … 'for the ENIGMA-MDD Consortium' (2020). Interactive impact of childhood maltreatment, depression, and age on cortical brain structure: mega-analytic findings from a large multi-site cohort. *Psychological medicine, 50*(6), 1020–1031. https://doi.org/10.1017/S003329171900093X

Uher R. (2008). The implications of gene-environment interactions in depression: will cause inform cure?. *Molecular psychiatry*, *13*(12), 1070–1078. https://doi.org/10.1038/mp.2008.92

van den Heuvel, M. P., & Sporns, O. (2011). Rich-club organization of the human connectome. *The Journal of Neuroscience : the official journal of the Society for Neuroscience*, *31*(44), 15775–15786. https://doi.org/10.1523/JNEUROSCI.3539-11.2011

van den Heuvel, M. P., & Sporns, O. (2013). Network hubs in the human brain. *Trends in Cognitive Sciences*, *17*(12), 683–696. https://doi.org/10.1016/j.tics.2013.09.012

van den Heuvel, M. P., Kahn, R. S., Goñi, J., & Sporns, O. (2012). High-cost, high-capacity backbone for global brain communication. *Proceedings of the National Academy of Sciences of the United States of America*, *109*(28), 11372–11377. https://doi.org/10.1073/pnas.1203593109

van Eijndhoven, P., van Wingen, G., Katzenbauer, M., Groen, W., Tepest, R., Fernández, G., … Tendolkar, I. (2013). Paralimbic cortical thickness in first-episode depression: evidence for trait-related differences in mood regulation. *The American journal of psychiatry*, *170*(12), 1477–1486. https://doi.org/10.1176/appi.ajp.2013.12121504

van Velzen, L. S., Kelly, S., Isaev, D., Aleman, A., Aftanas, L. I., Bauer, J., … Schmaal, L. (2020). White matter disturbances in major depressive disorder: a coordinated analysis across 20 international cohorts in the ENIGMA MDD working group. *Molecular Psychiatry*, *25*(7), 1511–1525. https://doi.org/10.1038/s41380-019-0477-2

Vandewouw, M. M., Pang, E. W., Lai, M. C., Kelley, E., Ayub, M., Lerch, J. P., … Anagnostou, E. (2023). Richer than we thought: neurophysiological methods reveal rich-club network development is frequency- and sex-dependent. *iScience, 26*(4), 106384. https://doi.org/10.1016/j.isci.2023.106384

Videbech, P., & Ravnkilde, B. (2004). Hippocampal volume and depression: a meta-analysis of MRI studies. *The American journal of psychiatry, 161*(11), 1957–1966. https://doi.org/10.1176/appi.ajp.161.11.1957

Vinkers, C. H., Joëls, M., Milaneschi, Y., Kahn, R. S., Penninx, B. W., & Boks, M. P. (2014). Stress exposure across the life span cumulatively increases depression risk and is moderated by neuroticism. *Depression and anxiety*, *31*(9), 737–745. https://doi.org/10.1002/da.22262

Wade, M., Wright, L., & Finegold, K. E. (2022). The effects of early life adversity on children's mental health and cognitive functioning. *Translational psychiatry, 12*(1), 244. https://doi.org/10.1038/s41398-022-02001-0

Wainberg, M., Forde, N. J., Mansour, S., Kerrebijn, I., Medland, S. E., Hawco, C., & Tripathy, S. J. (2024). Genetic architecture of the structural connectome. *Nature communications*, *15*(1), 1962. https://doi.org/10.1038/s41467-024-46023-2

Wang, R., Lifelines Cohort Study, Hartman, C. A., & Snieder, H. (2023). Stress-related exposures amplify the effects of genetic susceptibility on depression and anxiety. *Translational psychiatry*, *13*(1), 27. https://doi.org/10.1038/s41398-023-02327-3

Wang, Y., Wang, Q., Xie, J., Zhu, Y., Zhang, D., Li, G., Zhu, X., & Li, Y. (2022). Mediation on the Association Between Stressful Life Events and Depression by Abnormal White Matter Microstructures. *Biological psychiatry. Cognitive neuroscience and neuroimaging*, *7*(2), 162–170. https://doi.org/10.1016/j.bpsc.2021.03.009

Wang, Z., Yuan, Y., You, J., & Zhang, Z. (2020). Disrupted structural brain connectome underlying the cognitive deficits in remitted late-onset depression. *Brain imaging and behavior*, *14*(5), 1600–1611. https://doi.org/10.1007/s11682-019-00091-x

Warren, D. E., Power, J. D., Bruss, J., Denburg, N. L., Waldron, E. J., Sun, H., … Tranel, D. (2014). Network measures predict neuropsychological outcome after brain injury. *Proceedings of the National Academy of Sciences of the United States of America*, *111*(39), 14247–14252. https://doi.org/10.1073/pnas.1322173111

Waumans, R. C., Muntingh, A. D. T., Draisma, S., Huijbregts, K. M., van Balkom, A. J. L. M., & Batelaan, N. M. (2022). Barriers and facilitators for treatment-seeking in adults with a depressive or anxiety disorder in a Western-European health care setting: a qualitative study. *BMC psychiatry*, *22*(1), 165. https://doi.org/10.1186/s12888-022-03806-5

Wei, K., Cieslak, M., Greene, C., Grafton, S. T., & Carlson, J. M. (2017). Sensitivity analysis of human brain structural network construction. *Network Neuroscience (Cambridge, Mass.), 1*(4), 446–467. https://doi.org/10.1162/NETN_a_00025

Whiteford, H. A., Degenhardt, L., Rehm, J., Baxter, A. J., Ferrari, A. J., Erskine, H. E., … Vos, T. (2013). Global burden of disease attributable to mental and substance use disorders: findings from the Global Burden of Disease Study 2010. *Lancet (London, England)*, *382*(9904), 1575–1586. https://doi.org/10.1016/S0140-6736(13)61611-6

Wiersma, J. E., Hovens, J. G., van Oppen, P., Giltay, E. J., van Schaik, D. J., Beekman, A. T., & Penninx, B. W. (2009). The importance of childhood trauma and childhood life events for chronicity of depression in adults. *The Journal of clinical psychiatry*, *70*(7), 983–989. https://doi.org/10.4088/jcp.08m04521

Williams, L. M., Debattista, C., Duchemin, A. M., Schatzberg, A. F., & Nemeroff, C. B. (2016). Childhood trauma predicts antidepressant response in adults with major depression: data from the randomized international study to predict optimized treatment for depression. *Translational psychiatry*, *6*(5), e799. https://doi.org/10.1038/tp.2016.61

Winter, N. R., Leenings, R., Ernsting, J., Sarink, K., Fisch, L., Emden, D., … Hahn, T. (2022). Quantifying Deviations of Brain Structure and Function in Major Depressive Disorder Across Neuroimaging Modalities. *JAMA Psychiatry*, *79*(9), 879–888. https://doi.org/10.1001/jamapsychiatry.2022.1780

Witt, A., Öz, Y., Sachser, C., Brähler, E., Glaesmer, H., & Fegert, J. M. (2022). Validation and standardization of the Childhood Trauma Screener (CTS) in the general population. *Child and adolescent psychiatry and mental health, 16*(1), 73. https://doi.org/10.1186/s13034-022-00506-6

Woelfer, M., Kasties, V., Kahlfuss, S., & Walter, M. (2019). The Role of Depressive Subtypes within the Neuroinflammation Hypothesis of Major Depressive Disorder. *Neuroscience*, *403*, 93–110. https://doi.org/10.1016/j.neuroscience.2018.03.034

World Health Organization. Suicide worldwide in 2019: Global Health Estimates. Geneva, Switzerland: World Health Organization, 2021.

Wray, N. R., Pergadia, M. L., Blackwood, D. H., Penninx, B. W., Gordon, S. D., Nyholt, D. R., … Sullivan, P. F. (2012). Genome-wide association study of major depressive disorder: new results, meta-analysis, and lessons learned. *Molecular psychiatry*, *17*(1), 36–48. https://doi.org/10.1038/mp.2010.109

Wray, N. R., Ripke, S., Mattheisen, M., Trzaskowski, M., Byrne, E. M., Abdellaoui, A., … Major Depressive Disorder Working Group of the Psychiatric Genomics Consortium (2018). Genome-wide association analyses identify 44 risk variants and refine the genetic architecture of major depression. *Nature genetics*, *50*(5), 668–681. https://doi.org/10.1038/s41588-018-0090-3

Wray, N. R., Yang, J., Hayes, B. J., Price, A. L., Goddard, M. E., & Visscher, P. M. (2013). Pitfalls of predicting complex traits from SNPs. *Nature reviews. Genetics*, *14*(7), 507–515. https://doi.org/10.1038/nrg3457

Xia, C. H., Ma, Z., Ciric, R., Gu, S., Betzel, R. F., Kaczkurkin, A. N., … Satterthwaite, T. D. (2018). Linked dimensions of psychopathology and connectivity in functional brain networks. *Nature communications*, *9*(1), 3003. https://doi.org/10.1038/s41467-018-05317-y

Xie, Y., Sun, J., Man, W., Zhang, Z., & Zhang, N. (2023). Personalized estimates of brain cortical structural variability in individuals with Autism spectrum disorder: the predictor of

brain age and neurobiology relevance. *Molecular autism*, *14*(1), 27. https://doi.org/10.1186/s13229-023-00558-1

Xu, S. X., Deng, W. F., Qu, Y. Y., Lai, W. T., Huang, T. Y., Rong, H., & Xie, X. H. (2021). The integrated understanding of structural and functional connectomes in depression: A multimodal meta-analysis of graph metrics. *Journal of Affective Disorders*, *295*, 759–770. https://doi.org/10.1016/j.jad.2021.08.120

Yan, W., Pearlson, G. D., Fu, Z., Li, X., Iraji, A., Chen, J., … Calhoun, V. D. (2024). A Brainwide Risk Score for Psychiatric Disorder Evaluated in a Large Adolescent Population Reveals Increased Divergence Among Higher-Risk Groups Relative to Control Participants. *Biological psychiatry*, *95*(7), 699–708. https://doi.org/10.1016/j.biopsych.2023.09.017

Yekutieli D. (2008). Hierarchical False Discovery Rate–Controlling Methodology. *Journal of the American Statistical Association, 103*(481), 309-316. https://doi.org/10.1198/016214507000001373

Yeung, H. W., Stolicyn, A., Shen, X., Adams, M. J., Romaniuk, L., Thng, G., …Whalley, H. C. (2024). Classification accuracy of structural and functional connectomes across different depressive phenotypes. *Imaging Neurosicence, 2*, 1-24. https://doi.org/10.1162/imag_a_00064

Yu, M., Linn, K. A., Shinohara, R. T., Oathes, D. J., Cook, P. A., Duprat, R., … Sheline, Y. I. (2019). Childhood trauma history is linked to abnormal brain connectivity in major

depression. *Proceedings of the National Academy of Sciences of the United States of America, 116*(17), 8582–8590. https://doi.org/10.1073/pnas.1900801116

Yuan, P., & Raz, N. (2014). Prefrontal cortex and executive functions in healthy adults: a meta-analysis of structural neuroimaging studies. *Neuroscience and biobehavioral reviews, 42*, 180–192. https://doi.org/10.1016/j.neubiorev.2014.02.005

Yun, J. Y., & Kim, Y. K. (2021). Graph theory approach for the structural-functional brain connectome of depression. *Progress in Neuro-psychopharmacology & Biological Psychiatry*, *111*, 110401. https://doi.org/10.1016/j.pnpbp.2021.110401

Zalesky, A., Fornito, A., & Bullmore, E. T. (2010). Network-based statistic: identifying differences in brain networks. *NeuroImage*, *53*(4), 1197–1207. https://doi.org/10.1016/j.neuroimage.2010.06.041

Zhang, F. F., Peng, W., Sweeney, J. A., Jia, Z. Y., & Gong, Q. Y. (2018). Brain structure alterations in depression: Psychoradiological evidence. *CNS neuroscience & therapeutics, 24*(11), 994–1003. https://doi.org/10.1111/cns.12835

Zhang, X., Yan, H., Yu, H., Zhao, X., Shah, S., Dong, Z., … Tan, H. Y. (2021). Childhood urbanicity interacts with polygenic risk for depression to affect stress-related medial prefrontal function. *Translational psychiatry*, *11*(1), 522. https://doi.org/10.1038/s41398-021-01650-x

Zhang, Y., Zhang, Y., Ai, H., Van Dam, N. T., Qian, L., Hou, G., & Xu, P. (2022). Microstructural deficits of the thalamus in major depressive disorder. *Brain Communications*, *4*(5), fcac236. https://doi.org/10.1093/braincomms/fcac236

Zhao, S., Wang, G., Yan, T., Xiang, J., Yu, X., Li, H., & Wang, B. (2021). Sex Differences in Anatomical Rich-Club and Structural-Functional Coupling in the Human Brain Network. *Cerebral cortex (New York, N.Y. : 1991), 31*(4), 1987–1997. https://doi.org/10.1093/cercor/bhaa335

Zhao, T., Xu, Y., & He, Y. (2019). Graph theoretical modeling of baby brain networks. *NeuroImage*, *185*, 711–727. https://doi.org/10.1016/j.neuroimage.2018.06.038

Zheng, K., Wang, H., Li, J., Yan, B., Liu, J., Xi, Y., … Li, B. (2019). Structural networks analysis for depression combined with graph theory and the properties of fiber tracts via diffusion tensor imaging. *Neuroscience letters*, *694*, 34–40. https://doi.org/10.1016/j.neulet.2018.11.025

Zhou, H. X., Chen, X., Shen, Y. Q., Li, L., Chen, N. X., Zhu, Z. C., … Yan, C. G. (2020). Rumination and the default mode network: Meta-analysis of brain imaging studies and implications for depression. *NeuroImage*, *206*, 116287. https://doi.org/10.1016/j.neuroimage.2019.116287

Zhuo, C., Li, G., Lin, X., Jiang, D., Xu, Y., Tian, H., … Song, X. (2019). The rise and fall of MRI studies in major depressive disorder. *Translational psychiatry*, *9*(1), 335. https://doi.org/10.1038/s41398-019-0680-6

Zimmerman, M., Ellison, W., Young, D., Chelminski, I., & Dalrymple, K. (2015). How many different ways do patients meet the diagnostic criteria for major depressive disorder?. *Comprehensive psychiatry*, *56*, 29–34. https://doi.org/10.1016/j.comppsych.2014.09.007

Zou, K., Huang, X., Li, T., Gong, Q., Li, Z., Ou-yang, L., … Sun, X. (2008). Alterations of white matter integrity in adults with major depressive disorder: a magnetic resonance imaging study. *Journal of psychiatry & neuroscience : JPN*, *33*(6), 525–530.

Appendix 1: Supplementary materials for Chapter 2

A comprehensive hierarchical comparison of structural connectomes in Major Depressive Disorder cases v. controls in two large population samples

Supplementary Materials

Thng *et al*.

OVERVIEW

Supplementary text

Supplementary Figures

Supplementary Tables

1: Proportion of UKB and GS lifetime MDD cases with current MDD

For UKB, current MDD was assessed using questions based on the Patient's Health Questionnaire (PHQ; field IDs: 20514, 20510, 20517, 20519, 20511, 20507, 20508, 20518, 20513; see Davis et al (2020)). Among subjects that were identified as cases with lifetime MDD in our study, only 6% fulfilled the criteria (PHQ>=5) for current MDD. We also extracted the variable "frequency of depressed mood in last two weeks" (field ID: 2050) that was asked during the day of the imaging assessment. Among the MDD cases in our study, 67% responded "not at all", 26% responded "several days", 4% responded "more than half the days", and 3% responded "nearly every day".

For GS, current MDD was best assessed using the 16-item Quick Inventory of Depressive Symptomatology (QIDS), which looks at depressive symptoms over the past seven days (Yeung et al., 2012). It is rated on a four-point Likert scale from 0 to 3. Total QIDS scores range from 0 to 27 (0-5: no depression, 6-10: mild depression, 11-15: moderate depression, 16-20: severe depression, >21: very severe depression). For subjects that were identified as cases in our GS sample, they had a mean Total QIDS score of 4, suggesting that majority did not have current depressive symptoms. With majority of the cases not having current depressive symptoms in UKB and GS, it suggests that the observed effects are likely to be a generic MDD phenomenon rather than state effects.

2: Timeline of imaging and MDD assessment in UKB and GS

For UKB, the participants were imaged from 2014 onwards while lifetime history of MDD was assessed as part of the Mental Health Questionnaire administered from 2016 onwards. For GS, lifetime history of MDD was assessed during a recontact assessment and the participants were imaged a short while later starting the same year in 2015. To note, the use of lifetime MDD as a measure of MDD in this study helps to address complexities regarding the timing of assessments. To tie in with the above point, assessment of lifetime MDD is also more useful in capturing MDD cases as compared to "snapshots" of MDD at one point in time, given that onset of MDD is usually in the earlier years and have fluctuating courses.

Figure S1. Correlation coefficients of effect sizes (Cohen's d) for case-control differences of all global, tier and nodal network measures in UKB and GS.

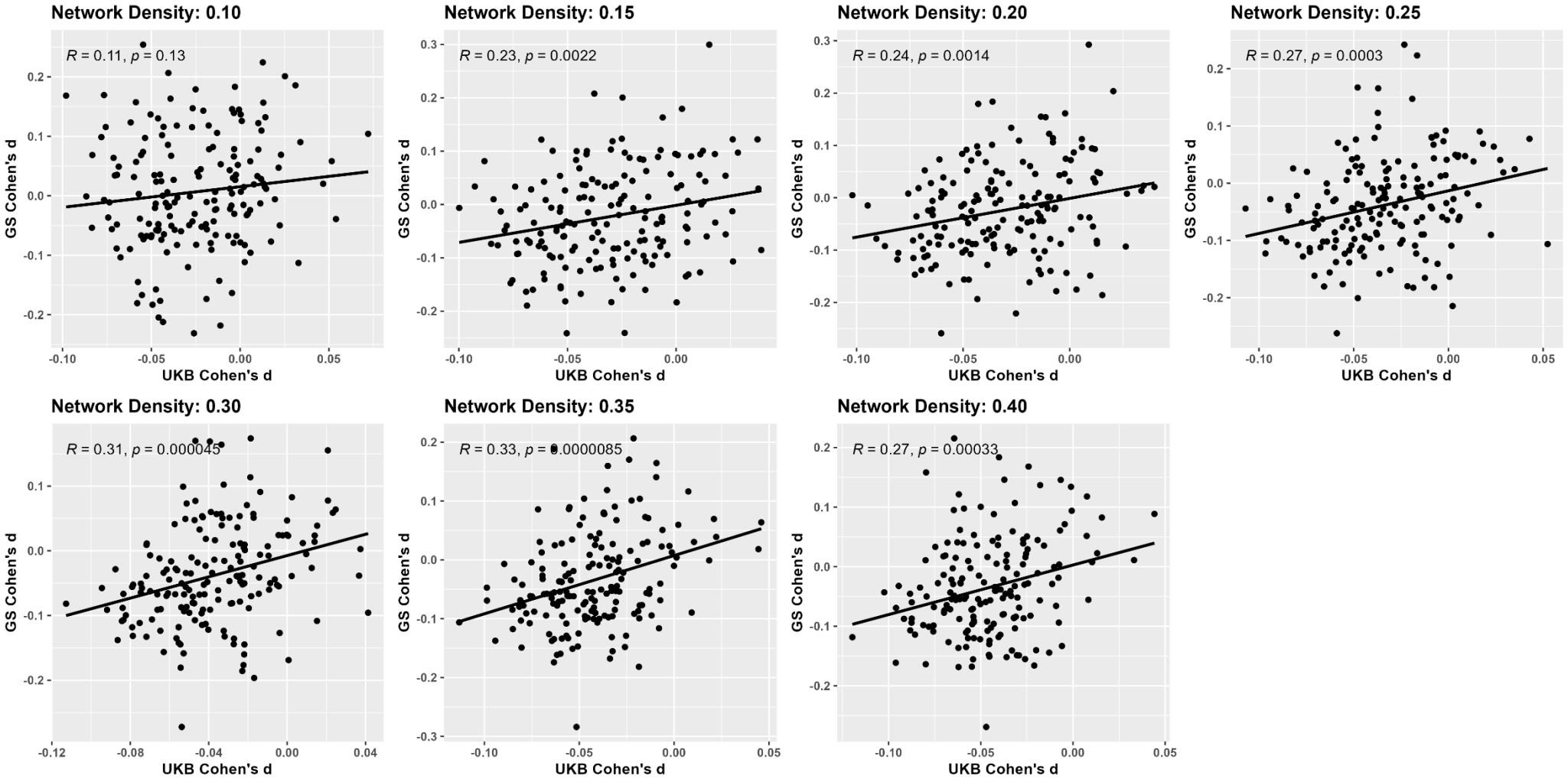

Figure S2. We tested for the presence of rich club organisation (i.e., whether hubs are more likely to be interconnected and have stronger connection among themselves than would occur by chance) in (A) cases and (B) controls in GS. For (A) and (B), the x-axis represents the range of degree (k) tested, the primary y-axis represents the rich club coefficients derived from the original network (Φ(k); black line) and the randomly generated networks ($\Phi_{rand}(k)$; grey line), and the secondary y-axis represents the normalised rich-club coefficients ($\Phi_{norm}(k)$; red line in (A), blue line in (B)). The shaded area represents the range of degree that showed significant rich club organisation, which is indicated by a $\Phi_{norm}(k)$ of greater than 1 over a continuous range of k. A comparison of $\Phi_{norm}(k)$ for cases and controls is shown in (C).

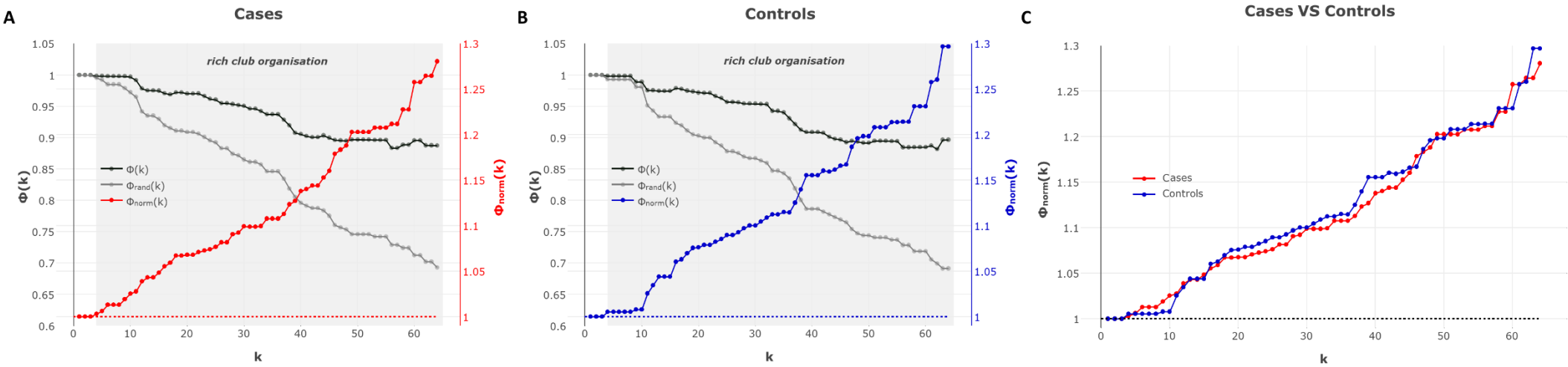

Figure S3. To statistically test whether the results replicated in both samples, we conducted a random-effects inverse-variance weighted meta-analysis for each network measure. We compared the effect sizes obtained in UKB with those obtained in the meta-analysis, in terms of their correlation, and the percentage of effect sizes that remained in the same direction / increased in value in the meta-analysis. (A) Comparison of the effect sizes obtained in UKB with the combined meta-analytic effect sizes showed a strong positive correlation, with 93.9% of effect sizes being in the same direction and more than half (51.9%) having higher values in the meta-analysis. (B) The skewed distribution of the I2 statistic (percentage of total variance explained by heterogeneity alone) also suggest that heterogeneity between cohorts was low.

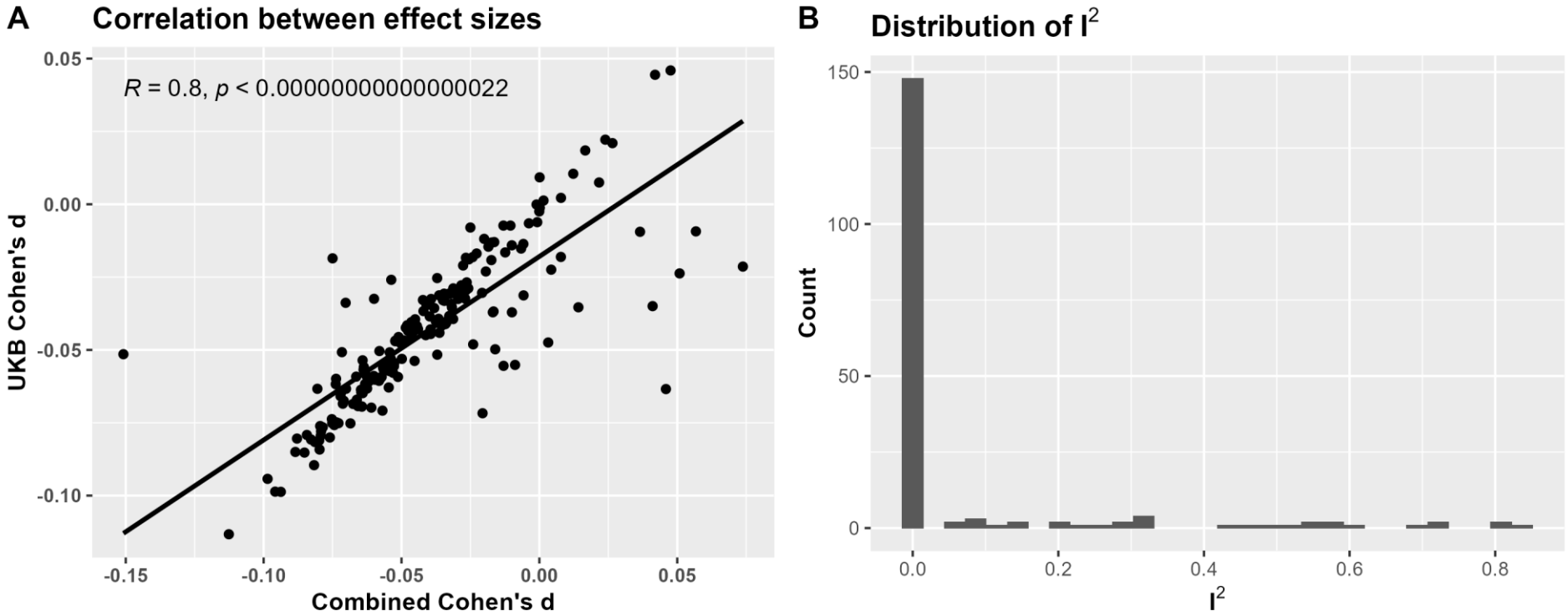

Table S1. List of all nodes and their abbreviations used in UKB and GS.

Region	Abbreviation
Left-Thalamus-Proper	L-thal
Left-Caudate	L-caud
Left-Putamen	L-puta
Left-Pallidum	L-pall
Brain-Stem	bSTEM
Left-Hippocampus	L-hipp
Left-Amygdala	L-amyg
Left-Accumbens-area	L-accu
Left-VentralDC	L-venDC
Right-Thalamus-Proper	R-thal
Right-Caudate	R-caud
Right-Putamen	R-puta
Right-Pallidum	R-pall
Right-Hippocampus	R-hipp
Right-Amygdala	R-amyg
Right-Accumbens-area	R-accu
Right-VentralDC	R-venDC
ctx-lh-bankssts	L-banks
ctx-lh-caudalanteriorcingulate	L-cauACG
ctx-lh-caudalmiddlefrontal	L-cauMFR
ctx-lh-cuneus	L-cune
ctx-lh-entorhinal	L-entorh
ctx-lh-fusiform	L-fusif
ctx-lh-inferiorparietal	L-infPAR
ctx-lh-inferiortemporal	L-infTEM
ctx-lh-isthmuscingulate	L-istCIN
ctx-lh-lateraloccipital	L-latOCC

ctx-lh-lateralorbitofrontal	L-latORB
ctx-lh-lingual	L-lingual
ctx-lh-medialorbitofrontal	L-medORB
ctx-lh-middletemporal	L-midTEM
ctx-lh-parahippocampal	L-parHIP
ctx-lh-paracentral	L-parCEN
ctx-lh-parsopercularis	L-parOPE
ctx-lh-parsorbitalis	L-parORB
ctx-lh-parstriangularis	L-parTRI
ctx-lh-pericalcarine	L-perCAR
ctx-lh-postcentral	L-posCEN
ctx-lh-posteriorcingulate	L-posCIN
ctx-lh-precentral	L-preCEN
ctx-lh-precuneus	L-preCUN
ctx-lh-rostralanteriorcingulate	L-rosACG
ctx-lh-rostralmiddlefrontal	L-rosMFR
ctx-lh-superiorfrontal	L-supFRO
ctx-lh-superiorparietal	L-supPAR
ctx-lh-superiortemporal	L-supTEM
ctx-lh-supramarginal	L-supMAR
ctx-lh-frontalpole	L-froPOL
ctx-lh-temporalpole	L-temPOL
ctx-lh-transversetemporal	L-traTEM
ctx-lh-insula	L-insula
ctx-rh-bankssts	R-banks
ctx-rh-caudalanteriorcingulate	R-cauACG
ctx-rh-caudalmiddlefrontal	R-cauMFR
ctx-rh-cuneus	R-cune
ctx-rh-entorhinal	R-entorh
ctx-rh-fusiform	R-fusif

ctx-rh-inferiorparietal	R-infPAR
ctx-rh-inferiortemporal	R-infTEM
ctx-rh-isthmuscingulate	R-istCIN
ctx-rh-lateraloccipital	R-latOCC
ctx-rh-lateralorbitofrontal	R-latORB
ctx-rh-lingual	R-lingual
ctx-rh-medialorbitofrontal	R-medORB
ctx-rh-middletemporal	R-midTEM
ctx-rh-parahippocampal	R-parHIP
ctx-rh-paracentral	R-parCEN
ctx-rh-parsopercularis	R-parOPE
ctx-rh-parsorbitalis	R-parORB
ctx-rh-parstriangularis	R-parTRI
ctx-rh-pericalcarine	R-perCAR
ctx-rh-postcentral	R-posCEN
ctx-rh-posteriorcingulate	R-posCIN
ctx-rh-precentral	R-preCEN
ctx-rh-precuneus	R-preCUN
ctx-rh-rostralanteriorcingulate	R-rosACG
ctx-rh-rostralmiddlefrontal	R-rosMFR
ctx-rh-superiorfrontal	R-supFRO
ctx-rh-superiorparietal	R-supPAR
ctx-rh-superiortemporal	R-supTEM
ctx-rh-supramarginal	R-supMAR
ctx-rh-frontalpole	R-froPOL
ctx-rh-temporalpole	R-temPOL
ctx-rh-transversetemporal	R-traTEM
ctx-rh-insula	R-insula

Table S2. List of antidepressants used in UKB and GS.

Code_in_UKB	Antidepressants
1140879616	amitriptyline
1140921600	citalopram
1140879540	fluoxetine
1140867878	sertraline
1140916282	venlafaxine
1140909806	dosulepin
1140867888	paroxetine
1141152732	mirtazapine
1141180212	escitalopram
1140879634	trazodone
1140867876	prozac
1140882236	seroxat
1141190158	cipralex
1141200564	duloxetine
1140867726	lofepramine
1140879620	clomipramine
1140867818	nortriptyline
1140879630	imipramine
1140879628	dothiepin
1141151946	cipramil
1140867948	amitriptyline
1140867624	prothiaden
1140867756	trimipramine
1140867884	lustral
1141151978	reboxetine
1141152736	zispin
1141201834	cymbalta

1140867690	anafranil
1140867640	doxepin
1140867920	moclobemide
1140867850	phenelzine
1140879544	fluvoxamine
1141200570	yentreve
1140867934	triptafen
1140867758	surmontil
1140867914	tranylcypromine
1140867820	allegron
1141151982	edronax
1140882244	molipaxin
1140879556	mianserin
1140867852	nardil
1140867860	faverin
1140917460	nefazodone
1140867938	amitriptyline+chlordiazepoxide
1140867856	isocarboxazid
1140867922	manerix
1140910820	maoi
1140882312	sinequan
1140867944	tranylcypromine+trifluoperazine
1140867784	ludiomil
1140867812	norval
1140867668	tryptizol

Table S3. Cohen's d for all network measures in UKB after controlling for age and sex in the main analysis comparing MDD cases and controls. Rows highlighted in yellow represent measures that were significantly different between cases and controls.

measure	region	abbreviation	beta	sd	tval	cohen_d	pval	pFDR	sig
GEFF	Global		-0.0778	0.0314	-2.4789	-0.0761	0.0170	0.033	*
TIER_NEFF	T1		-0.0781	0.0313	-2.4928	-0.0766	0.0150	0.020	*
TIER_NEFF	T2		-0.0698	0.0313	-2.2293	-0.0685	0.0200	0.020	*
TIER_NEFF	T3		-0.0768	0.0314	-2.4467	-0.0751	0.0140	0.020	*
TIER_NEFF	T4		-0.0813	0.0315	-2.5787	-0.0792	0.0110	0.020	*
NEFF	Left-Thalamus-Proper	L-thal	-0.0757	0.0315	-2.4020	-0.0738	0.0250	0.059	
NEFF	Left-Caudate	L-caud	-0.0915	0.0314	-2.9161	-0.0896	0.0080	0.112	
NEFF	Left-Putamen	L-puta	-0.1008	0.0314	-3.2122	-0.0986	0.0020	0.013	*
NEFF	Left-Pallidum	L-pall	-0.0798	0.0309	-2.5868	-0.0794	0.0120	0.035	*
NEFF	Brain-Stem	bSTEM	-0.0260	0.0308	-0.8445	-0.0259	0.4116	0.412	
NEFF	Left-Hippocampus	L-hipp	-0.0567	0.0311	-1.8190	-0.0559	0.0609	0.160	
NEFF	Left-Amygdala	L-amyg	-0.0305	0.0311	-0.9824	-0.0302	0.3327	0.393	
NEFF	Left-Accumbens-area	L-accu	-0.0399	0.0312	-1.2805	-0.0393	0.1958	0.322	
NEFF	Left-VentralDC	L-venDC	-0.0803	0.0305	-2.6296	-0.0808	0.0070	0.033	*
NEFF	Right-Thalamus-Proper	R-thal	-0.0859	0.0310	-2.7686	-0.0850	0.0100	0.035	*
NEFF	Right-Caudate	R-caud	-0.0839	0.0306	-2.7413	-0.0842	0.0070	0.056	
NEFF	Right-Putamen	R-puta	-0.0960	0.0313	-3.0692	-0.0943	0.0020	0.013	*
NEFF	Right-Pallidum	R-pall	-0.1147	0.0311	-3.6884	-0.1133	0.0010	0.013	*
NEFF	Right-Hippocampus	R-hipp	-0.0601	0.0312	-1.9267	-0.0592	0.0599	0.139	
NEFF	Right-Amygdala	R-amyg	-0.0454	0.0313	-1.4505	-0.0445	0.1419	0.297	
NEFF	Right-Accumbens-area	R-accu	-0.0345	0.0314	-1.1015	-0.0338	0.2567	0.369	
NEFF	Right-VentralDC	R-venDC	-0.0600	0.0311	-1.9292	-0.0592	0.0579	0.079	
NEFF	ctx-lh-bankssts	L-banks	-0.0709	0.0314	-2.2622	-0.0695	0.0240	0.112	
NEFF	ctx-lh-caudalanteriorcingulate	L-cauACG	-0.0341	0.0315	-1.0796	-0.0332	0.3137	0.335	
NEFF	ctx-lh-caudalmiddlefrontal	L-cauMFR	-0.0467	0.0315	-1.4836	-0.0456	0.1578	0.303	

NEFF	ctx-lh-cuneus	L-cune	-0.0525	0.0313	-1.6761	-0.0515	0.0989	0.160	
NEFF	ctx-lh-entorhinal	L-entorh	-0.0315	0.0315	-0.9994	-0.0307	0.3327	0.393	
NEFF	ctx-lh-fusiform	L-fusif	-0.0719	0.0312	-2.3069	-0.0708	0.0210	0.112	
NEFF	ctx-lh-inferiorparietal	L-infPAR	-0.0345	0.0306	-1.1274	-0.0346	0.2587	0.322	
NEFF	ctx-lh-inferiortemporal	L-infTEM	-0.0696	0.0312	-2.2317	-0.0685	0.0290	0.112	
NEFF	ctx-lh-isthmuscingulate	L-istCIN	-0.0600	0.0313	-1.9210	-0.0590	0.0579	0.079	
NEFF	ctx-lh-lateraloccipital	L-latOCC	-0.0578	0.0310	-1.8639	-0.0572	0.0639	0.081	
NEFF	ctx-lh-lateralorbitofrontal	L-latORB	-0.0521	0.0315	-1.6531	-0.0508	0.0999	0.160	
NEFF	ctx-lh-lingual	L-lingual	-0.0190	0.0314	-0.6046	-0.0186	0.5594	0.581	
NEFF	ctx-lh-medialorbitofrontal	L-medORB	-0.0832	0.0315	-2.6401	-0.0811	0.0140	0.075	
NEFF	ctx-lh-middletemporal	L-midTEM	-0.0273	0.0313	-0.8731	-0.0268	0.3716	0.418	
NEFF	ctx-lh-parahippocampal	L-parHIP	-0.0488	0.0314	-1.5528	-0.0477	0.1139	0.262	
NEFF	ctx-lh-paracentral	L-parCEN	-0.0603	0.0314	-1.9197	-0.0590	0.0709	0.147	
NEFF	ctx-lh-parsopercularis	L-parOPE	-0.0622	0.0315	-1.9736	-0.0606	0.0470	0.160	
NEFF	ctx-lh-parsorbitalis	L-parORB	-0.0836	0.0315	-2.6577	-0.0816	0.0090	0.100	
NEFF	ctx-lh-parstriangularis	L-parTRI	-0.0874	0.0315	-2.7757	-0.0852	0.0130	0.100	
NEFF	ctx-lh-pericalcarine	L-perCAR	-0.0478	0.0313	-1.5250	-0.0468	0.1259	0.212	
NEFF	ctx-lh-postcentral	L-posCEN	-0.0331	0.0314	-1.0572	-0.0325	0.2967	0.348	
NEFF	ctx-lh-posteriorcingulate	L-posCIN	-0.0629	0.0313	-2.0085	-0.0617	0.0519	0.079	
NEFF	ctx-lh-precentral	L-preCEN	-0.0236	0.0314	-0.7514	-0.0231	0.4466	0.482	
NEFF	ctx-lh-precuneus	L-preCUN	-0.0817	0.0313	-2.6068	-0.0801	0.0130	0.035	*
NEFF	ctx-lh-rostralanteriorcingulate	L-rosACG	-0.0543	0.0315	-1.7255	-0.0530	0.1049	0.262	
NEFF	ctx-lh-rostralmiddlefrontal	L-rosMFR	-0.0710	0.0314	-2.2602	-0.0694	0.0260	0.119	
NEFF	ctx-lh-superiorfrontal	L-supFRO	-0.0366	0.0315	-1.1604	-0.0356	0.2627	0.322	
NEFF	ctx-lh-superiorparietal	L-supPAR	-0.0609	0.0312	-1.9511	-0.0599	0.0579	0.079	
NEFF	ctx-lh-superiortemporal	L-supTEM	-0.0642	0.0314	-2.0479	-0.0629	0.0350	0.074	
NEFF	ctx-lh-supramarginal	L-supMAR	-0.0426	0.0314	-1.3574	-0.0417	0.1868	0.265	
NEFF	ctx-lh-frontalpole	L-froPOL	-0.0691	0.0315	-2.1973	-0.0675	0.0340	0.130	
NEFF	ctx-lh-temporalpole	L-temPOL	0.0213	0.0312	0.6831	0.0210	0.5095	0.558	

NEFF	ctx-lh-transversetemporal	L-traTEM	-0.0357	0.0313	-1.1386	-0.0350	0.2547	0.291	
NEFF	ctx-lh-insula	L-insula	-0.1002	0.0312	-3.2143	-0.0987	0.0010	0.016	*
NEFF	ctx-rh-bankssts	R-banks	-0.0409	0.0311	-1.3174	-0.0405	0.2068	0.279	
NEFF	ctx-rh-caudalanteriorcingulate	R-cauACG	-0.0395	0.0315	-1.2538	-0.0385	0.2507	0.291	
NEFF	ctx-rh-caudalmiddlefrontal	R-cauMFR	-0.0302	0.0314	-0.9611	-0.0295	0.3417	0.393	
NEFF	ctx-rh-cuneus	R-cune	-0.0544	0.0312	-1.7444	-0.0536	0.0869	0.160	
NEFF	ctx-rh-entorhinal	R-entorh	-0.0337	0.0315	-1.0703	-0.0329	0.2977	0.393	
NEFF	ctx-rh-fusiform	R-fusif	-0.0558	0.0311	-1.7957	-0.0551	0.0709	0.160	
NEFF	ctx-rh-inferiorparietal	R-infPAR	-0.0081	0.0312	-0.2602	-0.0080	0.7612	0.761	
NEFF	ctx-rh-inferiortemporal	R-infTEM	-0.0698	0.0309	-2.2568	-0.0693	0.0270	0.112	
NEFF	ctx-rh-isthmuscingulate	R-istCIN	-0.0541	0.0313	-1.7282	-0.0531	0.0809	0.096	
NEFF	ctx-rh-lateraloccipital	R-latOCC	-0.0416	0.0306	-1.3617	-0.0418	0.1868	0.197	
NEFF	ctx-rh-lateralorbitofrontal	R-latORB	-0.0509	0.0314	-1.6211	-0.0498	0.1119	0.163	
NEFF	ctx-rh-lingual	R-lingual	-0.0772	0.0313	-2.4681	-0.0758	0.0190	0.112	
NEFF	ctx-rh-medialorbitofrontal	R-medORB	-0.0483	0.0315	-1.5310	-0.0470	0.1429	0.190	
NEFF	ctx-rh-middletemporal	R-midTEM	-0.0475	0.0312	-1.5225	-0.0468	0.1249	0.212	
NEFF	ctx-rh-parahippocampal	R-parHIP	-0.0194	0.0315	-0.6160	-0.0189	0.5395	0.564	
NEFF	ctx-rh-paracentral	R-parCEN	-0.0652	0.0315	-2.0737	-0.0637	0.0450	0.135	
NEFF	ctx-rh-parsopercularis	R-parOPE	-0.0096	0.0315	-0.3031	-0.0093	0.7622	0.762	
NEFF	ctx-rh-parsorbitalis	R-parORB	-0.0659	0.0312	-2.1110	-0.0648	0.0490	0.161	
NEFF	ctx-rh-parstriangularis	R-parTRI	-0.0380	0.0314	-1.2077	-0.0371	0.2248	0.345	
NEFF	ctx-rh-pericalcarine	R-perCAR	-0.0508	0.0310	-1.6406	-0.0504	0.1199	0.212	
NEFF	ctx-rh-postcentral	R-posCEN	-0.0793	0.0313	-2.5381	-0.0779	0.0130	0.112	
NEFF	ctx-rh-posteriorcingulate	R-posCIN	-0.0648	0.0315	-2.0594	-0.0632	0.0420	0.135	
NEFF	ctx-rh-precentral	R-preCEN	-0.0258	0.0313	-0.8253	-0.0253	0.4046	0.405	
NEFF	ctx-rh-precuneus	R-preCUN	-0.0630	0.0314	-2.0109	-0.0618	0.0450	0.079	
NEFF	ctx-rh-rostralanteriorcingulate	R-rosACG	-0.0584	0.0316	-1.8503	-0.0568	0.0699	0.201	
NEFF	ctx-rh-rostralmiddlefrontal	R-rosMFR	-0.0582	0.0315	-1.8497	-0.0568	0.0779	0.160	

NEFF	ctx-rh-superiorfrontal	R-supFRO	-0.0459	0.0314	-1.4633	-0.0449	0.1548	0.246	
NEFF	ctx-rh-superiorparietal	R-supPAR	-0.0434	0.0314	-1.3803	-0.0424	0.1548	0.173	
NEFF	ctx-rh-superiortemporal	R-supTEM	-0.0432	0.0314	-1.3768	-0.0423	0.1748	0.262	
NEFF	ctx-rh-supramarginal	R-supMAR	-0.0605	0.0313	-1.9300	-0.0593	0.0619	0.139	
NEFF	ctx-rh-frontalpole	R-froPOL	-0.0425	0.0315	-1.3527	-0.0415	0.1928	0.322	
NEFF	ctx-rh-temporalpole	R-temPOL	-0.0704	0.0310	-2.2732	-0.0698	0.0230	0.119	
NEFF	ctx-rh-transversetemporal	R-traTEM	-0.0825	0.0315	-2.6189	-0.0804	0.0130	0.100	
NEFF	ctx-rh-insula	R-insula	-0.0578	0.0313	-1.8487	-0.0568	0.0500	0.135	
GCC	Global		-0.0587	0.0311	-1.8833	-0.0578	0.0509	0.051	
TIER_CC	T1		-0.0414	0.0312	-1.3255	-0.0407	0.1828	-	
TIER_CC	T2		-0.0408	0.0313	-1.3054	-0.0401	0.2028	-	
TIER_CC	T3		-0.0522	0.0311	-1.6815	-0.0516	0.0909	-	
TIER_CC	T4		-0.0762	0.0311	-2.4467	-0.0751	0.0180	-	
CC	Left-Thalamus-Proper	L-thal	-0.0377	0.0312	-1.2076	-0.0371	0.2278	-	
CC	Left-Caudate	L-caud	-0.0131	0.0310	-0.4229	-0.0130	0.7013	-	
CC	Left-Putamen	L-puta	-0.0025	0.0313	-0.0802	-0.0025	0.9231	-	
CC	Left-Pallidum	L-pall	0.0455	0.0314	1.4470	0.0444	0.1469	-	
CC	Brain-Stem	bSTEM	-0.0649	0.0315	-2.0621	-0.0633	0.0410	-	
CC	Left-Hippocampus	L-hipp	-0.0075	0.0314	-0.2384	-0.0073	0.8002	-	
CC	Left-Amygdala	L-amyg	0.0076	0.0314	0.2432	0.0075	0.8152	-	
CC	Left-Accumbens-area	L-accu	-0.0462	0.0311	-1.4830	-0.0455	0.1309	-	
CC	Left-VentralDC	L-venDC	-0.0001	0.0315	-0.0027	-0.0001	0.9970	-	
CC	Right-Thalamus-Proper	R-thal	-0.0309	0.0312	-0.9904	-0.0304	0.3546	-	
CC	Right-Caudate	R-caud	-0.0568	0.0310	-1.8300	-0.0562	0.0629	-	
CC	Right-Putamen	R-puta	-0.0284	0.0313	-0.9059	-0.0278	0.3786	-	
CC	Right-Pallidum	R-pall	0.0470	0.0314	1.4955	0.0459	0.1429	-	
CC	Right-Hippocampus	R-hipp	-0.0185	0.0314	-0.5888	-0.0181	0.5794	-	
CC	Right-Amygdala	R-amyg	-0.0649	0.0314	-2.0652	-0.0634	0.0360	-	
CC	Right-Accumbens-area	R-accu	-0.0437	0.0313	-1.3986	-0.0430	0.1598	-	
CC	Right-VentralDC	R-venDC	-0.0338	0.0315	-1.0725	-0.0329	0.2867	-	

CC	ctx-lh-bankssts	L-banks	0.0107	0.0313	0.3409	0.0105	0.7502	-	
CC	ctx-lh-caudalanteriorcingulate	L-cauACG	0.0188	0.0313	0.6012	0.0185	0.5305	-	
CC	ctx-lh-caudalmiddlefrontal	L-cauMFR	-0.0517	0.0313	-1.6550	-0.0508	0.1099	-	
CC	ctx-lh-cuneus	L-cune	-0.0622	0.0314	-1.9822	-0.0609	0.0480	-	
CC	ctx-lh-entorhinal	L-entorh	-0.0075	0.0316	-0.2377	-0.0073	0.8192	-	
CC	ctx-lh-fusiform	L-fusif	-0.0173	0.0315	-0.5506	-0.0169	0.5884	-	
CC	ctx-lh-inferiorparietal	L-infPAR	-0.0569	0.0315	-1.8061	-0.0555	0.0759	-	
CC	ctx-lh-inferiortemporal	L-infTEM	-0.0144	0.0314	-0.4588	-0.0141	0.6424	-	
CC	ctx-lh-isthmuscingulate	L-istCIN	-0.0545	0.0311	-1.7515	-0.0538	0.0939	-	
CC	ctx-lh-lateraloccipital	L-latOCC	-0.0314	0.0314	-1.0000	-0.0307	0.3147	-	
CC	ctx-lh-lateralorbitofrontal	L-latORB	-0.0676	0.0315	-2.1452	-0.0659	0.0410	-	
CC	ctx-lh-lingual	L-lingual	-0.0243	0.0314	-0.7730	-0.0237	0.4446	-	
CC	ctx-lh-medialorbitofrontal	L-medORB	0.0022	0.0315	0.0712	0.0022	0.9441	-	
CC	ctx-lh-middletemporal	L-midTEM	-0.0169	0.0313	-0.5383	-0.0165	0.6084	-	
CC	ctx-lh-parahippocampal	L-parHIP	-0.0571	0.0316	-1.8078	-0.0556	0.0629	-	
CC	ctx-lh-paracentral	L-parCEN	-0.0314	0.0308	-1.0178	-0.0313	0.3057	-	
CC	ctx-lh-parsopercularis	L-parOPE	-0.0188	0.0314	-0.5983	-0.0184	0.5315	-	
CC	ctx-lh-parsorbitalis	L-parORB	-0.0134	0.0315	-0.4275	-0.0131	0.6743	-	
CC	ctx-lh-parstriangularis	L-parTRI	-0.0661	0.0315	-2.1020	-0.0646	0.0380	-	
CC	ctx-lh-pericalcarine	L-perCAR	-0.0437	0.0313	-1.3962	-0.0429	0.1888	-	
CC	ctx-lh-postcentral	L-posCEN	-0.0592	0.0304	-1.9437	-0.0597	0.0430	-	
CC	ctx-lh-posteriorcingulate	L-posCIN	-0.0293	0.0311	-0.9403	-0.0289	0.3237	-	
CC	ctx-lh-precentral	L-preCEN	-0.0439	0.0310	-1.4153	-0.0435	0.1568	-	
CC	ctx-lh-precuneus	L-preCUN	-0.0149	0.0314	-0.4744	-0.0146	0.6194	-	
CC	ctx-lh-rostralanteriorcingulate	L-rosACG	-0.0659	0.0314	-2.0980	-0.0644	0.0350	-	
CC	ctx-lh-rostralmiddlefrontal	L-rosMFR	-0.0312	0.0315	-0.9917	-0.0305	0.2997	-	
CC	ctx-lh-superiorfrontal	L-supFRO	-0.0554	0.0312	-1.7738	-0.0545	0.0869	-	
CC	ctx-lh-superiorparietal	L-supPAR	-0.0613	0.0313	-1.9610	-0.0602	0.0539	-	

CC	ctx-lh-superiortemporal	L-supTEM	-0.0067	0.0314	-0.2131	-0.0065	0.8232	-	
CC	ctx-lh-supramarginal	L-supMAR	-0.0399	0.0310	-1.2859	-0.0395	0.2028	-	
CC	ctx-lh-frontalpole	L-froPOL	0.0227	0.0314	0.7218	0.0222	0.4955	-	
CC	ctx-lh-temporalpole	L-temPOL	-0.0403	0.0314	-1.2827	-0.0394	0.1928	-	
CC	ctx-lh-transversetemporal	L-traTEM	-0.0371	0.0311	-1.1940	-0.0367	0.2158	-	
CC	ctx-lh-insula	L-insula	-0.0096	0.0313	-0.3076	-0.0094	0.7632	-	
CC	ctx-rh-bankssts	R-banks	-0.0376	0.0314	-1.1982	-0.0368	0.2358	-	
CC	ctx-rh-caudalanteriorcingulate	R-cauACG	-0.0296	0.0311	-0.9526	-0.0293	0.3367	-	
CC	ctx-rh-caudalmiddlefrontal	R-cauMFR	-0.0347	0.0312	-1.1132	-0.0342	0.2747	-	
CC	ctx-rh-cuneus	R-cune	-0.0648	0.0314	-2.0627	-0.0633	0.0280	-	
CC	ctx-rh-entorhinal	R-entorh	-0.0422	0.0316	-1.3354	-0.0411	0.1848	-	
CC	ctx-rh-fusiform	R-fusif	-0.0364	0.0315	-1.1523	-0.0354	0.2507	-	
CC	ctx-rh-inferiorparietal	R-infPAR	-0.0219	0.0315	-0.6966	-0.0214	0.4845	-	
CC	ctx-rh-inferiortemporal	R-infTEM	-0.0140	0.0315	-0.4438	-0.0136	0.6803	-	
CC	ctx-rh-isthmuscingulate	R-istCIN	-0.0359	0.0311	-1.1517	-0.0354	0.2807	-	
CC	ctx-rh-lateraloccipital	R-latOCC	-0.0453	0.0315	-1.4369	-0.0441	0.1508	-	
CC	ctx-rh-lateralorbitofrontal	R-latORB	-0.0334	0.0315	-1.0586	-0.0325	0.2807	-	
CC	ctx-rh-lingual	R-lingual	-0.0012	0.0314	-0.0391	-0.0012	0.9700	-	
CC	ctx-rh-medialorbitofrontal	R-medORB	-0.0185	0.0313	-0.5913	-0.0182	0.5554	-	
CC	ctx-rh-middletemporal	R-midTEM	-0.0320	0.0315	-1.0186	-0.0313	0.2997	-	
CC	ctx-rh-parahippocampal	R-parHIP	0.0013	0.0313	0.0415	0.0013	0.9670	-	
CC	ctx-rh-paracentral	R-parCEN	-0.0213	0.0312	-0.6844	-0.0210	0.5085	-	
CC	ctx-rh-parsopercularis	R-parOPE	-0.0229	0.0314	-0.7311	-0.0225	0.4885	-	
CC	ctx-rh-parsorbitalis	R-parORB	-0.0563	0.0314	-1.7907	-0.0550	0.0809	-	
CC	ctx-rh-parstriangularis	R-parTRI	-0.0492	0.0314	-1.5663	-0.0481	0.1229	-	
CC	ctx-rh-pericalcarine	R-perCAR	-0.0391	0.0313	-1.2490	-0.0384	0.2298	-	
CC	ctx-rh-postcentral	R-posCEN	-0.0311	0.0312	-0.9978	-0.0306	0.3187	-	
CC	ctx-rh-posteriorcingulate	R-posCIN	-0.0292	0.0311	-0.9400	-0.0289	0.3656	-	
CC	ctx-rh-precentral	R-preCEN	-0.0683	0.0313	-2.1847	-0.0671	0.0250	-	

CC	ctx-rh-precuneus	R-preCUN	-0.0735	0.0315	-2.3358	-0.0717	0.0270	-	
CC	ctx-rh-rostralanteriorcingulate	R-rosACG	-0.0122	0.0315	-0.3869	-0.0119	0.6873	-	
CC	ctx-rh-rostralmiddlefrontal	R-rosMFR	-0.0331	0.0312	-1.0586	-0.0325	0.2647	-	
CC	ctx-rh-superiorfrontal	R-supFRO	-0.0441	0.0311	-1.4196	-0.0436	0.1618	-	
CC	ctx-rh-superiorparietal	R-supPAR	-0.0769	0.0314	-2.4493	-0.0752	0.0190	-	
CC	ctx-rh-superiortemporal	R-supTEM	-0.0063	0.0315	-0.2003	-0.0062	0.8272	-	
CC	ctx-rh-supramarginal	R-supMAR	-0.0330	0.0313	-1.0545	-0.0324	0.3127	-	
CC	ctx-rh-frontalpole	R-froPOL	-0.0196	0.0314	-0.6241	-0.0192	0.5175	-	
CC	ctx-rh-temporalpole	R-temPOL	-0.0481	0.0312	-1.5451	-0.0474	0.1179	-	
CC	ctx-rh-transversetemporal	R-traTEM	0.0094	0.0314	0.3003	0.0092	0.7582	-	
CC	ctx-rh-insula	R-insula	-0.0156	0.0314	-0.4952	-0.0152	0.6474	-	

Table S4. Cohen's d for all network measures in GS after controlling for age, sex and site in the main analysis comparing MDD cases and controls. To aid comparison, rows highlighted in yellow represent measures that were significantly different between cases and controls in the discovery cohort (UKB) in the main analysis.

measure	region	abbreviation	beta	sd	tval	cohen_d	pval	pFDR	sig
GEFF	Global		-0.101	0.091	-1.116	-0.108	0.246	0.737	
TIER_NEFF	T1		-0.094	0.094	-1.001	-0.097	0.312	0.416	
TIER_NEFF	T2		-0.096	0.095	-1.008	-0.097	0.306	0.416	
TIER_NEFF	T3		-0.069	0.088	-0.778	-0.075	0.429	0.429	
TIER_NEFF	T4		-0.111	0.087	-1.275	-0.123	0.205	0.416	
NEFF	Left-Thalamus-Proper	L-thal	-0.084	0.092	-0.912	-0.088	0.365	0.724	
NEFF	Left-Caudate	L-caud	-0.007	0.097	-0.072	-0.007	0.941	0.941	
NEFF	Left-Putamen	L-puta	-0.069	0.096	-0.717	-0.069	0.441	0.724	
NEFF	Left-Pallidum	L-pall	-0.079	0.099	-0.804	-0.078	0.401	0.724	
NEFF	Brain-Stem	bSTEM	-0.146	0.095	-1.534	-0.148	0.116	0.502	
NEFF	Left-Hippocampus	L-hipp	-0.128	0.093	-1.379	-0.133	0.161	0.502	
NEFF	Left-Amygdala	L-amyg	-0.045	0.097	-0.462	-0.045	0.626	0.752	
NEFF	Left-Accumbens-area	L-accu	-0.009	0.098	-0.096	-0.009	0.928	0.928	
NEFF	Left-VentralDC	L-venDC	-0.103	0.096	-1.069	-0.103	0.266	0.724	
NEFF	Right-Thalamus-Proper	R-thal	-0.110	0.090	-1.218	-0.118	0.214	0.724	
NEFF	Right-Caudate	R-caud	-0.034	0.098	-0.347	-0.034	0.723	0.858	
NEFF	Right-Putamen	R-puta	-0.134	0.094	-1.424	-0.137	0.140	0.724	
NEFF	Right-Pallidum	R-pall	-0.107	0.097	-1.100	-0.106	0.272	0.724	
NEFF	Right-Hippocampus	R-hipp	-0.132	0.095	-1.386	-0.134	0.168	0.502	
NEFF	Right-Amygdala	R-amyg	0.008	0.096	0.088	0.009	0.928	0.928	
NEFF	Right-Accumbens-area	R-accu	-0.166	0.096	-1.738	-0.168	0.095	0.621	
NEFF	Right-VentralDC	R-venDC	-0.037	0.096	-0.389	-0.038	0.689	0.881	
NEFF	ctx-lh-bankssts	L-banks	-0.015	0.097	-0.158	-0.015	0.852	0.858	
NEFF	ctx-lh-caudalanteriorcingulate	L-cauACG	-0.045	0.095	-0.477	-0.046	0.618	0.754	

NEFF	ctx-lh-caudalmiddlefrontal	L-cauMFR	-0.094	0.093	-1.019	-0.098	0.274	0.683	
NEFF	ctx-lh-cuneus	L-cune	-0.276	0.094	-2.941	-0.284	0.004	0.100	
NEFF	ctx-lh-entorhinal	L-entorh	-0.072	0.098	-0.742	-0.072	0.449	0.621	
NEFF	ctx-lh-fusiform	L-fusif	0.029	0.092	0.315	0.030	0.745	0.810	
NEFF	ctx-lh-inferiorparietal	L-infPAR	-0.093	0.092	-1.011	-0.098	0.298	0.858	
NEFF	ctx-lh-inferiortemporal	L-infTEM	-0.058	0.097	-0.603	-0.058	0.517	0.784	
NEFF	ctx-lh-isthmuscingulate	L-istCIN	-0.093	0.094	-0.988	-0.095	0.299	0.724	
NEFF	ctx-lh-lateraloccipital	L-latOCC	-0.027	0.095	-0.287	-0.028	0.767	0.858	
NEFF	ctx-lh-lateralorbitofrontal	L-latORB	-0.121	0.079	-1.525	-0.147	0.124	0.502	
NEFF	ctx-lh-lingual	L-lingual	-0.180	0.096	-1.882	-0.182	0.055	0.502	
NEFF	ctx-lh-medialorbitofrontal	L-medORB	-0.068	0.095	-0.710	-0.069	0.468	0.754	
NEFF	ctx-lh-middletemporal	L-midTEM	-0.022	0.098	-0.226	-0.022	0.811	0.928	
NEFF	ctx-lh-parahippocampal	L-parHIP	-0.077	0.098	-0.783	-0.076	0.432	0.621	
NEFF	ctx-lh-paracentral	L-parCEN	-0.069	0.095	-0.721	-0.070	0.418	0.858	
NEFF	ctx-lh-parsopercularis	L-parOPE	-0.035	0.093	-0.379	-0.037	0.700	0.796	
NEFF	ctx-lh-parsorbitalis	L-parORB	-0.078	0.094	-0.824	-0.080	0.437	0.621	
NEFF	ctx-lh-parstriangularis	L-parTRI	-0.084	0.095	-0.877	-0.085	0.389	0.737	
NEFF	ctx-lh-pericalcarine	L-perCAR	-0.098	0.094	-1.044	-0.101	0.301	0.683	
NEFF	ctx-lh-postcentral	L-posCEN	-0.155	0.097	-1.608	-0.155	0.094	0.858	
NEFF	ctx-lh-posteriorcingulate	L-posCIN	-0.078	0.097	-0.804	-0.078	0.395	0.858	
NEFF	ctx-lh-precentral	L-preCEN	0.015	0.096	0.158	0.015	0.858	0.858	
NEFF	ctx-lh-precuneus	L-preCUN	-0.039	0.090	-0.439	-0.042	0.648	0.877	
NEFF	ctx-lh-rostralanteriorcingulate	L-rosACG	-0.059	0.093	-0.640	-0.062	0.533	0.686	
NEFF	ctx-lh-rostralmiddlefrontal	L-rosMFR	-0.024	0.086	-0.277	-0.027	0.782	0.815	
NEFF	ctx-lh-superiorfrontal	L-supFRO	-0.052	0.087	-0.594	-0.057	0.545	0.784	
NEFF	ctx-lh-superiorparietal	L-supPAR	-0.149	0.090	-1.653	-0.160	0.082	0.724	
NEFF	ctx-lh-superiortemporal	L-supTEM	0.025	0.097	0.256	0.025	0.791	0.928	
NEFF	ctx-lh-supramarginal	L-supMAR	0.025	0.098	0.260	0.025	0.773	0.858	
NEFF	ctx-lh-frontalpole	L-froPOL	-0.080	0.082	-0.979	-0.095	0.317	0.621	

NEFF	ctx-lh-temporalpole	L-temPOL	0.063	0.087	0.719	0.069	0.448	0.621	
NEFF	ctx-lh-transversetemporal	L-traTEM	0.159	0.096	1.652	0.160	0.102	0.621	
NEFF	ctx-lh-insula	L-insula	-0.047	0.096	-0.490	-0.047	0.607	0.754	
NEFF	ctx-rh-bankssts	R-banks	-0.109	0.099	-1.103	-0.107	0.260	0.858	
NEFF	ctx-rh-caudalanteriorcingulate	R-cauACG	-0.048	0.092	-0.523	-0.051	0.633	0.754	
NEFF	ctx-rh-caudalmiddlefrontal	R-cauMFR	-0.003	0.089	-0.034	-0.003	0.972	0.972	
NEFF	ctx-rh-cuneus	R-cune	-0.144	0.092	-1.565	-0.151	0.117	0.502	
NEFF	ctx-rh-entorhinal	R-entorh	-0.132	0.097	-1.361	-0.131	0.183	0.621	
NEFF	ctx-rh-fusiform	R-fusif	0.085	0.092	0.926	0.089	0.383	0.737	
NEFF	ctx-rh-inferiorparietal	R-infPAR	-0.114	0.095	-1.204	-0.116	0.221	0.724	
NEFF	ctx-rh-inferiortemporal	R-infTEM	-0.032	0.095	-0.337	-0.033	0.729	0.858	
NEFF	ctx-rh-isthmuscingulate	R-istCIN	-0.019	0.097	-0.197	-0.019	0.847	0.928	
NEFF	ctx-rh-lateraloccipital	R-latOCC	-0.069	0.096	-0.722	-0.070	0.460	0.858	
NEFF	ctx-rh-lateralorbitofrontal	R-latORB	0.046	0.074	0.613	0.059	0.544	0.754	
NEFF	ctx-rh-lingual	R-lingual	-0.060	0.094	-0.638	-0.062	0.513	0.754	
NEFF	ctx-rh-medialorbitofrontal	R-medORB	-0.090	0.091	-0.991	-0.096	0.318	0.621	
NEFF	ctx-rh-middletemporal	R-midTEM	-0.072	0.097	-0.744	-0.072	0.441	0.724	
NEFF	ctx-rh-parahippocampal	R-parHIP	-0.086	0.096	-0.902	-0.087	0.368	0.621	
NEFF	ctx-rh-paracentral	R-parCEN	-0.075	0.097	-0.770	-0.074	0.419	0.858	
NEFF	ctx-rh-parsopercularis	R-parOPE	0.154	0.091	1.703	0.164	0.083	0.502	
NEFF	ctx-rh-parsorbitalis	R-parORB	-0.053	0.088	-0.602	-0.058	0.526	0.754	
NEFF	ctx-rh-parstriangularis	R-parTRI	0.076	0.092	0.831	0.080	0.413	0.737	
NEFF	ctx-rh-pericalcarine	R-perCAR	-0.119	0.092	-1.296	-0.125	0.181	0.502	
NEFF	ctx-rh-postcentral	R-posCEN	-0.091	0.097	-0.942	-0.091	0.330	0.858	
NEFF	ctx-rh-posteriorcingulate	R-posCIN	-0.055	0.095	-0.574	-0.055	0.559	0.858	
NEFF	ctx-rh-precentral	R-preCEN	-0.129	0.096	-1.336	-0.129	0.188	0.858	
NEFF	ctx-rh-precuneus	R-preCUN	-0.154	0.092	-1.672	-0.162	0.093	0.724	
NEFF	ctx-rh-rostralanteriorcingulate	R-rosACG	-0.093	0.083	-1.121	-0.108	0.273	0.621	

NEFF	ctx-rh-rostralmiddlefrontal	R-rosMFR	-0.046	0.082	-0.560	-0.054	0.584	0.858	
NEFF	ctx-rh-superiorfrontal	R-supFRO	-0.011	0.087	-0.128	-0.012	0.890	0.931	
NEFF	ctx-rh-superiorparietal	R-supPAR	-0.096	0.092	-1.041	-0.100	0.287	0.724	
NEFF	ctx-rh-superiortemporal	R-supTEM	-0.081	0.097	-0.839	-0.081	0.390	0.724	
NEFF	ctx-rh-supramarginal	R-supMAR	0.028	0.099	0.289	0.028	0.782	0.858	
NEFF	ctx-rh-frontalpole	R-froPOL	-0.076	0.081	-0.934	-0.090	0.366	0.621	
NEFF	ctx-rh-temporalpole	R-temPOL	0.012	0.089	0.130	0.013	0.897	0.928	
NEFF	ctx-rh-transversetemporal	R-traTEM	-0.139	0.090	-1.544	-0.149	0.135	0.621	
NEFF	ctx-rh-insula	R-insula	-0.128	0.095	-1.336	-0.129	0.165	0.858	
GCC	Global		-0.007	0.097	-0.069	-0.007	0.937	0.937	
TIER_CC	T1		0.033	0.097	0.342	0.033	0.735	-	
TIER_CC	T2		-0.014	0.095	-0.148	-0.014	0.880	-	
TIER_CC	T3		0.057	0.097	0.582	0.056	0.569	-	
TIER_CC	T4		-0.050	0.092	-0.549	-0.053	0.566	-	
CC	Left-Thalamus-Proper	L-thal	0.079	0.098	0.809	0.078	0.406	-	
CC	Left-Caudate	L-caud	-0.050	0.098	-0.515	-0.050	0.563	-	
CC	Left-Putamen	L-puta	0.024	0.098	0.244	0.024	0.802	-	
CC	Left-Pallidum	L-pall	0.018	0.097	0.188	0.018	0.848	-	
CC	Brain-Stem	bSTEM	-0.135	0.097	-1.395	-0.135	0.159	-	
CC	Left-Hippocampus	L-hipp	-0.070	0.098	-0.711	-0.069	0.494	-	
CC	Left-Amygdala	L-amyg	0.118	0.099	1.202	0.116	0.247	-	
CC	Left-Accumbens-area	L-accu	-0.055	0.097	-0.561	-0.054	0.570	-	
CC	Left-VentralDC	L-venDC	-0.010	0.099	-0.106	-0.010	0.921	-	
CC	Right-Thalamus-Proper	R-thal	0.066	0.095	0.698	0.067	0.468	-	
CC	Right-Caudate	R-caud	-0.062	0.098	-0.634	-0.061	0.528	-	
CC	Right-Putamen	R-puta	-0.032	0.095	-0.337	-0.033	0.739	-	
CC	Right-Pallidum	R-pall	0.064	0.098	0.659	0.064	0.496	-	
CC	Right-Hippocampus	R-hipp	0.105	0.097	1.073	0.104	0.296	-	
CC	Right-Amygdala	R-amyg	0.189	0.097	1.949	0.188	0.056	-	
CC	Right-Accumbens-area	R-accu	-0.007	0.096	-0.070	-0.007	0.949	-	

CC	Right-VentralDC	R-venDC	-0.051	0.093	-0.547	-0.053	0.555	-	
CC	ctx-lh-bankssts	L-banks	0.031	0.098	0.314	0.030	0.759	-	
CC	ctx-lh-caudalanteriorcingulate	L-cauACG	-0.001	0.097	-0.010	-0.001	0.992	-	
CC	ctx-lh-caudalmiddlefrontal	L-cauMFR	-0.084	0.095	-0.891	-0.086	0.392	-	
CC	ctx-lh-cuneus	L-cune	-0.072	0.097	-0.740	-0.071	0.459	-	
CC	ctx-lh-entorhinal	L-entorh	-0.041	0.097	-0.419	-0.040	0.653	-	
CC	ctx-lh-fusiform	L-fusif	-0.076	0.096	-0.797	-0.077	0.425	-	
CC	ctx-lh-inferiorparietal	L-infPAR	0.085	0.095	0.894	0.086	0.387	-	
CC	ctx-lh-inferiortemporal	L-infTEM	0.031	0.099	0.314	0.030	0.769	-	
CC	ctx-lh-isthmuscingulate	L-istCIN	0.034	0.095	0.357	0.034	0.725	-	
CC	ctx-lh-lateraloccipital	L-latOCC	-0.053	0.097	-0.550	-0.053	0.569	-	
CC	ctx-lh-lateralorbitofrontal	L-latORB	-0.122	0.093	-1.308	-0.126	0.190	-	
CC	ctx-lh-lingual	L-lingual	0.173	0.098	1.763	0.170	0.065	-	
CC	ctx-lh-medialorbitofrontal	L-medORB	0.059	0.095	0.616	0.060	0.540	-	
CC	ctx-lh-middletemporal	L-midTEM	0.027	0.097	0.283	0.027	0.784	-	
CC	ctx-lh-parahippocampal	L-parHIP	-0.024	0.102	-0.231	-0.023	0.823	-	
CC	ctx-lh-paracentral	L-parCEN	-0.084	0.095	-0.880	-0.085	0.373	-	
CC	ctx-lh-parsopercularis	L-parOPE	-0.096	0.093	-1.030	-0.099	0.303	-	
CC	ctx-lh-parsorbitalis	L-parORB	-0.058	0.098	-0.597	-0.058	0.529	-	
CC	ctx-lh-parstriangularis	L-parTRI	-0.066	0.097	-0.674	-0.065	0.451	-	
CC	ctx-lh-pericalcarine	L-perCAR	-0.056	0.098	-0.569	-0.055	0.554	-	
CC	ctx-lh-postcentral	L-posCEN	-0.037	0.096	-0.381	-0.037	0.683	-	
CC	ctx-lh-posteriorcingulate	L-posCIN	-0.054	0.097	-0.558	-0.054	0.565	-	
CC	ctx-lh-precentral	L-preCEN	-0.086	0.095	-0.900	-0.087	0.371	-	
CC	ctx-lh-precuneus	L-preCUN	-0.057	0.098	-0.584	-0.056	0.551	-	
CC	ctx-lh-rostralanteriorcingulate	L-rosACG	-0.134	0.094	-1.425	-0.138	0.158	-	
CC	ctx-lh-rostralmiddlefrontal	L-rosMFR	-0.021	0.099	-0.215	-0.021	0.836	-	
CC	ctx-lh-superiorfrontal	L-supFRO	-0.035	0.097	-0.360	-0.035	0.724	-	

CC	ctx-lh-superiorparietal	L-supPAR	-0.053	0.095	-0.561	-0.054	0.593	-	
CC	ctx-lh-superiortemporal	L-supTEM	0.023	0.097	0.234	0.023	0.820	-	
CC	ctx-lh-supramarginal	L-supMAR	-0.101	0.098	-1.038	-0.100	0.290	-	
CC	ctx-lh-frontalpole	L-froPOL	0.037	0.092	0.403	0.039	0.707	-	
CC	ctx-lh-temporalpole	L-temPOL	0.045	0.097	0.469	0.045	0.623	-	
CC	ctx-lh-transversetemporal	L-traTEM	-0.096	0.097	-0.983	-0.095	0.306	-	
CC	ctx-lh-insula	L-insula	0.143	0.098	1.455	0.140	0.161	-	
CC	ctx-rh-bankssts	R-banks	0.079	0.098	0.806	0.078	0.401	-	
CC	ctx-rh-caudalanteriorcingulate	R-cauACG	-0.017	0.097	-0.179	-0.017	0.853	-	
CC	ctx-rh-caudalmiddlefrontal	R-cauMFR	-0.010	0.097	-0.106	-0.010	0.914	-	
CC	ctx-rh-cuneus	R-cune	-0.175	0.097	-1.803	-0.174	0.055	-	
CC	ctx-rh-entorhinal	R-entorh	0.036	0.099	0.363	0.036	0.721	-	
CC	ctx-rh-fusiform	R-fusif	0.003	0.097	0.029	0.003	0.974	-	
CC	ctx-rh-inferiorparietal	R-infPAR	0.208	0.097	2.137	0.206	0.021	-	
CC	ctx-rh-inferiortemporal	R-infTEM	0.072	0.099	0.733	0.071	0.434	-	
CC	ctx-rh-isthmuscingulate	R-istCIN	0.119	0.097	1.226	0.118	0.201	-	
CC	ctx-rh-lateraloccipital	R-latOCC	0.041	0.098	0.414	0.040	0.666	-	
CC	ctx-rh-lateralorbitofrontal	R-latORB	-0.091	0.091	-0.992	-0.096	0.306	-	
CC	ctx-rh-lingual	R-lingual	0.013	0.096	0.131	0.013	0.893	-	
CC	ctx-rh-medialorbitofrontal	R-medORB	-0.075	0.093	-0.802	-0.077	0.442	-	
CC	ctx-rh-middletemporal	R-midTEM	0.092	0.098	0.936	0.090	0.370	-	
CC	ctx-rh-parahippocampal	R-parHIP	0.004	0.099	0.040	0.004	0.976	-	
CC	ctx-rh-paracentral	R-parCEN	-0.092	0.097	-0.949	-0.092	0.330	-	
CC	ctx-rh-parsopercularis	R-parOPE	0.102	0.098	1.043	0.101	0.287	-	
CC	ctx-rh-parsorbitalis	R-parORB	-0.062	0.097	-0.639	-0.062	0.523	-	
CC	ctx-rh-parstriangularis	R-parTRI	0.073	0.098	0.744	0.072	0.476	-	
CC	ctx-rh-pericalcarine	R-perCAR	0.021	0.096	0.218	0.021	0.822	-	
CC	ctx-rh-postcentral	R-posCEN	-0.046	0.097	-0.476	-0.046	0.619	-	
CC	ctx-rh-posteriorcingulate	R-posCIN	0.004	0.097	0.044	0.004	0.969	-	

CC	ctx-rh-precentral	R-preCEN	-0.058	0.097	-0.597	-0.058	0.550	-	
CC	ctx-rh-precuneus	R-preCUN	0.087	0.098	0.888	0.086	0.363	-	
CC	ctx-rh-rostralanteriorcingulate	R-rosACG	-0.093	0.095	-0.978	-0.094	0.331	-	
CC	ctx-rh-rostralmiddlefrontal	R-rosMFR	0.000	0.098	0.004	0.000	0.995	-	
CC	ctx-rh-superiorfrontal	R-supFRO	-0.066	0.097	-0.678	-0.065	0.484	-	
CC	ctx-rh-superiorparietal	R-supPAR	-0.004	0.097	-0.044	-0.004	0.961	-	
CC	ctx-rh-superiortemporal	R-supTEM	0.051	0.098	0.525	0.051	0.597	-	
CC	ctx-rh-supramarginal	R-supMAR	0.027	0.098	0.278	0.027	0.804	-	
CC	ctx-rh-frontalpole	R-froPOL	-0.002	0.093	-0.020	-0.002	0.983	-	
CC	ctx-rh-temporalpole	R-temPOL	0.099	0.092	1.076	0.104	0.318	-	
CC	ctx-rh-transversetemporal	R-traTEM	-0.089	0.098	-0.906	-0.090	0.353	-	
CC	ctx-rh-insula	R-insula	0.072	0.096	0.753	0.073	0.461	-	

Table S5. Cohen's d for all network measures in UKB after controlling for age, sex, body mass index, household income, and education level in the supplementary analysis comparing MDD cases and controls. To aid comparison, rows highlighted in yellow represent measures that were significantly different between cases and controls in the discovery cohort (UKB) in the main analysis.

measure	region	abb	beta	sd	tval	cohen_d	pval	pFDR	sig
GEFF	Global		-0.079	0.034	-2.298	-0.077	0.022	0.043	*
TIER_NEFF	T1		-0.082	0.034	-2.399	-0.080	0.016	0.035	*
TIER_NEFF	T2		-0.073	0.034	-2.116	-0.071	0.034	0.035	*
TIER_NEFF	T3		-0.072	0.034	-2.109	-0.070	0.035	0.035	*
TIER_NEFF	T4		-0.081	0.034	-2.360	-0.079	0.018	0.035	*
NEFF	Left-Thalamus-Proper	L-thal	-0.071	0.035	-2.042	-0.068	0.041	0.097	
NEFF	Left-Caudate	L-caud	-0.081	0.034	-2.377	-0.079	0.018	0.129	
NEFF	Left-Putamen	L-puta	-0.105	0.034	-3.066	-0.102	0.002	0.014	*
NEFF	Left-Pallidum	L-pall	-0.077	0.034	-2.281	-0.076	0.023	0.076	
NEFF	Brain-Stem	bSTEM	-0.030	0.034	-0.898	-0.030	0.369	0.369	
NEFF	Left-Hippocampus	L-hipp	-0.068	0.034	-2.025	-0.068	0.043	0.138	
NEFF	Left-Amygdala	L-amyg	-0.024	0.034	-0.718	-0.024	0.473	0.518	
NEFF	Left-Accumbens-area	L-accu	-0.041	0.034	-1.195	-0.040	0.232	0.333	
NEFF	Left-VentralDC	L-venDC	-0.075	0.033	-2.260	-0.075	0.024	0.076	
NEFF	Right-Thalamus-Proper	R-thal	-0.092	0.034	-2.698	-0.090	0.007	0.033	*
NEFF	Right-Caudate	R-caud	-0.072	0.034	-2.142	-0.071	0.032	0.129	
NEFF	Right-Putamen	R-puta	-0.113	0.034	-3.285	-0.110	0.001	0.010	*
NEFF	Right-Pallidum	R-pall	-0.125	0.034	-3.698	-0.123	0.000	0.004	*
NEFF	Right-Hippocampus	R-hipp	-0.060	0.034	-1.762	-0.059	0.078	0.162	
NEFF	Right-Amygdala	R-amyg	-0.050	0.034	-1.446	-0.048	0.148	0.263	
NEFF	Right-Accumbens-area	R-accu	-0.031	0.034	-0.893	-0.030	0.372	0.475	
NEFF	Right-VentralDC	R-venDC	-0.060	0.034	-1.759	-0.059	0.079	0.107	
NEFF	ctx-lh-bankssts	L-banks	-0.073	0.034	-2.140	-0.071	0.032	0.129	
NEFF	ctx-lh-caudalanteriorcingulate	L-cauACG	-0.032	0.035	-0.915	-0.031	0.360	0.384	

NEFF	ctx-lh-caudalmiddlefrontal	L-cauMFR	-0.062	0.034	-1.804	-0.060	0.071	0.205	
NEFF	ctx-lh-cuneus	L-cune	-0.049	0.034	-1.424	-0.048	0.154	0.228	
NEFF	ctx-lh-entorhinal	L-entorh	-0.015	0.034	-0.436	-0.015	0.663	0.693	
NEFF	ctx-lh-fusiform	L-fusif	-0.061	0.034	-1.787	-0.060	0.074	0.162	
NEFF	ctx-lh-inferiorparietal	L-infPAR	-0.039	0.033	-1.173	-0.039	0.241	0.312	
NEFF	ctx-lh-inferiortemporal	L-infTEM	-0.078	0.034	-2.296	-0.077	0.022	0.129	
NEFF	ctx-lh-isthmuscingulate	L-istCIN	-0.065	0.034	-1.895	-0.063	0.058	0.100	
NEFF	ctx-lh-lateraloccipital	L-latOCC	-0.047	0.034	-1.393	-0.046	0.164	0.194	
NEFF	ctx-lh-lateralorbitofrontal	L-latORB	-0.054	0.034	-1.577	-0.053	0.115	0.228	
NEFF	ctx-lh-lingual	L-lingual	0.001	0.034	0.033	0.001	0.974	0.974	
NEFF	ctx-lh-medialorbitofrontal	L-medORB	-0.081	0.034	-2.354	-0.079	0.019	0.129	
NEFF	ctx-lh-middletemporal	L-midTEM	-0.030	0.034	-0.884	-0.030	0.377	0.442	
NEFF	ctx-lh-parahippocampal	L-parHIP	-0.044	0.034	-1.307	-0.044	0.191	0.314	
NEFF	ctx-lh-paracentral	L-parCEN	-0.063	0.034	-1.837	-0.061	0.066	0.162	
NEFF	ctx-lh-parsopercularis	L-parOPE	-0.075	0.034	-2.193	-0.073	0.028	0.129	
NEFF	ctx-lh-parsorbitalis	L-parORB	-0.079	0.034	-2.296	-0.077	0.022	0.185	
NEFF	ctx-lh-parstriangularis	L-parTRI	-0.087	0.034	-2.544	-0.085	0.011	0.185	
NEFF	ctx-lh-pericalcarine	L-perCAR	-0.039	0.034	-1.153	-0.038	0.249	0.312	
NEFF	ctx-lh-postcentral	L-posCEN	-0.027	0.034	-0.779	-0.026	0.436	0.490	
NEFF	ctx-lh-posteriorcingulate	L-posCIN	-0.066	0.034	-1.933	-0.065	0.053	0.100	
NEFF	ctx-lh-precentral	L-preCEN	-0.017	0.034	-0.499	-0.017	0.618	0.642	
NEFF	ctx-lh-precuneus	L-preCUN	-0.073	0.034	-2.143	-0.072	0.032	0.087	
NEFF	ctx-lh-rostralanteriorcingulate	L-rosACG	-0.059	0.034	-1.732	-0.058	0.083	0.213	
NEFF	ctx-lh-rostralmiddlefrontal	L-rosMFR	-0.072	0.034	-2.109	-0.070	0.035	0.185	
NEFF	ctx-lh-superiorfrontal	L-supFRO	-0.039	0.035	-1.140	-0.038	0.254	0.312	
NEFF	ctx-lh-superiorparietal	L-supPAR	-0.051	0.034	-1.492	-0.050	0.136	0.172	
NEFF	ctx-lh-superiortemporal	L-supTEM	-0.062	0.034	-1.804	-0.060	0.071	0.107	
NEFF	ctx-lh-supramarginal	L-supMAR	-0.043	0.034	-1.268	-0.042	0.205	0.291	
NEFF	ctx-lh-frontalpole	L-froPOL	-0.066	0.034	-1.910	-0.064	0.056	0.185	

NEFF	ctx-lh-temporalpole	L-temPOL	-0.002	0.034	-0.052	-0.002	0.959	0.959	
NEFF	ctx-lh-transversetemporal	L-traTEM	-0.017	0.034	-0.512	-0.017	0.609	0.609	
NEFF	ctx-lh-insula	L-insula	-0.099	0.034	-2.898	-0.097	0.004	0.060	
NEFF	ctx-rh-bankssts	R-banks	-0.072	0.034	-2.124	-0.071	0.034	0.129	
NEFF	ctx-rh-caudalanteriorcingulate	R-cauACG	-0.049	0.034	-1.424	-0.048	0.155	0.228	
NEFF	ctx-rh-caudalmiddlefrontal	R-cauMFR	-0.050	0.034	-1.444	-0.048	0.149	0.263	
NEFF	ctx-rh-cuneus	R-cune	-0.053	0.034	-1.546	-0.052	0.122	0.228	
NEFF	ctx-rh-entorhinal	R-entorh	-0.041	0.034	-1.206	-0.040	0.228	0.333	
NEFF	ctx-rh-fusiform	R-fusif	-0.048	0.034	-1.417	-0.047	0.156	0.228	
NEFF	ctx-rh-inferiorparietal	R-infPAR	-0.023	0.034	-0.668	-0.022	0.504	0.545	
NEFF	ctx-rh-inferiortemporal	R-infTEM	-0.071	0.034	-2.097	-0.070	0.036	0.129	
NEFF	ctx-rh-isthmuscingulate	R-istCIN	-0.061	0.034	-1.770	-0.059	0.077	0.107	
NEFF	ctx-rh-lateraloccipital	R-latOCC	-0.031	0.034	-0.910	-0.030	0.363	0.369	
NEFF	ctx-rh-lateralorbitofrontal	R-latORB	-0.043	0.034	-1.267	-0.042	0.205	0.263	
NEFF	ctx-rh-lingual	R-lingual	-0.066	0.034	-1.917	-0.064	0.055	0.162	
NEFF	ctx-rh-medialorbitofrontal	R-medORB	-0.043	0.034	-1.245	-0.042	0.213	0.263	
NEFF	ctx-rh-middletemporal	R-midTEM	-0.052	0.034	-1.505	-0.050	0.132	0.210	
NEFF	ctx-rh-parahippocampal	R-parHIP	-0.026	0.034	-0.770	-0.026	0.442	0.518	
NEFF	ctx-rh-paracentral	R-parCEN	-0.054	0.034	-1.567	-0.052	0.117	0.198	
NEFF	ctx-rh-parsopercularis	R-parOPE	-0.025	0.034	-0.718	-0.024	0.473	0.518	
NEFF	ctx-rh-parsorbitalis	R-parORB	-0.068	0.034	-1.983	-0.066	0.047	0.185	
NEFF	ctx-rh-parstriangularis	R-parTRI	-0.033	0.034	-0.967	-0.032	0.333	0.451	
NEFF	ctx-rh-pericalcarine	R-perCAR	-0.058	0.034	-1.722	-0.057	0.085	0.164	
NEFF	ctx-rh-postcentral	R-posCEN	-0.082	0.034	-2.400	-0.080	0.016	0.129	
NEFF	ctx-rh-posteriorcingulate	R-posCIN	-0.081	0.034	-2.354	-0.079	0.019	0.129	
NEFF	ctx-rh-precentral	R-preCEN	-0.034	0.034	-0.996	-0.033	0.319	0.365	
NEFF	ctx-rh-precuneus	R-preCUN	-0.069	0.034	-1.995	-0.067	0.046	0.097	
NEFF	ctx-rh-rostralanteriorcingulate	R-rosACG	-0.051	0.034	-1.495	-0.050	0.135	0.263	

NEFF	ctx-rh-rostralmiddlefrontal	R-rosMFR	-0.063	0.035	-1.810	-0.060	0.070	0.187	
NEFF	ctx-rh-superiorfrontal	R-supFRO	-0.056	0.034	-1.628	-0.054	0.104	0.186	
NEFF	ctx-rh-superiorparietal	R-supPAR	-0.047	0.035	-1.351	-0.045	0.177	0.198	
NEFF	ctx-rh-superiortemporal	R-supTEM	-0.044	0.035	-1.286	-0.043	0.199	0.291	
NEFF	ctx-rh-supramarginal	R-supMAR	-0.071	0.034	-2.075	-0.069	0.038	0.129	
NEFF	ctx-rh-frontalpole	R-froPOL	-0.052	0.035	-1.518	-0.051	0.129	0.263	
NEFF	ctx-rh-temporalpole	R-temPOL	-0.073	0.034	-2.175	-0.073	0.030	0.185	
NEFF	ctx-rh-transversetemporal	R-traTEM	-0.067	0.034	-1.952	-0.065	0.051	0.185	
NEFF	ctx-rh-insula	R-insula	-0.064	0.034	-1.860	-0.062	0.063	0.162	
GCC	Global		-0.066	0.034	-1.925	-0.064	0.054	0.054	
TIER_CC	T1		-0.053	0.034	-1.564	-0.052	0.118	-	
TIER_CC	T2		-0.057	0.034	-1.674	-0.056	0.094	-	
TIER_CC	T3		-0.057	0.034	-1.667	-0.056	0.096	-	
TIER_CC	T4		-0.068	0.034	-1.988	-0.066	0.047	-	
CC	Left-Thalamus-Proper	L-thal	-0.039	0.034	-1.153	-0.038	0.249	-	
CC	Left-Caudate	L-caud	-0.023	0.034	-0.687	-0.023	0.492	-	
CC	Left-Putamen	L-puta	0.000	0.034	0.011	0.000	0.991	-	
CC	Left-Pallidum	L-pall	0.032	0.034	0.917	0.031	0.359	-	
CC	Brain-Stem	bSTEM	-0.059	0.034	-1.711	-0.057	0.087	-	
CC	Left-Hippocampus	L-hipp	-0.027	0.034	-0.776	-0.026	0.438	-	
CC	Left-Amygdala	L-amyg	0.000	0.034	0.004	0.000	0.996	-	
CC	Left-Accumbens-area	L-accu	-0.054	0.034	-1.586	-0.053	0.113	-	
CC	Left-VentralDC	L-venDC	-0.021	0.035	-0.603	-0.020	0.546	-	
CC	Right-Thalamus-Proper	R-thal	-0.030	0.034	-0.888	-0.030	0.375	-	
CC	Right-Caudate	R-caud	-0.060	0.034	-1.785	-0.060	0.074	-	
CC	Right-Putamen	R-puta	-0.027	0.034	-0.799	-0.027	0.424	-	
CC	Right-Pallidum	R-pall	0.037	0.034	1.095	0.037	0.274	-	
CC	Right-Hippocampus	R-hipp	-0.019	0.034	-0.551	-0.018	0.581	-	
CC	Right-Amygdala	R-amyg	-0.073	0.035	-2.106	-0.070	0.035	-	
CC	Right-Accumbens-area	R-accu	-0.025	0.034	-0.732	-0.024	0.464	-	

CC	Right-VentralDC	R-venDC	-0.042	0.034	-1.236	-0.041	0.217	-	
CC	ctx-lh-bankssts	L-banks	-0.003	0.034	-0.084	-0.003	0.933	-	
CC	ctx-lh-caudalanteriorcingulate	L-cauACG	0.011	0.034	0.335	0.011	0.737	-	
CC	ctx-lh-caudalmiddlefrontal	L-cauMFR	-0.059	0.034	-1.746	-0.058	0.081	-	
CC	ctx-lh-cuneus	L-cune	-0.069	0.034	-2.005	-0.067	0.045	-	
CC	ctx-lh-entorhinal	L-entorh	0.003	0.035	0.101	0.003	0.920	-	
CC	ctx-lh-fusiform	L-fusif	-0.031	0.034	-0.915	-0.031	0.360	-	
CC	ctx-lh-inferiorparietal	L-infPAR	-0.073	0.034	-2.124	-0.071	0.034	-	
CC	ctx-lh-inferiortemporal	L-infTEM	-0.045	0.034	-1.308	-0.044	0.191	-	
CC	ctx-lh-isthmuscingulate	L-istCIN	-0.072	0.034	-2.128	-0.071	0.033	-	
CC	ctx-lh-lateraloccipital	L-latOCC	-0.047	0.034	-1.374	-0.046	0.169	-	
CC	ctx-lh-lateralorbitofrontal	L-latORB	-0.076	0.034	-2.223	-0.074	0.026	-	
CC	ctx-lh-lingual	L-lingual	-0.037	0.034	-1.090	-0.036	0.276	-	
CC	ctx-lh-medialorbitofrontal	L-medORB	0.022	0.034	0.623	0.021	0.533	-	
CC	ctx-lh-middletemporal	L-midTEM	-0.044	0.034	-1.274	-0.043	0.203	-	
CC	ctx-lh-parahippocampal	L-parHIP	-0.039	0.034	-1.135	-0.038	0.256	-	
CC	ctx-lh-paracentral	L-parCEN	-0.034	0.034	-1.016	-0.034	0.310	-	
CC	ctx-lh-parsopercularis	L-parOPE	-0.020	0.034	-0.574	-0.019	0.566	-	
CC	ctx-lh-parsorbitalis	L-parORB	0.001	0.034	0.025	0.001	0.980	-	
CC	ctx-lh-parstriangularis	L-parTRI	-0.063	0.034	-1.856	-0.062	0.064	-	
CC	ctx-lh-pericalcarine	L-perCAR	-0.056	0.034	-1.647	-0.055	0.100	-	
CC	ctx-lh-postcentral	L-posCEN	-0.082	0.033	-2.468	-0.082	0.014	-	
CC	ctx-lh-posteriorcingulate	L-posCIN	-0.046	0.034	-1.348	-0.045	0.178	-	
CC	ctx-lh-precentral	L-preCEN	-0.050	0.034	-1.452	-0.048	0.147	-	
CC	ctx-lh-precuneus	L-preCUN	-0.029	0.034	-0.856	-0.029	0.392	-	
CC	ctx-lh-rostralanteriorcingulate	L-rosACG	-0.071	0.035	-2.064	-0.069	0.039	-	
CC	ctx-lh-rostralmiddlefrontal	L-rosMFR	-0.039	0.034	-1.147	-0.038	0.251	-	
CC	ctx-lh-superiorfrontal	L-supFRO	-0.038	0.034	-1.119	-0.037	0.263	-	

CC	ctx-lh-superiorparietal	L-supPAR	-0.074	0.034	-2.170	-0.072	0.030	-	
CC	ctx-lh-superiortemporal	L-supTEM	-0.022	0.034	-0.634	-0.021	0.526	-	
CC	ctx-lh-supramarginal	L-supMAR	-0.066	0.034	-1.940	-0.065	0.052	-	
CC	ctx-lh-frontalpole	L-froPOL	0.031	0.034	0.911	0.030	0.362	-	
CC	ctx-lh-temporalpole	L-temPOL	-0.048	0.034	-1.395	-0.047	0.163	-	
CC	ctx-lh-transversetemporal	L-traTEM	-0.047	0.034	-1.398	-0.047	0.162	-	
CC	ctx-lh-insula	L-insula	-0.003	0.034	-0.087	-0.003	0.931	-	
CC	ctx-rh-bankssts	R-banks	-0.044	0.034	-1.285	-0.043	0.199	-	
CC	ctx-rh-caudalanteriorcingulate	R-cauACG	-0.031	0.034	-0.929	-0.031	0.353	-	
CC	ctx-rh-caudalmiddlefrontal	R-cauMFR	-0.032	0.034	-0.937	-0.031	0.349	-	
CC	ctx-rh-cuneus	R-cune	-0.066	0.034	-1.926	-0.064	0.054	-	
CC	ctx-rh-entorhinal	R-entorh	-0.044	0.034	-1.272	-0.043	0.203	-	
CC	ctx-rh-fusiform	R-fusif	-0.032	0.035	-0.912	-0.030	0.362	-	
CC	ctx-rh-inferiorparietal	R-infPAR	-0.027	0.034	-0.783	-0.026	0.434	-	
CC	ctx-rh-inferiortemporal	R-infTEM	-0.031	0.034	-0.895	-0.030	0.371	-	
CC	ctx-rh-isthmuscingulate	R-istCIN	-0.032	0.034	-0.948	-0.032	0.343	-	
CC	ctx-rh-lateraloccipital	R-latOCC	-0.063	0.034	-1.818	-0.061	0.069	-	
CC	ctx-rh-lateralorbitofrontal	R-latORB	-0.042	0.034	-1.228	-0.041	0.219	-	
CC	ctx-rh-lingual	R-lingual	0.003	0.034	0.083	0.003	0.933	-	
CC	ctx-rh-medialorbitofrontal	R-medORB	0.004	0.034	0.115	0.004	0.909	-	
CC	ctx-rh-middletemporal	R-midTEM	-0.037	0.034	-1.096	-0.037	0.273	-	
CC	ctx-rh-parahippocampal	R-parHIP	-0.008	0.034	-0.238	-0.008	0.812	-	
CC	ctx-rh-paracentral	R-parCEN	-0.035	0.034	-1.021	-0.034	0.307	-	
CC	ctx-rh-parsopercularis	R-parOPE	-0.012	0.034	-0.344	-0.011	0.731	-	
CC	ctx-rh-parsorbitalis	R-parORB	-0.065	0.034	-1.885	-0.063	0.060	-	
CC	ctx-rh-parstriangularis	R-parTRI	-0.061	0.034	-1.805	-0.060	0.071	-	
CC	ctx-rh-pericalcarine	R-perCAR	-0.025	0.034	-0.730	-0.024	0.465	-	
CC	ctx-rh-postcentral	R-posCEN	-0.037	0.034	-1.080	-0.036	0.280	-	
CC	ctx-rh-posteriorcingulate	R-posCIN	-0.033	0.034	-0.960	-0.032	0.337	-	

CC	ctx-rh-precentral	R-preCEN	-0.070	0.034	-2.049	-0.068	0.040	-	
CC	ctx-rh-precuneus	R-preCUN	-0.087	0.034	-2.530	-0.084	0.011	-	
CC	ctx-rh-rostralanteriorcingulate	R-rosACG	0.007	0.034	0.189	0.006	0.850	-	
CC	ctx-rh-rostralmiddlefrontal	R-rosMFR	-0.024	0.034	-0.708	-0.024	0.479	-	
CC	ctx-rh-superiorfrontal	R-supFRO	-0.031	0.034	-0.897	-0.030	0.370	-	
CC	ctx-rh-superiorparietal	R-supPAR	-0.093	0.034	-2.715	-0.091	0.007	-	
CC	ctx-rh-superiortemporal	R-supTEM	-0.024	0.035	-0.689	-0.023	0.491	-	
CC	ctx-rh-supramarginal	R-supMAR	-0.044	0.034	-1.304	-0.044	0.192	-	
CC	ctx-rh-frontalpole	R-froPOL	-0.003	0.034	-0.102	-0.003	0.919	-	
CC	ctx-rh-temporalpole	R-temPOL	-0.054	0.034	-1.594	-0.053	0.111	-	
CC	ctx-rh-transversetemporal	R-traTEM	0.008	0.035	0.237	0.008	0.812	-	
CC	ctx-rh-insula	R-insula	-0.023	0.034	-0.678	-0.023	0.498	-	

Table S6. Cohen's d for all network measures in GS after controlling for age, sex, site, body mass index, household income, and education level in the supplementary analysis comparing MDD cases and controls. To aid comparison, rows highlighted in yellow represent measures that were significantly different between cases and controls in the discovery cohort (UKB) in the main analysis.

measure	region	abb	beta	sd	tval	cohen_d	pval	pFDR	sig
GEFF	Global		-0.165	0.096	-1.723	-0.174	0.085	0.171	
TIER_NEFF	T1		-0.167	0.099	-1.684	-0.170	0.093	-	
TIER_NEFF	T2		-0.173	0.100	-1.723	-0.174	0.085	-	
TIER_NEFF	T3		-0.127	0.094	-1.362	-0.138	0.174	-	
TIER_NEFF	T4		-0.147	0.091	-1.609	-0.163	0.108	-	
NEFF	Left-Thalamus-Proper	L-thal	-0.113	0.098	-1.151	-0.116	0.250	-	
NEFF	Left-Caudate	L-caud	-0.039	0.104	-0.372	-0.038	0.710	-	
NEFF	Left-Putamen	L-puta	-0.106	0.103	-1.028	-0.104	0.304	-	
NEFF	Left-Pallidum	L-pall	-0.110	0.106	-1.043	-0.105	0.297	-	
NEFF	Brain-Stem	bSTEM	-0.170	0.103	-1.643	-0.166	0.101	-	
NEFF	Left-Hippocampus	L-hipp	-0.208	0.100	-2.075	-0.210	0.038	-	
NEFF	Left-Amygdala	L-amyg	-0.085	0.104	-0.811	-0.082	0.417	-	
NEFF	Left-Accumbens-area	L-accu	-0.018	0.105	-0.175	-0.018	0.861	-	
NEFF	Left-VentralDC	L-venDC	-0.127	0.102	-1.244	-0.126	0.214	-	
NEFF	Right-Thalamus-Proper	R-thal	-0.160	0.096	-1.666	-0.168	0.096	-	
NEFF	Right-Caudate	R-caud	-0.039	0.106	-0.370	-0.037	0.712	-	
NEFF	Right-Putamen	R-puta	-0.192	0.099	-1.935	-0.196	0.053	-	
NEFF	Right-Pallidum	R-pall	-0.166	0.103	-1.607	-0.162	0.108	-	
NEFF	Right-Hippocampus	R-hipp	-0.243	0.102	-2.393	-0.242	0.017	-	
NEFF	Right-Amygdala	R-amyg	-0.048	0.104	-0.459	-0.046	0.647	-	
NEFF	Right-Accumbens-area	R-accu	-0.140	0.102	-1.376	-0.139	0.169	-	
NEFF	Right-VentralDC	R-venDC	-0.119	0.103	-1.165	-0.118	0.245	-	
NEFF	ctx-lh-bankssts	L-banks	-0.081	0.103	-0.789	-0.080	0.430	-	
NEFF	ctx-lh-caudalanteriorcingulate	L-cauACG	-0.053	0.103	-0.512	-0.052	0.609	-	

NEFF	ctx-lh-caudalmiddlefrontal	L-cauMFR	-0.155	0.100	-1.545	-0.156	0.123	-	
NEFF	ctx-lh-cuneus	L-cune	-0.271	0.100	-2.718	-0.275	0.007	-	
NEFF	ctx-lh-entorhinal	L-entorh	-0.042	0.104	-0.404	-0.041	0.686	-	
NEFF	ctx-lh-fusiform	L-fusif	0.010	0.098	0.098	0.010	0.922	-	
NEFF	ctx-lh-inferiorparietal	L-infPAR	-0.126	0.098	-1.283	-0.130	0.200	-	
NEFF	ctx-lh-inferiortemporal	L-infTEM	-0.118	0.101	-1.162	-0.117	0.245	-	
NEFF	ctx-lh-isthmuscingulate	L-istCIN	-0.138	0.100	-1.391	-0.140	0.165	-	
NEFF	ctx-lh-lateraloccipital	L-latOCC	-0.087	0.101	-0.863	-0.087	0.389	-	
NEFF	ctx-lh-lateralorbitofrontal	L-latORB	-0.145	0.084	-1.734	-0.175	0.083	-	
NEFF	ctx-lh-lingual	L-lingual	-0.168	0.102	-1.643	-0.166	0.101	-	
NEFF	ctx-lh-medialorbitofrontal	L-medORB	-0.115	0.102	-1.129	-0.114	0.259	-	
NEFF	ctx-lh-middletemporal	L-midTEM	-0.136	0.102	-1.332	-0.135	0.183	-	
NEFF	ctx-lh-parahippocampal	L-parHIP	-0.065	0.105	-0.619	-0.063	0.536	-	
NEFF	ctx-lh-paracentral	L-parCEN	-0.151	0.101	-1.495	-0.151	0.135	-	
NEFF	ctx-lh-parsopercularis	L-parOPE	-0.038	0.102	-0.375	-0.038	0.708	-	
NEFF	ctx-lh-parsorbitalis	L-parORB	-0.119	0.100	-1.184	-0.120	0.237	-	
NEFF	ctx-lh-parstriangularis	L-parTRI	-0.132	0.102	-1.291	-0.130	0.197	-	
NEFF	ctx-lh-pericalcarine	L-perCAR	-0.126	0.101	-1.242	-0.125	0.215	-	
NEFF	ctx-lh-postcentral	L-posCEN	-0.165	0.103	-1.597	-0.161	0.111	-	
NEFF	ctx-lh-posteriorcingulate	L-posCIN	-0.144	0.104	-1.387	-0.140	0.166	-	
NEFF	ctx-lh-precentral	L-preCEN	-0.005	0.104	-0.051	-0.005	0.959	-	
NEFF	ctx-lh-precuneus	L-preCUN	-0.079	0.095	-0.831	-0.084	0.406	-	
NEFF	ctx-lh-rostralanteriorcingulate	L-rosACG	-0.079	0.099	-0.804	-0.081	0.422	-	
NEFF	ctx-lh-rostralmiddlefrontal	L-rosMFR	-0.058	0.092	-0.625	-0.063	0.532	-	
NEFF	ctx-lh-superiorfrontal	L-supFRO	-0.082	0.094	-0.877	-0.089	0.381	-	
NEFF	ctx-lh-superiorparietal	L-supPAR	-0.204	0.095	-2.159	-0.218	0.031	-	
NEFF	ctx-lh-superiortemporal	L-supTEM	-0.034	0.101	-0.336	-0.034	0.737	-	
NEFF	ctx-lh-supramarginal	L-supMAR	-0.042	0.104	-0.406	-0.041	0.685	-	
NEFF	ctx-lh-frontalpole	L-froPOL	-0.105	0.087	-1.205	-0.122	0.229	-	

NEFF	ctx-lh-temporalpole	L-temPOL	0.034	0.094	0.358	0.036	0.720	-	
NEFF	ctx-lh-transversetemporal	L-traTEM	0.104	0.101	1.029	0.104	0.304	-	
NEFF	ctx-lh-insula	L-insula	-0.117	0.104	-1.125	-0.114	0.261	-	
NEFF	ctx-rh-bankssts	R-banks	-0.162	0.104	-1.561	-0.158	0.119	-	
NEFF	ctx-rh-caudalanteriorcingulate	R-cauACG	-0.072	0.099	-0.728	-0.074	0.467	-	
NEFF	ctx-rh-caudalmiddlefrontal	R-cauMFR	-0.041	0.096	-0.431	-0.044	0.666	-	
NEFF	ctx-rh-cuneus	R-cune	-0.136	0.098	-1.389	-0.140	0.165	-	
NEFF	ctx-rh-entorhinal	R-entorh	-0.115	0.105	-1.102	-0.111	0.271	-	
NEFF	ctx-rh-fusiform	R-fusif	0.041	0.099	0.415	0.042	0.678	-	
NEFF	ctx-rh-inferiorparietal	R-infPAR	-0.262	0.101	-2.590	-0.262	0.010	-	
NEFF	ctx-rh-inferiortemporal	R-infTEM	-0.094	0.101	-0.927	-0.094	0.354	-	
NEFF	ctx-rh-isthmuscingulate	R-istCIN	-0.052	0.103	-0.508	-0.051	0.611	-	
NEFF	ctx-rh-lateraloccipital	R-latOCC	-0.181	0.103	-1.767	-0.179	0.078	-	
NEFF	ctx-rh-lateralorbitofrontal	R-latORB	0.015	0.078	0.198	0.020	0.843	-	
NEFF	ctx-rh-lingual	R-lingual	-0.111	0.099	-1.129	-0.114	0.259	-	
NEFF	ctx-rh-medialorbitofrontal	R-medORB	-0.108	0.096	-1.126	-0.114	0.261	-	
NEFF	ctx-rh-middletemporal	R-midTEM	-0.154	0.103	-1.495	-0.151	0.135	-	
NEFF	ctx-rh-parahippocampal	R-parHIP	-0.126	0.101	-1.253	-0.127	0.211	-	
NEFF	ctx-rh-paracentral	R-parCEN	-0.122	0.104	-1.173	-0.118	0.241	-	
NEFF	ctx-rh-parsopercularis	R-parOPE	0.124	0.098	1.268	0.128	0.205	-	
NEFF	ctx-rh-parsorbitalis	R-parORB	-0.126	0.094	-1.341	-0.135	0.180	-	
NEFF	ctx-rh-parstriangularis	R-parTRI	0.042	0.098	0.427	0.043	0.669	-	
NEFF	ctx-rh-pericalcarine	R-perCAR	-0.169	0.097	-1.745	-0.176	0.081	-	
NEFF	ctx-rh-postcentral	R-posCEN	-0.139	0.103	-1.353	-0.137	0.176	-	
NEFF	ctx-rh-posteriorcingulate	R-posCIN	-0.139	0.103	-1.352	-0.137	0.177	-	
NEFF	ctx-rh-precentral	R-preCEN	-0.190	0.104	-1.829	-0.185	0.068	-	
NEFF	ctx-rh-precuneus	R-preCUN	-0.208	0.097	-2.145	-0.217	0.032	-	
NEFF	ctx-rh-rostralanteriorcingulate	R-rosACG	-0.117	0.089	-1.324	-0.134	0.186	-	

NEFF	ctx-rh-rostralmiddlefrontal	R-rosMFR	-0.089	0.086	-1.030	-0.104	0.304	-	
NEFF	ctx-rh-superiorfrontal	R-supFRO	-0.085	0.093	-0.917	-0.093	0.359	-	
NEFF	ctx-rh-superiorparietal	R-supPAR	-0.176	0.097	-1.805	-0.182	0.072	-	
NEFF	ctx-rh-superiortemporal	R-supTEM	-0.150	0.101	-1.481	-0.150	0.139	-	
NEFF	ctx-rh-supramarginal	R-supMAR	-0.039	0.104	-0.376	-0.038	0.707	-	
NEFF	ctx-rh-frontalpole	R-froPOL	-0.113	0.085	-1.335	-0.135	0.182	-	
NEFF	ctx-rh-temporalpole	R-temPOL	-0.066	0.097	-0.680	-0.069	0.497	-	
NEFF	ctx-rh-transversetemporal	R-traTEM	-0.123	0.096	-1.278	-0.129	0.202	-	
NEFF	ctx-rh-insula	R-insula	-0.156	0.101	-1.555	-0.157	0.120	-	
GCC	Global		-0.057	0.103	-0.554	-0.056	0.580	0.580	
TIER_CC	T1		-0.066	0.103	-0.640	-0.065	0.522	-	
TIER_CC	T2		-0.071	0.100	-0.712	-0.072	0.477	-	
TIER_CC	T3		0.031	0.104	0.301	0.030	0.764	-	
TIER_CC	T4		-0.040	0.099	-0.405	-0.041	0.686	-	
CC	Left-Thalamus-Proper	L-thal	-0.031	0.105	-0.297	-0.030	0.766	-	
CC	Left-Caudate	L-caud	-0.158	0.106	-1.494	-0.151	0.136	-	
CC	Left-Putamen	L-puta	-0.069	0.104	-0.666	-0.067	0.506	-	
CC	Left-Pallidum	L-pall	-0.092	0.103	-0.900	-0.091	0.369	-	
CC	Brain-Stem	bSTEM	-0.201	0.106	-1.897	-0.192	0.058	-	
CC	Left-Hippocampus	L-hipp	-0.070	0.106	-0.658	-0.066	0.511	-	
CC	Left-Amygdala	L-amyg	0.102	0.106	0.962	0.097	0.336	-	
CC	Left-Accumbens-area	L-accu	-0.006	0.104	-0.054	-0.005	0.957	-	
CC	Left-VentralDC	L-venDC	-0.146	0.104	-1.400	-0.141	0.162	-	
CC	Right-Thalamus-Proper	R-thal	-0.020	0.102	-0.194	-0.020	0.846	-	
CC	Right-Caudate	R-caud	-0.084	0.106	-0.792	-0.080	0.429	-	
CC	Right-Putamen	R-puta	-0.099	0.101	-0.980	-0.099	0.327	-	
CC	Right-Pallidum	R-pall	-0.001	0.105	-0.009	-0.001	0.993	-	
CC	Right-Hippocampus	R-hipp	0.107	0.105	1.018	0.103	0.309	-	
CC	Right-Amygdala	R-amyg	0.138	0.105	1.305	0.132	0.192	-	
CC	Right-Accumbens-area	R-accu	0.055	0.104	0.534	0.054	0.594	-	

CC	Right-VentralDC	R-venDC	-0.113	0.099	-1.142	-0.115	0.254	-	
CC	ctx-lh-bankssts	L-banks	0.050	0.107	0.473	0.048	0.636	-	
CC	ctx-lh-caudalanteriorcingulate	L-cauACG	-0.021	0.106	-0.200	-0.020	0.842	-	
CC	ctx-lh-caudalmiddlefrontal	L-cauMFR	-0.095	0.101	-0.946	-0.096	0.344	-	
CC	ctx-lh-cuneus	L-cune	-0.072	0.104	-0.687	-0.069	0.492	-	
CC	ctx-lh-entorhinal	L-entorh	-0.016	0.103	-0.159	-0.016	0.874	-	
CC	ctx-lh-fusiform	L-fusif	-0.091	0.102	-0.894	-0.090	0.372	-	
CC	ctx-lh-inferiorparietal	L-infPAR	0.003	0.101	0.029	0.003	0.977	-	
CC	ctx-lh-inferiortemporal	L-infTEM	-0.059	0.106	-0.561	-0.057	0.575	-	
CC	ctx-lh-isthmuscingulate	L-istCIN	-0.071	0.101	-0.699	-0.071	0.485	-	
CC	ctx-lh-lateraloccipital	L-latOCC	-0.112	0.103	-1.085	-0.110	0.278	-	
CC	ctx-lh-lateralorbitofrontal	L-latORB	-0.143	0.101	-1.411	-0.143	0.159	-	
CC	ctx-lh-lingual	L-lingual	0.134	0.106	1.270	0.128	0.204	-	
CC	ctx-lh-medialorbitofrontal	L-medORB	0.076	0.104	0.736	0.074	0.462	-	
CC	ctx-lh-middletemporal	L-midTEM	0.013	0.104	0.122	0.012	0.903	-	
CC	ctx-lh-parahippocampal	L-parHIP	0.020	0.111	0.179	0.019	0.858	-	
CC	ctx-lh-paracentral	L-parCEN	-0.132	0.102	-1.300	-0.131	0.194	-	
CC	ctx-lh-parsopercularis	L-parOPE	-0.170	0.099	-1.717	-0.173	0.087	-	
CC	ctx-lh-parsorbitalis	L-parORB	-0.097	0.106	-0.923	-0.093	0.356	-	
CC	ctx-lh-parstriangularis	L-parTRI	-0.031	0.106	-0.289	-0.029	0.773	-	
CC	ctx-lh-pericalcarine	L-perCAR	-0.130	0.103	-1.264	-0.128	0.207	-	
CC	ctx-lh-postcentral	L-posCEN	-0.038	0.102	-0.369	-0.037	0.712	-	
CC	ctx-lh-posteriorcingulate	L-posCIN	-0.130	0.102	-1.270	-0.128	0.204	-	
CC	ctx-lh-precentral	L-preCEN	-0.140	0.100	-1.397	-0.141	0.163	-	
CC	ctx-lh-precuneus	L-preCUN	-0.136	0.104	-1.307	-0.132	0.192	-	
CC	ctx-lh-rostralanteriorcingulate	L-rosACG	-0.150	0.101	-1.488	-0.150	0.137	-	
CC	ctx-lh-rostralmiddlefrontal	L-rosMFR	-0.030	0.106	-0.280	-0.028	0.779	-	
CC	ctx-lh-superiorfrontal	L-supFRO	-0.084	0.105	-0.795	-0.080	0.427	-	

CC	ctx-lh-superiorparietal	L-supPAR	-0.146	0.102	-1.427	-0.144	0.154	-	
CC	ctx-lh-superiortemporal	L-supTEM	-0.009	0.104	-0.090	-0.009	0.928	-	
CC	ctx-lh-supramarginal	L-supMAR	-0.123	0.105	-1.175	-0.119	0.240	-	
CC	ctx-lh-frontalpole	L-froPOL	0.013	0.099	0.127	0.013	0.899	-	
CC	ctx-lh-temporalpole	L-temPOL	0.054	0.104	0.521	0.053	0.602	-	
CC	ctx-lh-transversetemporal	L-traTEM	-0.201	0.104	-1.936	-0.196	0.053	-	
CC	ctx-lh-insula	L-insula	0.119	0.105	1.132	0.114	0.258	-	
CC	ctx-rh-bankssts	R-banks	0.083	0.104	0.793	0.080	0.428	-	
CC	ctx-rh-caudalanteriorcingulate	R-cauACG	-0.063	0.105	-0.596	-0.060	0.552	-	
CC	ctx-rh-caudalmiddlefrontal	R-cauMFR	0.010	0.104	0.098	0.010	0.922	-	
CC	ctx-rh-cuneus	R-cune	-0.203	0.104	-1.951	-0.197	0.052	-	
CC	ctx-rh-entorhinal	R-entorh	0.096	0.107	0.900	0.092	0.368	-	
CC	ctx-rh-fusiform	R-fusif	-0.038	0.104	-0.362	-0.037	0.717	-	
CC	ctx-rh-inferiorparietal	R-infPAR	0.240	0.104	2.306	0.233	0.021	-	
CC	ctx-rh-inferiortemporal	R-infTEM	0.003	0.105	0.031	0.003	0.976	-	
CC	ctx-rh-isthmuscingulate	R-istCIN	0.012	0.104	0.111	0.011	0.911	-	
CC	ctx-rh-lateraloccipital	R-latOCC	0.010	0.105	0.091	0.009	0.927	-	
CC	ctx-rh-lateralorbitofrontal	R-latORB	-0.092	0.096	-0.957	-0.097	0.339	-	
CC	ctx-rh-lingual	R-lingual	-0.005	0.101	-0.045	-0.004	0.964	-	
CC	ctx-rh-medialorbitofrontal	R-medORB	-0.058	0.100	-0.575	-0.058	0.566	-	
CC	ctx-rh-middletemporal	R-midTEM	0.037	0.105	0.354	0.036	0.724	-	
CC	ctx-rh-parahippocampal	R-parHIP	-0.013	0.106	-0.119	-0.012	0.906	-	
CC	ctx-rh-paracentral	R-parCEN	-0.084	0.103	-0.813	-0.082	0.416	-	
CC	ctx-rh-parsopercularis	R-parOPE	0.054	0.105	0.509	0.051	0.611	-	
CC	ctx-rh-parsorbitalis	R-parORB	-0.067	0.103	-0.654	-0.066	0.513	-	
CC	ctx-rh-parstriangularis	R-parTRI	0.065	0.105	0.618	0.062	0.537	-	
CC	ctx-rh-pericalcarine	R-perCAR	-0.005	0.103	-0.046	-0.005	0.964	-	
CC	ctx-rh-postcentral	R-posCEN	-0.030	0.104	-0.288	-0.029	0.774	-	
CC	ctx-rh-posteriorcingulate	R-posCIN	-0.040	0.104	-0.386	-0.039	0.699	-	

CC	ctx-rh-precentral	R-preCEN	-0.059	0.104	-0.570	-0.058	0.569	-	
CC	ctx-rh-precuneus	R-preCUN	0.009	0.104	0.083	0.008	0.934	-	
CC	ctx-rh-rostralanteriorcingulate	R-rosACG	-0.079	0.102	-0.771	-0.078	0.441	-	
CC	ctx-rh-rostralmiddlefrontal	R-rosMFR	-0.020	0.105	-0.192	-0.019	0.848	-	
CC	ctx-rh-superiorfrontal	R-supFRO	-0.085	0.104	-0.821	-0.083	0.412	-	
CC	ctx-rh-superiorparietal	R-supPAR	-0.032	0.103	-0.313	-0.032	0.754	-	
CC	ctx-rh-superiortemporal	R-supTEM	0.040	0.105	0.384	0.039	0.701	-	
CC	ctx-rh-supramarginal	R-supMAR	0.005	0.106	0.048	0.005	0.962	-	
CC	ctx-rh-frontalpole	R-froPOL	-0.040	0.101	-0.394	-0.040	0.694	-	
CC	ctx-rh-temporalpole	R-temPOL	0.064	0.101	0.637	0.064	0.524	-	
CC	ctx-rh-transversetemporal	R-traTEM	-0.054	0.106	-0.510	-0.053	0.610	-	
CC	ctx-rh-insula	R-insula	-0.016	0.103	-0.154	-0.016	0.878	-	

Table S7. Cohen's d for all network measures in UKB after controlling for age and sex in the supplementary analysis comparing MDD cases with and without antidepressant use. Among the cases, 14% took antidepressants and 86% did not. To aid comparison, rows highlighted in yellow represent measures that were significantly different between cases and controls in the discovery cohort (UKB) in the main analysis.

measure	region	abb	beta	sd	tval	cohen_d	pval	pFDR	sig
GEFF	Global		-0.143	0.071	-1.995	-0.146	0.046	0.092	
TIER_NEFF	T1		-0.127	0.071	-1.778	-0.130	0.076	-	
TIER_NEFF	T2		-0.144	0.071	-2.021	-0.148	0.043	-	
TIER_NEFF	T3		-0.147	0.071	-2.068	-0.152	0.039	-	
TIER_NEFF	T4		-0.130	0.072	-1.812	-0.133	0.070	-	
NEFF	Left-Thalamus-Proper	L-thal	-0.167	0.072	-2.309	-0.169	0.021	-	
NEFF	Left-Caudate	L-caud	-0.090	0.072	-1.260	-0.092	0.208	-	
NEFF	Left-Putamen	L-puta	-0.104	0.071	-1.464	-0.107	0.144	-	
NEFF	Left-Pallidum	L-pall	-0.081	0.070	-1.153	-0.085	0.249	-	
NEFF	Brain-Stem	bSTEM	-0.073	0.072	-1.025	-0.075	0.305	-	
NEFF	Left-Hippocampus	L-hipp	-0.085	0.071	-1.211	-0.089	0.226	-	
NEFF	Left-Amygdala	L-amyg	-0.053	0.069	-0.773	-0.057	0.440	-	
NEFF	Left-Accumbens-area	L-accu	-0.143	0.072	-1.999	-0.147	0.046	-	
NEFF	Left-VentralDC	L-venDC	-0.064	0.070	-0.911	-0.067	0.362	-	
NEFF	Right-Thalamus-Proper	R-thal	-0.116	0.071	-1.630	-0.120	0.103	-	
NEFF	Right-Caudate	R-caud	-0.112	0.070	-1.596	-0.117	0.111	-	
NEFF	Right-Putamen	R-puta	-0.103	0.071	-1.442	-0.106	0.149	-	
NEFF	Right-Pallidum	R-pall	-0.037	0.072	-0.515	-0.038	0.607	-	
NEFF	Right-Hippocampus	R-hipp	0.004	0.073	0.053	0.004	0.958	-	
NEFF	Right-Amygdala	R-amyg	-0.037	0.074	-0.499	-0.037	0.618	-	
NEFF	Right-Accumbens-area	R-accu	-0.193	0.074	-2.614	-0.192	0.009	-	
NEFF	Right-VentralDC	R-venDC	-0.086	0.072	-1.206	-0.088	0.228	-	
NEFF	ctx-lh-bankssts	L-banks	-0.114	0.073	-1.560	-0.114	0.119	-	
NEFF	ctx-lh-caudalanteriorcingulate	L-cauACG	-0.108	0.073	-1.487	-0.109	0.137	-	

NEFF	ctx-lh-caudalmiddlefrontal	L-cauMFR	-0.068	0.073	-0.924	-0.068	0.356	-	
NEFF	ctx-lh-cuneus	L-cune	-0.147	0.071	-2.072	-0.152	0.038	-	
NEFF	ctx-lh-entorhinal	L-entorh	-0.042	0.072	-0.581	-0.043	0.562	-	
NEFF	ctx-lh-fusiform	L-fusif	-0.200	0.071	-2.834	-0.208	0.005	-	
NEFF	ctx-lh-inferiorparietal	L-infPAR	-0.128	0.070	-1.833	-0.134	0.067	-	
NEFF	ctx-lh-inferiortemporal	L-infTEM	-0.160	0.071	-2.240	-0.164	0.025	-	
NEFF	ctx-lh-isthmuscingulate	L-istCIN	-0.097	0.071	-1.361	-0.100	0.174	-	
NEFF	ctx-lh-lateraloccipital	L-latOCC	-0.147	0.070	-2.113	-0.155	0.035	-	
NEFF	ctx-lh-lateralorbitofrontal	L-latORB	-0.209	0.073	-2.870	-0.210	0.004	-	
NEFF	ctx-lh-lingual	L-lingual	-0.058	0.072	-0.798	-0.059	0.425	-	
NEFF	ctx-lh-medialorbitofrontal	L-medORB	-0.118	0.072	-1.639	-0.120	0.101	-	
NEFF	ctx-lh-middletemporal	L-midTEM	-0.141	0.072	-1.962	-0.144	0.050	-	
NEFF	ctx-lh-parahippocampal	L-parHIP	-0.103	0.073	-1.417	-0.104	0.157	-	
NEFF	ctx-lh-paracentral	L-parCEN	-0.094	0.072	-1.315	-0.096	0.189	-	
NEFF	ctx-lh-parsopercularis	L-parOPE	-0.083	0.074	-1.132	-0.083	0.258	-	
NEFF	ctx-lh-parsorbitalis	L-parORB	-0.140	0.073	-1.931	-0.142	0.054	-	
NEFF	ctx-lh-parstriangularis	L-parTRI	0.000	0.073	0.000	0.000	1.000	-	
NEFF	ctx-lh-pericalcarine	L-perCAR	-0.111	0.071	-1.571	-0.115	0.116	-	
NEFF	ctx-lh-postcentral	L-posCEN	-0.134	0.071	-1.886	-0.138	0.060	-	
NEFF	ctx-lh-posteriorcingulate	L-posCIN	-0.147	0.072	-2.057	-0.151	0.040	-	
NEFF	ctx-lh-precentral	L-preCEN	-0.135	0.073	-1.853	-0.136	0.064	-	
NEFF	ctx-lh-precuneus	L-preCUN	-0.096	0.071	-1.343	-0.099	0.179	-	
NEFF	ctx-lh-rostralanteriorcingulate	L-rosACG	-0.007	0.074	-0.092	-0.007	0.927	-	
NEFF	ctx-lh-rostralmiddlefrontal	L-rosMFR	-0.058	0.073	-0.799	-0.059	0.424	-	
NEFF	ctx-lh-superiorfrontal	L-supFRO	-0.068	0.074	-0.917	-0.067	0.359	-	
NEFF	ctx-lh-superiorparietal	L-supPAR	-0.086	0.071	-1.223	-0.090	0.222	-	
NEFF	ctx-lh-superiortemporal	L-supTEM	-0.117	0.072	-1.622	-0.119	0.105	-	
NEFF	ctx-lh-supramarginal	L-supMAR	-0.104	0.072	-1.431	-0.105	0.153	-	
NEFF	ctx-lh-frontalpole	L-froPOL	-0.094	0.072	-1.296	-0.095	0.195	-	

NEFF	ctx-lh-temporalpole	L-temPOL	-0.109	0.070	-1.563	-0.115	0.118	-	
NEFF	ctx-lh-transversetemporal	L-traTEM	-0.182	0.073	-2.502	-0.184	0.012	-	
NEFF	ctx-lh-insula	L-insula	-0.170	0.072	-2.375	-0.174	0.018	-	
NEFF	ctx-rh-bankssts	R-banks	-0.091	0.072	-1.258	-0.092	0.208	-	
NEFF	ctx-rh-caudalanteriorcingulate	R-cauACG	-0.219	0.073	-2.981	-0.219	0.003	-	
NEFF	ctx-rh-caudalmiddlefrontal	R-cauMFR	-0.048	0.072	-0.671	-0.049	0.502	-	
NEFF	ctx-rh-cuneus	R-cune	-0.156	0.071	-2.190	-0.161	0.029	-	
NEFF	ctx-rh-entorhinal	R-entorh	0.067	0.074	0.896	0.066	0.370	-	
NEFF	ctx-rh-fusiform	R-fusif	-0.085	0.072	-1.187	-0.087	0.235	-	
NEFF	ctx-rh-inferiorparietal	R-infPAR	-0.052	0.072	-0.728	-0.053	0.467	-	
NEFF	ctx-rh-inferiortemporal	R-infTEM	-0.106	0.070	-1.510	-0.111	0.131	-	
NEFF	ctx-rh-isthmuscingulate	R-istCIN	-0.192	0.072	-2.675	-0.196	0.008	-	
NEFF	ctx-rh-lateraloccipital	R-latOCC	-0.190	0.071	-2.687	-0.197	0.007	-	
NEFF	ctx-rh-lateralorbitofrontal	R-latORB	-0.068	0.073	-0.931	-0.068	0.352	-	
NEFF	ctx-rh-lingual	R-lingual	-0.058	0.072	-0.817	-0.060	0.414	-	
NEFF	ctx-rh-medialorbitofrontal	R-medORB	-0.069	0.073	-0.943	-0.069	0.346	-	
NEFF	ctx-rh-middletemporal	R-midTEM	-0.078	0.071	-1.098	-0.081	0.272	-	
NEFF	ctx-rh-parahippocampal	R-parHIP	-0.048	0.070	-0.689	-0.051	0.491	-	
NEFF	ctx-rh-paracentral	R-parCEN	-0.145	0.072	-2.006	-0.147	0.045	-	
NEFF	ctx-rh-parsopercularis	R-parOPE	-0.104	0.072	-1.437	-0.105	0.151	-	
NEFF	ctx-rh-parsorbitalis	R-parORB	-0.101	0.073	-1.383	-0.101	0.167	-	
NEFF	ctx-rh-parstriangularis	R-parTRI	-0.115	0.073	-1.563	-0.115	0.118	-	
NEFF	ctx-rh-pericalcarine	R-perCAR	-0.140	0.070	-2.000	-0.147	0.046	-	
NEFF	ctx-rh-postcentral	R-posCEN	-0.072	0.071	-1.006	-0.074	0.314	-	
NEFF	ctx-rh-posteriorcingulate	R-posCIN	-0.165	0.073	-2.276	-0.167	0.023	-	
NEFF	ctx-rh-precentral	R-preCEN	-0.073	0.070	-1.038	-0.076	0.300	-	
NEFF	ctx-rh-precuneus	R-preCUN	-0.100	0.070	-1.421	-0.104	0.155	-	
NEFF	ctx-rh-rostralanteriorcingulate	R-rosACG	-0.115	0.074	-1.556	-0.114	0.120	-	

NEFF	ctx-rh-rostralmiddlefrontal	R-rosMFR	-0.108	0.073	-1.471	-0.108	0.141	-	
NEFF	ctx-rh-superiorfrontal	R-supFRO	-0.096	0.072	-1.333	-0.098	0.183	-	
NEFF	ctx-rh-superiorparietal	R-supPAR	-0.038	0.071	-0.528	-0.039	0.598	-	
NEFF	ctx-rh-superiortemporal	R-supTEM	-0.132	0.071	-1.858	-0.136	0.063	-	
NEFF	ctx-rh-supramarginal	R-supMAR	-0.129	0.072	-1.807	-0.133	0.071	-	
NEFF	ctx-rh-frontalpole	R-froPOL	-0.038	0.075	-0.509	-0.037	0.611	-	
NEFF	ctx-rh-temporalpole	R-temPOL	0.014	0.072	0.189	0.014	0.850	-	
NEFF	ctx-rh-transversetemporal	R-traTEM	-0.145	0.072	-2.007	-0.147	0.045	-	
NEFF	ctx-rh-insula	R-insula	-0.160	0.071	-2.251	-0.165	0.025	-	
GCC	Global		-0.051	0.071	-0.717	-0.053	0.473	0.473	
TIER_CC	T1		-0.078	0.073	-1.070	-0.078	0.285	-	
TIER_CC	T2		-0.007	0.072	-0.092	-0.007	0.927	-	
TIER_CC	T3		-0.042	0.071	-0.596	-0.044	0.552	-	
TIER_CC	T4		-0.057	0.070	-0.814	-0.060	0.416	-	
CC	Left-Thalamus-Proper	L-thal	-0.024	0.073	-0.321	-0.024	0.748	-	
CC	Left-Caudate	L-caud	-0.029	0.071	-0.406	-0.030	0.685	-	
CC	Left-Putamen	L-puta	-0.043	0.072	-0.602	-0.044	0.547	-	
CC	Left-Pallidum	L-pall	0.017	0.073	0.233	0.017	0.816	-	
CC	Brain-Stem	bSTEM	-0.007	0.069	-0.099	-0.007	0.921	-	
CC	Left-Hippocampus	L-hipp	0.036	0.071	0.509	0.037	0.611	-	
CC	Left-Amygdala	L-amyg	0.038	0.073	0.526	0.039	0.599	-	
CC	Left-Accumbens-area	L-accu	-0.100	0.067	-1.488	-0.109	0.137	-	
CC	Left-VentralDC	L-venDC	-0.024	0.074	-0.331	-0.024	0.740	-	
CC	Right-Thalamus-Proper	R-thal	-0.020	0.073	-0.280	-0.021	0.780	-	
CC	Right-Caudate	R-caud	-0.114	0.072	-1.569	-0.115	0.117	-	
CC	Right-Putamen	R-puta	-0.079	0.073	-1.077	-0.079	0.282	-	
CC	Right-Pallidum	R-pall	-0.092	0.075	-1.240	-0.091	0.215	-	
CC	Right-Hippocampus	R-hipp	-0.126	0.073	-1.721	-0.126	0.085	-	
CC	Right-Amygdala	R-amyg	0.015	0.076	0.202	0.015	0.840	-	
CC	Right-Accumbens-area	R-accu	-0.218	0.073	-2.989	-0.219	0.003	-	

CC	Right-VentralDC	R-venDC	-0.109	0.075	-1.451	-0.106	0.147	-	
CC	ctx-lh-bankssts	L-banks	-0.003	0.072	-0.035	-0.003	0.972	-	
CC	ctx-lh-caudalanteriorcingulate	L-cauACG	-0.033	0.072	-0.454	-0.033	0.650	-	
CC	ctx-lh-caudalmiddlefrontal	L-cauMFR	-0.042	0.072	-0.573	-0.042	0.566	-	
CC	ctx-lh-cuneus	L-cune	-0.030	0.071	-0.422	-0.031	0.673	-	
CC	ctx-lh-entorhinal	L-entorh	-0.009	0.073	-0.123	-0.009	0.902	-	
CC	ctx-lh-fusiform	L-fusif	-0.025	0.073	-0.345	-0.025	0.730	-	
CC	ctx-lh-inferiorparietal	L-infPAR	0.000	0.073	0.002	0.000	0.998	-	
CC	ctx-lh-inferiortemporal	L-infTEM	-0.030	0.072	-0.423	-0.031	0.672	-	
CC	ctx-lh-isthmuscingulate	L-istCIN	-0.146	0.072	-2.022	-0.148	0.043	-	
CC	ctx-lh-lateraloccipital	L-latOCC	-0.035	0.073	-0.482	-0.035	0.630	-	
CC	ctx-lh-lateralorbitofrontal	L-latORB	-0.072	0.072	-0.998	-0.073	0.318	-	
CC	ctx-lh-lingual	L-lingual	-0.251	0.072	-3.478	-0.255	0.001	-	
CC	ctx-lh-medialorbitofrontal	L-medORB	-0.092	0.073	-1.267	-0.093	0.205	-	
CC	ctx-lh-middletemporal	L-midTEM	-0.003	0.072	-0.043	-0.003	0.966	-	
CC	ctx-lh-parahippocampal	L-parHIP	-0.148	0.075	-1.987	-0.146	0.047	-	
CC	ctx-lh-paracentral	L-parCEN	0.019	0.072	0.268	0.020	0.789	-	
CC	ctx-lh-parsopercularis	L-parOPE	0.058	0.073	0.786	0.058	0.432	-	
CC	ctx-lh-parsorbitalis	L-parORB	0.043	0.069	0.620	0.046	0.535	-	
CC	ctx-lh-parstriangularis	L-parTRI	0.041	0.073	0.562	0.041	0.574	-	
CC	ctx-lh-pericalcarine	L-perCAR	-0.105	0.073	-1.447	-0.106	0.148	-	
CC	ctx-lh-postcentral	L-posCEN	0.022	0.068	0.329	0.024	0.742	-	
CC	ctx-lh-posteriorcingulate	L-posCIN	0.025	0.072	0.346	0.025	0.729	-	
CC	ctx-lh-precentral	L-preCEN	0.029	0.072	0.405	0.030	0.686	-	
CC	ctx-lh-precuneus	L-preCUN	-0.042	0.071	-0.592	-0.043	0.554	-	
CC	ctx-lh-rostralanteriorcingulate	L-rosACG	-0.048	0.072	-0.670	-0.049	0.503	-	
CC	ctx-lh-rostralmiddlefrontal	L-rosMFR	-0.059	0.073	-0.811	-0.059	0.417	-	
CC	ctx-lh-superiorfrontal	L-supFRO	-0.029	0.070	-0.414	-0.030	0.679	-	

CC	ctx-lh-superiorparietal	L-supPAR	0.017	0.071	0.233	0.017	0.816	-	
CC	ctx-lh-superiortemporal	L-supTEM	-0.075	0.073	-1.024	-0.075	0.306	-	
CC	ctx-lh-supramarginal	L-supMAR	0.011	0.070	0.151	0.011	0.880	-	
CC	ctx-lh-frontalpole	L-froPOL	0.041	0.075	0.551	0.040	0.581	-	
CC	ctx-lh-temporalpole	L-temPOL	-0.080	0.068	-1.166	-0.085	0.244	-	
CC	ctx-lh-transversetemporal	L-traTEM	0.041	0.071	0.582	0.043	0.561	-	
CC	ctx-lh-insula	L-insula	-0.125	0.074	-1.691	-0.124	0.091	-	
CC	ctx-rh-bankssts	R-banks	-0.109	0.072	-1.522	-0.112	0.128	-	
CC	ctx-rh-caudalanteriorcingulate	R-cauACG	0.126	0.073	1.735	0.127	0.083	-	
CC	ctx-rh-caudalmiddlefrontal	R-cauMFR	0.107	0.071	1.501	0.110	0.134	-	
CC	ctx-rh-cuneus	R-cune	-0.051	0.070	-0.717	-0.053	0.473	-	
CC	ctx-rh-entorhinal	R-entorh	0.049	0.075	0.652	0.048	0.515	-	
CC	ctx-rh-fusiform	R-fusif	-0.083	0.072	-1.152	-0.085	0.249	-	
CC	ctx-rh-inferiorparietal	R-infPAR	0.006	0.072	0.086	0.006	0.932	-	
CC	ctx-rh-inferiortemporal	R-infTEM	-0.095	0.073	-1.302	-0.096	0.193	-	
CC	ctx-rh-isthmuscingulate	R-istCIN	0.020	0.074	0.267	0.020	0.789	-	
CC	ctx-rh-lateraloccipital	R-latOCC	-0.089	0.072	-1.245	-0.091	0.213	-	
CC	ctx-rh-lateralorbitofrontal	R-latORB	-0.028	0.070	-0.402	-0.029	0.688	-	
CC	ctx-rh-lingual	R-lingual	-0.185	0.074	-2.506	-0.184	0.012	-	
CC	ctx-rh-medialorbitofrontal	R-medORB	-0.028	0.074	-0.375	-0.028	0.708	-	
CC	ctx-rh-middletemporal	R-midTEM	-0.039	0.073	-0.533	-0.039	0.594	-	
CC	ctx-rh-parahippocampal	R-parHIP	0.021	0.071	0.287	0.021	0.774	-	
CC	ctx-rh-paracentral	R-parCEN	0.058	0.073	0.795	0.058	0.427	-	
CC	ctx-rh-parsopercularis	R-parOPE	-0.029	0.070	-0.414	-0.030	0.679	-	
CC	ctx-rh-parsorbitalis	R-parORB	-0.074	0.070	-1.048	-0.077	0.295	-	
CC	ctx-rh-parstriangularis	R-parTRI	0.007	0.069	0.102	0.007	0.919	-	
CC	ctx-rh-pericalcarine	R-perCAR	-0.036	0.070	-0.507	-0.037	0.612	-	
CC	ctx-rh-postcentral	R-posCEN	0.049	0.072	0.675	0.049	0.500	-	
CC	ctx-rh-posteriorcingulate	R-posCIN	0.073	0.071	1.021	0.075	0.307	-	

CC	ctx-rh-precentral	R-preCEN	0.063	0.071	0.885	0.065	0.376	-	
CC	ctx-rh-precuneus	R-preCUN	-0.030	0.073	-0.413	-0.030	0.679	-	
CC	ctx-rh-rostralanteriorcingulate	R-rosACG	-0.101	0.074	-1.368	-0.100	0.171	-	
CC	ctx-rh-rostralmiddlefrontal	R-rosMFR	0.072	0.072	1.006	0.074	0.314	-	
CC	ctx-rh-superiorfrontal	R-supFRO	0.040	0.069	0.580	0.043	0.562	-	
CC	ctx-rh-superiorparietal	R-supPAR	-0.075	0.073	-1.038	-0.076	0.300	-	
CC	ctx-rh-superiortemporal	R-supTEM	-0.008	0.073	-0.114	-0.008	0.909	-	
CC	ctx-rh-supramarginal	R-supMAR	0.046	0.072	0.630	0.046	0.529	-	
CC	ctx-rh-frontalpole	R-froPOL	-0.071	0.070	-1.008	-0.074	0.314	-	
CC	ctx-rh-temporalpole	R-temPOL	0.054	0.072	0.750	0.055	0.454	-	
CC	ctx-rh-transversetemporal	R-traTEM	-0.065	0.073	-0.894	-0.066	0.372	-	
CC	ctx-rh-insula	R-insula	-0.036	0.073	-0.490	-0.036	0.624	-	

Table S8. Cohen's d for all network measures in UKB after controlling for age and sex in the supplementary analysis comparing MDD cases and controls, excluding MDD cases with antidepressant use. Among the cases, 14% took antidepressants and 86% did not. To aid comparison, rows highlighted in yellow represent measures that were significantly different between cases and controls in the discovery cohort (UKB) in the main analysis.

measure	region	abb	beta	sd	tval	cohen_d	pval	pFDR	sig
GEFF	Global		-0.059	0.033	-1.774	-0.058	0.076	0.117	
TIER_NEFF	T1		-0.061	0.033	-1.856	-0.060	0.063	-	
TIER_NEFF	T2		-0.051	0.033	-1.544	-0.050	0.123	-	
TIER_NEFF	T3		-0.058	0.033	-1.738	-0.057	0.082	-	
TIER_NEFF	T4		-0.063	0.033	-1.899	-0.062	0.058	-	
NEFF	Left-Thalamus-Proper	L-thal	-0.052	0.033	-1.568	-0.051	0.117	-	
NEFF	Left-Caudate	L-caud	-0.079	0.033	-2.377	-0.077	0.017	-	
NEFF	Left-Putamen	L-puta	-0.088	0.033	-2.660	-0.086	0.008	-	
NEFF	Left-Pallidum	L-pall	-0.070	0.033	-2.147	-0.070	0.032	-	
NEFF	Brain-Stem	bSTEM	-0.018	0.033	-0.562	-0.018	0.574	-	
NEFF	Left-Hippocampus	L-hipp	-0.044	0.033	-1.332	-0.043	0.183	-	
NEFF	Left-Amygdala	L-amyg	-0.022	0.033	-0.674	-0.022	0.501	-	
NEFF	Left-Accumbens-area	L-accu	-0.019	0.033	-0.570	-0.019	0.569	-	
NEFF	Left-VentralDC	L-venDC	-0.072	0.032	-2.230	-0.073	0.026	-	
NEFF	Right-Thalamus-Proper	R-thal	-0.069	0.033	-2.112	-0.069	0.035	-	
NEFF	Right-Caudate	R-caud	-0.067	0.032	-2.085	-0.068	0.037	-	
NEFF	Right-Putamen	R-puta	-0.083	0.033	-2.504	-0.081	0.012	-	
NEFF	Right-Pallidum	R-pall	-0.111	0.033	-3.390	-0.110	0.001	-	
NEFF	Right-Hippocampus	R-hipp	-0.063	0.033	-1.909	-0.062	0.056	-	
NEFF	Right-Amygdala	R-amyg	-0.039	0.033	-1.195	-0.039	0.232	-	
NEFF	Right-Accumbens-area	R-accu	-0.007	0.033	-0.203	-0.007	0.839	-	
NEFF	Right-VentralDC	R-venDC	-0.048	0.033	-1.478	-0.048	0.139	-	
NEFF	ctx-lh-bankssts	L-banks	-0.057	0.033	-1.726	-0.056	0.084	-	

NEFF	ctx-lh-caudalanteriorcingulate	L-cauACG	-0.017	0.033	-0.525	-0.017	0.600	-	
NEFF	ctx-lh-caudalmiddlefrontal	L-cauMFR	-0.035	0.033	-1.063	-0.035	0.288	-	
NEFF	ctx-lh-cuneus	L-cune	-0.035	0.033	-1.058	-0.034	0.290	-	
NEFF	ctx-lh-entorhinal	L-entorh	-0.023	0.033	-0.702	-0.023	0.483	-	
NEFF	ctx-lh-fusiform	L-fusif	-0.045	0.033	-1.379	-0.045	0.168	-	
NEFF	ctx-lh-inferiorparietal	L-infPAR	-0.015	0.032	-0.460	-0.015	0.645	-	
NEFF	ctx-lh-inferiortemporal	L-infTEM	-0.048	0.033	-1.453	-0.047	0.146	-	
NEFF	ctx-lh-isthmuscingulate	L-istCIN	-0.047	0.033	-1.423	-0.046	0.155	-	
NEFF	ctx-lh-lateraloccipital	L-latOCC	-0.037	0.033	-1.123	-0.037	0.262	-	
NEFF	ctx-lh-lateralorbitofrontal	L-latORB	-0.023	0.033	-0.696	-0.023	0.486	-	
NEFF	ctx-lh-lingual	L-lingual	-0.013	0.033	-0.403	-0.013	0.687	-	
NEFF	ctx-lh-medialorbitofrontal	L-medORB	-0.067	0.033	-2.008	-0.065	0.045	-	
NEFF	ctx-lh-middletemporal	L-midTEM	-0.007	0.033	-0.219	-0.007	0.827	-	
NEFF	ctx-lh-parahippocampal	L-parHIP	-0.040	0.033	-1.193	-0.039	0.233	-	
NEFF	ctx-lh-paracentral	L-parCEN	-0.046	0.033	-1.387	-0.045	0.165	-	
NEFF	ctx-lh-parsopercularis	L-parOPE	-0.051	0.033	-1.531	-0.050	0.126	-	
NEFF	ctx-lh-parsorbitalis	L-parORB	-0.066	0.033	-1.981	-0.064	0.048	-	
NEFF	ctx-lh-parstriangularis	L-parTRI	-0.090	0.033	-2.723	-0.089	0.007	-	
NEFF	ctx-lh-pericalcarine	L-perCAR	-0.037	0.033	-1.108	-0.036	0.268	-	
NEFF	ctx-lh-postcentral	L-posCEN	-0.014	0.033	-0.435	-0.014	0.663	-	
NEFF	ctx-lh-posteriorcingulate	L-posCIN	-0.043	0.033	-1.297	-0.042	0.195	-	
NEFF	ctx-lh-precentral	L-preCEN	-0.006	0.033	-0.191	-0.006	0.849	-	
NEFF	ctx-lh-precuneus	L-preCUN	-0.069	0.033	-2.068	-0.067	0.039	-	
NEFF	ctx-lh-rostralanteriorcingulate	L-rosACG	-0.054	0.033	-1.630	-0.053	0.103	-	
NEFF	ctx-lh-rostralmiddlefrontal	L-rosMFR	-0.065	0.033	-1.975	-0.064	0.048	-	
NEFF	ctx-lh-superiorfrontal	L-supFRO	-0.028	0.033	-0.847	-0.028	0.397	-	
NEFF	ctx-lh-superiorparietal	L-supPAR	-0.048	0.033	-1.463	-0.048	0.144	-	
NEFF	ctx-lh-superiortemporal	L-supTEM	-0.048	0.033	-1.445	-0.047	0.148	-	

NEFF	ctx-lh-supramarginal	L-supMAR	-0.028	0.033	-0.855	-0.028	0.392	-	
NEFF	ctx-lh-frontalpole	L-froPOL	-0.055	0.033	-1.664	-0.054	0.096	-	
NEFF	ctx-lh-temporalpole	L-temPOL	0.038	0.033	1.155	0.038	0.248	-	
NEFF	ctx-lh-transversetemporal	L-traTEM	-0.011	0.033	-0.338	-0.011	0.735	-	
NEFF	ctx-lh-insula	L-insula	-0.078	0.033	-2.380	-0.077	0.017	-	
NEFF	ctx-rh-bankssts	R-banks	-0.030	0.033	-0.923	-0.030	0.356	-	
NEFF	ctx-rh-caudalanteriorcingulate	R-cauACG	-0.010	0.033	-0.301	-0.010	0.764	-	
NEFF	ctx-rh-caudalmiddlefrontal	R-cauMFR	-0.024	0.033	-0.728	-0.024	0.467	-	
NEFF	ctx-rh-cuneus	R-cune	-0.033	0.033	-1.013	-0.033	0.311	-	
NEFF	ctx-rh-entorhinal	R-entorh	-0.043	0.033	-1.290	-0.042	0.197	-	
NEFF	ctx-rh-fusiform	R-fusif	-0.047	0.033	-1.422	-0.046	0.155	-	
NEFF	ctx-rh-inferiorparietal	R-infPAR	-0.001	0.033	-0.020	-0.001	0.984	-	
NEFF	ctx-rh-inferiortemporal	R-infTEM	-0.058	0.033	-1.761	-0.057	0.078	-	
NEFF	ctx-rh-isthmuscingulate	R-istCIN	-0.029	0.033	-0.868	-0.028	0.386	-	
NEFF	ctx-rh-lateraloccipital	R-latOCC	-0.018	0.032	-0.552	-0.018	0.581	-	
NEFF	ctx-rh-lateralorbitofrontal	R-latORB	-0.041	0.033	-1.232	-0.040	0.218	-	
NEFF	ctx-rh-lingual	R-lingual	-0.071	0.033	-2.155	-0.070	0.031	-	
NEFF	ctx-rh-medialorbitofrontal	R-medORB	-0.039	0.033	-1.169	-0.038	0.243	-	
NEFF	ctx-rh-middletemporal	R-midTEM	-0.039	0.033	-1.177	-0.038	0.239	-	
NEFF	ctx-rh-parahippocampal	R-parHIP	-0.015	0.033	-0.439	-0.014	0.661	-	
NEFF	ctx-rh-paracentral	R-parCEN	-0.045	0.033	-1.363	-0.044	0.173	-	
NEFF	ctx-rh-parsopercularis	R-parOPE	0.005	0.033	0.162	0.005	0.871	-	
NEFF	ctx-rh-parsorbitalis	R-parORB	-0.054	0.033	-1.658	-0.054	0.097	-	
NEFF	ctx-rh-parstriangularis	R-parTRI	-0.022	0.033	-0.664	-0.022	0.507	-	
NEFF	ctx-rh-pericalcarine	R-perCAR	-0.033	0.033	-1.004	-0.033	0.315	-	
NEFF	ctx-rh-postcentral	R-posCEN	-0.068	0.033	-2.068	-0.067	0.039	-	
NEFF	ctx-rh-posteriorcingulate	R-posCIN	-0.044	0.033	-1.334	-0.043	0.182	-	
NEFF	ctx-rh-precentral	R-preCEN	-0.015	0.033	-0.463	-0.015	0.643	-	
NEFF	ctx-rh-precuneus	R-preCUN	-0.049	0.033	-1.471	-0.048	0.141	-	

NEFF	ctx-rh-rostralanteriorcingulate	R-rosACG	-0.045	0.033	-1.340	-0.044	0.180	-	
NEFF	ctx-rh-rostralmiddlefrontal	R-rosMFR	-0.043	0.033	-1.296	-0.042	0.195	-	
NEFF	ctx-rh-superiorfrontal	R-supFRO	-0.033	0.033	-0.993	-0.032	0.321	-	
NEFF	ctx-rh-superiorparietal	R-supPAR	-0.039	0.033	-1.161	-0.038	0.246	-	
NEFF	ctx-rh-superiortemporal	R-supTEM	-0.026	0.033	-0.786	-0.026	0.432	-	
NEFF	ctx-rh-supramarginal	R-supMAR	-0.042	0.033	-1.280	-0.042	0.201	-	
NEFF	ctx-rh-frontalpole	R-froPOL	-0.037	0.033	-1.101	-0.036	0.271	-	
NEFF	ctx-rh-temporalpole	R-temPOL	-0.070	0.033	-2.146	-0.070	0.032	-	
NEFF	ctx-rh-transversetemporal	R-traTEM	-0.061	0.033	-1.817	-0.059	0.069	-	
NEFF	ctx-rh-insula	R-insula	-0.036	0.033	-1.079	-0.035	0.281	-	
GCC	Global		-0.052	0.033	-1.567	-0.051	0.117	0.117	
TIER_CC	T1		-0.031	0.033	-0.942	-0.031	0.346	-	
TIER_CC	T2		-0.041	0.033	-1.225	-0.040	0.221	-	
TIER_CC	T3		-0.046	0.033	-1.398	-0.045	0.162	-	
TIER_CC	T4		-0.068	0.033	-2.050	-0.067	0.040	-	
CC	Left-Thalamus-Proper	L-thal	-0.036	0.033	-1.094	-0.036	0.274	-	
CC	Left-Caudate	L-caud	-0.007	0.033	-0.201	-0.007	0.841	-	
CC	Left-Putamen	L-puta	0.003	0.033	0.079	0.003	0.937	-	
CC	Left-Pallidum	L-pall	0.046	0.033	1.375	0.045	0.169	-	
CC	Brain-Stem	bSTEM	-0.063	0.033	-1.893	-0.062	0.058	-	
CC	Left-Hippocampus	L-hipp	-0.015	0.033	-0.442	-0.014	0.659	-	
CC	Left-Amygdala	L-amyg	0.003	0.033	0.082	0.003	0.934	-	
CC	Left-Accumbens-area	L-accu	-0.032	0.033	-0.967	-0.031	0.334	-	
CC	Left-VentralDC	L-venDC	0.003	0.033	0.091	0.003	0.928	-	
CC	Right-Thalamus-Proper	R-thal	-0.029	0.033	-0.885	-0.029	0.376	-	
CC	Right-Caudate	R-caud	-0.041	0.033	-1.235	-0.040	0.217	-	
CC	Right-Putamen	R-puta	-0.017	0.033	-0.508	-0.017	0.612	-	
CC	Right-Pallidum	R-pall	0.061	0.033	1.833	0.060	0.067	-	
CC	Right-Hippocampus	R-hipp	0.000	0.033	0.006	0.000	0.995	-	

CC	Right-Amygdala	R-amyg	-0.068	0.033	-2.056	-0.067	0.040	-	
CC	Right-Accumbens-area	R-accu	-0.012	0.033	-0.354	-0.012	0.724	-	
CC	Right-VentralDC	R-venDC	-0.019	0.033	-0.577	-0.019	0.564	-	
CC	ctx-lh-bankssts	L-banks	0.012	0.033	0.349	0.011	0.727	-	
CC	ctx-lh-caudalanteriorcingulate	L-cauACG	0.023	0.033	0.707	0.023	0.480	-	
CC	ctx-lh-caudalmiddlefrontal	L-cauMFR	-0.047	0.033	-1.424	-0.046	0.154	-	
CC	ctx-lh-cuneus	L-cune	-0.057	0.033	-1.736	-0.056	0.083	-	
CC	ctx-lh-entorhinal	L-entorh	-0.004	0.033	-0.116	-0.004	0.908	-	
CC	ctx-lh-fusiform	L-fusif	-0.015	0.033	-0.463	-0.015	0.643	-	
CC	ctx-lh-inferiorparietal	L-infPAR	-0.061	0.033	-1.842	-0.060	0.066	-	
CC	ctx-lh-inferiortemporal	L-infTEM	-0.012	0.033	-0.360	-0.012	0.718	-	
CC	ctx-lh-isthmuscingulate	L-istCIN	-0.035	0.033	-1.082	-0.035	0.279	-	
CC	ctx-lh-lateraloccipital	L-latOCC	-0.028	0.033	-0.832	-0.027	0.405	-	
CC	ctx-lh-lateralorbitofrontal	L-latORB	-0.056	0.033	-1.701	-0.055	0.089	-	
CC	ctx-lh-lingual	L-lingual	0.011	0.033	0.318	0.010	0.750	-	
CC	ctx-lh-medialorbitofrontal	L-medORB	0.014	0.033	0.411	0.013	0.681	-	
CC	ctx-lh-middletemporal	L-midTEM	-0.018	0.033	-0.530	-0.017	0.596	-	
CC	ctx-lh-parahippocampal	L-parHIP	-0.042	0.033	-1.269	-0.041	0.204	-	
CC	ctx-lh-paracentral	L-parCEN	-0.032	0.033	-0.993	-0.032	0.321	-	
CC	ctx-lh-parsopercularis	L-parOPE	-0.029	0.033	-0.874	-0.028	0.382	-	
CC	ctx-lh-parsorbitalis	L-parORB	-0.019	0.033	-0.573	-0.019	0.567	-	
CC	ctx-lh-parstriangularis	L-parTRI	-0.071	0.033	-2.137	-0.069	0.033	-	
CC	ctx-lh-pericalcarine	L-perCAR	-0.028	0.033	-0.838	-0.027	0.402	-	
CC	ctx-lh-postcentral	L-posCEN	-0.063	0.032	-1.941	-0.063	0.052	-	
CC	ctx-lh-posteriorcingulate	L-posCIN	-0.032	0.033	-0.986	-0.032	0.324	-	
CC	ctx-lh-precentral	L-preCEN	-0.048	0.033	-1.467	-0.048	0.142	-	
CC	ctx-lh-precuneus	L-preCUN	-0.011	0.033	-0.317	-0.010	0.751	-	
CC	ctx-lh-rostralanteriorcingulate	L-rosACG	-0.060	0.033	-1.823	-0.059	0.068	-	

CC	ctx-lh-rostralmiddlefrontal	L-rosMFR	-0.022	0.033	-0.656	-0.021	0.512	-	
CC	ctx-lh-superiorfrontal	L-supFRO	-0.052	0.033	-1.576	-0.051	0.115	-	
CC	ctx-lh-superiorparietal	L-supPAR	-0.065	0.033	-1.977	-0.064	0.048	-	
CC	ctx-lh-superiortemporal	L-supTEM	0.004	0.033	0.122	0.004	0.903	-	
CC	ctx-lh-supramarginal	L-supMAR	-0.043	0.033	-1.305	-0.042	0.192	-	
CC	ctx-lh-frontalpole	L-froPOL	0.019	0.033	0.564	0.018	0.573	-	
CC	ctx-lh-temporalpole	L-temPOL	-0.027	0.033	-0.816	-0.027	0.414	-	
CC	ctx-lh-transversetemporal	L-traTEM	-0.042	0.033	-1.281	-0.042	0.200	-	
CC	ctx-lh-insula	L-insula	0.010	0.033	0.293	0.010	0.770	-	
CC	ctx-rh-bankssts	R-banks	-0.022	0.033	-0.657	-0.021	0.511	-	
CC	ctx-rh-caudalanteriorcingulate	R-cauACG	-0.047	0.033	-1.437	-0.047	0.151	-	
CC	ctx-rh-caudalmiddlefrontal	R-cauMFR	-0.051	0.033	-1.544	-0.050	0.123	-	
CC	ctx-rh-cuneus	R-cune	-0.059	0.033	-1.766	-0.057	0.078	-	
CC	ctx-rh-entorhinal	R-entorh	-0.048	0.033	-1.443	-0.047	0.149	-	
CC	ctx-rh-fusiform	R-fusif	-0.025	0.033	-0.738	-0.024	0.461	-	
CC	ctx-rh-inferiorparietal	R-infPAR	-0.024	0.033	-0.726	-0.024	0.468	-	
CC	ctx-rh-inferiortemporal	R-infTEM	-0.002	0.033	-0.065	-0.002	0.948	-	
CC	ctx-rh-isthmuscingulate	R-istCIN	-0.040	0.033	-1.211	-0.039	0.226	-	
CC	ctx-rh-lateraloccipital	R-latOCC	-0.031	0.033	-0.935	-0.030	0.350	-	
CC	ctx-rh-lateralorbitofrontal	R-latORB	-0.027	0.033	-0.807	-0.026	0.420	-	
CC	ctx-rh-lingual	R-lingual	0.028	0.033	0.833	0.027	0.405	-	
CC	ctx-rh-medialorbitofrontal	R-medORB	-0.014	0.033	-0.416	-0.014	0.677	-	
CC	ctx-rh-middletemporal	R-midTEM	-0.027	0.033	-0.823	-0.027	0.411	-	
CC	ctx-rh-parahippocampal	R-parHIP	0.000	0.033	0.001	0.000	0.999	-	
CC	ctx-rh-paracentral	R-parCEN	-0.029	0.033	-0.866	-0.028	0.387	-	
CC	ctx-rh-parsopercularis	R-parOPE	-0.018	0.033	-0.542	-0.018	0.588	-	
CC	ctx-rh-parsorbitalis	R-parORB	-0.047	0.033	-1.407	-0.046	0.160	-	
CC	ctx-rh-parstriangularis	R-parTRI	-0.054	0.033	-1.629	-0.053	0.103	-	
CC	ctx-rh-pericalcarine	R-perCAR	-0.034	0.033	-1.028	-0.033	0.304	-	

CC	ctx-rh-postcentral	R-posCEN	-0.036	0.033	-1.087	-0.035	0.277	-	
CC	ctx-rh-posteriorcingulate	R-posCIN	-0.040	0.033	-1.207	-0.039	0.227	-	
CC	ctx-rh-precentral	R-preCEN	-0.078	0.033	-2.366	-0.077	0.018	-	
CC	ctx-rh-precuneus	R-preCUN	-0.070	0.033	-2.096	-0.068	0.036	-	
CC	ctx-rh-rostralanteriorcingulate	R-rosACG	0.003	0.033	0.081	0.003	0.936	-	
CC	ctx-rh-rostralmiddlefrontal	R-rosMFR	-0.046	0.033	-1.376	-0.045	0.169	-	
CC	ctx-rh-superiorfrontal	R-supFRO	-0.051	0.033	-1.545	-0.050	0.122	-	
CC	ctx-rh-superiorparietal	R-supPAR	-0.066	0.033	-1.972	-0.064	0.049	-	
CC	ctx-rh-superiortemporal	R-supTEM	-0.004	0.033	-0.125	-0.004	0.901	-	
CC	ctx-rh-supramarginal	R-supMAR	-0.037	0.033	-1.115	-0.036	0.265	-	
CC	ctx-rh-frontalpole	R-froPOL	-0.009	0.033	-0.265	-0.009	0.791	-	
CC	ctx-rh-temporalpole	R-temPOL	-0.056	0.033	-1.690	-0.055	0.091	-	
CC	ctx-rh-transversetemporal	R-traTEM	0.017	0.033	0.518	0.017	0.605	-	
CC	ctx-rh-insula	R-insula	-0.010	0.033	-0.314	-0.010	0.753	-	

Table S9. Bayes factor analysis looking at network differences between MDD cases and controls in GS. For the model, we used network measures as the dependent variable, MDD status as the grouping factor, and age, sex and site as covariates. This model was compared to a null model, which also included age, sex, and site as covariates, to derive BF_{10}. To aid comparison, rows highlighted in yellow represent measures that were significantly different between cases and controls in the discovery cohort (UKB) in the main analysis.

Note: Briefly, in comparing the alternative hypothesis to the null hypothesis (BF_{10}), a BF_{10} of value *X* would mean that the data are *X* times more likely under the alternative hypothesis than under the null. To determine the strength of evidence, we used the suggested reference values, where $BF_{10}>3$ can be interpreted as being roughly similar to $p<0.05$. $BF_{10}<1/3$ would suggest moderate evidence for the absence of an effect, $1/3<BF_{10}<3$ would suggest absence of evidence (i.e., study not informative enough), and $BF_{10}>3$ would suggest moderate evidence for the presence of an effect (Keysers, Gazzola & Wagenmakers, 2020).

The results show that majority of the measures had BF_{10} below 1 (i.e., less likely to occur as compared to the null) and fall under the category of $BF_{10}<1/3$, suggesting moderate evidence for the absence of effect. However, we would like to highlight that the correlation between the case-control Cohen's d for all the network measures between those derived in UKB and GS were rather strong and significant ($r_s=0.37$, $p=7.1\times10\text{-}7$), suggesting that the effects observed in UKB are likely to be consistent in GS. The lack of significant findings might be a matter of insufficient sample size and not necessarily an absence of effect, especially since previous studies have reported that a sample size of at least N=1000 is needed to reliably detect brain-behaviour associations (Marek et al., 2022).

measure	region	abb	BF_{10}	BF_{10}_error
GEFF	Global		0.16115411	0.15696768
TIER_LNEF	T1		0.1330622	0.02372637
TIER_LNEF	T2		0.13692971	0.04360612
TIER_LNEF	T3		0.1220917	0.0293749
TIER_LNEF	T4		0.19829608	0.2006628
LNEF	Left-Thalamus-Proper	L-thal	0.15083621	0.0270096
LNEF	Left-Caudate	L-caud	0.13478229	0.02544543
LNEF	Left-Putamen	L-puta	0.16002935	0.04247565
LNEF	Left-Pallidum	L-pall	0.16250855	0.03222233
LNEF	Brain-Stem	bSTEM	0.18425498	0.03403999

LNEF	Left-Hippocampus	L-hipp	0.14588602	0.08306244
LNEF	Left-Amygdala	L-amyg	0.11861926	0.03176265
LNEF	Left-Accumbens-area	L-accu	0.09504783	0.13753686
LNEF	Left-VentralDC	L-venDC	0.15883309	0.03948545
LNEF	Right-Thalamus-Proper	R-thal	0.15814095	0.02119135
LNEF	Right-Caudate	R-caud	0.12772797	0.03130398
LNEF	Right-Putamen	R-puta	0.28841983	0.03865176
LNEF	Right-Pallidum	R-pall	0.21954407	0.05386256
LNEF	Right-Hippocampus	R-hipp	0.12499978	0.02231405
LNEF	Right-Amygdala	R-amyg	0.14409981	0.04541631
LNEF	Right-Accumbens-area	R-accu	0.45694309	0.05087775
LNEF	Right-VentralDC	R-venDC	0.11909494	0.04389136
LNEF	ctx-lh-bankssts	L-banks	0.13579644	0.05617556
LNEF	ctx-lh-caudalanteriorcingulate	L-cauACG	0.14191245	0.02259783
LNEF	ctx-lh-caudalmiddlefrontal	L-cauMFR	0.14781244	0.02380726
LNEF	ctx-lh-cuneus	L-cune	1.26465961	0.06586829
LNEF	ctx-lh-entorhinal	L-entorh	0.1160552	0.04823371
LNEF	ctx-lh-fusiform	L-fusif	0.15293092	0.03276657
LNEF	ctx-lh-inferiorparietal	L-infPAR	0.15207149	0.02405598
LNEF	ctx-lh-inferiortemporal	L-infTEM	0.13017855	0.03242282
LNEF	ctx-lh-isthmuscingulate	L-istCIN	0.16669664	0.0211162
LNEF	ctx-lh-lateraloccipital	L-latOCC	0.11446774	0.03209847
LNEF	ctx-lh-lateralorbitofrontal	L-latORB	0.35663411	0.03333823
LNEF	ctx-lh-lingual	L-lingual	0.26173804	0.03420066
LNEF	ctx-lh-medialorbitofrontal	L-medORB	0.1504379	0.0320086
LNEF	ctx-lh-middletemporal	L-midTEM	0.08832218	0.22643338
LNEF	ctx-lh-parahippocampal	L-parHIP	0.11579994	0.07074013
LNEF	ctx-lh-paracentral	L-parCEN	0.12556455	0.04882464
LNEF	ctx-lh-parsopercularis	L-parOPE	0.20691228	0.45121519
LNEF	ctx-lh-parsorbitalis	L-parORB	0.15506163	0.04947517

LNEF	ctx-lh-parstriangularis	L-parTRI	0.16602285	0.0500814
LNEF	ctx-lh-pericalcarine	L-perCAR	0.18265883	0.06232319
LNEF	ctx-lh-postcentral	L-posCEN	0.40008265	0.0488138
LNEF	ctx-lh-posteriorcingulate	L-posCIN	0.14726067	0.03364983
LNEF	ctx-lh-precentral	L-preCEN	0.12751994	0.04324029
LNEF	ctx-lh-precuneus	L-preCUN	0.11528551	0.02518855
LNEF	ctx-lh-rostralanteriorcingulate	L-rosACG	0.15343462	0.0333054
LNEF	ctx-lh-rostralmiddlefrontal	L-rosMFR	0.12004891	0.02329184
LNEF	ctx-lh-superiorfrontal	L-supFRO	0.12939953	0.04903821
LNEF	ctx-lh-superiorparietal	L-supPAR	0.22612295	0.02737812
LNEF	ctx-lh-superiortemporal	L-supTEM	0.13009271	0.04078699
LNEF	ctx-lh-supramarginal	L-supMAR	0.26907552	0.84953399
LNEF	ctx-lh-frontalpole	L-froPOL	0.19305654	0.06207071
LNEF	ctx-lh-temporalpole	L-temPOL	0.21524709	0.0302919
LNEF	ctx-lh-transversetemporal	L-traTEM	0.34242874	0.02250714
LNEF	ctx-lh-insula	L-insula	0.13664826	0.02403309
LNEF	ctx-rh-bankssts	R-banks	0.14377869	0.04416332
LNEF	ctx-rh-caudalanteriorcingulate	R-cauACG	0.12694851	0.08610289
LNEF	ctx-rh-caudalmiddlefrontal	R-cauMFR	0.11710021	0.02143745
LNEF	ctx-rh-cuneus	R-cune	0.16679219	0.02209158
LNEF	ctx-rh-entorhinal	R-entorh	0.26672156	0.06683795
LNEF	ctx-rh-fusiform	R-fusif	0.28478987	0.03233084
LNEF	ctx-rh-inferiorparietal	R-infPAR	0.17650011	0.02105307
LNEF	ctx-rh-inferiortemporal	R-infTEM	0.1010021	0.18258712
LNEF	ctx-rh-isthmuscingulate	R-istCIN	0.12543461	0.03388579
LNEF	ctx-rh-lateraloccipital	R-latOCC	0.11968064	0.07473535
LNEF	ctx-rh-lateralorbitofrontal	R-latORB	0.15852023	0.02205961
LNEF	ctx-rh-lingual	R-lingual	0.1201137	0.04683142
LNEF	ctx-rh-medialorbitofrontal	R-medORB	0.15396901	0.02112863
LNEF	ctx-rh-middletemporal	R-midTEM	0.12706729	0.03520928

LNEF	ctx-rh-parahippocampal	R-parHIP	0.13888401	0.03808925
LNEF	ctx-rh-paracentral	R-parCEN	0.12491481	0.06990945
LNEF	ctx-rh-parsopercularis	R-parOPE	0.42301928	0.04502333
LNEF	ctx-rh-parsorbitalis	R-parORB	0.11423656	0.02631305
LNEF	ctx-rh-parstriangularis	R-parTRI	0.14331802	0.02571658
LNEF	ctx-rh-pericalcarine	R-perCAR	0.12203971	0.04968352
LNEF	ctx-rh-postcentral	R-posCEN	0.17370452	0.02475531
LNEF	ctx-rh-posteriorcingulate	R-posCIN	0.13545381	0.03117073
LNEF	ctx-rh-precentral	R-preCEN	0.26101651	0.02238347
LNEF	ctx-rh-precuneus	R-preCUN	0.23402818	0.03858195
LNEF	ctx-rh-rostralanteriorcingulate	R-rosACG	0.16509765	0.02113082
LNEF	ctx-rh-rostralmiddlefrontal	R-rosMFR	0.12638377	0.03882118
LNEF	ctx-rh-superiorfrontal	R-supFRO	0.11047395	0.01964023
LNEF	ctx-rh-superiorparietal	R-supPAR	0.13809604	0.03548247
LNEF	ctx-rh-superiortemporal	R-supTEM	0.11120316	0.20204433
LNEF	ctx-rh-supramarginal	R-supMAR	0.09594432	0.18228997
LNEF	ctx-rh-frontalpole	R-froPOL	0.1223241	0.02617827
LNEF	ctx-rh-temporalpole	R-temPOL	0.11757652	0.04070014
LNEF	ctx-rh-transversetemporal	R-traTEM	0.17697539	0.01994915
LNEF	ctx-rh-insula	R-insula	0.1575456	0.06457639
GCC	Global		0.11634358	0.03421479
TIER_LCC	T4		0.14243643	0.08663579
TIER_LCC	T1		0.12277424	0.04124247
TIER_LCC	T2		0.11997807	0.02861867
TIER_LCC	T3		0.19411091	0.22454987
LCC	Left-Thalamus-Proper	L-thal	0.17438553	0.24538222
LCC	Left-Caudate	L-caud	0.17189786	0.02551096
LCC	Left-Putamen	L-puta	0.13036023	0.03657811
LCC	Left-Pallidum	L-pall	0.12371839	0.0943803
LCC	Brain-Stem	bSTEM	0.25515326	0.08036026

LCC	Left-Hippocampus	L-hipp	0.17332785	0.08181673
LCC	Left-Amygdala	L-amyg	0.32449911	0.02695624
LCC	Left-Accumbens-area	L-accu	0.67698466	0.0560877
LCC	Left-VentralDC	L-venDC	0.12290402	0.03715117
LCC	Right-Thalamus-Proper	R-thal	0.16746518	0.04140049
LCC	Right-Caudate	R-caud	0.14894568	0.0652848
LCC	Right-Putamen	R-puta	0.12101104	0.02172291
LCC	Right-Pallidum	R-pall	0.13914248	0.02472246
LCC	Right-Hippocampus	R-hipp	0.11789203	0.05189223
LCC	Right-Amygdala	R-amyg	2.45490842	0.05350073
LCC	Right-Accumbens-area	R-accu	6.51839124	0.98076464
LCC	Right-VentralDC	R-venDC	0.15720347	0.07467294
LCC	ctx-lh-bankssts	L-banks	0.12116573	0.03878084
LCC	ctx-lh-caudalanteriorcingulate	L-cauACG	0.11113763	0.1115267
LCC	ctx-lh-caudalmiddlefrontal	L-cauMFR	0.22543476	0.04910314
LCC	ctx-lh-cuneus	L-cune	0.13300241	0.03318202
LCC	ctx-lh-entorhinal	L-entorh	0.11149816	0.09746281
LCC	ctx-lh-fusiform	L-fusif	0.16854242	0.06873485
LCC	ctx-lh-inferiorparietal	L-infPAR	0.13639207	0.09944227
LCC	ctx-lh-inferiortemporal	L-infTEM	0.13305417	0.05189519
LCC	ctx-lh-isthmuscingulate	L-istCIN	0.13516589	0.03421247
LCC	ctx-lh-lateraloccipital	L-latOCC	0.11780524	0.03286496
LCC	ctx-lh-lateralorbitofrontal	L-latORB	0.89119405	0.02214524
LCC	ctx-lh-lingual	L-lingual	0.54040065	0.02839444
LCC	ctx-lh-medialorbitofrontal	L-medORB	0.15687578	0.04144085
LCC	ctx-lh-middletemporal	L-midTEM	0.12443853	0.0339458
LCC	ctx-lh-parahippocampal	L-parHIP	0.11143187	0.0408074
LCC	ctx-lh-paracentral	L-parCEN	0.18952023	0.05598854
LCC	ctx-lh-parsopercularis	L-parOPE	0.24697503	0.04153441
LCC	ctx-lh-parsorbitalis	L-parORB	0.14783557	0.04387814

LCC	ctx-lh-parstriangularis	L-parTRI	0.18440829	0.04898933
LCC	ctx-lh-pericalcarine	L-perCAR	0.13047466	0.03082269
LCC	ctx-lh-postcentral	L-posCEN	0.13182352	0.03132139
LCC	ctx-lh-posteriorcingulate	L-posCIN	0.15730876	0.0424746
LCC	ctx-lh-precentral	L-preCEN	0.37089989	0.03823101
LCC	ctx-lh-precuneus	L-preCUN	0.14625061	0.02515656
LCC	ctx-lh-rostralanteriorcingulate	L-rosACG	0.18822436	0.02462713
LCC	ctx-lh-rostralmiddlefrontal	L-rosMFR	0.12886576	0.03458263
LCC	ctx-lh-superiorfrontal	L-supFRO	0.12730217	0.02406275
LCC	ctx-lh-superiorparietal	L-supPAR	0.11086489	0.03529768
LCC	ctx-lh-superiortemporal	L-supTEM	0.1364857	0.02345061
LCC	ctx-lh-supramarginal	L-supMAR	0.31286786	0.04912556
LCC	ctx-lh-frontalpole	L-froPOL	0.11990528	0.02069123
LCC	ctx-lh-temporalpole	L-temPOL	0.14857474	0.05348019
LCC	ctx-lh-transversetemporal	L-traTEM	0.18320921	0.09881816
LCC	ctx-lh-insula	L-insula	0.15542712	0.03413163
LCC	ctx-rh-bankssts	R-banks	0.13469865	0.02409235
LCC	ctx-rh-caudalanteriorcingulate	R-cauACG	0.11390732	0.04262898
LCC	ctx-rh-caudalmiddlefrontal	R-cauMFR	0.12877372	0.10047992
LCC	ctx-rh-cuneus	R-cune	0.38964623	0.04010708
LCC	ctx-rh-entorhinal	R-entorh	0.11697274	0.0362858
LCC	ctx-rh-fusiform	R-fusif	0.12567745	0.02335213
LCC	ctx-rh-inferiorparietal	R-infPAR	0.67842239	0.05586979
LCC	ctx-rh-inferiortemporal	R-infTEM	0.12938697	0.03694808
LCC	ctx-rh-isthmuscingulate	R-istCIN	0.19372544	0.1087856
LCC	ctx-rh-lateraloccipital	R-latOCC	0.1407557	0.06972331
LCC	ctx-rh-lateralorbitofrontal	R-latORB	0.13418814	0.05308628
LCC	ctx-rh-lingual	R-lingual	0.12949191	0.03280416
LCC	ctx-rh-medialorbitofrontal	R-medORB	0.23461768	0.02473386
LCC	ctx-rh-middletemporal	R-midTEM	0.17912316	0.02540408

LCC	ctx-rh-parahippocampal	R-parHIP	0.12363149	0.03826873
LCC	ctx-rh-paracentral	R-parCEN	0.29023368	0.03310488
LCC	ctx-rh-parsopercularis	R-parOPE	0.16609547	0.06591768
LCC	ctx-rh-parsorbitalis	R-parORB	0.13045692	0.02735672
LCC	ctx-rh-parstriangularis	R-parTRI	0.15679574	0.0566699
LCC	ctx-rh-pericalcarine	R-perCAR	0.11655808	0.04418457
LCC	ctx-rh-postcentral	R-posCEN	0.18580708	0.03635432
LCC	ctx-rh-posteriorcingulate	R-posCIN	0.1326434	0.03900991
LCC	ctx-rh-precentral	R-preCEN	0.18424626	0.09690667
LCC	ctx-rh-precuneus	R-preCUN	0.12113881	0.07025331
LCC	ctx-rh-rostralanteriorcingulate	R-rosACG	0.23902214	0.11450339
LCC	ctx-rh-rostralmiddlefrontal	R-rosMFR	0.10842206	0.04293403
LCC	ctx-rh-superiorfrontal	R-supFRO	0.20832068	0.0372779
LCC	ctx-rh-superiorparietal	R-supPAR	0.11013535	0.03973776
LCC	ctx-rh-superiortemporal	R-supTEM	0.13948605	0.03275478
LCC	ctx-rh-supramarginal	R-supMAR	0.11388066	0.0966321
LCC	ctx-rh-frontalpole	R-froPOL	0.12191341	0.03370643
LCC	ctx-rh-temporalpole	R-temPOL	0.17797268	0.02543795
LCC	ctx-rh-transversetemporal	R-traTEM	0.22563626	0.08925254
LCC	ctx-rh-insula	R-insula	0.1731277	0.03948812

Table S10. Bayes factor analysis looking at network differences between MDD cases with and without antidepressant use in UKB. For the model, we used network measures as the dependent variable, antidepressant use as the grouping factor, and age and sex as covariates. This model was compared to a null model, which also included age and sex as covariates, to derive BF_{10}. To aid comparison, rows highlighted in yellow represent measures that were significantly different between cases and controls in the discovery cohort (UKB) in the main analysis.

Note: Briefly, in comparing the alternative hypothesis to the null hypothesis (BF_{10}), a BF_{10} of value *X* would mean that the data are *X* times more likely under the alternative hypothesis than under the null. To determine the strength of evidence, we used the suggested reference values, where $BF_{10}>3$ can be interpreted as being roughly similar to $p<0.05$. $BF_{10}<1/3$ would suggest moderate evidence for the absence of an effect, $1/3<BF_{10}<3$ would suggest absence of evidence (i.e., study not informative enough), and $BF_{10}>3$ would suggest moderate evidence for the presence of an effect (Keysers, Gazzola & Wagenmakers, 2020).

The results show that majority of the measures had BF_{10} below 1 (i.e., less likely to occur as compared to the null) and fall under the category of $BF_{10}<1/3$ and even $BF_{10}<1/10$, suggesting moderate and strong evidence for the absence of effect, respectively. However, a considerable number of variables also fall under the category of absence of evidence, and even some under the category of evidence of effect. However, we would like to highlight that the analysis between MDD cases not on antidepressant use and controls had highly consistent results with the main findings ($r_s=0.934$, $p<0.001$), thus showing that our main findings are unlikely to be driven by the effects of antidepressants.

measure	region	abb	BF_{10}	BF_{10}_error
GEFF	Global		0.51659083	0.02731845
TIER_LNEF	T1		0.33084819	0.03721299
TIER_LNEF	T2		0.54014859	0.03183695
TIER_LNEF	T3		0.59135881	0.03416457
TIER_LNEF	T4		0.45241506	0.05773054
LNEF	Left-Thalamus-Proper	L-thal	1.12844966	0.04015115
LNEF	Left-Caudate	L-caud	0.1700984	0.03347781
LNEF	Left-Putamen	L-puta	0.20179169	0.04773076
LNEF	Left-Pallidum	L-pall	0.14464577	0.07251843
LNEF	Brain-Stem	bSTEM	0.13112779	0.01763863
LNEF	Left-Hippocampus	L-hipp	0.16960088	0.01981275

LNEF	Left-Amygdala	L-amyg	0.11692364	0.04393909
LNEF	Left-Accumbens-area	L-accu	0.42391597	0.02958313
LNEF	Left-VentralDC	L-venDC	0.10931274	0.02341447
LNEF	Right-Thalamus-Proper	R-thal	0.28657252	0.02648195
LNEF	Right-Caudate	R-caud	0.25047049	0.02488406
LNEF	Right-Putamen	R-puta	0.23411908	0.08555397
LNEF	Right-Pallidum	R-pall	0.08948262	0.02332008
LNEF	Right-Hippocampus	R-hipp	0.08099524	0.03530827
LNEF	Right-Amygdala	R-amyg	0.08424015	0.02804033
LNEF	Right-Accumbens-area	R-accu	2.24901355	0.01959196
LNEF	Right-VentralDC	R-venDC	0.1539964	0.06860288
LNEF	ctx-lh-bankssts	L-banks	0.2308982	0.03439726
LNEF	ctx-lh-caudalanteriorcingulate	L-cauACG	0.23609535	0.02194809
LNEF	ctx-lh-caudalmiddlefrontal	L-cauMFR	0.12582514	0.04184666
LNEF	ctx-lh-cuneus	L-cune	0.57814853	0.03004241
LNEF	ctx-lh-entorhinal	L-entorh	0.09625934	0.03051983
LNEF	ctx-lh-fusiform	L-fusif	3.68932129	0.01696132
LNEF	ctx-lh-inferiorparietal	L-infPAR	0.37360268	0.03357381
LNEF	ctx-lh-inferiortemporal	L-infTEM	0.95817845	0.0437011
LNEF	ctx-lh-isthmuscingulate	L-istCIN	0.13686292	0.25855551
LNEF	ctx-lh-lateraloccipital	L-latOCC	0.67581537	0.03133219
LNEF	ctx-lh-lateralorbitofrontal	L-latORB	5.73534481	0.05854164
LNEF	ctx-lh-lingual	L-lingual	0.11487866	0.02482856
LNEF	ctx-lh-medialorbitofrontal	L-medORB	0.30089707	0.0413005
LNEF	ctx-lh-middletemporal	L-midTEM	0.43019205	0.01848759
LNEF	ctx-lh-parahippocampal	L-parHIP	0.30771851	0.02752576
LNEF	ctx-lh-paracentral	L-parCEN	0.20222502	0.03511604
LNEF	ctx-lh-parsopercularis	L-parOPE	0.13821857	0.0203937
LNEF	ctx-lh-parsorbitalis	L-parORB	0.45997552	0.06813927
LNEF	ctx-lh-parstriangularis	L-parTRI	0.07622113	0.10428335
LNEF	ctx-lh-pericalcarine	L-perCAR	0.28485809	0.0273292
LNEF	ctx-lh-postcentral	L-posCEN	0.48399931	0.01917721

LNEF	ctx-lh-posteriorcingulate	L-posCIN	0.55420687	0.04562344
LNEF	ctx-lh-precentral	L-preCEN	0.41920897	0.04891265
LNEF	ctx-lh-precuneus	L-preCUN	0.18996549	0.04479445
LNEF	ctx-lh-rostralanteriorcingulate	L-rosACG	0.07733936	0.04374407
LNEF	ctx-lh-rostralmiddlefrontal	L-rosMFR	0.10760079	0.04565695
LNEF	ctx-lh-superiorfrontal	L-supFRO	0.11713873	0.02790567
LNEF	ctx-lh-superiorparietal	L-supPAR	0.15851528	0.05117136
LNEF	ctx-lh-superiortemporal	L-supTEM	0.260148	0.02861393
LNEF	ctx-lh-supramarginal	L-supMAR	0.20227416	0.01948296
LNEF	ctx-lh-frontalpole	L-froPOL	0.17760096	0.03968224
LNEF	ctx-lh-temporalpole	L-temPOL	0.27636565	0.03364887
LNEF	ctx-lh-transversetemporal	L-traTEM	1.16806585	0.0300553
LNEF	ctx-lh-insula	L-insula	1.31249723	0.03704653
LNEF	ctx-rh-bankssts	R-banks	0.13841653	0.06422881
LNEF	ctx-rh-caudalanteriorcingulate	R-cauACG	5.26705751	0.02295781
LNEF	ctx-rh-caudalmiddlefrontal	R-cauMFR	0.10285205	0.04521328
LNEF	ctx-rh-cuneus	R-cune	0.78536767	0.02530346
LNEF	ctx-rh-entorhinal	R-entorh	0.11878727	0.07317349
LNEF	ctx-rh-fusiform	R-fusif	0.15460731	0.02243272
LNEF	ctx-rh-inferiorparietal	R-infPAR	0.10494441	0.02463602
LNEF	ctx-rh-inferiortemporal	R-infTEM	0.22486544	0.01733734
LNEF	ctx-rh-isthmuscingulate	R-istCIN	2.83755487	0.03519937
LNEF	ctx-rh-lateraloccipital	R-latOCC	2.16625294	0.04024875
LNEF	ctx-rh-lateralorbitofrontal	R-latORB	0.11913321	0.07917363
LNEF	ctx-rh-lingual	R-lingual	0.11631546	0.02687188
LNEF	ctx-rh-medialorbitofrontal	R-medORB	0.12739844	0.04490671
LNEF	ctx-rh-middletemporal	R-midTEM	0.12583033	0.07926122
LNEF	ctx-rh-parahippocampal	R-parHIP	0.1022401	0.05642382
LNEF	ctx-rh-paracentral	R-parCEN	0.72593183	0.02915285
LNEF	ctx-rh-parsopercularis	R-parOPE	0.23833951	0.02241006
LNEF	ctx-rh-parsorbitalis	R-parORB	0.21289438	0.05619676
LNEF	ctx-rh-parstriangularis	R-parTRI	0.30018594	0.10872929

LNEF	ctx-rh-pericalcarine	R-perCAR	0.66898388	0.06647589
LNEF	ctx-rh-postcentral	R-posCEN	0.14806922	0.05719865
LNEF	ctx-rh-posteriorcingulate	R-posCIN	1.02948256	0.06285358
LNEF	ctx-rh-precentral	R-preCEN	0.14467343	0.02042506
LNEF	ctx-rh-precuneus	R-preCUN	0.22206458	0.04662745
LNEF	ctx-rh-rostralanteriorcingulate	R-rosACG	0.23998594	0.0238111
LNEF	ctx-rh-rostralmiddlefrontal	R-rosMFR	0.24530232	0.01978748
LNEF	ctx-rh-superiorfrontal	R-supFRO	0.19240971	0.02898439
LNEF	ctx-rh-superiorparietal	R-supPAR	0.08772746	0.03210656
LNEF	ctx-rh-superiortemporal	R-supTEM	0.42679911	0.09059185
LNEF	ctx-rh-supramarginal	R-supMAR	0.37916171	0.03456918
LNEF	ctx-rh-frontalpole	R-froPOL	0.08752916	0.02084906
LNEF	ctx-rh-temporalpole	R-temPOL	0.08616067	0.02132094
LNEF	ctx-rh-transversetemporal	R-traTEM	0.79529523	0.02620074
LNEF	ctx-rh-insula	R-insula	0.98695961	0.03078779
GCC	Global		0.10537334	0.02083691
TIER_LCC	T4		0.11304725	0.01840815
TIER_LCC	T1		0.13562455	0.01959982
TIER_LCC	T2		0.09055637	0.10003995
TIER_LCC	T3		0.09098258	0.02674643
LCC	Left-Thalamus-Proper	L-thal	0.07612428	0.06707713
LCC	Left-Caudate	L-caud	0.08390641	0.03912916
LCC	Left-Putamen	L-puta	0.09174775	0.08127935
LCC	Left-Pallidum	L-pall	0.08666992	0.01985115
LCC	Brain-Stem	bSTEM	0.08148073	0.01978652
LCC	Left-Hippocampus	L-hipp	0.09656095	0.0534517
LCC	Left-Amygdala	L-amyg	0.08830678	0.03716608
LCC	Left-Accumbens-area	L-accu	0.18026791	0.01836676
LCC	Left-VentralDC	L-venDC	0.09103072	0.02197416
LCC	Right-Thalamus-Proper	R-thal	0.07597372	0.02717488
LCC	Right-Caudate	R-caud	0.26959095	0.10662872
LCC	Right-Putamen	R-puta	0.126177	0.04214453

LCC	Right-Pallidum	R-pall	0.16738595	0.02972443
LCC	Right-Hippocampus	R-hipp	0.33712385	0.03637027
LCC	Right-Amygdala	R-amyg	0.08150796	0.08810541
LCC	Right-Accumbens-area	R-accu	7.94184058	0.17175212
LCC	Right-VentralDC	R-venDC	0.21878459	0.04229412
LCC	ctx-lh-bankssts	L-banks	0.08432898	0.02896968
LCC	ctx-lh-caudalanteriorcingulate	L-cauACG	0.09211549	0.06662343
LCC	ctx-lh-caudalmiddlefrontal	L-cauMFR	0.08192273	0.02124155
LCC	ctx-lh-cuneus	L-cune	0.08474095	0.03185455
LCC	ctx-lh-entorhinal	L-entorh	0.08318074	0.03014179
LCC	ctx-lh-fusiform	L-fusif	0.09793358	0.20898445
LCC	ctx-lh-inferiorparietal	L-infPAR	0.08330766	0.05889723
LCC	ctx-lh-inferiortemporal	L-infTEM	0.08110197	0.06326355
LCC	ctx-lh-isthmuscingulate	L-istCIN	0.56097404	0.02658327
LCC	ctx-lh-lateraloccipital	L-latOCC	0.09239657	0.03992808
LCC	ctx-lh-lateralorbitofrontal	L-latORB	0.12731975	0.03709617
LCC	ctx-lh-lingual	L-lingual	23.8704701	0.01760166
LCC	ctx-lh-medialorbitofrontal	L-medORB	0.16413365	0.02368031
LCC	ctx-lh-middletemporal	L-midTEM	0.0819485	0.05839175
LCC	ctx-lh-parahippocampal	L-parHIP	0.80832376	0.26584348
LCC	ctx-lh-paracentral	L-parCEN	0.08628796	0.07155319
LCC	ctx-lh-parsopercularis	L-parOPE	0.1152226	0.01973289
LCC	ctx-lh-parsorbitalis	L-parORB	0.09434836	0.03149267
LCC	ctx-lh-parstriangularis	L-parTRI	0.10586626	0.13601887
LCC	ctx-lh-pericalcarine	L-perCAR	0.19773735	0.02660659
LCC	ctx-lh-postcentral	L-posCEN	0.0873558	0.02927382
LCC	ctx-lh-posteriorcingulate	L-posCIN	0.08943677	0.02599637
LCC	ctx-lh-precentral	L-preCEN	0.09063304	0.03771244
LCC	ctx-lh-precuneus	L-preCUN	0.09334888	0.03171153
LCC	ctx-lh-rostralanteriorcingulate	L-rosACG	0.09021436	0.0359107
LCC	ctx-lh-rostralmiddlefrontal	L-rosMFR	0.12097025	0.0300524
LCC	ctx-lh-superiorfrontal	L-supFRO	0.08864277	0.08655403

LCC	ctx-lh-superiorparietal	L-supPAR	0.09051392	0.02110573
LCC	ctx-lh-superiortemporal	L-supTEM	0.12046357	0.03712691
LCC	ctx-lh-supramarginal	L-supMAR	0.08778446	0.0309568
LCC	ctx-lh-frontalpole	L-froPOL	0.0979122	0.03054582
LCC	ctx-lh-temporalpole	L-temPOL	0.16726512	0.10302688
LCC	ctx-lh-transversetemporal	L-traTEM	0.09302018	0.02871877
LCC	ctx-lh-insula	L-insula	0.31992494	0.02672149
LCC	ctx-rh-bankssts	R-banks	0.26506076	0.03852671
LCC	ctx-rh-caudalanteriorcingulate	R-cauACG	0.34092352	0.15497107
LCC	ctx-rh-caudalmiddlefrontal	R-cauMFR	0.33782663	0.0188864
LCC	ctx-rh-cuneus	R-cune	0.10490085	0.01906464
LCC	ctx-rh-entorhinal	R-entorh	0.0998781	0.03317983
LCC	ctx-rh-fusiform	R-fusif	0.16378646	0.02204565
LCC	ctx-rh-inferiorparietal	R-infPAR	0.09440326	0.14017076
LCC	ctx-rh-inferiortemporal	R-infTEM	0.15525881	0.03503535
LCC	ctx-rh-isthmuscingulate	R-istCIN	0.08196783	0.03044492
LCC	ctx-rh-lateraloccipital	R-latOCC	0.17639361	0.07034082
LCC	ctx-rh-lateralorbitofrontal	R-latORB	0.0798884	0.06336161
LCC	ctx-rh-lingual	R-lingual	1.55499751	0.02529382
LCC	ctx-rh-medialorbitofrontal	R-medORB	0.09024026	0.03795262
LCC	ctx-rh-middletemporal	R-midTEM	0.08927574	0.02817434
LCC	ctx-rh-parahippocampal	R-parHIP	0.07905559	0.02099929
LCC	ctx-rh-paracentral	R-parCEN	0.12625182	0.02961629
LCC	ctx-rh-parsopercularis	R-parOPE	0.08854862	0.05643596
LCC	ctx-rh-parsorbitalis	R-parORB	0.13218257	0.03296867
LCC	ctx-rh-parstriangularis	R-parTRI	0.08307117	0.03694569
LCC	ctx-rh-pericalcarine	R-perCAR	0.07897337	0.04939035
LCC	ctx-rh-postcentral	R-posCEN	0.12195295	0.03075111
LCC	ctx-rh-posteriorcingulate	R-posCIN	0.14785382	0.03386091
LCC	ctx-rh-precentral	R-preCEN	0.16836323	0.15055524
LCC	ctx-rh-precuneus	R-preCUN	0.08344151	0.02541291
LCC	ctx-rh-rostralanteriorcingulate	R-rosACG	0.17358415	0.03971958

LCC	ctx-rh-rostralmiddlefrontal	R-rosMFR	0.15719158	0.0457432
LCC	ctx-rh-superiorfrontal	R-supFRO	0.11006605	0.02687783
LCC	ctx-rh-superiorparietal	R-supPAR	0.11442108	0.02684386
LCC	ctx-rh-superiortemporal	R-supTEM	0.07805659	0.02358742
LCC	ctx-rh-supramarginal	R-supMAR	0.10022813	0.01977657
LCC	ctx-rh-frontalpole	R-froPOL	0.12180699	0.02852578
LCC	ctx-rh-temporalpole	R-temPOL	0.11433383	0.07403618
LCC	ctx-rh-transversetemporal	R-traTEM	0.10836511	0.02498548
LCC	ctx-rh-insula	R-insula	0.08814204	0.04975702

References

Davis, K. A. S., Coleman, J. R. I., Adams, M., Allen, N., Breen, G., Cullen, B., … Hotopf, M. (2020). Mental health in UK Biobank - development, implementation and results from an online questionnaire completed by 157 366 participants: a reanalysis. BJPsych Open, 6(2), e18. https://doi.org/10.1192/bjo.2019.100

Keysers, C., Gazzola, V., & Wagenmakers, E. J. (2020). Using Bayes factor hypothesis testing in neuroscience to establish evidence of absence. Nature neuroscience, 23(7), 788–799. https://doi.org/10.1038/s41593-020-0660-4

Marek, S., Tervo-Clemmens, B., Calabro, F. J., Montez, D. F., Kay, B. P., Hatoum, A. S., … Dosenbach, N. U. F. (2022). Reproducible brain-wide association studies require thousands of individuals. Nature, 603(7902), 654–660. https://doi.org/10.1038/s41586-022-04492-9

Yeung, A., Feldman, G., Pedrelli, P., Hails, K., Fava, M., Reyes, T., & Mundt, J. C. (2012). The Quick Inventory of Depressive Symptomatology, clinician rated and self-report: a psychometric assessment in Chinese Americans with major depressive disorder. The Journal of nervous and mental disease, 200(8), 712–715. https://doi.org/10.1097/NMD.0b013e318261413d

Appendix 2: Supplementary materials for Chapter 3

A sex-stratified analysis on the impact of polygenic risk for Major Depressive Disorder on the structural connectome and the moderating effects of childhood trauma in the UK Biobank

Supplementary Materials

Thng *et al*.

OVERVIEW

Supplementary Text

Supplementary Figures

Supplementary Tables

1: Details on exclusion criteria

Participants were excluded if they had (1) neurological or other mental health conditions, and (2) if they were related and non-European.

Presence of neurological and other psychiatric conditions

For neurological conditions, we searched through the official records and self-reported data for all neurological conditions in UKB. Subjects who were excluded had at least one of the following neurological conditions: stroke, TIA, epilepsy, meningitis, multiple sclerosis, Parkinson's, brain injury, CNS tumours, dementia, subarachnoid haemorrhage, other degenerative CNS unclassified, intracerebral haemorrhage, other demyelination CNS disease, Guillain Barre, encephalitis, motor neurone, neurological injury, brain haemorrhage, intracranial abscess, spina bifida, neoplasm brain, cerebral cysts, cerebral oedema, cerebral aneurysm, other degenerative basal ganglia, encephalopathy, other congenital brain malformations, cerebral palsy, spinal cord other congenital, brain compression, hydrocephalus, anoxic brain damage, other degenerative CNS classified, progressive supranuclear palsy, other demyelinating acute disseminated, Huntington's, neurosyphilis, anencephaly, encephalocele, microencephaly, congenital hydrocephalus, TB nervous system, cerebral cryptococcosis, amoebic brain abscess, neuronal ceroid lipofuscinosis, reduction deformities of brain, senile degeneration of brain unclassified, systemic atrophy in CNS. For psychiatric conditions, we excluded subjects that had any official diagnosis for the following conditions: bipolar disorder, multiple personality disorder, schizophrenia, autism, or intellectual disability.

Relatedness

We had to restrict our sample to unrelated and European-only sample, as MDD-PRS generated using summary statistics based on European-only subjects will have low generalisability to other ethnicities. Full details can be found in Howard et al (2018). Briefly, related individuals were initially excluded based on a shared relatedness of up to the 3rd degree using kinship coefficients (>0.044) calculated using the KING toolset (Manichaikul et al., 2010). One member of each group of related individuals was then subsequently added back in, by creating a genomic relationship matrix and selecting individuals with a genetic relatedness of <0.025 with any other participant.

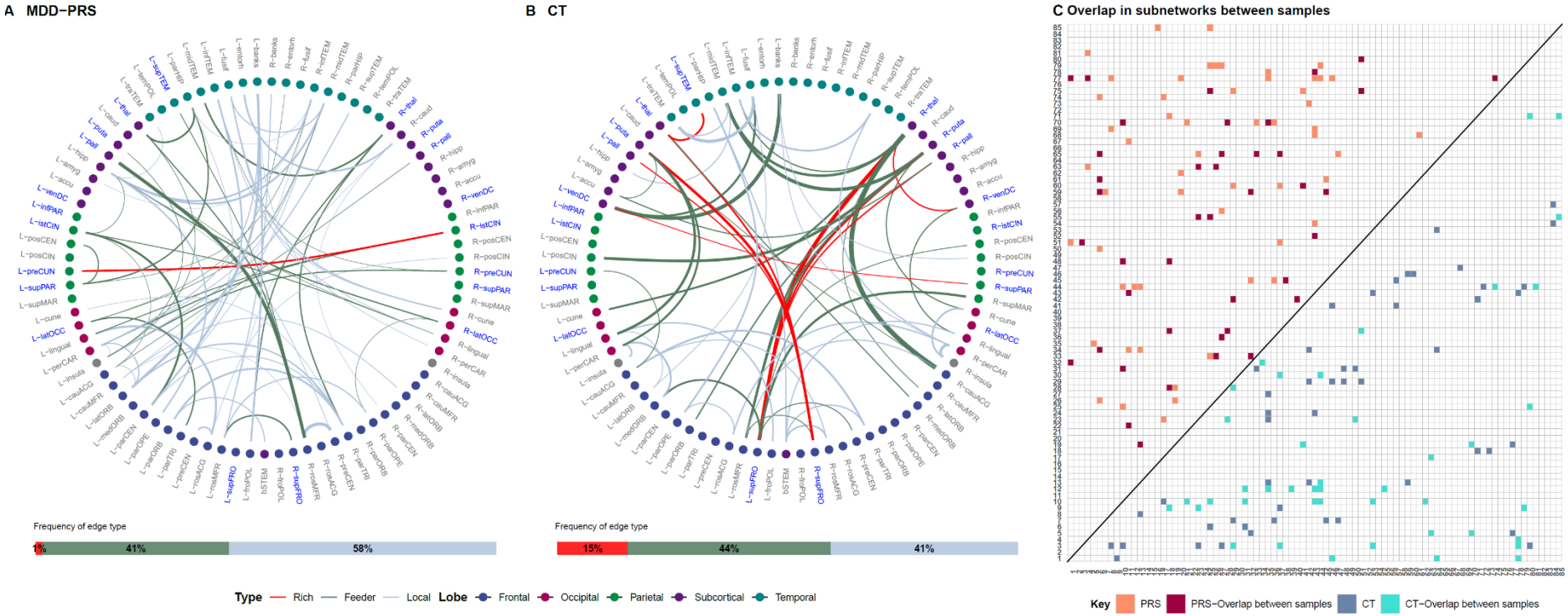

D

	PRS-associated subnetwork			CT-associated subnetwork		
	# Rich connections	# Feeder connections	# Local connections	# Rich connections	# Feeder connections	# Local connections
Females (main, N=8,069)	9	28	34	14	36	27
Females (matched, N=6,812)	1	28	40	9	26	24
Overlap	1	18	23	8	22	13

Figure S1. (A, B) PRS- and CT-associated subnetwork for the matched female sample. (C) Comparison of overlapping edges between main and matched female sample for the PRS- and CT-associated subnetworks. The upper triangle represent PRS-associated subnetworks and the lower triangle represent CT-associated subnetworks. Regions highlighted in orange/blue represent all edges in the subnetworks being compared, regions in red/turquoise represent the overlapping edges. The Jaccard Indexes for the PRS- and CT-associated subnetworks was 0.428 and 0.462, respectively. (D) Details on the number of overlapping edges between the main and matched female sample for each type of edge.

Figure S2. Results for the mediation and moderated mediation analyses for the matched female sample.

Mediation (PRS)

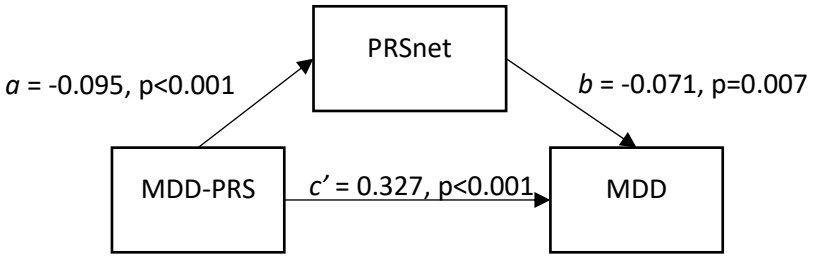

ab = 0.007, 95% CI [0.002, 0.012]

Mediation (CT)

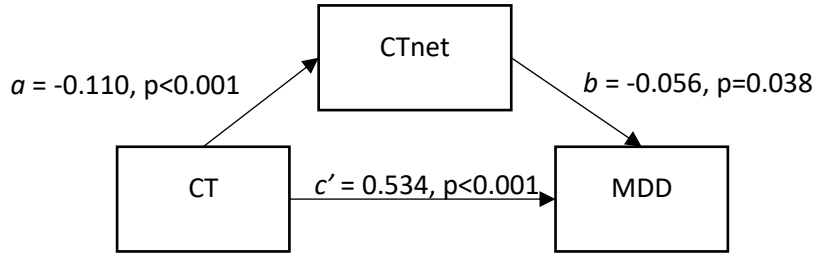

ab = 0.006, 95% CI [0.0002, 0.013]

Moderated mediation

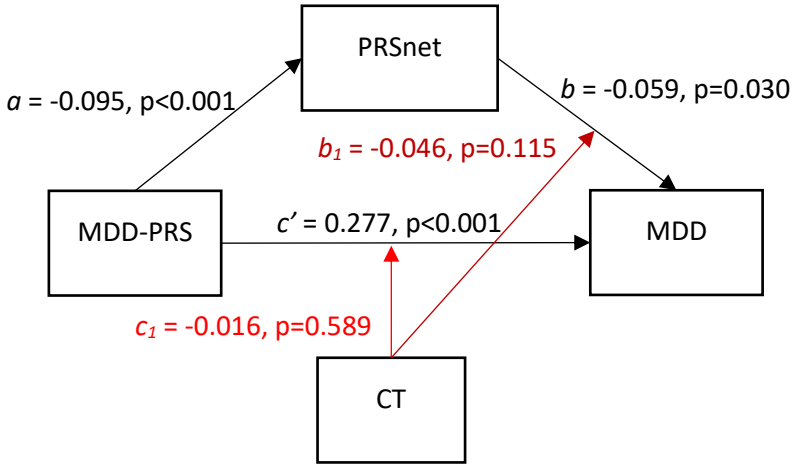

Index of moderated mediation: 0.004, 95% CI [-0.001, 0.010]

Table S1. List of all nodes and their abbreviations used in UKB.

Region	Abbreviation	Node position
Left-Thalamus-Proper	L-thal	1
Left-Caudate	L-caud	2
Left-Putamen	L-puta	3
Left-Pallidum	L-pall	4
Brain-Stem	bSTEM	5
Left-Hippocampus	L-hipp	6
Left-Amygdala	L-amyg	7
Left-Accumbens-area	L-accu	8
Left-VentralDC	L-venDC	9
Right-Thalamus-Proper	R-thal	10
Right-Caudate	R-caud	11
Right-Putamen	R-puta	12
Right-Pallidum	R-pall	13
Right-Hippocampus	R-hipp	14
Right-Amygdala	R-amyg	15
Right-Accumbens-area	R-accu	16
Right-VentralDC	R-venDC	17
ctx-lh-bankssts	L-banks	18
ctx-lh-caudalanteriorcingulate	L-cauACG	19
ctx-lh-caudalmiddlefrontal	L-cauMFR	20
ctx-lh-cuneus	L-cune	21
ctx-lh-entorhinal	L-entorh	22
ctx-lh-fusiform	L-fusif	23
ctx-lh-inferiorparietal	L-infPAR	24
ctx-lh-inferiortemporal	L-infTEM	25
ctx-lh-isthmuscingulate	L-istCIN	26
ctx-lh-lateraloccipital	L-latOCC	27

ctx-lh-lateralorbitofrontal	L-latORB	28
ctx-lh-lingual	L-lingual	29
ctx-lh-medialorbitofrontal	L-medORB	30
ctx-lh-middletemporal	L-midTEM	31
ctx-lh-parahippocampal	L-parHIP	32
ctx-lh-paracentral	L-parCEN	33
ctx-lh-parsopercularis	L-parOPE	34
ctx-lh-parsorbitalis	L-parORB	35
ctx-lh-parstriangularis	L-parTRI	36
ctx-lh-pericalcarine	L-perCAR	37
ctx-lh-postcentral	L-posCEN	38
ctx-lh-posteriorcingulate	L-posCIN	39
ctx-lh-precentral	L-preCEN	40
ctx-lh-precuneus	L-preCUN	41
ctx-lh-rostralanteriorcingulate	L-rosACG	42
ctx-lh-rostralmiddlefrontal	L-rosMFR	43
ctx-lh-superiorfrontal	L-supFRO	44
ctx-lh-superiorparietal	L-supPAR	45
ctx-lh-superiortemporal	L-supTEM	46
ctx-lh-supramarginal	L-supMAR	47
ctx-lh-frontalpole	L-froPOL	48
ctx-lh-temporalpole	L-temPOL	49
ctx-lh-transversetemporal	L-traTEM	50
ctx-lh-insula	L-insula	51
ctx-rh-bankssts	R-banks	52
ctx-rh-caudalanteriorcingulate	R-cauACG	53
ctx-rh-caudalmiddlefrontal	R-cauMFR	54
ctx-rh-cuneus	R-cune	55
ctx-rh-entorhinal	R-entorh	56
ctx-rh-fusiform	R-fusif	57

ctx-rh-inferiorparietal	R-infPAR	58
ctx-rh-inferiortemporal	R-infTEM	59
ctx-rh-isthmuscingulate	R-istCIN	60
ctx-rh-lateraloccipital	R-latOCC	61
ctx-rh-lateralorbitofrontal	R-latORB	62
ctx-rh-lingual	R-lingual	63
ctx-rh-medialorbitofrontal	R-medORB	64
ctx-rh-middletemporal	R-midTEM	65
ctx-rh-parahippocampal	R-parHIP	66
ctx-rh-paracentral	R-parCEN	67
ctx-rh-parsopercularis	R-parOPE	68
ctx-rh-parsorbitalis	R-parORB	69
ctx-rh-parstriangularis	R-parTRI	70
ctx-rh-pericalcarine	R-perCAR	71
ctx-rh-postcentral	R-posCEN	72
ctx-rh-posteriorcingulate	R-posCIN	73
ctx-rh-precentral	R-preCEN	74
ctx-rh-precuneus	R-preCUN	75
ctx-rh-rostralanteriorcingulate	R-rosACG	76
ctx-rh-rostralmiddlefrontal	R-rosMFR	77
ctx-rh-superiorfrontal	R-supFRO	78
ctx-rh-superiorparietal	R-supPAR	79
ctx-rh-superiortemporal	R-supTEM	80
ctx-rh-supramarginal	R-supMAR	81
ctx-rh-frontalpole	R-froPOL	82
ctx-rh-temporalpole	R-temPOL	83
ctx-rh-transversetemporal	R-traTEM	84
ctx-rh-insula	R-insula	85

Table S2. List of all connections in the PRS-associated subnetwork for females. Note: "t-stat" represents the t-statistic derived in the first step of the NBS analysis and "frequency" represents the number of times the type of "Region1-Region2" connection appears in the network. The table is ordered according to the "frequency" column in a descending manner.

Node1	Node2	Region1	Region2	Region1Region2	tstat	frequency
Right-Pallidum	ctx-lh-caudalanteriorcingulate	subcortical	frontal	frontal_subcortical	2.6106513	15
Left-Hippocampus	ctx-lh-parsopercularis	subcortical	frontal	frontal_subcortical	2.39442273	15
Right-Caudate	ctx-lh-parsopercularis	subcortical	frontal	frontal_subcortical	2.57032932	15
Right-Pallidum	ctx-lh-parsopercularis	subcortical	frontal	frontal_subcortical	2.66800245	15
Right-Caudate	ctx-lh-rostralmiddlefrontal	subcortical	frontal	frontal_subcortical	2.71246841	15
Right-Thalamus-Proper	ctx-lh-superiorfrontal	subcortical	frontal	frontal_subcortical	2.54093398	15
Right-Putamen	ctx-lh-superiorfrontal	subcortical	frontal	frontal_subcortical	2.45187314	15
Right-Pallidum	ctx-lh-superiorfrontal	subcortical	frontal	frontal_subcortical	2.63170622	15
Right-Thalamus-Proper	ctx-lh-frontalpole	subcortical	frontal	frontal_subcortical	2.39429931	15
Left-Accumbens-area	ctx-rh-parsorbitalis	subcortical	frontal	frontal_subcortical	2.36137306	15
Right-Thalamus-Proper	ctx-rh-parstriangularis	subcortical	frontal	frontal_subcortical	3.18688952	15
Right-VentralDC	ctx-rh-precentral	subcortical	frontal	frontal_subcortical	2.44639666	15
Left-Thalamus-Proper	ctx-rh-rostralmiddlefrontal	subcortical	frontal	frontal_subcortical	2.64847909	15
Left-Pallidum	ctx-rh-rostralmiddlefrontal	subcortical	frontal	frontal_subcortical	4.08128858	15
Left-Accumbens-area	ctx-rh-rostralmiddlefrontal	subcortical	frontal	frontal_subcortical	2.32021494	15
ctx-lh-precentral	ctx-lh-rostralanteriorcingulate	frontal	frontal	frontal_frontal	2.82275831	12
ctx-lh-rostralmiddlefrontal	ctx-rh-caudalmiddlefrontal	frontal	frontal	frontal_frontal	2.58085256	12
ctx-lh-rostralmiddlefrontal	ctx-rh-parsorbitalis	frontal	frontal	frontal_frontal	3.16616455	12
ctx-lh-lateralorbitofrontal	ctx-rh-parstriangularis	frontal	frontal	frontal_frontal	3.1672745	12
ctx-lh-parsorbitalis	ctx-rh-parstriangularis	frontal	frontal	frontal_frontal	3.33329198	12
ctx-lh-parstriangularis	ctx-rh-parstriangularis	frontal	frontal	frontal_frontal	2.61089753	12
ctx-lh-parsorbitalis	ctx-rh-rostralmiddlefrontal	frontal	frontal	frontal_frontal	2.71716892	12
ctx-lh-rostralmiddlefrontal	ctx-rh-rostralmiddlefrontal	frontal	frontal	frontal_frontal	2.53248361	12
ctx-lh-superiorfrontal	ctx-rh-rostralmiddlefrontal	frontal	frontal	frontal_frontal	3.35604724	12
ctx-rh-precentral	ctx-rh-rostralmiddlefrontal	frontal	frontal	frontal_frontal	3.5874837	12

ctx-lh-parsorbitalis	ctx-rh-superiorfrontal	frontal	frontal	frontal_frontal	2.55403389	12
ctx-lh-rostralmiddlefrontal	ctx-rh-superiorfrontal	frontal	frontal	frontal_frontal	3.82404747	12
Right-Caudate	ctx-lh-entorhinal	subcortical	temporal	subcortical_temporal	2.54020568	7
Right-VentralDC	ctx-lh-fusiform	subcortical	temporal	subcortical_temporal	2.58280287	7
Right-Thalamus-Proper	ctx-lh-inferiortemporal	subcortical	temporal	subcortical_temporal	2.45610754	7
Right-Thalamus-Proper	ctx-lh-middletemporal	subcortical	temporal	subcortical_temporal	2.86301349	7
Left-Thalamus-Proper	ctx-lh-parahippocampal	subcortical	temporal	subcortical_temporal	2.87230359	7
Left-Hippocampus	ctx-rh-inferiortemporal	subcortical	temporal	subcortical_temporal	2.379022	7
Left-Hippocampus	ctx-rh-middletemporal	subcortical	temporal	subcortical_temporal	2.77280173	7
ctx-lh-bankssts	ctx-lh-pericalcarine	temporal	occipital	occipital_temporal	2.69031417	6
ctx-lh-fusiform	ctx-rh-cuneus	temporal	occipital	occipital_temporal	2.63942071	6
ctx-lh-inferiortemporal	ctx-rh-cuneus	temporal	occipital	occipital_temporal	2.70730587	6
ctx-lh-fusiform	ctx-rh-lingual	temporal	occipital	occipital_temporal	2.35361174	6
ctx-lh-lateraloccipital	ctx-rh-middletemporal	occipital	temporal	occipital_temporal	2.78511214	6
ctx-lh-pericalcarine	ctx-rh-middletemporal	occipital	temporal	occipital_temporal	2.54948544	6
ctx-lh-bankssts	ctx-lh-lateralorbitofrontal	temporal	frontal	frontal_temporal	2.84808857	5
ctx-lh-parahippocampal	ctx-lh-paracentral	temporal	frontal	frontal_temporal	2.61718975	5
ctx-lh-bankssts	ctx-lh-frontalpole	temporal	frontal	frontal_temporal	2.65518592	5
ctx-lh-rostralmiddlefrontal	ctx-rh-bankssts	frontal	temporal	frontal_temporal	2.46987431	5
ctx-lh-paracentral	ctx-rh-middletemporal	frontal	temporal	frontal_temporal	2.91500361	5
ctx-lh-superiorparietal	ctx-rh-inferiortemporal	parietal	temporal	parietal_temporal	2.6982894	4
ctx-lh-supramarginal	ctx-rh-middletemporal	parietal	temporal	parietal_temporal	2.59666856	4
ctx-lh-inferiortemporal	ctx-rh-precuneus	temporal	parietal	parietal_temporal	2.88876153	4
ctx-lh-inferiortemporal	ctx-rh-superiorparietal	temporal	parietal	parietal_temporal	2.5328817	4
ctx-lh-postcentral	ctx-lh-superiorparietal	parietal	parietal	parietal_parietal	2.55223902	4
ctx-lh-precuneus	ctx-rh-isthmuscingulate	parietal	parietal	parietal_parietal	2.74126737	4
ctx-lh-precuneus	ctx-rh-precuneus	parietal	parietal	parietal_parietal	2.64373483	4
ctx-lh-isthmuscingulate	ctx-rh-superiorparietal	parietal	parietal	parietal_parietal	2.32415675	4
ctx-lh-superiorparietal	ctx-rh-lateraloccipital	parietal	occipital	occipital_parietal	2.46111301	4
ctx-lh-isthmuscingulate	ctx-rh-lingual	parietal	occipital	occipital_parietal	2.33393341	4

ctx-lh-lingual	ctx-rh-precuneus	occipital	parietal	occipital_parietal	2.41065671	4
ctx-lh-lateraloccipital	ctx-rh-superiorparietal	occipital	parietal	occipital_parietal	2.46695677	4
ctx-lh-isthmuscingulate	ctx-lh-paracentral	parietal	frontal	frontal_parietal	2.91378639	3
ctx-lh-parstriangularis	ctx-lh-superiorparietal	frontal	parietal	frontal_parietal	2.35759207	3
ctx-lh-superiorfrontal	ctx-rh-superiorparietal	frontal	parietal	frontal_parietal	2.79524391	3
ctx-lh-lateraloccipital	ctx-lh-parstriangularis	occipital	frontal	frontal_occipital	2.81801929	3
ctx-lh-lateralorbitofrontal	ctx-lh-pericalcarine	frontal	occipital	frontal_occipital	2.46226532	3
ctx-lh-lingual	ctx-lh-rostralanteriorcingulate	occipital	frontal	frontal_occipital	3.22165107	3
ctx-lh-insula	ctx-rh-superiortemporal	insula	temporal	insula_temporal	2.83896664	2
ctx-lh-inferiortemporal	ctx-rh-insula	temporal	insula	insula_temporal	2.97232307	2
Left-Putamen	ctx-lh-insula	subcortical	insula	insula_subcortical	2.36847531	2
Right-Accumbens-area	ctx-rh-insula	subcortical	insula	insula_subcortical	2.51789602	2
ctx-lh-parahippocampal	ctx-rh-inferiortemporal	temporal	temporal	temporal_temporal	2.91131823	1
Left-Pallidum	ctx-rh-supramarginal	subcortical	parietal	parietal_subcortical	2.4953346	1
Left-Hippocampus	ctx-rh-lateraloccipital	subcortical	occipital	occipital_subcortical	2.89822388	1
ctx-lh-insula	ctx-rh-precuneus	insula	parietal	insula_parietal	2.36507593	1

Table S3. List of all connections in the PRS-associated subnetwork for males. Note: "t-stat" represents the t-statistic derived in the first step of the NBS analysis and "frequency" represents the number of times the type of "Region1-Region2" connection appears in the network. The table is ordered according to the "frequency" column in a descending manner.

Node1	Node2	Region1	Region2	Region1Region2	tstat	frequency
ctx-lh-postcentral	ctx-rh-caudalmiddlefrontal	parietal	frontal	frontal_parietal	2.51004267	13
ctx-lh-rostralmiddlefrontal	ctx-rh-isthmuscingulate	frontal	parietal	frontal_parietal	2.42529679	13
ctx-lh-postcentral	ctx-rh-parsopercularis	parietal	frontal	frontal_parietal	2.68351873	13
ctx-lh-postcentral	ctx-rh-parstriangularis	parietal	frontal	frontal_parietal	2.69599187	13
ctx-lh-supramarginal	ctx-rh-parstriangularis	parietal	frontal	frontal_parietal	2.73276811	13
ctx-lh-superiorfrontal	ctx-rh-postcentral	frontal	parietal	frontal_parietal	2.93242802	13
ctx-lh-supramarginal	ctx-rh-precentral	parietal	frontal	frontal_parietal	3.41791243	13
ctx-lh-lateralorbitofrontal	ctx-rh-precuneus	frontal	parietal	frontal_parietal	2.36596465	13
ctx-lh-postcentral	ctx-rh-rostralmiddlefrontal	parietal	frontal	frontal_parietal	3.04157896	13
ctx-lh-precuneus	ctx-rh-rostralmiddlefrontal	parietal	frontal	frontal_parietal	2.43338677	13
ctx-lh-paracentral	ctx-rh-superiorparietal	frontal	parietal	frontal_parietal	2.5889736	13
ctx-lh-paracentral	ctx-rh-supramarginal	frontal	parietal	frontal_parietal	2.42712466	13
ctx-rh-isthmuscingulate	ctx-rh-frontalpole	parietal	frontal	frontal_parietal	2.4059433	13
ctx-lh-caudalmiddlefrontal	ctx-rh-caudalanteriorcingulate	frontal	frontal	frontal_frontal	2.495369	12
ctx-lh-rostralmiddlefrontal	ctx-rh-caudalanteriorcingulate	frontal	frontal	frontal_frontal	2.71791155	12
ctx-lh-superiorfrontal	ctx-rh-paracentral	frontal	frontal	frontal_frontal	3.09222806	12
ctx-lh-parsopercularis	ctx-rh-parsopercularis	frontal	frontal	frontal_frontal	2.7853682	12
ctx-lh-lateralorbitofrontal	ctx-rh-parsorbitalis	frontal	frontal	frontal_frontal	2.67358956	12
ctx-lh-frontalpole	ctx-rh-parsorbitalis	frontal	frontal	frontal_frontal	2.63068627	12
ctx-lh-parstriangularis	ctx-rh-parstriangularis	frontal	frontal	frontal_frontal	2.33571208	12
ctx-lh-superiorfrontal	ctx-rh-parstriangularis	frontal	frontal	frontal_frontal	2.377432	12
ctx-lh-parstriangularis	ctx-rh-superiorfrontal	frontal	frontal	frontal_frontal	2.7718725	12
ctx-lh-rostralmiddlefrontal	ctx-rh-superiorfrontal	frontal	frontal	frontal_frontal	2.52818613	12
ctx-lh-superiorfrontal	ctx-rh-superiorfrontal	frontal	frontal	frontal_frontal	2.61570431	12
ctx-rh-rostralanteriorcingulate	ctx-rh-frontalpole	frontal	frontal	frontal_frontal	2.60557407	12

Right-Caudate	ctx-lh-caudalanteriorcingulate	subcortical	frontal	frontal_subcortical	2.91352295	6
Right-Putamen	ctx-lh-rostralmiddlefrontal	subcortical	frontal	frontal_subcortical	2.39588044	6
Left-Thalamus-Proper	ctx-rh-parsopercularis	subcortical	frontal	frontal_subcortical	2.68239929	6
Left-Putamen	ctx-rh-parsopercularis	subcortical	frontal	frontal_subcortical	2.73737352	6
Left-Caudate	ctx-rh-rostralmiddlefrontal	subcortical	frontal	frontal_subcortical	2.49070637	6
Left-Accumbens-area	ctx-rh-rostralmiddlefrontal	subcortical	frontal	frontal_subcortical	2.55816186	6
ctx-lh-bankssts	ctx-lh-paracentral	temporal	frontal	frontal_temporal	2.47010315	4
ctx-lh-caudalanteriorcingulate	ctx-rh-bankssts	frontal	temporal	frontal_temporal	2.35504282	4
ctx-lh-superiortemporal	ctx-rh-caudalmiddlefrontal	temporal	frontal	frontal_temporal	2.37785651	4
ctx-lh-parahippocampal	ctx-rh-paracentral	temporal	frontal	frontal_temporal	2.34405102	4
ctx-lh-bankssts	ctx-rh-superiorparietal	temporal	parietal	parietal_temporal	2.85410418	3
ctx-lh-bankssts	ctx-rh-supramarginal	temporal	parietal	parietal_temporal	2.65426848	3
ctx-lh-postcentral	ctx-rh-transversetemporal	parietal	temporal	parietal_temporal	3.04911588	3
ctx-lh-supramarginal	ctx-rh-inferiorparietal	parietal	parietal	parietal_parietal	2.37801538	3
ctx-lh-supramarginal	ctx-rh-postcentral	parietal	parietal	parietal_parietal	2.72241864	3
ctx-rh-precuneus	ctx-rh-supramarginal	parietal	parietal	parietal_parietal	3.01729025	3
ctx-lh-inferiortemporal	ctx-rh-cuneus	temporal	occipital	occipital_temporal	2.66146233	2
ctx-rh-bankssts	ctx-rh-cuneus	temporal	occipital	occipital_temporal	2.7812501	2
ctx-rh-pericalcarine	ctx-rh-precuneus	occipital	parietal	occipital_parietal	2.41670195	2
ctx-rh-cuneus	ctx-rh-supramarginal	occipital	parietal	occipital_parietal	4.10015019	2
ctx-lh-insula	ctx-rh-parsopercularis	insula	frontal	frontal_insula	2.35485209	2
ctx-lh-rostralmiddlefrontal	ctx-rh-insula	frontal	insula	frontal_insula	2.81210891	2
ctx-lh-bankssts	ctx-lh-parahippocampal	temporal	temporal	temporal_temporal	2.64476183	1
Left-Accumbens-area	ctx-rh-inferiorparietal	subcortical	parietal	parietal_subcortical	2.35385597	1
ctx-lh-insula	ctx-rh-supramarginal	insula	parietal	insula_parietal	3.37309478	1

Table S4. List of all connections in the CT-associated subnetwork for females. Note: "t-stat" represents the t-statistic derived in the first step of the NBS analysis and "frequency" represents the number of times the type of "Region1-Region2" connection appears in the network. The table is ordered according to the "frequency" column in a descending manner.

Node1	Node2	Region1	Region2	Region1Region2	tstat	frequency
Right-Putamen	ctx-lh-parsorbitalis	subcortical	frontal	frontal_subcortical	2.81553469	17
Right-Pallidum	ctx-lh-parsorbitalis	subcortical	frontal	frontal_subcortical	2.92965494	17
Left-Amygdala	ctx-lh-parstriangularis	subcortical	frontal	frontal_subcortical	2.43075882	17
Right-Pallidum	ctx-lh-rostralanteriorcingulate	subcortical	frontal	frontal_subcortical	2.49441504	17
Right-Thalamus-Proper	ctx-lh-rostralmiddlefrontal	subcortical	frontal	frontal_subcortical	2.52931979	17
Right-Putamen	ctx-lh-rostralmiddlefrontal	subcortical	frontal	frontal_subcortical	2.99595406	17
Right-Thalamus-Proper	ctx-lh-superiorfrontal	subcortical	frontal	frontal_subcortical	4.05371772	17
Right-Putamen	ctx-lh-superiorfrontal	subcortical	frontal	frontal_subcortical	3.37935308	17
Right-Pallidum	ctx-lh-superiorfrontal	subcortical	frontal	frontal_subcortical	2.76317762	17
Left-Putamen	ctx-rh-caudalanteriorcingulate	subcortical	frontal	frontal_subcortical	2.4214649	17
Right-Thalamus-Proper	ctx-rh-caudalanteriorcingulate	subcortical	frontal	frontal_subcortical	3.3323793	17
Right-Thalamus-Proper	ctx-rh-lateralorbitofrontal	subcortical	frontal	frontal_subcortical	2.38405542	17
Left-Thalamus-Proper	ctx-rh-medialorbitofrontal	subcortical	frontal	frontal_subcortical	2.48479315	17
Brain-Stem	ctx-rh-parstriangularis	subcortical	frontal	frontal_subcortical	2.36518027	17
Left-Thalamus-Proper	ctx-rh-superiorfrontal	subcortical	frontal	frontal_subcortical	3.11450359	17
Left-Putamen	ctx-rh-superiorfrontal	subcortical	frontal	frontal_subcortical	3.14774128	17
Left-Pallidum	ctx-rh-superiorfrontal	subcortical	frontal	frontal_subcortical	3.57708071	17
Left-VentralDC	ctx-lh-bankssts	subcortical	temporal	subcortical_temporal	3.66066417	10
Left-Putamen	ctx-lh-fusiform	subcortical	temporal	subcortical_temporal	2.487933	10
Left-VentralDC	ctx-lh-fusiform	subcortical	temporal	subcortical_temporal	3.31273845	10
Left-Hippocampus	ctx-lh-inferiortemporal	subcortical	temporal	subcortical_temporal	2.36448321	10
Right-Thalamus-Proper	ctx-lh-inferiortemporal	subcortical	temporal	subcortical_temporal	2.39306499	10
Right-Thalamus-Proper	ctx-lh-middletemporal	subcortical	temporal	subcortical_temporal	3.01166001	10
Right-Putamen	ctx-lh-middletemporal	subcortical	temporal	subcortical_temporal	3.18452338	10
Left-Thalamus-Proper	ctx-lh-superiortemporal	subcortical	temporal	subcortical_temporal	3.20939293	10

Right-Pallidum	ctx-rh-inferiortemporal	subcortical	temporal	subcortical_temporal	2.41861399	10
Left-Putamen	ctx-rh-superiortemporal	subcortical	temporal	subcortical_temporal	2.39916491	10
Right-Thalamus-Proper	ctx-lh-cuneus	subcortical	occipital	occipital_subcortical	2.49547212	9
Left-Putamen	ctx-lh-lateraloccipital	subcortical	occipital	occipital_subcortical	2.3447007	9
Left-Putamen	ctx-lh-lingual	subcortical	occipital	occipital_subcortical	3.38027985	9
Left-Amygdala	ctx-lh-lingual	subcortical	occipital	occipital_subcortical	2.43778837	9
Left-Putamen	ctx-lh-pericalcarine	subcortical	occipital	occipital_subcortical	3.3327696	9
Left-VentralDC	ctx-lh-pericalcarine	subcortical	occipital	occipital_subcortical	2.4374812	9
Right-Putamen	ctx-rh-cuneus	subcortical	occipital	occipital_subcortical	3.15546799	9
Brain-Stem	ctx-rh-lingual	subcortical	occipital	occipital_subcortical	2.43482128	9
Right-VentralDC	ctx-rh-lingual	subcortical	occipital	occipital_subcortical	2.49128136	9
ctx-lh-fusiform	ctx-lh-lateralorbitofrontal	temporal	frontal	frontal_temporal	2.73619425	6
ctx-lh-middletemporal	ctx-lh-paracentral	temporal	frontal	frontal_temporal	2.62275926	6
ctx-lh-parahippocampal	ctx-lh-parsopercularis	temporal	frontal	frontal_temporal	2.7924129	6
ctx-lh-fusiform	ctx-lh-parsorbitalis	temporal	frontal	frontal_temporal	2.67544578	6
ctx-lh-middletemporal	ctx-lh-frontalpole	temporal	frontal	frontal_temporal	2.38131108	6
ctx-rh-caudalmiddlefrontal	ctx-rh-transversetemporal	frontal	temporal	frontal_temporal	2.72034033	6
ctx-lh-inferiorparietal	ctx-lh-parsorbitalis	parietal	frontal	frontal_parietal	2.45219897	6
ctx-lh-caudalanteriorcingulate	ctx-lh-precuneus	frontal	parietal	frontal_parietal	2.82862094	6
ctx-lh-inferiorparietal	ctx-lh-rostralmiddlefrontal	parietal	frontal	frontal_parietal	2.40413939	6
ctx-lh-supramarginal	ctx-rh-parsopercularis	parietal	frontal	frontal_parietal	2.65371516	6
ctx-lh-superiorfrontal	ctx-rh-superiorparietal	frontal	parietal	frontal_parietal	2.4452293	6
ctx-lh-superiorfrontal	ctx-rh-supramarginal	frontal	parietal	frontal_parietal	3.0883178	6
ctx-lh-medialorbitofrontal	ctx-lh-superiorfrontal	frontal	frontal	frontal_frontal	2.52762888	5
ctx-lh-parsopercularis	ctx-rh-medialorbitofrontal	frontal	frontal	frontal_frontal	2.55076357	5
ctx-rh-caudalanteriorcingulate	ctx-rh-medialorbitofrontal	frontal	frontal	frontal_frontal	2.38776586	5
ctx-lh-caudalanteriorcingulate	ctx-rh-parstriangularis	frontal	frontal	frontal_frontal	2.80141748	5
ctx-lh-superiorfrontal	ctx-rh-precentral	frontal	frontal	frontal_frontal	2.60252698	5
ctx-lh-fusiform	ctx-lh-transversetemporal	temporal	temporal	temporal_temporal	3.41149674	4
ctx-lh-superiortemporal	ctx-rh-inferiortemporal	temporal	temporal	temporal_temporal	2.40918479	4

ctx-lh-inferiortemporal	ctx-rh-superiortemporal	temporal	temporal	temporal_temporal	3.21803497	4
ctx-rh-fusiform	ctx-rh-transversetemporal	temporal	temporal	temporal_temporal	2.43494576	4
ctx-lh-precuneus	ctx-lh-superiortemporal	parietal	temporal	parietal_temporal	2.40131465	4
ctx-lh-precuneus	ctx-rh-fusiform	parietal	temporal	parietal_temporal	2.99020272	4
ctx-lh-superiorparietal	ctx-rh-fusiform	parietal	temporal	parietal_temporal	2.85644991	4
ctx-lh-superiortemporal	ctx-rh-isthmuscingulate	temporal	parietal	parietal_temporal	2.38929313	4
Right-Putamen	ctx-lh-posteriorcingulate	subcortical	parietal	parietal_subcortical	2.84386452	4
Left-Amygdala	ctx-lh-superiorparietal	subcortical	parietal	parietal_subcortical	3.18236032	4
Left-Amygdala	ctx-lh-supramarginal	subcortical	parietal	parietal_subcortical	2.8190479	4
Left-VentralDC	ctx-rh-superiorparietal	subcortical	parietal	parietal_subcortical	2.46741867	4
ctx-lh-lingual	ctx-lh-insula	occipital	insula	insula_occipital	2.66583356	4
ctx-lh-pericalcarine	ctx-lh-insula	occipital	insula	insula_occipital	3.23828555	4
ctx-rh-cuneus	ctx-rh-insula	occipital	insula	insula_occipital	2.78376746	4
ctx-rh-pericalcarine	ctx-rh-insula	occipital	insula	insula_occipital	2.87209382	4
ctx-lh-lateralorbitofrontal	ctx-lh-lingual	frontal	occipital	frontal_occipital	2.83191733	4
ctx-lh-lateraloccipital	ctx-lh-parsorbitalis	occipital	frontal	frontal_occipital	2.46407641	4
ctx-lh-medialorbitofrontal	ctx-lh-pericalcarine	frontal	occipital	frontal_occipital	2.48841902	4
ctx-lh-lingual	ctx-lh-rostralanteriorcingulate	occipital	frontal	frontal_occipital	2.41585387	4
Left-Thalamus-Proper	Left-VentralDC	subcortical	subcortical	subcortical_subcortical	2.59433164	2
Left-Putamen	Right-Thalamus-Proper	subcortical	subcortical	subcortical_subcortical	2.37487374	2
ctx-lh-lingual	ctx-lh-superiortemporal	occipital	temporal	occipital_temporal	2.38868472	2
ctx-rh-pericalcarine	ctx-rh-superiortemporal	occipital	temporal	occipital_temporal	2.3966643	2

Table S5. List of all connections in the CT-associated subnetwork for males. Note: “t-stat” represents the t-statistic derived in the first step of the NBS analysis and “frequency” represents the number of times the type of “Region1-Region2” connection appears in the network. The table is ordered according to the “frequency” column in a descending manner.

Node1	Node2	Region1	Region2	Region1Region2	tstat	frequency
Left-Amygdala	ctx-lh-inferiorparietal	subcortical	parietal	parietal_subcortical	2.44943158	7
Right-Thalamus-Proper	ctx-lh-inferiorparietal	subcortical	parietal	parietal_subcortical	3.5673433	7
Right-Thalamus-Proper	ctx-lh-postcentral	subcortical	parietal	parietal_subcortical	4.09461823	7
Left-VentralDC	ctx-lh-supramarginal	subcortical	parietal	parietal_subcortical	2.79528074	7
Left-Pallidum	ctx-rh-inferiorparietal	subcortical	parietal	parietal_subcortical	2.39651196	7
Left-Pallidum	ctx-rh-isthmuscingulate	subcortical	parietal	parietal_subcortical	2.62718734	7
Left-VentralDC	ctx-rh-precuneus	subcortical	parietal	parietal_subcortical	2.54285732	7
ctx-lh-lateraloccipital	ctx-lh-transversetemporal	occipital	temporal	occipital_temporal	2.53437373	6
ctx-lh-inferiortemporal	ctx-rh-cuneus	temporal	occipital	occipital_temporal	2.7225458	6
ctx-lh-bankssts	ctx-rh-lateraloccipital	temporal	occipital	occipital_temporal	2.74156428	6
ctx-lh-inferiortemporal	ctx-rh-lateraloccipital	temporal	occipital	occipital_temporal	2.48568266	6
ctx-lh-parahippocampal	ctx-rh-lateraloccipital	temporal	occipital	occipital_temporal	2.60515586	6
ctx-lh-lateraloccipital	ctx-rh-superiortemporal	occipital	temporal	occipital_temporal	3.96668703	6
Right-Thalamus-Proper	ctx-lh-lateralorbitofrontal	subcortical	frontal	frontal_subcortical	2.36422228	5
Left-Pallidum	ctx-rh-parstriangularis	subcortical	frontal	frontal_subcortical	3.63245871	5
Right-Pallidum	ctx-rh-parstriangularis	subcortical	frontal	frontal_subcortical	3.09278943	5
Left-Pallidum	ctx-rh-rostralanteriorcingulate	subcortical	frontal	frontal_subcortical	3.68074056	5
Left-Accumbens-area	ctx-rh-rostralanteriorcingulate	subcortical	frontal	frontal_subcortical	2.6480299	5
ctx-lh-inferiortemporal	ctx-rh-isthmuscingulate	temporal	parietal	parietal_temporal	2.44642306	4
ctx-lh-fusiform	ctx-rh-precuneus	temporal	parietal	parietal_temporal	3.76365068	4
ctx-lh-superiortemporal	ctx-rh-precuneus	temporal	parietal	parietal_temporal	2.46176321	4
ctx-lh-fusiform	ctx-rh-superiorparietal	temporal	parietal	parietal_temporal	2.63257566	4
Left-VentralDC	ctx-lh-transversetemporal	subcortical	temporal	subcortical_temporal	3.0432666	3
Right-Thalamus-Proper	ctx-lh-transversetemporal	subcortical	temporal	subcortical_temporal	2.46610342	3
Left-Amygdala	ctx-rh-bankssts	subcortical	temporal	subcortical_temporal	3.0791631	3

ctx-lh-postcentral	ctx-rh-isthmuscingulate	parietal	parietal	parietal_parietal	2.39777849	3
ctx-lh-inferiorparietal	ctx-rh-precuneus	parietal	parietal	parietal_parietal	3.01566993	3
ctx-lh-inferiorparietal	ctx-rh-superiorparietal	parietal	parietal	parietal_parietal	3.14661552	3
ctx-lh-lateraloccipital	ctx-rh-isthmuscingulate	occipital	parietal	occipital_parietal	2.66445688	3
ctx-lh-inferiorparietal	ctx-rh-lateraloccipital	parietal	occipital	occipital_parietal	2.78725854	3
ctx-lh-lateraloccipital	ctx-rh-superiorparietal	occipital	parietal	occipital_parietal	3.06653496	3
Left-Pallidum	Right-Putamen	subcortical	subcortical	subcortical_subcortical	2.41786652	2
Left-Pallidum	Right-Pallidum	subcortical	subcortical	subcortical_subcortical	2.96604764	2
ctx-lh-parahippocampal	ctx-rh-paracentral	temporal	frontal	frontal_temporal	2.47136076	2
ctx-lh-superiortemporal	ctx-rh-frontalpole	temporal	frontal	frontal_temporal	2.36251488	2
ctx-lh-isthmuscingulate	ctx-lh-lateralorbitofrontal	parietal	frontal	frontal_parietal	2.49902218	2
ctx-rh-isthmuscingulate	ctx-rh-parsopercularis	parietal	frontal	frontal_parietal	2.38042547	2
Right-Pallidum	ctx-lh-insula	subcortical	insula	insula_subcortical	2.50411619	1
ctx-lh-insula	ctx-rh-isthmuscingulate	insula	parietal	insula_parietal	2.55866561	1

Table S6. List of all connections in the PRS-associated subnetwork for the matched female sample. Note: “t-stat” represents the t-statistic derived in the first step of the NBS analysis and “frequency” represents the number of times the type of “Region1-Region2” connection appears in the network. The table is ordered according to the “frequency” column in a descending manner.

Node1	Node2	Region1	Region2	Region1Region2	tstat	frequency
Right-Pallidum	ctx-lh-caudalanteriorcingulate	subcortical	frontal	frontal_subcortical	2.29369012	10
Left-Hippocampus	ctx-lh-parsopercularis	subcortical	frontal	frontal_subcortical	2.6974574	10
Brain-Stem	ctx-lh-parsorbitalis	subcortical	frontal	frontal_subcortical	2.4792543	10
Right-Caudate	ctx-lh-rostralmiddlefrontal	subcortical	frontal	frontal_subcortical	2.24062093	10
Right-Thalamus-Proper	ctx-lh-frontalpole	subcortical	frontal	frontal_subcortical	2.5659767	10
Right-Caudate	ctx-rh-paracentral	subcortical	frontal	frontal_subcortical	2.22022797	10
Right-Thalamus-Proper	ctx-rh-parstriangularis	subcortical	frontal	frontal_subcortical	2.59285183	10
Left-Hippocampus	ctx-rh-precentral	subcortical	frontal	frontal_subcortical	2.35184137	10
Left-Thalamus-Proper	ctx-rh-rostralmiddlefrontal	subcortical	frontal	frontal_subcortical	2.51528216	10
Left-Pallidum	ctx-rh-rostralmiddlefrontal	subcortical	frontal	frontal_subcortical	3.62845923	10
ctx-lh-caudalanteriorcingulate	ctx-lh-lateralorbitofrontal	frontal	frontal	frontal_frontal	2.3410645	10
ctx-lh-precentral	ctx-lh-rostralanteriorcingulate	frontal	frontal	frontal_frontal	2.74861678	10
ctx-lh-caudalmiddlefrontal	ctx-rh-lateralorbitofrontal	frontal	frontal	frontal_frontal	2.4001502	10
ctx-lh-rostralmiddlefrontal	ctx-rh-parsopercularis	frontal	frontal	frontal_frontal	2.5268291	10
ctx-lh-lateralorbitofrontal	ctx-rh-parstriangularis	frontal	frontal	frontal_frontal	2.66835902	10
ctx-lh-paracentral	ctx-rh-parstriangularis	frontal	frontal	frontal_frontal	2.44918036	10
ctx-lh-parsorbitalis	ctx-rh-parstriangularis	frontal	frontal	frontal_frontal	2.86927863	10
ctx-lh-caudalmiddlefrontal	ctx-rh-rostralmiddlefrontal	frontal	frontal	frontal_frontal	2.23608425	10
ctx-rh-precentral	ctx-rh-rostralmiddlefrontal	frontal	frontal	frontal_frontal	3.54304672	10
ctx-lh-rostralmiddlefrontal	ctx-rh-superiorfrontal	frontal	frontal	frontal_frontal	2.6703695	10
ctx-lh-bankssts	ctx-lh-pericalcarine	temporal	occipital	occipital_temporal	2.45917712	8
ctx-lh-fusiform	ctx-rh-cuneus	temporal	occipital	occipital_temporal	2.65579382	8
ctx-lh-inferiortemporal	ctx-rh-cuneus	temporal	occipital	occipital_temporal	2.32536693	8
ctx-lh-lateraloccipital	ctx-rh-entorhinal	occipital	temporal	occipital_temporal	2.24613883	8
ctx-lh-fusiform	ctx-rh-lingual	temporal	occipital	occipital_temporal	2.34009756	8

ctx-lh-lateraloccipital	ctx-rh-middletemporal	occipital	temporal	occipital_temporal	2.27360484	8
ctx-lh-pericalcarine	ctx-rh-middletemporal	occipital	temporal	occipital_temporal	2.41708696	8
ctx-lh-bankssts	ctx-rh-pericalcarine	temporal	occipital	occipital_temporal	2.28967466	8
ctx-lh-bankssts	ctx-lh-lateralorbitofrontal	temporal	frontal	frontal_temporal	3.14616859	8
ctx-lh-inferiortemporal	ctx-lh-paracentral	temporal	frontal	frontal_temporal	2.78283503	8
ctx-lh-parahippocampal	ctx-lh-paracentral	temporal	frontal	frontal_temporal	2.3014331	8
ctx-lh-bankssts	ctx-lh-frontalpole	temporal	frontal	frontal_temporal	2.83263294	8
ctx-lh-rostralmiddlefrontal	ctx-rh-bankssts	frontal	temporal	frontal_temporal	2.47275888	8
ctx-lh-caudalmiddlefrontal	ctx-rh-inferiortemporal	frontal	temporal	frontal_temporal	2.24747998	8
ctx-lh-paracentral	ctx-rh-middletemporal	frontal	temporal	frontal_temporal	2.34282518	8
ctx-lh-superiortemporal	ctx-rh-rostralmiddlefrontal	temporal	frontal	frontal_temporal	2.36914281	8
Right-Caudate	ctx-lh-entorhinal	subcortical	temporal	subcortical_temporal	2.82997571	7
Right-Thalamus-Proper	ctx-lh-middletemporal	subcortical	temporal	subcortical_temporal	2.78697629	7
Left-Thalamus-Proper	ctx-lh-parahippocampal	subcortical	temporal	subcortical_temporal	2.86697646	7
Left-Hippocampus	ctx-lh-transversetemporal	subcortical	temporal	subcortical_temporal	2.2944339	7
Left-Hippocampus	ctx-rh-inferiortemporal	subcortical	temporal	subcortical_temporal	2.83772404	7
Left-Amygdala	ctx-rh-inferiortemporal	subcortical	temporal	subcortical_temporal	2.23088323	7
Left-Hippocampus	ctx-rh-middletemporal	subcortical	temporal	subcortical_temporal	2.89457708	7
ctx-lh-lateraloccipital	ctx-lh-parstriangularis	occipital	frontal	frontal_occipital	2.63728064	5
ctx-lh-lateralorbitofrontal	ctx-lh-pericalcarine	frontal	occipital	frontal_occipital	2.5408466	5
ctx-lh-lingual	ctx-lh-rostralanteriorcingulate	occipital	frontal	frontal_occipital	2.98551073	5
ctx-rh-lateraloccipital	ctx-rh-parsopercularis	occipital	frontal	frontal_occipital	2.21689413	5
ctx-lh-cuneus	ctx-rh-parstriangularis	occipital	frontal	frontal_occipital	2.30472446	5
ctx-lh-parahippocampal	ctx-lh-superiorparietal	temporal	parietal	parietal_temporal	2.62436867	3
ctx-lh-superiorparietal	ctx-rh-inferiortemporal	parietal	temporal	parietal_temporal	2.2473444	3
ctx-lh-inferiortemporal	ctx-rh-precuneus	temporal	parietal	parietal_temporal	2.21651415	3
ctx-lh-lingual	ctx-rh-isthmuscingulate	occipital	parietal	occipital_parietal	2.43709039	3
ctx-lh-pericalcarine	ctx-rh-isthmuscingulate	occipital	parietal	occipital_parietal	2.52983363	3
ctx-lh-isthmuscingulate	ctx-rh-lingual	parietal	occipital	occipital_parietal	2.44761075	3

ctx-lh-caudalanteriorcingulate	ctx-lh-isthmuscingulate	frontal	parietal	frontal_parietal	2.2001909	3
ctx-lh-isthmuscingulate	ctx-lh-paracentral	parietal	frontal	frontal_parietal	3.00243919	3
ctx-lh-rostralanteriorcingulate	ctx-rh-posteriorcingulate	frontal	parietal	frontal_parietal	2.26922653	3
ctx-lh-parahippocampal	ctx-rh-inferiortemporal	temporal	temporal	temporal_temporal	2.21672069	2
ctx-lh-fusiform	ctx-rh-middletemporal	temporal	temporal	temporal_temporal	2.52685841	2
ctx-lh-postcentral	ctx-lh-superiorparietal	parietal	parietal	parietal_parietal	2.51605374	2
ctx-lh-precuneus	ctx-rh-isthmuscingulate	parietal	parietal	parietal_parietal	2.88443997	2
Left-Hippocampus	ctx-rh-lateraloccipital	subcortical	occipital	occipital_subcortical	2.56799872	2
Left-Pallidum	ctx-rh-lingual	subcortical	occipital	occipital_subcortical	2.21332298	2
Left-Thalamus-Proper	ctx-lh-insula	subcortical	insula	insula_subcortical	2.30360212	2
Left-Putamen	ctx-lh-insula	subcortical	insula	insula_subcortical	2.27943045	2
Left-Hippocampus	ctx-lh-isthmuscingulate	subcortical	parietal	parietal_subcortical	2.30370893	1
ctx-lh-insula	ctx-rh-superiortemporal	insula	temporal	insula_temporal	2.50518088	1
ctx-lh-insula	ctx-rh-precuneus	insula	parietal	insula_parietal	2.53391878	1
ctx-lh-pericalcarine	ctx-lh-insula	occipital	insula	insula_occipital	2.27945912	1

Table S7. List of all connections in the CT-associated subnetwork for the matched female sample. Note: “t-stat” represents the t-statistic derived in the first step of the NBS analysis and “frequency” represents the number of times the type of “Region1-Region2” connection appears in the network. The table is ordered according to the “frequency” column in a descending manner.

Node1	Node2	Region1	Region2	Region1Region2	tstat	frequency
Right-Putamen	ctx-lh-parsorbitalis	subcortical	frontal	frontal_subcortical	2.62758778	15
Right-Thalamus-Proper	ctx-lh-rostralmiddlefrontal	subcortical	frontal	frontal_subcortical	2.91979843	15
Right-Putamen	ctx-lh-rostralmiddlefrontal	subcortical	frontal	frontal_subcortical	3.25026223	15
Right-Thalamus-Proper	ctx-lh-superiorfrontal	subcortical	frontal	frontal_subcortical	3.85601291	15
Right-Putamen	ctx-lh-superiorfrontal	subcortical	frontal	frontal_subcortical	2.80474079	15
Right-Pallidum	ctx-lh-superiorfrontal	subcortical	frontal	frontal_subcortical	2.62773155	15
Left-Putamen	ctx-rh-caudalanteriorcingulate	subcortical	frontal	frontal_subcortical	2.34677402	15
Right-Thalamus-Proper	ctx-rh-caudalanteriorcingulate	subcortical	frontal	frontal_subcortical	4.41937786	15
Right-Thalamus-Proper	ctx-rh-lateralorbitofrontal	subcortical	frontal	frontal_subcortical	2.38524281	15
Left-Thalamus-Proper	ctx-rh-medialorbitofrontal	subcortical	frontal	frontal_subcortical	2.48408457	15
Brain-Stem	ctx-rh-parstriangularis	subcortical	frontal	frontal_subcortical	2.62138088	15
Brain-Stem	ctx-rh-rostralmiddlefrontal	subcortical	frontal	frontal_subcortical	2.79423778	15
Left-Thalamus-Proper	ctx-rh-superiorfrontal	subcortical	frontal	frontal_subcortical	2.79935919	15
Left-Putamen	ctx-rh-superiorfrontal	subcortical	frontal	frontal_subcortical	3.31345414	15
Left-Pallidum	ctx-rh-superiorfrontal	subcortical	frontal	frontal_subcortical	2.50766265	15
Left-VentralDC	ctx-lh-bankssts	subcortical	temporal	subcortical_temporal	3.81671815	8
Left-VentralDC	ctx-lh-fusiform	subcortical	temporal	subcortical_temporal	3.01425191	8
Right-Thalamus-Proper	ctx-lh-inferiortemporal	subcortical	temporal	subcortical_temporal	2.5514713	8
Left-Hippocampus	ctx-lh-middletemporal	subcortical	temporal	subcortical_temporal	2.46880838	8
Right-Thalamus-Proper	ctx-lh-middletemporal	subcortical	temporal	subcortical_temporal	3.27309175	8
Right-Putamen	ctx-lh-middletemporal	subcortical	temporal	subcortical_temporal	3.71694271	8
Brain-Stem	ctx-lh-parahippocampal	subcortical	temporal	subcortical_temporal	2.57711627	8
Left-Thalamus-Proper	ctx-lh-superiortemporal	subcortical	temporal	subcortical_temporal	2.88415368	8
ctx-lh-parsopercularis	ctx-lh-rostralanteriorcingulate	frontal	frontal	frontal_frontal	2.49438178	7
ctx-lh-medialorbitofrontal	ctx-lh-superiorfrontal	frontal	frontal	frontal_frontal	2.87598852	7

ctx-lh-rostralmiddlefrontal	ctx-rh-caudalanteriorcingulate	frontal	frontal	frontal_frontal	2.52785691	7
ctx-lh-caudalanteriorcingulate	ctx-rh-parstriangularis	frontal	frontal	frontal_frontal	2.91420557	7
ctx-lh-superiorfrontal	ctx-rh-precentral	frontal	frontal	frontal_frontal	2.42634383	7
ctx-lh-caudalanteriorcingulate	ctx-rh-rostralmiddlefrontal	frontal	frontal	frontal_frontal	2.46792993	7
ctx-lh-rostralmiddlefrontal	ctx-rh-superiorfrontal	frontal	frontal	frontal_frontal	2.37817291	7
Right-Thalamus-Proper	ctx-lh-cuneus	subcortical	occipital	occipital_subcortical	2.95180863	6
Left-Putamen	ctx-lh-lingual	subcortical	occipital	occipital_subcortical	3.27022937	6
Left-Putamen	ctx-lh-pericalcarine	subcortical	occipital	occipital_subcortical	2.98567659	6
Right-Putamen	ctx-rh-cuneus	subcortical	occipital	occipital_subcortical	2.49871027	6
Brain-Stem	ctx-rh-lingual	subcortical	occipital	occipital_subcortical	2.54285909	6
Right-VentralDC	ctx-rh-lingual	subcortical	occipital	occipital_subcortical	2.50123503	6
ctx-lh-lateralorbitofrontal	ctx-lh-lingual	frontal	occipital	frontal_occipital	2.41995312	4
ctx-lh-medialorbitofrontal	ctx-lh-pericalcarine	frontal	occipital	frontal_occipital	2.95093462	4
ctx-lh-lingual	ctx-lh-frontalpole	occipital	frontal	frontal_occipital	2.65910724	4
ctx-lh-rostralanteriorcingulate	ctx-rh-pericalcarine	frontal	occipital	frontal_occipital	2.6662298	4
ctx-lh-fusiform	ctx-lh-transversetemporal	temporal	temporal	temporal_temporal	3.52688379	3
ctx-lh-middletemporal	ctx-lh-transversetemporal	temporal	temporal	temporal_temporal	2.52977902	3
ctx-lh-inferiortemporal	ctx-rh-superiortemporal	temporal	temporal	temporal_temporal	2.88229506	3
Left-Putamen	Left-Accumbens-area	subcortical	subcortical	subcortical_subcortical	2.41267228	3
Left-Accumbens-area	Right-Pallidum	subcortical	subcortical	subcortical_subcortical	2.50178089	3
Right-Thalamus-Proper	Right-VentralDC	subcortical	subcortical	subcortical_subcortical	2.58416134	3
ctx-lh-pericalcarine	ctx-lh-insula	occipital	insula	insula_occipital	2.79733001	3
ctx-rh-cuneus	ctx-rh-insula	occipital	insula	insula_occipital	2.8494636	3
ctx-rh-pericalcarine	ctx-rh-insula	occipital	insula	insula_occipital	3.38066287	3
ctx-lh-caudalanteriorcingulate	ctx-lh-precuneus	frontal	parietal	frontal_parietal	2.37786862	3
ctx-lh-superiorfrontal	ctx-rh-postcentral	frontal	parietal	frontal_parietal	2.38958365	3
ctx-lh-superiorfrontal	ctx-rh-supramarginal	frontal	parietal	frontal_parietal	3.14292953	3
Right-Putamen	ctx-lh-posteriorcingulate	subcortical	parietal	parietal_subcortical	3.4249314	2
Left-VentralDC	ctx-rh-superiorparietal	subcortical	parietal	parietal_subcortical	2.38855179	2
ctx-lh-bankssts	ctx-rh-pericalcarine	temporal	occipital	occipital_temporal	2.39565698	2

ctx-rh-pericalcarine	ctx-rh-superiortemporal	occipital	temporal	occipital_temporal	2.57422842	2
ctx-lh-fusiform	ctx-lh-lateralorbitofrontal	temporal	frontal	frontal_temporal	2.38618156	2
ctx-lh-parahippocampal	ctx-lh-parsopercularis	temporal	frontal	frontal_temporal	2.81773767	2
ctx-lh-bankssts	ctx-rh-posteriorcingulate	temporal	parietal	parietal_temporal	2.40343061	1

References

Howard, D. M., Adams, M. J., Shirali, M., Clarke, T. K., Marioni, R. E., Davies, G., … McIntosh, A. M. (2018). Genome-wide association study of depression phenotypes in UK Biobank identifies variants in excitatory synaptic pathways. *Nature communications, 9*(1), 1470. https://doi.org/10.1038/s41467-018-03819-3

Manichaikul, A., Mychaleckyj, J. C., Rich, S. S., Daly, K., Sale, M., & Chen, W. M. (2010). Robust relationship inference in genome-wide association studies. *Bioinformatics (Oxford, England), 26*(22), 2867–2873. https://doi.org/10.1093/bioinformatics/btq559

Appendix 3: Supplementary materials for Chapter 4

Comparing personalised brain-based and genetic risk scores for Major Depressive Disorder in large population samples of adults and adolescents

Supplementary Materials

Thng *et al*.

OVERVIEW

Supplementary Text

Supplementary Figures

Supplementary Tables

1: Exclusion criteria for GS-Imaging and ABCD

For GS-Imaging, we excluded (a) individuals with neurological problems (brain tumour, hemotoma, stroke, epilepsy, haemorrhage, cerebral palsy and aneurysm, N=33), (b) related individuals, and (c) individuals with poor brain image quality (see Section 4 on Quality control measures for imaging data). As GS-Imaging is a family-based cohort, each participant within a family was assigned a random number and only one individual with the highest random number in each family was included. For ABCD, we excluded (a) individuals with neurological problems (N=114), (b) related individuals following the approach described for GS-Imaging, (3) individuals of non-European ancestry to match the MDD genome-wide association study discovery cohorts used to calculate PRS (see Section 2 on Selection of individuals of European ancestry in ABCD), and (4) individuals with poor image quality (see Section 4 on Quality control measures for imaging data).

2: Selection of individuals of European ancestry in ABCD

We restricted our sample to include only individuals of European ancestry to ensure the accuracy of polygenic risk scores, as summary statistics from genome wide association studies are typically based on European populations. Principal component analysis (PCA) was undertaken on ABCD genotyped data to generate the top 15 genetic principal components (PC). 4-means clustering was then performed on the top two PCs corresponding to White, Black, Hispanic and Asian. We created an intersection between the White clusters for PC1 and PC2 to generate a final White cluster. Individuals who self-reported as White, have parents that self-reported as White, and fall under the final White cluster were

selected (N=4160). A PCA plot was done together with data from The 1000 Genomes Project Consortium (2015) – European Population to confirm that subjects were selected accurately (Figure S1).

3: Quality control steps for ABCD imputed genetics data

The ABCD team conducted quality control (QC) on the genotyped data following the Ricopili pipeline (Lam et al., 2020) and then imputation using mixed ancestry and Eagle v2.4 phasing on the TOPMed imputation server (https://topmedimpute.readthedocs.io/en/latest) using the full sample. We filtered for INFO score<0.8 and then converted the genome build from hg38/GRCH38 to hg19/GRCh37 using LiftOver (https://github.com/sritchie73/liftOverPlink). As minor allele frequencies can differ between different ancestries, we further filtered for minor allele frequency <0.005 only after obtaining the European-only subsample.

4: Quality control measures for imaging data

For GS-Imaging, full image acquisition details can be found in Habota el al (2021) T1 data were acquired from N=1,080 individuals. The FreeSurfer processed scans were visually inspected and minor errors were manually corrected. Errors included incorrect skull stripping, exclusion of grey or white matter in tissue segmentation maps, or incorrect brain parcellation into separate regions as detailed in Neilson et al (2019). Individuals were excluded when there was at least one major error that could not be corrected (e.g., in segmentation or cortical parcellation) or when there

were multiple minor errors (N=12). Within those included, data was edited for N=424 individuals. Diffusion tensor imaging (DTI) data were acquired from N=1,058 individuals and processed using the TBSS toolkit. QC was performed following ENIGMA DTI protocols (http://enigma.ini.usc.edu/protocols/dti-protocols/), which included (1) correcting for eddy current-induced distortions and subject movement in the scanner, (2) skull stripping using BET at a threshold of 0.2, (3) using DTIFIT in order to compute diffusion tensor characteristics, and (4) visually checking the quality of FA images at this stage in order to exclude distorted images. In total, N=21 individuals were excluded due to errors during diffusion tensor fitting (N=14) and errors during registration/skeleton fitting (N=7). More details on QC measures can be found in Green et al (2021) and Stolicyn et al (2020). The final analysis sample for GS-Imaging (N=702 after applying all exclusion criteria and merging with genetic and clinical data) included individuals with either T1 (N=702) or DTI (N=686) data, with N=680 having both.

For ABCD, full image acquisition details are detailed in Hagler et al (2019). The minimally processed data for the full sample were downloaded from the ABCD repository. Further QC following the QC recommendations by the ABCD team [7] were conducted for the unrelated European-only subsample. For morphometric measures, only individuals who had satisfactory T1 scans (field name: iqc_t1_ok_ser > 0) and passed FreeSurfer quality control (field name: fsqc_qc =1) were included (N=243 excluded). For white matter microstructural measures, only individuals who had satisfactory T1 scans, satisfactory diffusion MRI scans (field name: iqc_dmri_ok_ser > 0) and passed FreeSurfer QC were included (N=377 excluded). In addition to the standard quality control steps above, for baseline data only, average FA and MD values that were five standard

deviations from mean were also removed to reduce skewness (N=18), as described in Shen et al (2021). The final analysis sample for ABCD baseline (N=3,825 after applying all exclusion criteria and merging with genetic and clinical data) included individuals with either T1 (N=3,825) or DTI (N=3,630) data, with N=3,630 having both. The QC process was repeated for the two-year follow-up assessment. In total, N=30 and N=79 individuals were excluded for morphometric measures and white matter microstructural measures, respectively at two-year follow-up. The final analysis sample for ABCD two-year follow-up (N=2,081 after applying all exclusion criteria and merging with genetic and clinical data) included individuals with either T1 (N=2,081) or DTI (N=2,032) data, with N=2,032 having both.

5: Calculation of Regional Vulnerability Index (RVI)

Using RVI-Sub as an example, the residuals for each of the 7 subcortical structures were first estimated by regressing out the effects of the same covariates used in the ENIGMA meta-analysis (refer to Table S1 to S4 for covariates used), and then z-score transformed using the mean and standard deviation of healthy individuals. In our sample, subjects were deemed as healthy if they did not self-report any psychiatric diagnoses and were not taking antidepressants at the point of assessment (Table 1 in main text). This procedure yielded a vector comprising 7 region-wise z-scores for each subject. Subject-specific RVI-Sub was then calculated as a single Pearson's correlation coefficient between the vector of the 7 region-wise z-values and the corresponding regional effect sizes in the ENIGMA meta-analyses. This procedure was repeated for cortical thickness and surface area measures (using 33 cortical regions each), and for FA and MD measures (using 24 white matter tracts each), each

yielding a single RVI. For ABCD, only 12 white matter tracts were used upon matching the tracts defined by AtlasTrack used in ABCD and the John Hopkins University atlas used in ENIGMA and GS-Imaging (Table S3). Measures from the left and right hemisphere were averaged. The RVI computation was implemented in the RVIpkg package version 0.2.3 in R (https://cran.r-project.org/web/packages/RVIpkg/RVIpkg.pdf).

6: Phenotypes included in summary statistics used for PRS calculation

Summary statistics were obtained from Howard et al (Howard et al., 2019). Three different cohorts were included in the meta-analysis: UK Biobank, 23nMe and Psychiatric Genetics Consortium (PGC). Within UK Biobank, the broad definition of depression was used, where subjects were asked: 'Have you ever seen a general practitioner for nerves, anxiety, tension or depression?' or 'Have you ever seen a psychiatrist for nerves, anxiety, tension or depression?'. Within 23nMe, phenotypic status was based on responses to web-based surveys, with individuals that self-reported as having received a clinical diagnosis or treatment for depression classified as cases. For PGC, cases were required to meet international consensus criteria (DSM-IV, ICD-9, or ICD-10) for a lifetime diagnosis of MDD established using structured diagnostic instruments from assessments by trained interviewers, clinician-administered checklists, or medical record review.

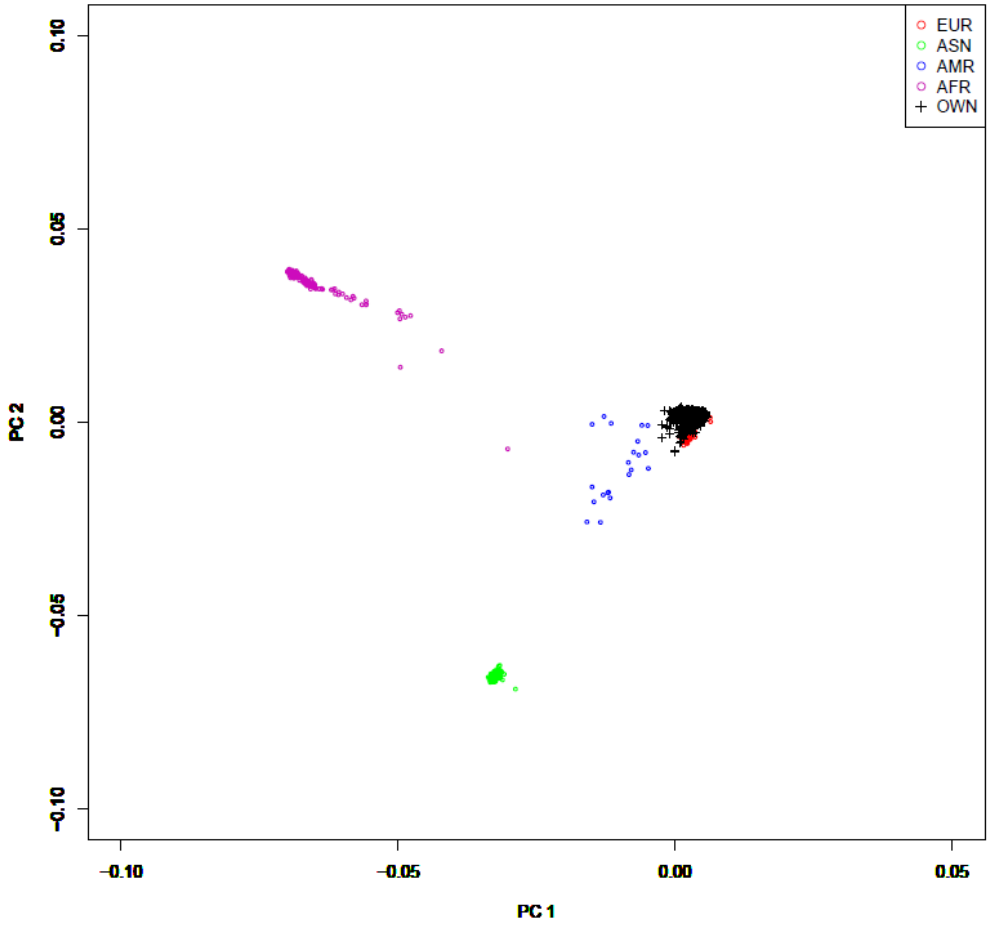

Figure S1. PCA plot using ABCD genotyped data and 1000 Genomes genetic data. The ABCD sample used in the current analyses were mostly of European ancestry, as indicated by the overlap with the 1000 Genomes European population. Figure legend: EUR – European, ASN – Asian, AMR – American, AFR – African, OWN – ABCD European-only sample.

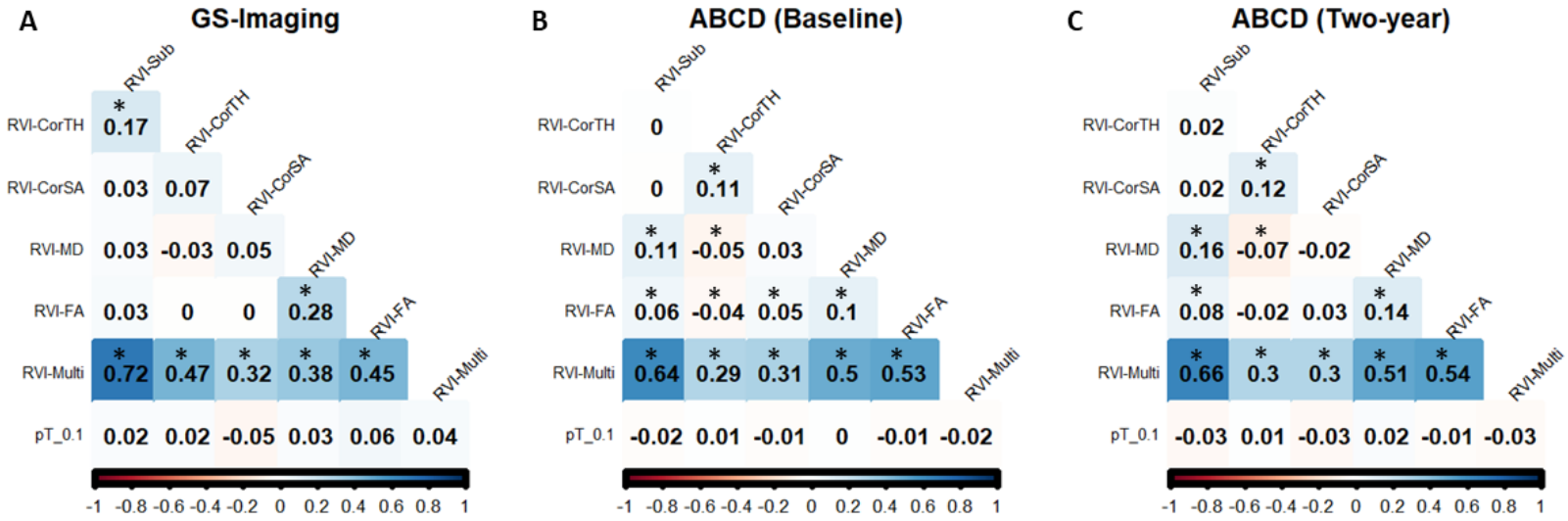

Figure S2. Correlation coefficients between the different MDD-RVIs and MDD-PRS at pT_0.1 for (A) GS-Imaging, (B) ABCD (Baseline), and (C) ABCD (Two-year). Boxes with "*" indicate that the correlation coefficient is significant at $p<0.05$.

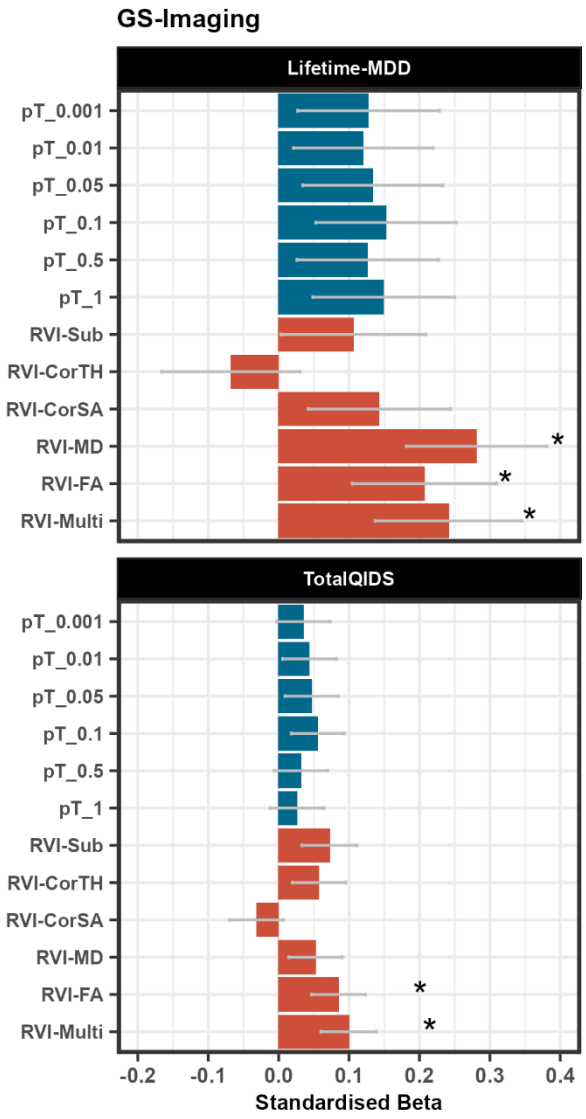

Figure S3. Association between MDD-RVIs/MDD-PRS (all thresholds) with Lifetime-MDD and TotalQIDS in GS-Imaging. The x-axis represents the standardised effect sizes and the y-axis represent the different RVI types and the MDD-PRS calculated at the different p-value thresholds.

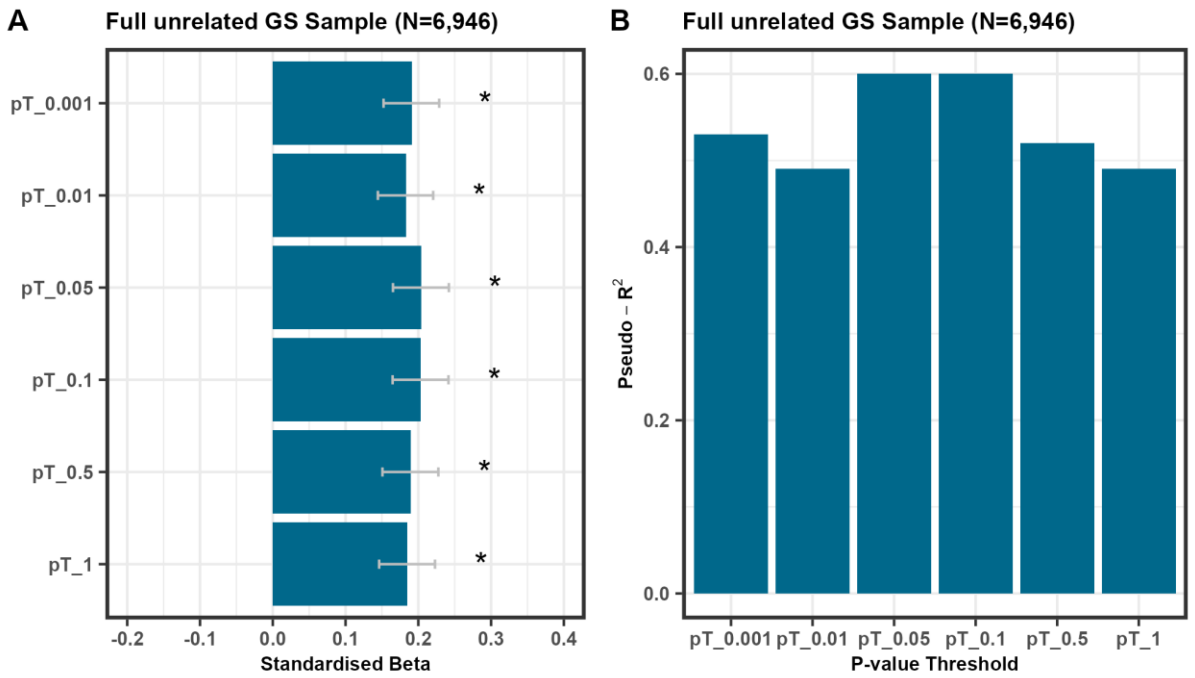

Figure S4. (A) Association between MDD-PRS and lifetime MDD diagnosis in the full unrelated GS sample (N=6,946) defined in Howard et al (2019). Individuals were defined as cases if they were given a MDD diagnosis using the Structured Clinical Interview for DSM disorders (975 cases and 5,975 controls). The x-axis represents the standardised effect sizes and the y-axis represent the different RVI types and the MDD-PRS calculated at the different p-value thresholds. (B) The change in McFadden Pseudo-R^2 was calculated for each p-value threshold to assess the improvement in model fit upon adding MDD-PRS as a predictor, relative to the null model including only covariates.

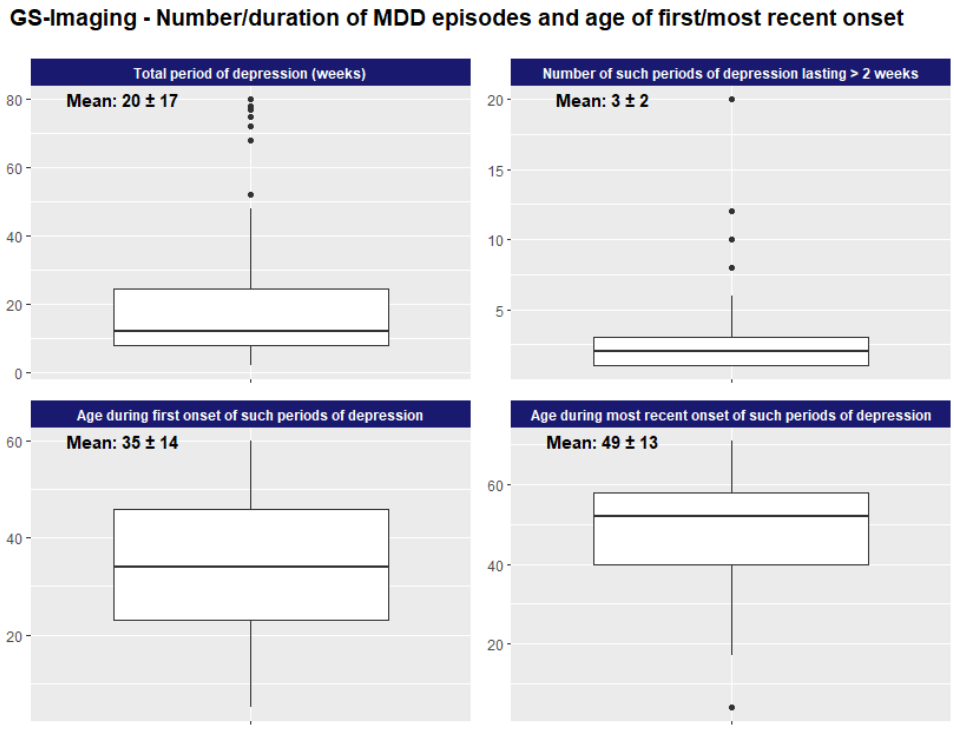

Figure S5. Additional information on number/duration of MDD episodes and age of first/most recent onset in GS-Imaging.

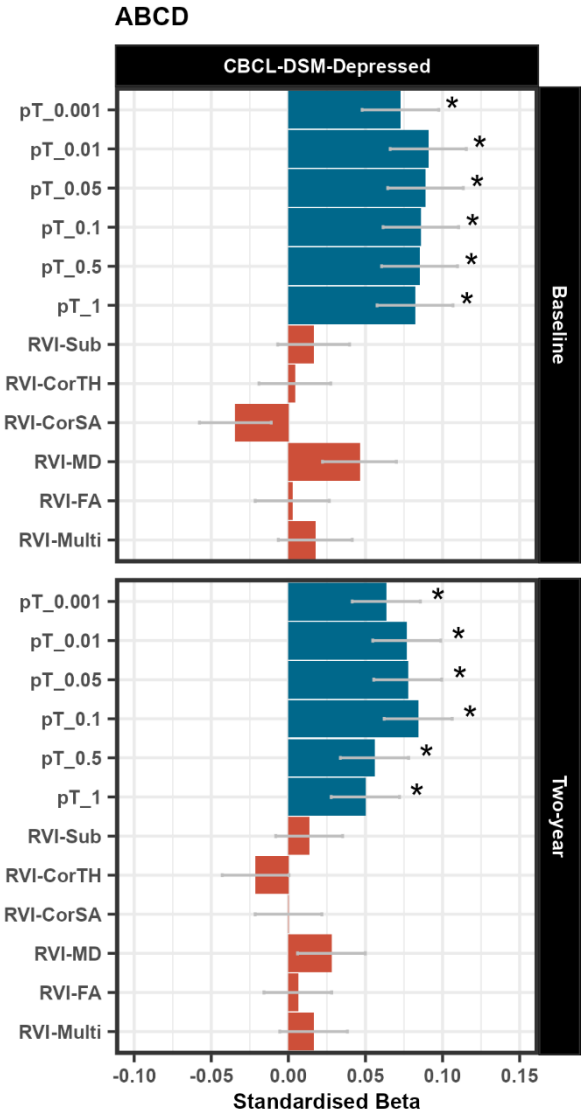

Figure S6. Association between MDD-RVIs/ MDD-PRS with CBCL-DSM-Depressed at baseline and two-year follow-up. The x-axis represents the standardised effect sizes and the y-axis represent the different RVI types and the MDD-PRS calculated at the different p-value thresholds.

Table S1. MDD case-control effect sizes for subcortical volume obtained from Table 1 in Schmaal et al (2016). Covariates included age, sex, site and ICV.

Region	**Cohen's d**
Accumbens	-0.019
Amygdala	-0.060
Caudate	-0.023
Hippocampus	-0.144
Pallidum	-0.001
Putamen	0.012
Thalamus	-0.044

Table S2. MDD case-control effect sizes for cortical surface area and thickness obtained from Table S19 and Table 1 in Schmaal et al (2017), respectively. Covariates included age, sex and site. The left and right hemispheres were averaged to calculate cortical-based RVIs in the current analysis.

Region	**Cohen's d – Cortical SA**	**Cohen's d – Cortical Thickness**
Left banks superior temporal sulcus	-0.024	−0.058
Left caudal anterior cingulate cortex	0.021	−0.042
Left caudal middle frontal gyrus	0.045	−0.014
Left cuneus	-0.007	0.05
Left entorhinal cortex	0.008	−0.041
Left frontal pole	-0.049	−0.011
Left fusiform gyrus	0.012	−0.117
Left hemisphere total surface area	0.026	−0.057
Left inferior parietal cortex	-0.005	−0.063
Left inferior temporal gyrus	0.046	−0.049
Left insula	0.014	−0.111
Left isthmus cingulate cortex	0.063	−0.104
Left lateral occipital cortex	0.016	−0.023
Left lateral orbitofrontal cortex	0.041	−0.046
Left lingual gyrus	0.028	0.01
Left medial orbitofrontal cortex	0.035	−0.134
Left middle temporal gyrus	-0.034	−0.090
Left paracentral lobule	0.018	−0.003
Left parahippocampal gyrus	-0.017	−0.072
Left pars opercularis	-0.015	−0.063
Left pars orbitalis	-0.002	−0.073
Left pars triangularis	-0.063	−0.054
Left pericalcarine cortex	-0.008	0.09
Left postcentral gyrus	0.006	0.04

Left posterior cingulate cortex	0.006	−0.099
Left precentral gyrus	0.034	−0.020
Left precuneus	0.011	−0.024
Left rostral anterior cingulate cortex	0.04	−0.130
Left rostral middle frontal gyrus	0.025	−0.037
Left superior frontal gyrus	0.052	−0.066
Left superior parietal cortex	0.017	−0.005
Left superior temporal gyrus	0.011	0.01
Left supramarginal gyrus	0.04	−0.045
Left temporal pole	0.066	0.01
Left transverse temporal gyrus	0.013	−0.035
Right banks superior temporal sulcus	0.01	−0.074
Right caudal anterior cingulate cortex	0.011	−0.080
Right caudal middle frontal gyrus	0.009	0.01
Right cuneus	0.058	0.05
Right entorhinal cortex	0.036	−0.055
Right frontal pole	0.024	−0.062
Right fusiform gyrus	-0.034	−0.116
Right hemisphere total surface area	0.007	−0.049
Right inferior parietal cortex	-0.024	−0.041
Right inferior temporal gyrus	0.005	−0.117
Right insula	-0.004	−0.115
Right isthmus cingulate cortex	0.04	−0.071
Right lateral occipital cortex	0.067	0.01
Right lateral orbitofrontal cortex	0.026	−0.120
Right lingual gyrus	0.016	−0.012
Right medial orbitofrontal cortex	0.027	−0.131
Right middle temporal gyrus	0.027	−0.088
Right paracentral lobule	0.014	−0.006
Right parahippocampal gyrus	-0.04	−0.061

Right pars opercularis	-0.011	−0.017
Right pars orbitalis	0.022	−0.070
Right pars triangularis	-0.012	−0.031
Right pericalcarine cortex	0.007	0.08
Right postcentral gyrus	0.022	0.03
Right posterior cingulate cortex	0.016	−0.093
Right precentral gyrus	0.009	−0.022
Right precuneus	0.006	0.01
Right rostral anterior cingulate cortex	0.029	−0.098
Right rostral middle frontal gyrus	0.054	−0.038
Right superior frontal gyrus	0.028	−0.078
Right superior parietal cortex	-0.008	0.03
Right superior temporal gyrus	0.029	−0.031
Right supramarginal gyrus	0.004	−0.053
Right temporal pole	0.051	0.01
Right transverse temporal gyrus	-0.021	−0.051

Table S3. Tracts of interest listed in van Velzen et al (2020). Regions that match with ABCD and are used for the analyses are highlighted in yellow.

Abbreviation	Full tract name
AverageFA	Full skeleton average FA
ACR (L+R)	Anterior corona radiata
ALIC (L+R)	Anterior limb of internal capsule
BCC	Body of corpus callosum
CC (BCC+GCC+SCC)	Corpus callosum
CGC (L+R)	Cingulum (cingulate gyrus)
CGH (L+R)	Cingulum (hippocampal portion)
CR (L+R)	Corona radiata
CST (L+R)	Corticospinal tract
EC (L+R)	External capsule
FX	Fornix
FXST (L+R)	Fornix (cres) / Stria terminalis
GCC	Genu of corpus callosum
IC (L+R)	Internal capsule
IFO (L+R)	Inferior fronto-occipital fasciculus
PCR (L+R)	Posterior corona radiata
PLIC (L+R)	Posterior limb of internal capsule
PTR (L+R)	Posterior thalamic radiation

RLIC (L+R)	Retrolenticular part of internal capsule
SCC	Splenium of corpus callosum
SCR (L+R)	Superior corona radiata
SFO (L+R)	Superior fronto-occipital fasciculus
SLF (L+R)	Superior longitudinal fasciculus
SS (L+R)	Sagittal stratum
UNC (L+R)	Uncinate fasciculus

Table S4. Effect sizes for MD and FA obtained from Table S6 and Table S4 in van Velzen et al (2020), respectively. Covariates included age, age^2, sex, age*sex, age^2*sex and site.

Region	Cohen's d – MD	Cohen's d – FA
AACR	0.065	-0.253
ALIC	0.124	-0.232
BCC	0.192	-0.243
CC	0.17	-0.249
CGC	0.085	-0.165
CGH	0.14	-0.068
CR	0.12	-0.25
CST	0.104	-0.101
EC	0.148	-0.16
FX	0.123	-0.083
FXST	0.18	-0.183
GCC	0.102	-0.247
IC	0.104	-0.229
IFO	0.093	-0.121
PCR	0.143	-0.202
PLIC	0.105	-0.154
PTR	0.111	-0.135
RLIC	0.075	-0.151
SCC	0.143	-0.13
SCR	0.192	-0.197
SFO	0.164	-0.232
SLF	0.126	-0.169
SS	0.12	-0.23
UNC	0.052	-0.12
Average	0.176	-0.258

Table S5. Standardised betas from linear regression analyses examining the association between FA values and severity of symptoms measured by the Beck Depression Inventory in adults only. This table was obtained from Table S92 in van Velzen et al (2020).

Region	Beta	SE	CI LB	CI UB	P-value	FDR P-value	I^2	N
ACR	0.000313	0.000187	-0.000053	0.000679	0.093	0.883	34.109	477
ALIC	0.000088	0.000139	-0.000184	0.000360	0.528	0.975	19.424	477
BCC	0.000020	0.000165	-0.000304	0.000344	0.904	0.975	0.000	477
CC	0.000006	0.000123	-0.000235	0.000246	0.963	0.975	0.276	477
CGC	0.000029	0.000261	-0.000482	0.000539	0.913	0.975	41.845	477
CGH	-0.000359	0.000326	-0.000997	0.000279	0.269	0.975	50.839	477
CR	0.000165	0.000131	-0.000091	0.000420	0.208	0.975	17.340	477
CST	-0.000346	0.000502	-0.001331	0.000638	0.491	0.975	81.332	477
EC	0.000018	0.000202	-0.000378	0.000414	0.928	0.975	56.521	477
FX	-0.000419	0.000259	-0.000926	0.000089	0.106	0.883	0.000	477
FXST	-0.000389	0.000214	-0.000809	0.000031	0.069	0.883	31.235	477
GCC	-0.000075	0.000236	-0.000537	0.000388	0.752	0.975	47.584	477
IC	-0.000019	0.000096	-0.000206	0.000169	0.847	0.975	0.000	477
IFO	-0.000330	0.000487	-0.001285	0.000625	0.498	0.975	78.024	477
PCR	0.000054	0.000112	-0.000167	0.000274	0.633	0.975	0.000	477
PLIC	-0.000032	0.000124	-0.000276	0.000211	0.794	0.975	0.000	477

PTR	-0.000131	0.000133	-0.000392	0.000130	0.326	0.975	0.000	477
RLIC	-0.000129	0.000118	-0.000361	0.000103	0.276	0.975	0.000	477
SCC	0.000055	0.000099	-0.000139	0.000249	0.576	0.975	0.000	477
SCR	0.000208	0.000215	-0.000214	0.000631	0.333	0.975	53.738	477
SFO	0.000122	0.000365	-0.000593	0.000837	0.738	0.975	71.573	477
SLF	0.000045	0.000114	-0.000178	0.000267	0.695	0.975	0.000	477
SS	0.000050	0.000119	-0.000183	0.000282	0.677	0.975	0.000	477
UNC	-0.000023	0.000232	-0.000477	0.000431	0.921	0.975	5.682	477
AverageFA	0.000003	0.000078	-0.000151	0.000156	0.975	0.975	5.459	477

Table S6. Standardised betas from linear regression analyses examining the association between MD values and severity of symptoms measured by the Beck Depression Inventory in adults only. This table was obtained from Table S94 in van Velzen et al (2020).

Region	Beta	SE	CI LB	CI UB	P-value	FDR P-value	I^2	N
ACR	-0.00000001	0.00000031	-0.00000061	0.00000059	0.975	0.975	61.795	477
ALIC	-0.00000006	0.00000012	-0.00000029	0.00000017	0.620	0.902	2.768	477
BCC	0.00000011	0.00000018	-0.00000024	0.00000047	0.541	0.902	0.000	477
CC	0.00000005	0.00000015	-0.00000025	0.00000035	0.745	0.902	1.767	477
CGC	0.00000016	0.00000015	-0.00000014	0.00000046	0.297	0.902	9.121	477
CGH	0.00000025	0.00000020	-0.00000014	0.00000064	0.207	0.902	15.588	477
CR	0.00000005	0.00000020	-0.00000034	0.00000044	0.794	0.902	41.998	477
CST	0.00000013	0.00000024	-0.00000034	0.00000061	0.586	0.902	41.516	477
EC	0.00000003	0.00000011	-0.00000019	0.00000025	0.794	0.902	0.000	477
FX	-0.00000023	0.00000112	-0.00000243	0.00000197	0.838	0.908	11.894	477
FXST	0.00000017	0.00000013	-0.00000009	0.00000043	0.191	0.902	14.567	477
GCC	0.00000003	0.00000017	-0.00000031	0.00000037	0.872	0.908	0.000	477
IC	-0.00000008	0.00000010	-0.00000027	0.00000012	0.441	0.902	0.000	477
IFO	0.00000043	0.00000034	-0.00000025	0.00000111	0.213	0.902	78.643	477
PCR	0.00000013	0.00000013	-0.00000012	0.00000038	0.301	0.902	0.000	477
PLIC	-0.00000004	0.00000013	-0.00000028	0.00000021	0.761	0.902	0.000	477

PTR	0.00000016	0.00000016	-0.00000015	0.00000047	0.316	0.902	11.768	477
RLIC	-0.00000012	0.00000011	-0.00000033	0.00000010	0.298	0.902	0.000	477
SCC	-0.00000005	0.00000016	-0.00000037	0.00000027	0.775	0.902	15.737	477
SCR	0.00000011	0.00000010	-0.00000009	0.00000031	0.284	0.902	0.000	477
SFO	0.00000005	0.00000015	-0.00000023	0.00000034	0.718	0.902	0.000	477
SLF	0.00000003	0.00000010	-0.00000016	0.00000023	0.737	0.902	0.000	477
SS	0.00000009	0.00000016	-0.00000023	0.00000040	0.585	0.902	20.731	477
UNC	0.00000022	0.00000024	-0.00000025	0.00000070	0.353	0.902	0.000	477
AverageMD	0.00000005	0.00000009	-0.00000013	0.00000024	0.562	0.902	0.000	477

Table S7. Delta AIC values (e.g., "M2-M1" refers to the difference between M2 and M1 AIC values) for each model type (M1 to M5) when MDD-RVIs and MDD-PRS are used as predictors individually or in conjunction with each other. For model comparison, negative delta AIC values are indicative of better model fit. The results for both GS-Imaging and ABCD are reported.

GS-Imaging

		Lifetime-MDD						TotalQIDS					
Model	**Variables**	**RVI-Sub**	**RVI-CorTH**	**RVI-CorSA**	**RVI-MD**	**RVI-FA**	**RVI-Multi**	**RVI-Sub**	**RVI-CorTH**	**RVI-CorSA**	**RVI-MD**	**RVI-FA**	**RVI-Multi**
M1	Covs (for RVI)	NIL						NIL					
M2-M1	RVI+Covs (for RVI)	-38.428	-24.372	-13.828	-21.965	-18.047	-57.694	-122.529	-89.208	-37.53	-52.889	-56.001	-174.54
M3	Covs	NIL						NIL					
M4-M3	PRS+Covs	-0.363						-0.273					
M5-M4	PRS+RVI+Covs	-38.347	-24.715	-12.897	-22.276	-19.151	-58.55	-124.326	-90.384	-39.086	-54.432	-56.834	-177.55

ABCD

		CBCL-DSM-Depressed (Baseline)						CBCL-DSM-Depressed (Two-year)					
Model	**Variables**	**RVI-Sub**	**RVI-CorTH**	**RVI-CorSA**	**RVI-MD**	**RVI-FA**	**RVI-Multi**	**RVI-Sub**	**RVI-CorTH**	**RVI-CorSA**	**RVI-MD**	**RVI-FA**	**RVI-Multi**
M1	Covs (for RVI)	NIL						NIL					
M2-M1	RVI+Covs (for RVI)	1.497	1.966	-0.212	-256.563	-252.825	-253.354	1.605	1.017	2	-163.139	-161.579	-162.062
M3	Covs	NIL						NIL					
M4-M3	PRS+Covs	-11.385						-12.823					
M5-M4	PRS+RVI+Covs	0.892	1.988	0.494	-253.625	-249.971	-251.168	1.504	0.734	1.977	-164.721	-163.399	-163.875

*Covs: Covariates; "Covs (for RVI)" models do not include the 15 genetic principal components and genotype plate number that were included in the "Covs" models

Table S8. Association between baseline MDD-RVIs and MDD-PRS with the residualised CBCL-DSM-Depressed scores from baseline to two-year follow up for all RVI types and p-value thresholds.

Dependent variable	Predictor	*B*	SD	t-value	p-value
CBCL-DSM-Depressed (residualised)	pT_0.001	0.022	0.028	0.784	0.433
	pT_0.01	0.034	0.028	1.201	0.230
	pT_0.05	0.026	0.028	0.914	0.361
	pT_0.1	0.030	0.028	1.087	0.277
	pT_0.5	0.004	0.028	0.146	0.884
	pT_1	-0.001	0.028	-0.046	0.963
	RVI-Sub	0.009	0.026	0.331	0.741
	RVI-CorTH	-0.024	0.026	-0.916	0.360
	RVI-CorSA	0.022	0.026	0.842	0.400
	RVI-MD	-0.003	0.027	-0.095	0.924
	RVI-FA	-0.007	0.027	-0.248	0.804
	RVI-Multi	-0.008	0.026	-0.284	0.777

References

The 1000 Genomes Project Consortium, Auton, A., Brooks, L. D., Durbin, R. M., Garrison, E. P., Kang, H. M., … Abecasis, G. R. (2015). A global reference for human genetic variation. *Nature*, *526*(7571), 68–74. https://doi.org/10.1038/nature15393

Lam, M., Awasthi, S., Watson, H. J., Goldstein, J., Panagiotaropoulou, G., Trubetskoy, V., … Ripke, S. (2020). RICOPILI: Rapid Imputation for COnsortias PIpeLIne. *Bioinformatics (Oxford, England)*, *36*(3), 930–933. https://doi.org/10.1093/bioinformatics/btz633

Habota, T., Sandu, A. L., Waiter, G. D., McNeil, C. J., Steele, J. D., Macfarlane, J. A., … McIntosh, A. M. (2021). Cohort profile for the STratifying Resilience and Depression Longitudinally (STRADL) study: A depression-focused investigation of Generation Scotland, using detailed clinical, cognitive, and neuroimaging assessments. *Wellcome Open Research, 4*, 185. https://doi.org/10.12688/wellcomeopenres.15538.2

Neilson, E., Shen, X., Cox, S. R., Clarke, T. K., Wigmore, E. M., Gibson, J., … Lawrie, S. M. (2019). Impact of Polygenic Risk for Schizophrenia on Cortical Structure in UK Biobank. *Biological psychiatry*, *86*(7), 536–544. https://doi.org/10.1016/j.biopsych.2019.04.013

Green, C., Shen, X., Stevenson, A. J., Conole, E. L. S., Harris, M. A., Barbu, M. C., … Whalley, H. C. (2021). Structural brain correlates of serum and epigenetic markers of inflammation in major depressive disorder. *Brain, behavior, and immunity*, *92*, 39–48. https://doi.org/10.1016/j.bbi.2020.11.024

Stolicyn, A., Harris, M. A., Shen, X., Barbu, M. C., Adams, M. J., Hawkins, E. L., … Whalley, H. C. (2020). Automated classification of depression from structural brain measures across two independent community-based cohorts. *Human brain mapping*, *41*(14), 3922–3937. https://doi.org/10.1002/hbm.25095

Hagler, D. J., Jr, Hatton, S., Cornejo, M. D., Makowski, C., Fair, D. A., Dick, A. S., … Dale, A. M. (2019). Image processing and analysis methods for the Adolescent Brain Cognitive Development Study. *NeuroImage*, *202*, 116091. https://doi.org/10.1016/j.neuroimage.2019.116091

Shen, X., MacSweeney, N., Chan, S. W. Y., Barbu, M. C., Adams, M. J., Lawrie, S. M., … Whalley, H. C. (2021). Brain structural associations with depression in a large early adolescent sample (the ABCD study®). *EClinicalMedicine*, *42*, 101204. https://doi.org/10.1016/j.eclinm.2021.101204

Howard, D. M., Adams, M. J., Clarke, T. K., Hafferty, J. D., Gibson, J., Shirali, M., … McIntosh, A. M. (2019). Genome-wide meta-analysis of depression identifies 102 independent variants and highlights the importance of the prefrontal brain regions. *Nature neuroscience, 22*(3), 343–352. https://doi.org/10.1038/s41593-018-0326-7

Schmaal, L., Veltman, D. J., van Erp, T. G., Sämann, P. G., Frodl, T., Jahanshad, N., … Hibar, D. P. (2016). Subcortical brain alterations in major depressive disorder: findings from the

ENIGMA Major Depressive Disorder working group. *Molecular psychiatry, 21*(6), 806–812. https://doi.org/10.1038/mp.2015.69
Schmaal, L., Hibar, D. P., Sämann, P. G., Hall, G. B., Baune, B. T., Jahanshad, N., … Veltman, D. J. (2017). Cortical abnormalities in adults and adolescents with major depression based on brain scans from 20 cohorts worldwide in the ENIGMA Major Depressive Disorder Working Group. *Molecular psychiatry, 22*(6), 900–909. https://doi.org/10.1038/mp.2016.60

van Velzen, L. S., Kelly, S., Isaev, D., Aleman, A., Aftanas, L. I., Bauer, J., … Schmaal, L. (2020). White matter disturbances in major depressive disorder: a coordinated analysis across 20 international cohorts in the ENIGMA MDD working group. *Molecular Psychiatry*, *25*(7), 1511–1525. https://doi.org/10.1038/s41380-019-0477-2